



**Russian Academy of Sciences
Karelian Scientific Centre
Northern Water Problems Institute**

**Proceedings of the 7th Workshop on
PHYSICAL PROCESSES
IN NATURAL WATERS**

**2-5 July 2003
Petrozavodsk, Russia**



Edited by Arkady Terzhevik

Petrozavodsk, 2003

Proceedings of the 7th Workshop on
PHYSICAL PROCESSES IN
NATURAL WATERS

2-5 July 2003
Petrozavodsk, Russia

Edited by Arkady Terzhevik

Northern Water Problems Institute
Karelian Scientific Centre
Russian Academy of Sciences

Petrozavodsk, 2003

Arkady Terzhevik (Ed.)

Proceedings of the 7th Workshop on Physical Processes In Natural Waters. Petrozavodsk, Karelian Scientific Centre, Russian Academy of Sciences, 2003, 168 p.

Keywords: coastal zones; ice-covered lakes; Lake Baikal; Lake Ladoga; Langmuir circulation; mixing; numerical modeling; thermal structure of lakes; tidal seas.

This volume contains the extended abstracts of presentations at the 7th Workshop “Physical Processes In Natural Waters”. The researchers from different European and Russian institutions contribute their up-to-date results from studies of physical processes that play an essential role in the development of lake and sea ecosystems. A wide range of subjects is considered, with a certain focus on numerical modeling of hydrodynamics and parameterization of sub-grid-scale processes in water bodies. Different approaches to solving the issues of modern physical limnology are discussed.

Preface

The workshop “Physical Processes in Natural Waters” was initiated in 1996 and eventually became a periodic event. It gathers physical limnologists and oceanographers to discuss the hottest issues related to the processes in lakes and coastal zones of seas. To preserve the numerous lakes as a part of the European landscape, to provide the sustainable management of their resources, the efficient tools that allow effectively solving these tasks are essential. The numerical models of lake ecosystems are on the list of tools. One of the bottlenecks typical for models developed up to now is a description of the processes that take place in the sub-grid scales, i.e. the development of the frontal zones, mixing, heat/mass transfer through the interfaces, etc. To successfully implement the comprehensive parameterizations of such processes into the models, a better knowledge of their physics is strongly required. This a challenge sent to the community of physical limnologists and oceanographers. To my mind, the main idea of the workshop, that is to present the state of the art and get criticisms, to discuss results achieved and formulate further steps in research, is the most fruitful approach to resolving such problems. I do hope that the seventh Workshop will be as productive as all previous.

Arkady Terzhevik
Petrozavodsk, July 2003

List of PPNW7 participants

- Bengtsson, Lars – Department of Water Resources Engineering, Lund University, Sweden; E-mail: Lars.Bengtsson@tvrl.lth.se
- Bondur, Valery – Scientific-educational center “Aerokosmos”, Moscow State University of Geodesy and Cartography, Russia
- Bäuerle, Erich – Limnological Institute, University of Konstanz, Germany; E-mail: erich.baeyerle@uni-konstanz.de
- Böhrer, Bertram – Umweltforschungszentrum, Germany; E-mail: boehrer@gm.ufz.de
- Filatov, Nikolai – Northern Water Problems Institute, Karelian Scientific Centre, Russ. Acad. Sci., Russia; E-mail: nfilatov@nwpi.karelia.ru
- Golosoov, Sergei – Institute of Limnology, Russ. Acad. Sci., Russia; E-mail: sergey_golosoov@mail.ru
- Granin, Nikolai – Limnological Institute, Siberian Branch, Russ. Acad. Sci., Russia; E-mail: nick@lin.irk.ru
- Ivanov, Vyacheslav – Limnological Institute, Siberian Branch, Russ. Acad. Sci., Russia; E-mail: ppshest@lin.irk.ru
- Jones, Ian – CEH, Windermere, UK; E-mail: ianj@ceh.ac.uk
- Karetnikov, Sergei – Institute of Limnology, Russ. Acad. Sci., Russia; E-mail: naumenko@limno.org.ru
- Kay, Anthony – Department of Mathematical Sciences, Loughborough University, UK; E-mail: a.kay@lboro.ac.uk
- Kirillin, Georgiy – Institute of Freshwater Ecology and Inland Fisheries, Germany; E-mail: kirillin@igb-berlin.de
- Kuimova, Lyubov – Limnological Institute, Siberian Branch, Russ. Acad. Sci., Russia; E-mail: ppshest@lin.irk.ru
- Lepparanta, Matti – Division of Geophysics, University of Helsinki, Finland; E-mail: Matti.Lepparanta@phnet.fi
- Little, John – Department of Civil and Environmental Engineering, Virginia Tech, Blacksburg, USA; E-mail: jcl@vt.edu
- Maher, Osama Ali – Department of Water Resources Engineering, Lund University, Sweden; E-mail: Osama.Maher@tvrl.lth.se
- Mironov, Dmitrii – German Weather Service (DWD), Germany; E-mail: Dmitrii.Mironov@dwd.de
- Petrov, Michail – Northern Water Problems Institute, Karelian Scientific Centre, Russ. Acad. Sci., Russia; E-mail: petrov@nwpi.karelia.ru
- Podsetchin, Viktor – Pirkanmaa Regional Environment Centre, Tampere, Finland; E-mail: Victor.Podsetchine@ymparisto.fi
- Rukhovets, Leonid – St. Petersburg Institute of Economics and Mathematics, Russ. Acad. Sci., Russia; E-mail: leor@emi.spb.su
- Ryanzhin, Sergei – Institute of Limnology, Russ. Acad. Sci., St. Petersburg, Russia; E-mail: ryanzhin@peterlink.ru
- Schmid, Martin – Applied Aquatic Ecology, Swiss Federal Institute of Environmental Science and Technology (EAWAG), Switzerland; E-mail: Martin.Schmid@eawag.ch

Terzhevik, Arkady – Northern Water Problems Institute, Karelian Scientific Centre, Russ. Acad. Sci., Russia; E-mail: ark@nwpi.krc.karelia.ru

Tsvetova, Elena – Institute of Computational Mathematics and Mathematical Geophysics, Siberian Branch, Russ. Acad. Sci., Russia; E-mail: tsvet@OMMFAO.sscs.ru

Wüest, Alfred – Applied Aquatic Ecology, Federal Institute for Environmental Science and Technology (EAWAG), Switzerland; E-mail: wuest@eawag.ch

Zdorovenov, Roman – Northern Water Problems Institute, Karelian Scientific Centre, Russ. Acad. Sci., Russia; E-mail: romga@nwpi.karelia.ru

Zdorovenova, Galina – Northern Water Problems Institute, Karelian Scientific Centre, Russ. Acad. Sci., Russia; E-mail: romga@nwpi.karelia.ru

Zyryanov, Valery – Institute of Water Problems, Russ. Acad. Sci., Russia; E-mail: zyryanov@aqua.laser.ru

Kochkov, Nikolai - Institute of Limnology, Russ. Acad. Sci., St. Petersburg, Russia; E-mail: ryanzhin@peterlink.ru

Neelov, Ivan - Nansen International Environmental and Remote Sensing Centre, St. Petersburg, Russia; E-mail: neelov@aari.nw.ru

Physical Processes in Natural Waters
7th Workshop, 2-5 July, 2003, Petrozavodsk, Russia

Work Program

Wednesday, 2 July

9-40 – 10-00

Registration of participants, etc.

10-00 – 10-15:

Nikolai Filatov, Welcome words, etc.

Physical processes in great lakes (chair: Johny Wüest)

10-15 – 10-45:

Erich Bäuerle, Indirect forcing of topographic waves in large stratified lakes

10-45 – 11-15:

Nikolai Granin, R. Yu. Gnatovsky, A.A. Zhdanov, M.N. Granin and V.V. Blinov,
Temperature as indicator of the methane escape from the bottom sediments

11-15 - 11-45:

Coffee break

11-45 – 12-15:

Lyubov Kuimova and Pavel Sherstyankin, On Types of Thermal Convection in Lake
Baikal During Last Five Million Years

12-15 – 12-45

Pavel Sherstyankin, Lyubov Kuimova and V.G. Ivanov, About the Potential Temperature
and Adiabatic Parameter (the ratio C_p/C_v) of Deep Fresh Waters in Lake Baikal.

12-45 – 14-15:

Lunch

Physical processes in great lakes (chair: Erich Bäuerle)

14-15 – 14-45:

John Little and Alfred Wüest, Meromixis: The Effect Of Wind, River Inflow, And Primary
Productivity

14-45 – 15-15:

Martin Schmid, Andre Masson, Michael Schurter, Alfred Wüest, Yury Parfenov and
Nikolai Granin, The contribution of near-inertial waves to stratified turbulence and
diapycnal mixing in Lake Baikal

15-15 – 15-30:

Coffee break

15-30 – 16-00:

Martin Schmid, Andreas Lorke, Christian Dinkel, and Alfred Wüest, Observation of
double diffusive convection in Lake Nyos, Cameroon

16-00 – 16-30:

Michail Naumenko, Sergei Karetnikov and Vadim Guzivaty, 3-D thermal structure of
Lake Ladoga: a new approach and results

16-30 – 17-00:

Sergei Ryzanjin, Peter Chu, Lev Karlin and Nikolai Kochkov, Developing LANGMUIR-
1 and LANGMUIR-2 – the databases for a study of Langmuir circulation

17-00 – 17-30:

Sergei Ryzanin and Peter Chu, Selected statistics calculated for streak spacing of Langmuir circulation measured in natural waters

19-00 –

Ice-breaking party on the coast of Lake Onega

Thursday, 3 July

Physical processes in ice-covered lakes (chair: Lars Bengtsson)

9-30 – 10-00:

Matti Lepparanta, The Seasonal Cycle of the Ice Cover in Lake Paajarvi, Southern Finland

10-00 – 10-30:

Michail Petrov, Arkady Terzhevik, Roman Zdrovennov and Galina Zdrovennova, Motions in ice-covered lakes

10-30 – 11-00:

Michail Petrov, Arkady Terzhevik, Roman Zdrovennov and Galina Zdrovennova, Thermal structure of shallow lakes in early winter

11-00 – 11-15:

Coffee break

Physical processes in ice-covered lakes (chair: Matti Lepparanta)

11-15 – 11-45:

Sergei Golosov, Ilya Zverev, and Arkady Terzhevik, Modelling thermal structure and heat interaction between water column and bottom sediments in ice-covered lakes

11-45 – 12-15:

Osama Ali Maher, Dissolved oxygen content and distribution in a shallow ice covered lake

12-15 – 12-45:

Lars Bengtsson, Water quality problems in urban lakes and ponds in winter and during snowmelt

12-45 – 14-15

Lunch

14-15 – 15-15:

Alfred Wüest, Andreas Lorke and Michael Schurter, The effect of the bottom boundary on diapycnal mixing (plenary talk)

Physical processes in shallow lakes (chair: Viktor Podsechin)

15-15 – 15-45:

Bertram Boehrer and Stephanie Kastner, Measuring water storage with high resolution pressure sensors in a small lake

15-45 – 16-15

Dmitrii Mironov, Sergei Golosov and Ilya Zverev, On the Self-Similarity of the Temperature Profile in Lake Bottom Sediments

16-15 – 16-30

Coffee break

Coastal zones of tidal seas (chairs: Valery Bondur / Nikolai Filatov)

16-30 – 17-00

Valery Bondur and Nikolai Filatov, Study of physical processes in coastal zone for detecting anthropogenic impact by means of remote sensing

17-00 – 17-30

Valery Zyryanov, Differentiation of Suspended Bottom Deposits by Tidal Waves in Shallow Water

19-00:

Dinner

Friday, 4 July

Excursion to the Kizhi Archipelago

Saturday, 5 July

Modelling physical processes in lakes (chair: Dmitrii Mironov)

9-30 – 10-00:

Paul Holland, Anthony Kay and Vincenzo Botte, Numerical model of the thermal bar and its ecological consequences in a river-dominated lake

10-00 – 10-30:

Georgy Kirillin and Arkady Terzhevik, Radiative Damping Of Convection Near The Maximum Density Temperature: A Specific Mixing Regime In Ice-Covered Lakes

10-30 – 11-00:

Elena Tsvetova, Lake Baikal as Source and Receptor of Perturbations in the Region: Numerical Study

11-00 – 11-15:

Coffee break

11-15 – 11-45:

Elena Tsvetova and Erich Bäuerle, Response of a small stratified lake to a sudden midsummer change in weather conditions: 3-D simulation

Modelling physical processes in lakes (chair: Sergei Golosov)

11-45 – 12-45:

Dmitrii Mironov, Georgy Kirillin, Erdmann Heise, Sergei Golosov, Arkady Terzhevik and Ilya Zverev, Parameterization of lakes in numerical models for environmental applications (plenary talk)

12-45 – 13-00:

Coffee break

13-00 – 13-30

Georgy Kirillin, Modelling of the shallow lake response to climate variability

13-30-14-00

Viktor Podsetchin, A comparison of several turbulent closure schemes in 1-D lake models

14-00 – 14-30:

Leonid Rukhovets and Gennady Astrakhantsev, Modeling circulation and temperature regime of great stratified lakes

14-30-15-00:

Nikolai Filatov, Ivan Neelov, Dmitry Pozdnyakov and Andrei Filatov, Comprehensive investigations of hydrophysical processes in tidal and non-tidal estuaries of the Baltic and White Seas

15-00:

Nikolai Filatov, Farewell words to participants

Workshop Committee:

Adolf Stips
Alfred Wüest
Bertram Böhler
Erich Bäuerle
Lars Bengtsson
Madis-Jaak Lilover
Nikolai Filatov
Xavier Casamitjana

Local Organising Committee (NWPI)

Nikolai Filatov, Director
Nina Kiseleva, Deputy Director
Tatyana Regerand, Scientific Secretary
Arkady Terzhevik, Lab. Of Hydrophysics, Head

Technical Personnel

Roman Zdorovenov (room 511)

Table of Contents

Physical processes in great lakes

E. Bäuerle

Indirect forcing of topographic waves in large stratified lakes

N.G.Granin, R. Yu. Gnatovsky, A.A.Zhdanov, M.N.Granin, V.V.Blinov

Temperature as indicator of the methane escape from the bottom sediments

L.N. Kuimova and P.P. Sherstyankin

About Types of Thermal Convection in Lake Baikal During Last Five Million Years

P.P. Sherstyankin P.P., L.N. Kuimova and V.G. Ivanov

About the Potential Temperature and Adiabatic Parameter (the ratio C_p/C_v) of Deep Fresh Waters on Lake Baikal.

J.C. Little and A. Wuest

Meromixis: The Effect Of Wind, River Inflow, And Primary Productivity

M. Schmid, A. Masson, M. Schurter, A. Wuest, Yu. Parfenov and N. Granin,

The contribution of near-inertial waves to stratified turbulence and diapycnal mixing in Lake Baikal

M. Schmid and A. Wuest

Observation of double diffusive convection in Lake Nyos, Cameroon

M. Naumenko, S.Karetnikov and V.Guzivaty

3-D thermal structure of Lake Ladoga: a new approach and results

S. Ryzanzhin, P. Chu, L. Karlin and N. Kochkov

Developing LANGMUIR-1 and LANGMUIR-2 – the databases for a study of Langmuir circulation

S. Ryzanzhin and P. Chu

Selected statistics calculated for streak spacing of Langmuir circulation measured in natural waters

Alfred Wüest, Andreas Lorke and Michael Schurter

The effect of the bottom boundary on diapycnal mixing

Physical processes in ice-covered lakes

M. Lepparanta

The Seasonal Cycle of the Ice Cover in Lake Paajarvi, Southern Finland

M. Petrov, A. Terzhevik, R. Zdrovennov and G. Zdrovennova

Motions in ice-covered lakes

M. Petrov, A. Terzhevik, R. Zdrovennov and G. Zdrovennova

Thermal structure of shallow lakes in early winter

S. Golosov, I. Zverev, and A. Terzhevik

Modelling thermal structure and heat interaction between water column and bottom sediments in ice-covered lakes

Physical processes in shallow lakes

B. Boehrer and Stephanie Kastner

Measuring water storage with high resolution pressure sensors in a small lake

D. Mironov S. Golosov and I. Zverev

On the Self-Similarity of the Temperature Profile in Lake Bottom Sediments

Coastal zones of tidal seas

V. Bondur and N. Filatov

Study of physical processes in coastal zone for detecting anthropogenic impact by means of remote sensing

V. Zyryanov

Differentiation of Suspended Bottom Deposits by Tidal Waves in Shallow Water

Modelling physical processes in lakes

P. Holland, A. Kay and V. Botte

Numerical model of the thermal bar and its ecological consequences in a river-dominated lake

G. Kirillin and A. Terzhevik

Radiative Damping Of Convection Near The Maximum Density Temperature: A Specific Mixing Regime In Ice-Covered Lakes

E. Tsvetova

Hydrodynamics of Lake Baikal region: numerical study

E. Tsvetova and E. Bauerle

Response of a small stratified lake to a sudden midsummer change in weather conditions: 3-D simulation

D. Mironov, G. Kirillin, E. Heise, S. Golosov, A. Terzhevik and I. Zverev

Parameterization of lakes in numerical models for environmental applications

G. Kirillin

Modelling of the shallow lake response to climate variability

V. Podsetchin

A comparison of several turbulent closure schemes in 1-D lake models

L. Rukhovets and G. Astrakhantsev

Modeling circulation and temperature regime of great stratified lakes

N. Filatov, I. Neelov, D. Pozdnyakov and A. Filatov

Comprehensive investigations of hydrophysical processes in tidal and non-tidal estuaries of the Baltic and White Seas

Indirect forcing of topographic waves in large stratified lakes.

E. Bäuerle

Limnological Institute, Environmental Physics, University of Constance, Germany
(E-mail: erich.baeuerle@t-online.de)

Abstract

In large and/or weakly stratified lakes the oscillatory response to wind forcing at the water surface consists of subinertial and superinertial internal basin-wide oscillations which often are classified as Kelvin-type and Poincaré-type waves. Furthermore, it is known that a non-flat bottom in large rotating basins causes topographic Rossby waves which exclusively appear with frequencies smaller than the inertial. On the other hand, in many lakes during the stratified seasons due to extent and stratification the familiar "internal seiches" get eigenperiods larger than the local inertial period. In consequence, and analogous to the theory of topographic Rossby waves on stratified marine shelves, long internal Kelvin waves in stratified lakes undergo substantial modifications if the frequencies of internal gravitational modes and rotational modes overlap. By means of numerical calculations with a simple two-layer model in the frequency-domain it is shown that the low order horizontal modes of internal oscillations ("seiches") if subinertial in frequency may get coupled with local "periodic vortices". Calculations with a time-stepping two-layer model show how part of the initial basin-wide response to wind forcing is transferred to regions of the basin which favour the appearance of topographic waves. In accordance with the processes on stratified shelves the modes appear to be bottom-trapped. Observations from Lake Constance (Germany) confirm the theoretical findings.

Introduction

One of the most obvious features of a lake is the rich variety of bottom topography possessed by even the simplest lake basins. In this respect it may be surprising that so many theories of lake water motions, especially of periodic motions in stratified basins, ignore variations in depth by assuming flat bottom and vertical walls instead of sloping boundaries. The reason is simply that the interactions between stratified flows and topography are extremely complicated. We know from investigations on the stratified flow over the oceanic boundary, the shelf region, that even for a relatively smooth topography a variety of waves occurs, which in the presence of topographic disturbances are scattered, trapped or transmitted in highly complicated ways. We thus lack a kind of simple rule of thumb of the effects, which occur near and at the topographic disturbance. Rather the interaction problem appears intractable if considered in full extent.

The numerical models

The principle of coupling between internal gravitational oscillations (internal seiches) and rotational modes induced by topography can be worked out rather clearly by investigating the processes in a rectangular basin which is large enough that with realistic summerly stratification the internal seiche (at least the fundamental one) exhibits periods somewhat larger than the inertial period. The basin is kept predominantly flat-bottomed such that the sub-inertial motions, aside from the topographical disturbances, may be of internal Kelvin wave-like form. Above flat bottom and at some distance from the topographic disturbance the vertical distribution of the variables (internal pressure and horizontal velocity, respectively) follows the vertical eigenfunctions of the Sturm-Liouville problem. In the case of a two-layer model, the transports in the layers are (nearly) compensating.

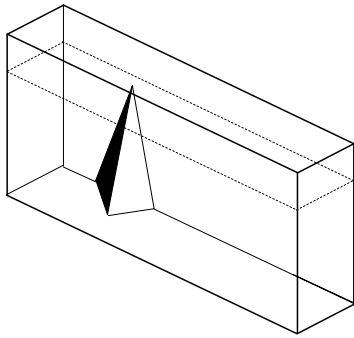


Fig.1: Sketch of the triangular hump disturbing the flat bottom.

The “lake” of the present investigation is given by a 5 x 1 rectangular basin (60 km x 12 km) which aside from the topographic disturbance is 100 m deep. Stratification is approximated by two layers of slightly different densities ($\rho_2 > \rho_1$, $\Delta\rho/\rho_2 = O(10^{-3})$). The upper layer depth is 10 m throughout the calculations. The internal Rossby radius (the phase velocity divided by the inertial frequency) is in the order of 2 – 6 km. The flat bottom is disturbed locally by a triangular hump which is leaning against the vertical boundary sloping linearly from the mid of the basin towards the shoreline (see Fig.1).

The model is run in two different ways: (i) in the frequency mode where the eigenfrequencies of the system are sought, and (ii) in the time-stepping mode with some idealized wind-forcing.

The eigenfrequencies

The eigenfrequencies of the two-layered basin in dependence of the stratification are shown in Fig.2. We distinguish two different classes of dispersion curves, which exhibit the strange behaviour of “kissing”: the strongly increasing curves and the nearly constant ones when approaching one another do not intersect themselves but seem to be repelled.

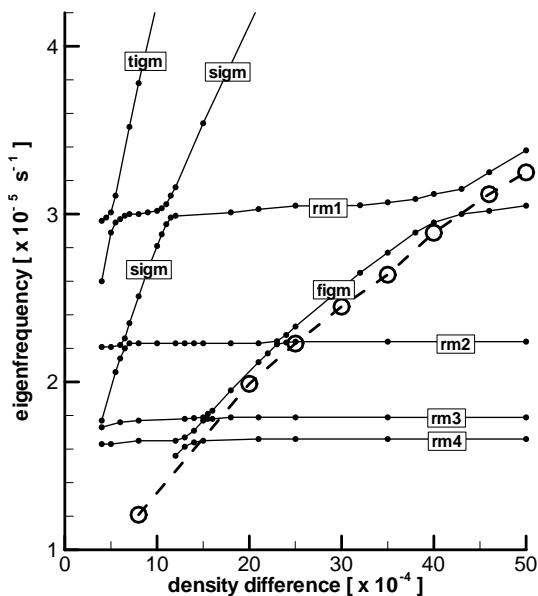


Fig.2: Dependence of the eigenfrequencies of a 5x1 rectangular basin on the density difference between upper and lower layer of a two-layered model (rmi (i=1-4) stands for rotational modes; figm, sigm, and tigm stands for first, second, and third internal gravitational mode, respectively). The dashed line refers to results of the time-stepping model.

Far from the “kissing” regions, the structures of the modes with nearly no dependence on stratification resemble those of pure rotational modes as they occur without stratification, whereas

the structure of the modes with strongly increasing eigenfrequencies resemble those of pure internal gravitational modes. In the “kissing” regions the modes get coupled and the structures are determined by both gravitational and rotational effects (no superposition!).

Indirect forcing

The structures of pure rotational modes which are trapped on topographical features as small as the triangular hump are much too small to be excited directly by any realistic wind. Basin-wide internal seiches driven by the wind, on the other hand, are known to be most familiar in stratified lakes. The question arises, how the coupled modes look like if large-scale wind is forcing the water surface.

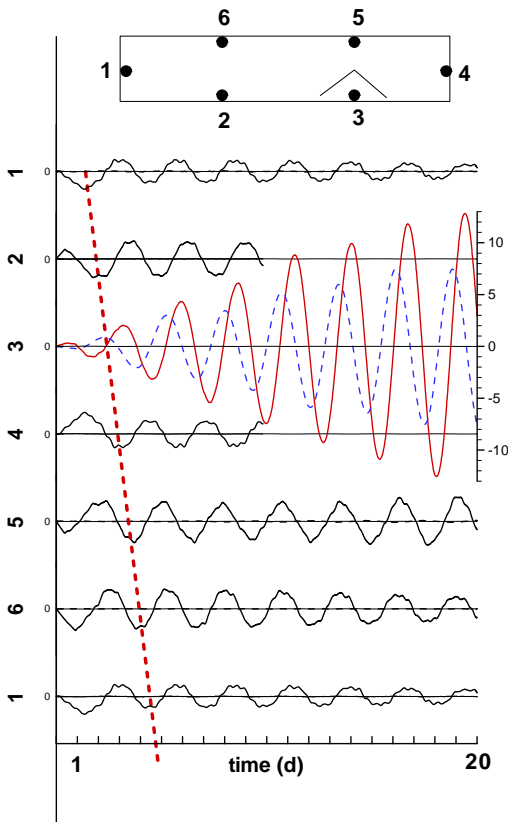


Fig.3: The alongshore and offshore components of the transports in the lower layer of the two-layer model ($\varepsilon = 35 \times 10^{-4}$; $h_{2min} = 10$ m) at the positions indicated in the inset. The alongshore component is taken positive in direction of the cyclonically propagating internal Kelvin wave. The phase propagation ($c_i=0.56$ m s $^{-1}$) is indicated by the dashed line.

The time series of the transports in the lower layer of the two-layer model (Fig.3) show the response of the basin on a 2 days wind forcing in longitudinal direction.

Obviously, the dominating process is the fundamental internal oscillation with a period which differs only slightly from the value of a flat-bottomed 5 x 1 basin with the same stratification. Two effects of the topographic disturbance (the hump) should be emphasized: (i) the current field of the Kelvin wave-like internal oscillation with an amphidromic point in the basins center is altered substantially in the immediate vicinity of the hump and (ii) the internal oscillation exhibits a significant “damping” although the calculations of the numerical model are done neither with bottom friction nor interfacial friction.

Whereas at the near-shore positions far away from the hump (P1, P2, P4, P6) the currents are purely shore-parallel, at position P3 (directly on the crest of the hump) the situation is totally different: the component normal to the shore leads the shore-parallel component by 90° indicating an anti-cyclonically rotating current. The linearly increasing amplitude is typical of resonant forcing of a linear system and is in total contrast to the slightly decreasing amplitudes at the other positions away from the hump.

Another way to present the current field is given by means of hodographs which are formed by the tips of the current vectors at certain instants. In Fig.4 we present 3 examples from the hump region. At position P(121,06) which is situated on the flat-bottomed base of the hump the time series of the components of the horizontal transports (uppermost row of the second column of Fig.4) reveal that the shore-parallel component leads the shore-normal component by 90°

indicating a cyclonically rotating current vector. Admittedly, the hodograph of the whole episode (third column) not really clarifies the facts. That is more likely done by the hodograph of the time segment with the length of one period. The second row of Fig.4 with time series from a position on the slope of the hump shows that the components are out of phase. Consequently, the hodograph (nearly) degenerates to a straight line. Most illuminating is the hodograph from the crest of the hump which reveals both the anti-cyclonic rotation and the increase of the transport.

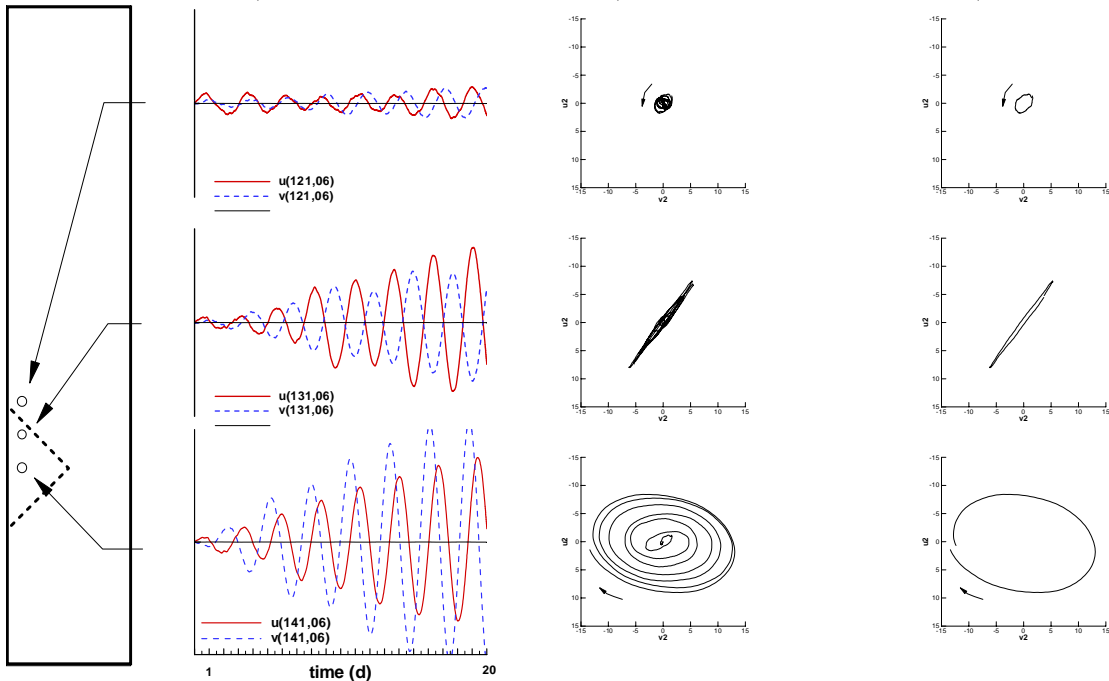


Fig.4: The response of a two-layered 5x1 rectangular basin on a 2 day wind in longitudinal direction. Time series of the alongshore and cross-shore components of the transport in the lower layer and hodographs at the points which are marked by the arrows. The baseline of the hump is indicated by dashed lines. The hodographs on the right side of the figure are drawn for one period of the lowest mode. Notice that the wind lasted only at the first 10 % of the interval.

Results from Lake Constance

The principles outlined above with respect to a 5x1 rectangular basin with an isolated disturbance of the bottom topography were transferred to stratified Upper Lake Constance. Special interest was given to an underwater sill near the Island of Mainau where records of temperature and current constantly differ in many respects from what is expected with regard to the familiar signal of the fundamental internal oscillation of the lake's basin. It will be shown at the workshop that the observations from Lake Constance are consistent with the theory outlined above. Conclusions with respect to other parts of the lake are made and consequences concerning other lakes will be discussed.

Temperature as indicator of the methane escape from the bottom sediments

N.G.Granin, R. Yu. Gnatovsky, A.A.Zhdanov, M.N.Granin, V.V.Blinov
Limnological Institute SB RAS, , Irkutsk, Russia; E-mail: nick@lin.irk.ru

and

J. Klerkx
IBES, Belgium

An application of a high-precision instrument CTD-probe (SBE-25) allowed us to obtain a high quality data on the peculiarities of the patterns of vertical temperature distribution in deep waters of Lake Baikal. Long-term observations of the vertical temperature profiles show that rather thick deep-water mixed layer (DML) intermittently appears in the northern part of Southern Lake Baikal (Fig.1). It is characterized by the temperature increase with depth. The temperature gradient is close or equal to the adiabatic one thus testifying for complete water mixing within this layer; therefore we consider this layer is the adiabatic. In the Pacific, the adiabatic layer was found in the deep-water zone of the ocean (Millard et al., 1990).

In Baikal, the mechanism of mixing processes within the adiabatic layer was not evident. Based on 1995-1996 data, which showed DML existence in the near-bottom zone of 1150 to 1400 m, we supposed that mixing process could be a result of the shear instability of the near bottom currents. However, during 1997-2003, DML was observed within the intermediate zone of 900 to 1100 m (Fig. 1). In such a case, mixing cannot be a result of the shear instability since the bottom area at these depths (727 km²) is considerably less compared to that at 1200 m water depth (2767 km²).

Discovery of mud volcanoes in Southern Lake Baikal (De Batist et al., 2002) put a new light on this problem. The formation of mud volcanoes is caused by the methane escapes from the uppermost sediments. We suggest that the mechanism of DML formation could be related to convection due to the methane flux from the bottom sediments. As a matter of fact, both the methane dissolution and temperature increase result in decrease of the water density. Thus, when a rather high volume of the methane is escaping from the lake floor, a stability of the stratification may be disturbed thus leading to convection.

An appearance and existence of the adiabatic layer is not possible without generation of convection, which prevents decrease of the layer's thickness due to the vertical turbulent diffusion. When there are no mechanisms supporting convection within the layer, decreasing of the thickness of the mixed layer is described by the following equation (Gloor et al., 2000)

$$\frac{dh_{mix}}{dt} = -\frac{k_z}{h_{mix}}; \rightarrow h_{mix} = \sqrt{h_{mix0}^2 - 2k_z t},$$

where h_{mix} – the thickness of the mixed layer; k_z – the coefficient of vertical turbulent exchange. Based on the measurements of temperature microstructure and the currents velocity within the near-bottom layer, the coefficients of vertical turbulent exchange was determined for Southern Lake Baikal (Wuest et al., 2000). We used these coefficients as well as our data on the thickness of the mixed layer to calculate the lifetime of the layer, when there is no convection supporting the layer's existence.

The calculated lifetime of the near-bottom mixed layer observed during 1995 – 1996 (Fig. 1) was about 120 days. The intermediate layer observed since 1997 until 2000 (Fig. 1) had the lifetime 80 days. In both cases the real time of the adiabatic layer existence essentially exceeded that calculated from the equation. This means that there should be some mechanisms that support mixing within the layer.

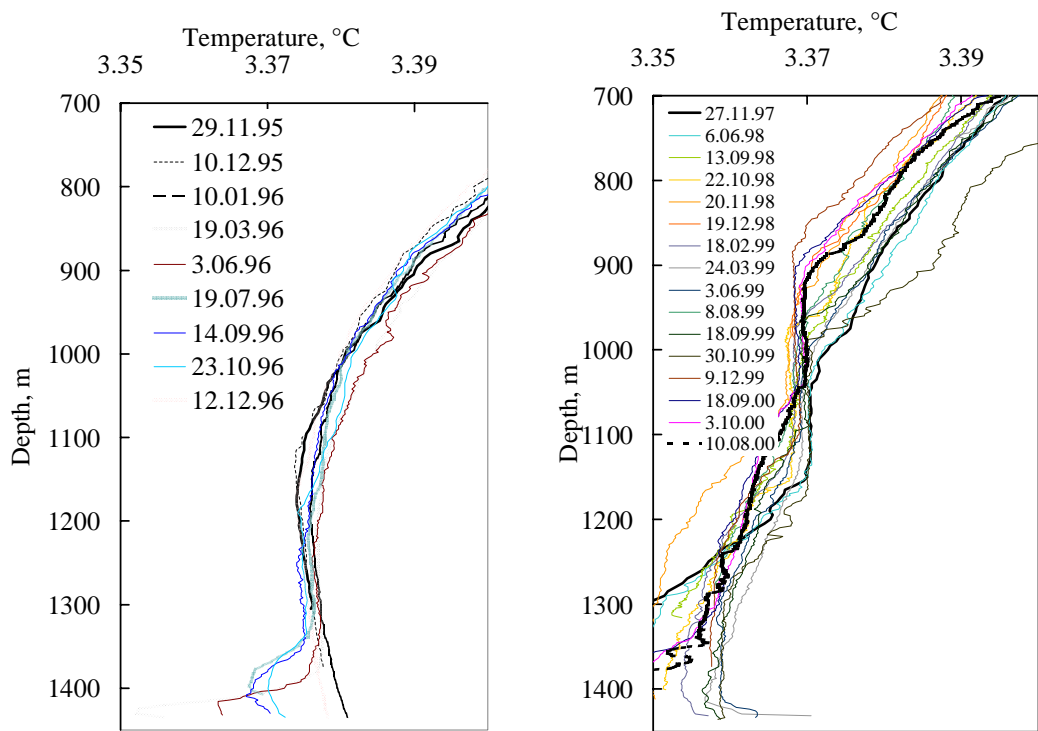


Fig. 1. Patterns of the vertical temperature distribution in the northern part of Southern Baikal. Center of the section cape Kadil'ny- the Mishikha River, 1995-1996 and 1997-2000.

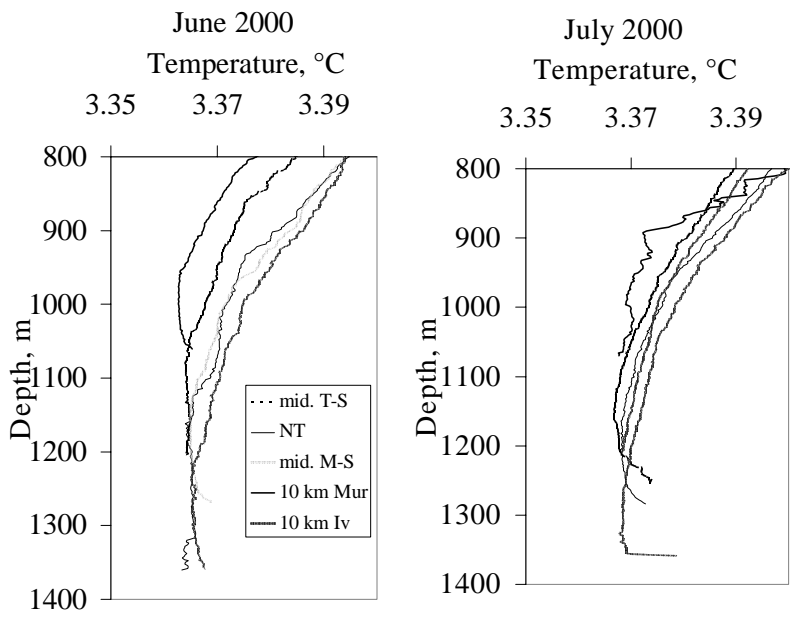


Fig. 2. Patterns of the vertical temperature distribution in the western part of Southern Baikal (June and July, 2000).

Our data show that the adiabatic layer constantly exists in the northern part of Southern Lake Baikal (Fig. 1). In addition, some of the data testify to episodic appearance of the adiabatic layer within the near-bottom zone in the western part of Southern Lake Baikal. For example, such layer was observed in June 2000 and we calculated its lifetime to be 20 - 40 days. Actually, in July 2000, the layer was not observed already (Fig. 2). Other words, the real time of the mixed layer's existence agrees with the theoretically estimated lifetime. We suggest that the layer appearance could be related to the gas escape initiated by the earthquake that has happened in early June 2000.

The temperature data obtained at some sites in Southern Lake Baikal reflect an existence of the gas hydrates within the uppermost sediments (Fig. 3). There is substantial difference ($>0.01^{\circ}\text{C}$) between the temperature profiles recorded during sink and rise of the instrument. It might be if the sediment material containing the gas hydrates has entered inside the enclosure of temperature sensor.

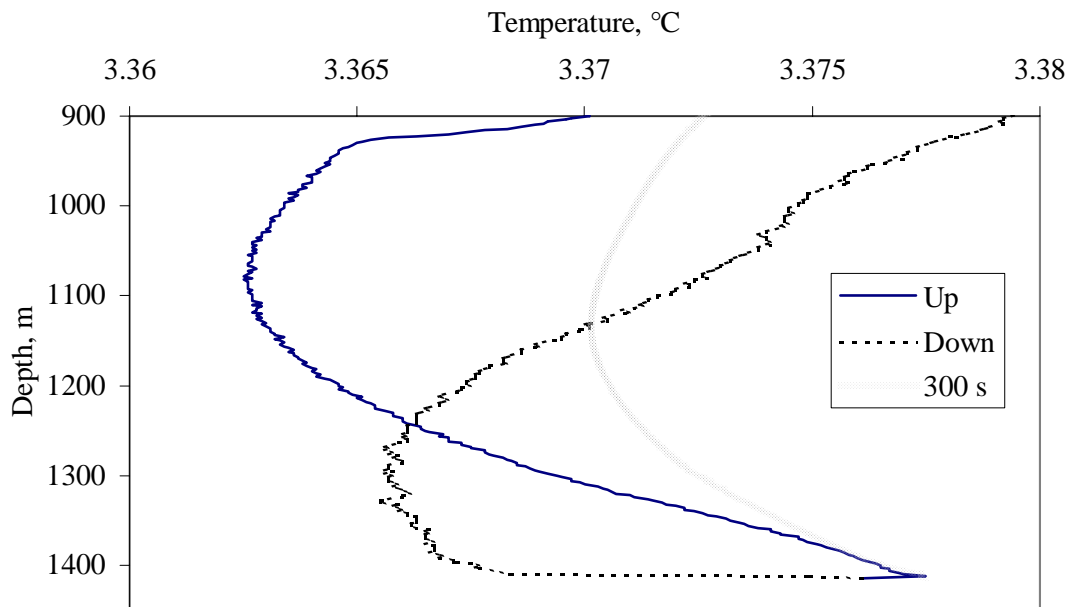


Fig. 3. Temperature of the sensor during sink (Down) and rise (Up) of CTD probe, vent structure “Novyi”. Temperature is calculated for the response time 300 s.

Assuming that there was the same water temperature during rise and sink of the instrument, computations have been made for the different response times of the sensor. Results of computations show that the temperature fluctuations cannot be explained only by the changes of the sensor's response time (Fig. 3). It follows from the similarity between the calculated temperature profile and the profile of the sensor's temperature at the initial part of rise (from 1410 to 1350 m water depths) that the response time of the sensor with enclosure filled with the sediment is close to 300 sec. During further rise of the sensor, the profile of measured temperature is different from that of the calculated temperature. Any changes in the response time of the instrument cannot explain the temperature minimum recorded at 1100 m depth. Such low temperature at this horizon was not observed during sink of the instrument. Temperature decrease of the sensor may be due to the phase transition of the gas hydrates thrilled with the sediment material that has entered inside the enclosure of temperature sensor. This may serve as an

additional confirmation of the gas hydrates existence within the uppermost sediments in the region of vent structure “Novyi”. Similar data were obtained at some other sites in Southern Lake Baikal.

We attempt to explain possible reasons responsible for the specific pattern of vertical temperature distribution within the near-bottom zone at the region, where the vent structures have been found. Due to gas escapes from the bottom sediments the following temperature changes might take place:

- a) increase and decrease of the water temperature due to the phase transition of gas hydrates;
- b) decrease of the temperature gradient and change of its sign because of convective mixing, which is provided by ascending flux of bubbles and diminution of water density due to the methane dissolution.

When the methane bubbles are escaping from the pelagic bottom sediments (at the water depths > 400 m), the crystals of gas hydrates may be formed at the gas-water boundary, because TP conditions necessary for the gas hydrates existence are accomplished. In this case the water temperature in the near-bottom zone may increase. The nascent gas hydrates are unstable within the water media and their further destruction is accompanied by cooling of the environment. Decrease of the temperature may be also caused by destruction of the crystals of gas hydrates floating from the bottom.

Gas escapes contribute to the vertical water mixing within the near-bottom layer changing this way the temperature stratification. The water temperature is a sensitive indicator of the manifestation of gas hydrates and gas escapes within the deep layers of the water column. Temperature measurements may be used during preliminary studies, which aim to discovery the regions forward-looking for the gas hydrates occurrence. At systematic observations, data on the spatial-temporal structure of the deep homogeneous water layer may be used for evaluation of the methane flux from the pelagic bottom sediments.

In the region characterized by existence of the vent structures, whose formation is caused by the methane escapes from the uppermost sediments, hydrophysical studies allow obtaining the specific data. The latter indicate both the specific pattern of the vertical temperature distribution within the near-bottom zone and a difference between the temperatures of the sensor measured during rise and sink of the instrument. The phase transitions during formation and decomposition of the gas hydrates may serve as a reason for increase and decrease of the water temperature.

This work was supported by the Royal Society of UK, INTAS grant N 01-2309 and RFBR grant N 03-05-65255.

References

- Millard RC, Owens WB, Fofonoff NP (1990) On the calculation of the Brunt-Vaisala frequency. *Deep-Sea Research* 37: 167-181
- De Batist M, Klerkx J, Van Rensbergen et al. (2002) Active hydrate destabilization in Lake Baikal, Siberia. *Terra Nova* 14: 436-442
- Gloor M, Wuest A, Imboden DM (2000) Dynamics of mixed bottom boundary layers and its implications for diapycnal transport in a stratified, natural waters. *J. Geophysical Research* 105: 8629-8646
- Wuest A, Granin N, Kocsis O, Ravens TM, Schurter M, Sturm M. (2000) Deep water renewal in Lake Baikal – Matching turbulent kinetic energy and internal cycling. *Terra Nostra* 9: 60-74

On Types of Thermal Convection in Lake Baikal During Last Five Million Years

Kuimova L.N., Sherstyankin P.P.

Limnological Institute, Siberian Branch, Russ. Acad. Sci., Irkutsk, 664033, Russia; E-mail: ppsherst@lin.irk.ru

For the last five million years, the history of Lake Baikal has been rich of active geological, climatic, hydrophysical and biological events. A subtropical climate, which was characterized for ten million years by high average annual air temperature T_{air} on the level of 20°C and then approximately 15°C, was replaced by a moderate climate with the periods of great glaciations until it gained the features of a modern climate (Vorobjeva et al., 1995; Yasamanov, 1985; Kuzmin, Grachev, Williams et al., 1997). Let us consider all these three types of thermal convections using real analogs and analyzing recent materials.

Subtropical climate before and during systematic lowering of air temperature T_{air} . In the beginning let us imagine what could happen to Lake Baikal if the climate were tropical or close to it as T_{air} was about 20°C before the origin of Lake Baikal and the period studied. Lake Tanganyika is an analogue of such example. The average annual temperature is about 26°C with almost complete absence of seasonal (annual) run. The pycnocline (thermocline) in this lake is located at depths of 100-150 m; below there is a hydrogen sulphide zone. It exists because of the absence of vertical mixing in deep layers. Vertical mixing in the upper layers (higher than pycnocline), which provides proper distribution and mixing of oxygen necessary for biota, is caused by daily convection and slight cooling of water at the expense of seasonal winds and trade wind. Convection at the expense of this cooling reaches 400 m. However, the hydrogen sulphide zone only slightly decreases and does not disappear completely (Edmond, Stallard, Craig et al., 1993).

Due to some reasons, there were no such phenomena in Lake Baikal during subtropical climate: firstly, in the annual (seasonal) run there was a period of air temperature decrease (accordingly, that of surface waters) at the expense of minimal annual input of solar radiation (for the water of absorbed radiation) in the period of winter solstice; secondly, due to considerable daily cooling (convection) in comparison with Lake Tanganyika. Systematic decrease of average annual temperature of air, surface and deep waters caused the intensification of convection.

Approximate annual run of T_{air} , T_{sw} and T_{dw} is shown in Fig. 1a. The main peculiarity of temperature regimes and hydrophysical processes was the fact that the temperature of air and water was not lower than 10°C.

The difference in temperatures of surface and deep waters decreased and in dynamically active regions (convergent zones of fronts) it dropped to zero (incomplete analog – modern autumn homothermy in Lake Baikal and complete analog – MEDOC (1970) convection in the Mediterranean Sea). The pycnocline of temperature and density deepened considerably or disappeared completely. In vertical mixing of waters, the main dominant role belonged to water temperature and there was observed a T-type mixing (Sherstyankin, Kuimova, Shimaraev, 1995).

Transitional period lasted for a short time (~2.6-2.4 mln. years ago) in the Middle Upper Pliocene during the replacement of paleomagnetic epochs: Gauss replaced the epoch of Matuyama. For about 200 thousand years (Vorobjeva et al., 1995) T_{air} had been changing from 9-10°C to -4÷-10°C. The air temperature decrease was accompanied by astronomic (orbital effects, increase of planetary albedo and others) and planetary events (long storms and dust storms, changes in the systems of currents in the World Ocean, changes of types of circulations, etc.), and by the activity of geological processes (mountain formation, increase of depths up to 1 km and deeper, earthquakes, etc.).

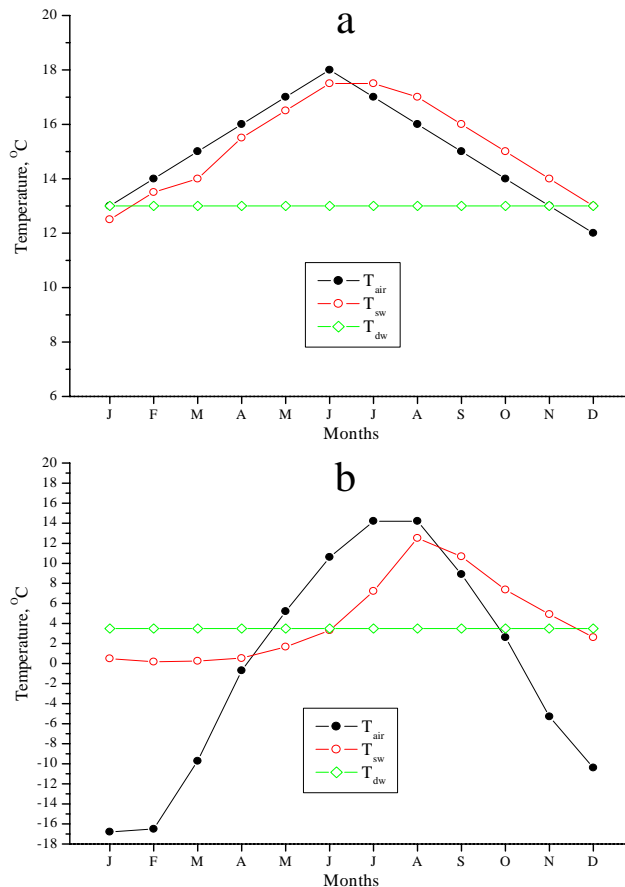


Fig. 1. Annual run of average annual air temperatures T_{air} , temperatures of surface water layers T_{sw} and deep waters T_{dw} (depth of about 500m): for subtropical climate (according to the data of Vorobjova et al., 1995), $T_{air} \sim 15^\circ\text{C}$; b. for moderate modern climate $T_{air} \sim 0^\circ\text{C}$ for Southern Baikal (Kuimova, Sherstyankin, 1998), T_{sw} - according to Verbolov's data, 1965, T_{dw} for depth of about 500 m.

A severe impact was brought to biota, especially to its warm-loving species (rhinoceros, warm-loving vegetation, and other organisms could not survive; see exhibits of Baikal Museum). During drastic decrease of T_{air} in the polar region of the World Ocean and in Lake Baikal intensive convections of MEDOC type were developed, which caused rapid cooling of deep waters. T_{air} reached 0°C , however, this temperature completely differed from modern one as in the seasonal run there had not been regular negative temperatures yet. The temperatures of surface waters began to reach 4°C and lower values, there appeared the first ice phenomena, and thin ice cover was destroyed quickly.

Establishment of moderate climate (2.4 mln. years ago – till present time) happened very fast in the geological scale of time. Lake Baikal began to gain recent features (Logachev et al., 1996; Mats, 1995; Popova et al., 1989), see Fig.2. A paleoclimate of the Baikal Region beginning from the Pliocene (5 mln. years ago, GEOL. TIME TABLE, 1994) is clearly distinguished in paleo-soils (Vorobjova et al., 1995). Based on the characteristics of changes of paleoclimates of the Baikal Region in Late Cenozoic (Vorobjova et al., 1995), it should be noted that the first stable transition of T_{air} to negative values, which could be connected to the appearance of ice phenomena in Lake Baikal, occurred in the Upper Pliocene about 2.4 mln. years ago. However, according to Vorobjova et al. (1995), the most vivid cooling when ice phenomena appeared in Lake Baikal, took place in the Upper Eopleistocene about 0.9 mln. years ago. At the same time the constant ice cover in the Arctic appeared (Khusid et al., 1993). As for the later period (Late

Pleistocene), which differed in lower temperatures of air, the ice regime of the lake was characterized by annual long periods without ice (Shimaraev et al., 1995). A more severe cooling than nowadays was observed. However, the ice cover broke in summer every year. The period of open water could be shortened up to 3-2 months, and in the coldest years the ice cover could break into ice fields and the ice of porridge-like state in Northern Baikal where the average temperature of air was 4°C lower than that in Southern Baikal. However, the break-up of ice always happened and annually there was a period of open water every year (Kuimova and Sherstyankin, 1998).

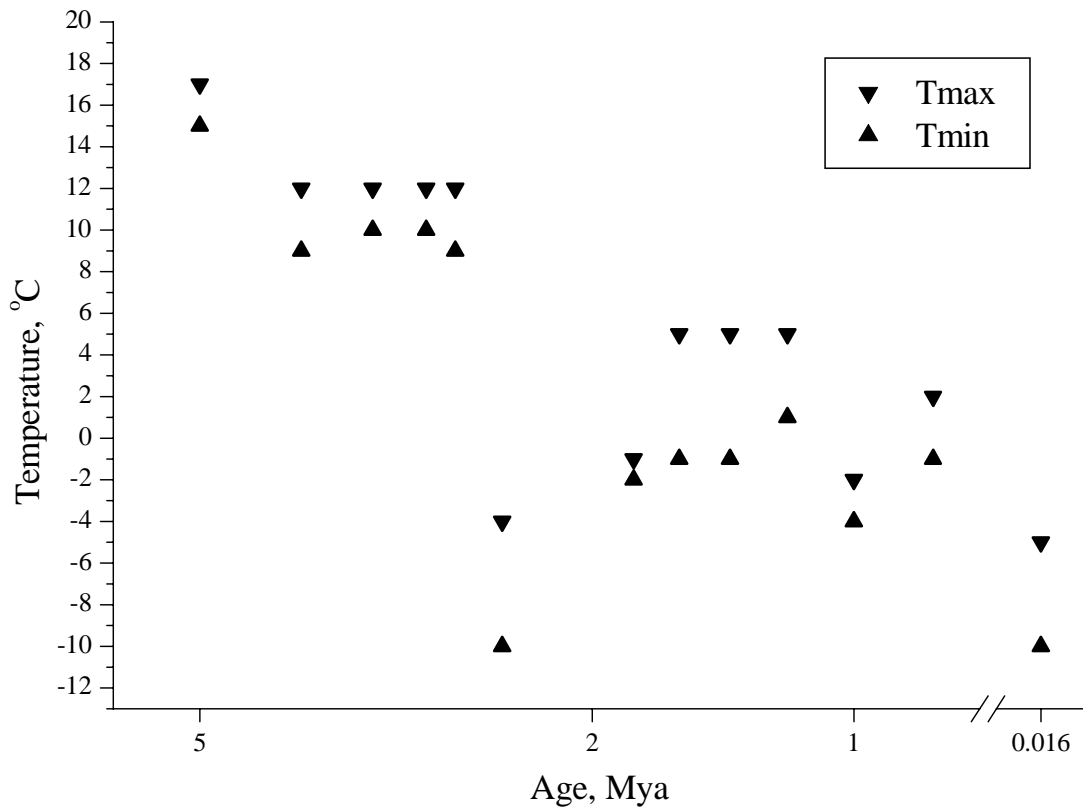


Fig.2. Average annual air temperatures T_{air} of the Baikal Region for the last five million years according to the data of Vorobjova et al., 1995.

The negative temperature stratification is such a strong retardation for freezing of a water column that Lake Vostok in the Antarctic, which appeared to be in the ice captivity, could not have frozen so far (Zotikov and Duxbury, 2000). The ice cover on Lake Baikal has never existed for the whole year.

Conclusions

Main peculiarities of cooling of water in Lake Baikal can be distinguished at transition from a subtropical climate with positive average annual air temperature to a moderate climate with negative T_{air} with a simultaneous increase of depth. Intensity of cooling gradually exceeded intensity of warming. Cooling of deep waters was of seasonal character and occurred only during the cold period of a year. Analogs of cooling processes are: a) Mediterranean convection with T_w significantly exceeding the temperature of maximal density T_{md} , b) autumn homothermy in Lake

Baikal. Due to gradual cooling of climate, Lake Baikal turns from a warm monomictic reservoir to the reservoir of a dimictic type, which is characterized by the development of convection twice a year – in spring and autumn.

Acknowledgements

This work was supported by the Russian Foundation of Basic Research, grant No.01-05-65097.

References

- Vorobjoeva G.A., Mats V.D., Shimaraeva M.K., 1995. Paleoklimaty pozdnego kainozoya Baikalskogo regiona [Late-Cenozoic paleoclimates in the Baikal region]. *Geologiya and Geofizika*, 36 (8): 82-96 (In Russian).
- Yasamanov N.A., 1985. *Drevnie klimaty Zemli* [Ancient climates of the Earth]. Leningrad, Gidrometeoizdat, 295 pp. (In Russian).
- Kuzmin M.I., Grachev M.A., Williams et al., 1997. Nepreryvnaya letopis paleoklimatov poslednikh 4,5 millionov let iz ozera Baikal [The continuous annals of paleoclimates for the last 4,5 million years from Lake Baikal] (first information). *Geology and geophysics*, 38 (5): 1021-1023. (In Russian).
- MEDOC GROUP, 1969. 1970. Observation of Formation of Deep Water in the Mediterranean Sea. *Nature*, 227: 1037-1040.
- Edmond J.M., R.F.Stallard, H. Craig, V.Graig., R.F.Weiss, G.W.Coulter, 1993. Nutrient chemistry of the water column of Lake Tanganyika. *Limnol. Oceanogr.*, 38(4): 725-738.
- Sherstyankin P.P., Kuimova L.N., Shimaraev M.N. 1995. On Paleothermohaline Regime of Lake Baikal. The Second Vereshchagin Baikal Conference, October 5-10, 1995. Abstracts. Irkutsk, p.231.
- Kuimova L.N., Sherstyankin P.P., 1998. Climate change and extreme hydrological events on Lake Baikal during the last 250,000 years. *In The Second International Conference on Climate and Water*. Espoo, Finland, 17-20 August 1998, 3: 1197-1204.
- Verbolov V.I., 1964. Temperaturnyi rezhim zal. Listvenichnogo na Baikale [The Temperature Regime of Bay Listvenichnyi on Lake Baikal]. *In Elements of a hydrometeorological Regime of Lake Baikal*. Moskva – Leningrad, “Nauka”: 38-51. (In Russian).
- Logachev N.A., Rasskazov S.V., Ivanov A.V., Levi K.G., Bukharov A.A.,Kashik S.A., Sherman S.I., 1996. Kainozoiskii riftogenez v kontinentalnoi litosfere [Cenozoic rift genesis in continental litosphere]. *In Litosfera tsentralnoi Asii*: 57-80. (In Russian).
- Mats V.D., 1995. Development of the Baikal depression: chronology of the transformation of zoogeographic barriers. The Second Vereshchagin Baikal Conference, October 5-10, 1995. Abstracts. Irkutsk, p.131.
- Popova S.M., Mats V.D., Chernyaeva G.P. et al., 1989. *Paleolimnologicheskie rekonstruktsii (Baikalskaya riftovaya zona)*. [Paleolimnological reconstructions (In the Baikal rift zone)]. Novosibirsk, “Nauka”, 112 pp. (In Russian).
- Khusid T.A., Belyaeva V.N., Burmistrova I.I., 1993. K istorii glubokovodnogo Arkticheskogo Basseina [On the History of Deep Arctic Ocean]. *Oceanologiya*, 33 (6): 930-934. (In Russian).
- Shimaraev M.N., Granin N.G., Kuimova L.N., 1995. Opyt rekonstruktsii gidrofizicheskikh uslovii v Baikale v pozdnem pleistotsene i golotsene [Experience of reconstruction of hydrophysical conditions in Baikal in Late Pleistocene and Holocene]. *Geologiya and Geofizika*, 36 (8): 97-102. (In Russian).
- Zotikov I.A., Duxbury N.S., 2000. O genezise ozera Vostok (Antarktika) [On Genesis of Vostok Lake (Antarctica)]. *Doklady Akademii Nauk*, 374 (6): 824-626. (In Russian).

On Potential Temperature and Adiabatic Parameter (ratio C_p/C_v) of Deep Fresh Waters of Lake Baikal

Sherstyankin P.P., Kuimova L.N., Ivanov V.G.

Limnological Institute, Siberian Branch, Russ. Acad. Sci., Irkutsk, 664033, Russia.

E-mail: ppshest@lin.irk.ru

Lake Baikal, the deepest freshwater basin on our Planet, has a temperate type of climate. Every year the lake is covered with ice of about 60-100 cm thick for several months. Due to these circumstances, some unique thermodynamic characteristics of natural water become apparent in the Baikal water:

- during half a year in the uppermost water layers there is a reverse temperature stratification with the water temperature T lower than that of maximum density T_{md} and with negative coefficient of temperature expansion α ;
- in deep water layers (over 300 m) there is always a direct temperature stratification, i.e. T in situ is always higher than T_{md} and α is always positive like in marine waters (Vereshchagin, 1927; Mamaev, 1987; Wüest, Carmack, 2000).

Proximity of Baikal waters temperatures to the temperature of maximum density reveals interesting and surprising features first observed in Lake Baikal (Vereshchagin, 1927; 1936). Unfortunately, a lot of limnologists and oceanologists have not understood and accepted them.

One of the most unique characteristics of them is that the differences in temperatures of deep water T and temperatures of maximum density in situ – $T_{md} - (T - T_{md})$ – with an increase of depth (pressure) “are gradually increasing” in Vereshchagin’s point of view (1927, 1936). This fact has been proved by numerous observations carried out in Lake Baikal after Vereshchagin (Rossolimo, 1957; Weiss et al., 1991; Hohmann et al., 1997). Inevitable growth of true potential temperatures and the deficit of potential densities result from $T - T_{md}$. P.P. Sherstyankin, L.N. Kuimova and V.L. Potemkin first noticed the deficit of potential densities in 1997 (Sherstyankin et al., 1997a, b).

The problem on correct determination of true potential temperature is very simple. It is necessary to know which contribution adiabatic changes of temperature (Helland-Hansen method) and of T_{md} make at changes of depths (pressure). How important are these factors for the conditions of Lake Baikal? The calculations show that adiabatic corrections for the depth of 1600 m are lower than 0.04°C. Due to the changes of T_{md} , the maximum correction of the same conditions reaches about 3.4°C, i.e. the corrections that are not taken into account by Helland-Hansen method, are almost by two orders higher (in about 100 times). Knowing this, Vereshchagin (1927) animo neglected adiabatic corrections. The potential temperature of Helland-Hansen method (1912) takes into account not all the corrections (only one of the two and the least correction, which may be neglected for Baikal conditions): it is incomplete and incorrect. That’s why we define it as false, θ_{false} . The potential temperature defined by our method that take into account adiabatic changes and changes of T_{md} , is called complete or true (Sherstyankin et al. 1997; 1998, 2001; Sherstyankin and Kuimova, 2002). In Lake Baikal for the deep zone below 300 m, temperatures T in situ are higher than T_{md} . After their transformation into “potential” temperature with the help of Helland-Hansen method, they are lower than T_{md} for surface waters. This contradicts physical sense of potential transformation of temperatures responsible for the transmission of thermodynamic properties of waters without falsification (Fig. 1). Potential temperatures θ_{false} determined with Helland-Hansen method (1912) for deep Baikal waters decrease with the increase of depths, α changes its sign and becomes negative (!?) (Weiss et al.,

1991; Hohmann et al., 1997; etc). This does not agree with the observed growth of the temperature differences $T(Z)-T_{md}(Z)$ with the depth increase Z and with the sign α

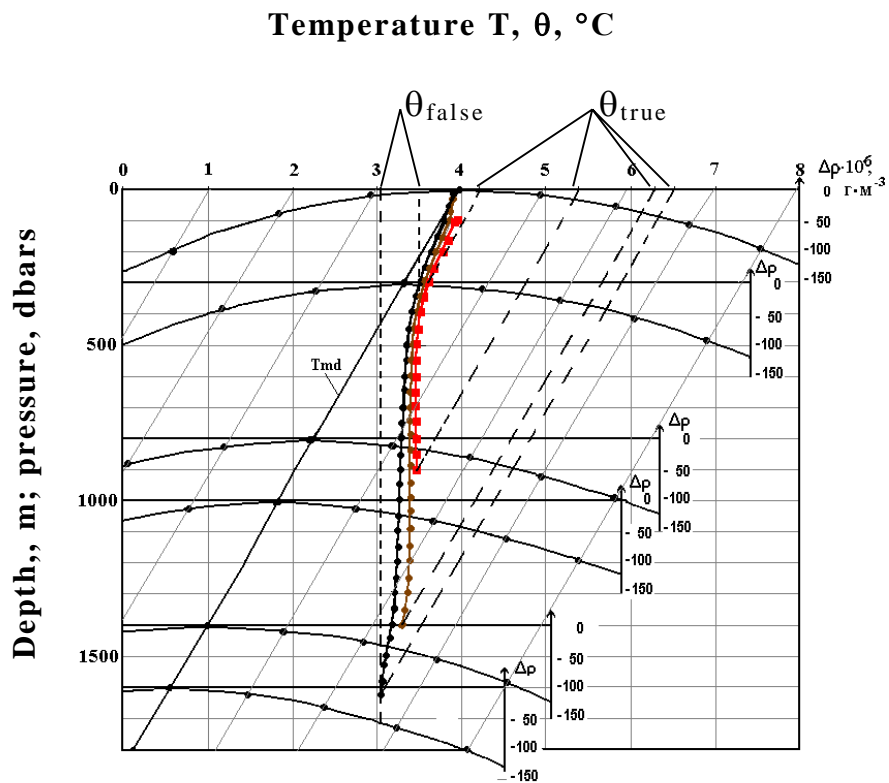


Fig. 1. Potential temperatures in the northern, southern, and middle basins of Lake Baikal (Weiss et al., 1991) θ_{false} obtained by the traditional method and θ_{true} for the same conditions obtained with regard for the decrease in the maximum density temperatures T_{md} with an increase in pressure P or depth Z . The graphs of the water density diminishing vs. the departure of the *in situ* temperature from T_{md} or the water density deficit D_r with the centers at pressures equal to 0, 300, 800, 1000, 1400, and 1600 dbar (meters) are presented in the same figure.

(Fig. 1). Potential temperatures θ_{true} for deep layers are higher than T_{md} , and temperature differences grow stably with the depth; the sign α is positive (Vereshchagin, 1927; 1936; Sherstyankin et al., 1997; 1998; Sherstyankin and Kuimova, 2002). This corresponds to the observations (Fig. 1).

Why are the incorrect ideas of potential temperature so stable in spite of discrepancy between experimental (observed) facts?

Evidently, there are some reasons for this. Firstly, for oceanologists working with marine waters where the real temperatures of waters are far from those of maximum density, inaccuracy in the definition of potential temperature and density is not so vivid as for Baikal water, especially since the sign α does not change. Secondly, to explain why potential temperatures with the increase of depth grow and potential densities accordingly decrease without losing stability is not simple. These characteristics of deep waters, which we see on the example of Lake Baikal, seem

to be surprising and strange at first sight. As they do not contradict the experiment, this is a law of nature that we cannot understand infinitely long, however to change it is beyond our power. We carried out the detailed theoretical and experimental analysis of these phenomena called thermobaric stability caused by the presence of temperature of maximum density T_{md} and its decrease with the growth of depth (pressure) (Sherstyankin and Kuimova, 2002).

At one of the conferences where we (P.P.Sherstyankin and L.N.Kuimova) were reporting on our viewpoint about the problems of potential temperature and density, Alfred Wüest (personal report) said that our theory misapprehended mainly because of the growth of potential temperatures in the deep zone of Lake Baikal.

The study of adiabatic character of processes occurring in the water is a very important problem connected with the understanding of thermodynamic characteristics of deep natural waters. It is necessary to know the parameter of the adiabat κ equal to the ratio of specific heat at constant pressure C_p and constant volume C_v , as well as the adiabatic gradient Γ of the temperature or adiabatic correction ΔT_{ad} to the temperature T in situ. We again encounter anomalous effects of the water. At $T=T_{md}$, the adiabat parameter $\kappa=C_p/C_v \equiv 1$, the coefficient of temperature expansion $\alpha \equiv 1$, the adiabatic correction $\Delta T_{ad} \equiv 0$, i.e. adiabatic character of processes is reduced to zero or degenerates. From the physical point of view it means that buoyancy forces of some volume of water also equal to zero. Infinitesimal increase of the density ρ at $T \equiv T_{md}$ can lead to infinite large vertical movements of this volume. This effect is experimentally proved by the thermal bar observations in situ when at the transition of the temperature of surface water layers through the temperature of maximum density (about 4°C for fresh waters), vertical mixing of Baikal waters exceeds 200 m according to L.L. Rossolimo's data (1957) and over 400 m – to P.P. Sherstyankin's data (1977).

Such important thermodynamic parameter of natural waters as the sound speed is entirely determined by adiabatic characteristics of water. The sound speed C in the water is the square root of the reverse number of adiabatic compressibility (derivation of water density ρ of pressure P at constant entropy η and salinity S - $(\partial\rho/\partial P)_{\eta,S}$), and depends greatly on the index of adiabat C_p/C_v . Adiabatic compressibility is κ times lower than isothermal compressibility; at $T=T_{md}$, adiabatic and isothermal compressibilities become equal to each other.

The values of adiabat parameters κ , α and ΔT_{ad} increase at temperatures $T>T_{md}$ with an increase of T (having $\kappa > 1$, $\alpha > 0$ and $\Delta T_{ad} < 0$). At $T<T_{md}$, the values of these parameters also rise; however, α and ΔT_{ad} change their signs, while κ retains its sign forming, as in the case with the water density ρ , two branches of positive values.

The sound speed is closely connected with the equation of state of the lake water and can be used for proving its justification test (Sherstyankin et al., 2002).

The formula of Chen and Millero (1986) is usually used for the equation of the Baikal water state, which simulates well a very important effect connected with the temperature of maximum density T_{md} (Sherstyankin et al., 2000). However, there have been not experimental evidences of application of such equation of the Baikal water state. This became possible comparing the values of the sound speed calculated for Baikal waters using the Chen-Millero equation of state in our formula (Sherstyankin et al., 2002) with the values of sound speed obtained in the experiment by Chenskii et al. (1998), which are stipulated by real but unknown equation of the water state (Fig. 2). The differences of sound speeds derived from these formulae appeared to be 0.2 m/s (Sherstyankin et al., 2002) and are comparable with absolute errors of experimental calculations (+/- 0.2 m/s, Chenskii et al., 1998). Hence, the experimental evidences of the validity of the equation of the state of lacustrine waters in the Chen-Millero form (1986) for Baikal conditions have been obtained.

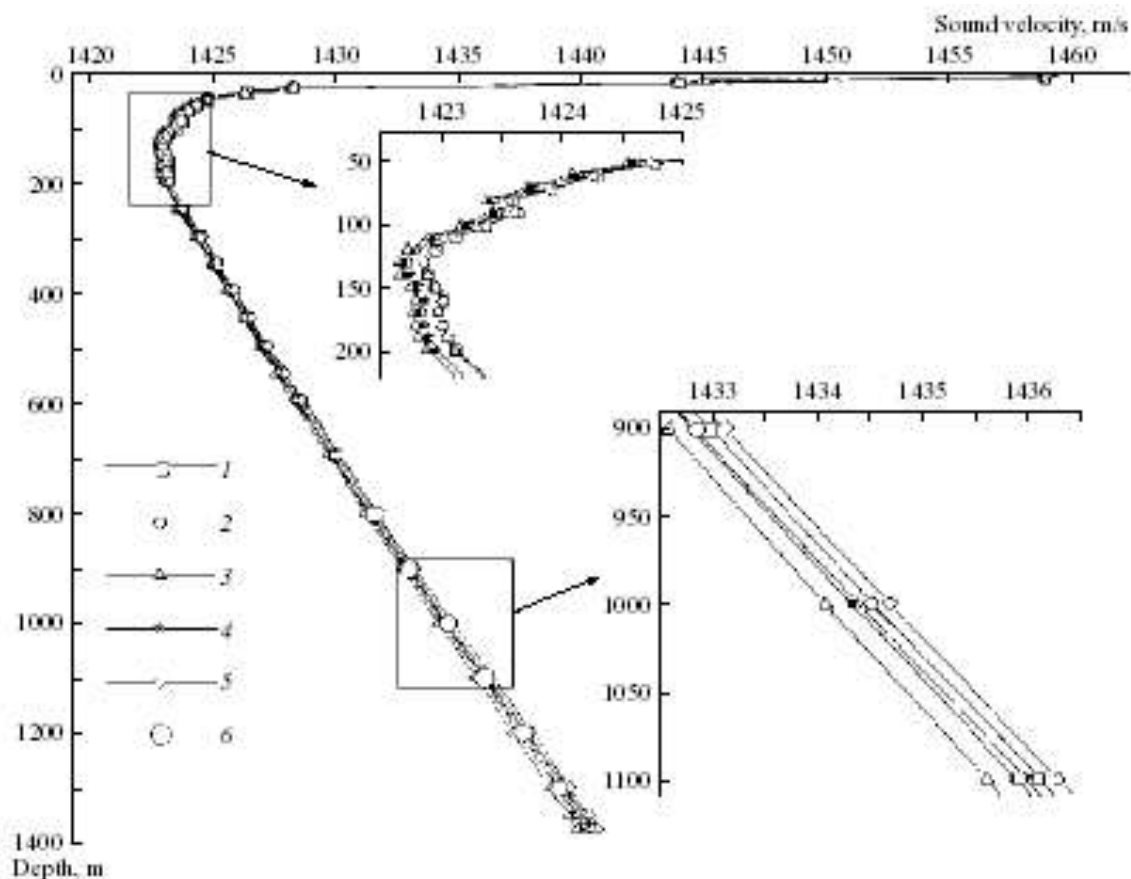


Fig.2. Sound velocities at station located 5.5 km south of Cape Listvennichnyi in the southern Lake Baikal area. Curves based on: (1) Chen and Millero (1977), (2) Chen and Millero (1986), (3) Kolotilo and Sherstyankin (1985), (4) modified after Kolotilo and Sherstyankin, (5) Eq. (4), (6) values measured near Cape Polovinnyi Chenskii et al. (1998).

Acknowledgements

This work was supported by Russian Foundation for Basic Research (grants No. 01-05-97229, No. 01-05-65097, No.02-05-65337 and No. 02-05-65345).

References

- Chen, C.T. and Millero, F.J., 1977. Speed of sound in seawater at high pressures. *J. Acoust. Soc. Am.*, **62**: 1129-1135.
- Chen, C.T. and Millero, F.J., 1986. Precise thermodynamic properties for natural waters covering only the limnological range. *Limnol. Oceanogr.*, **31**: 657-662.
- Chenskii, A.G. et al. 1998. The hydroacoustic System for measurements of Neutrino Telescope coordinates and long-term monitoring of hydrophysical processes on Lake Baikal. *Akustika okeana* (Acoustics of the Ocean), Moscow: GEOS, 1998, pp. 344-347. (In Russian).
- Helland-Hansen, B.1912. *The ocean waters, An introduction to physical oceanography*. Intern. Rev. d. Hydrobiol., Suppl. to Bd.III, Ser.1, H.2, 84 pp., Leipzig.
- Hohmann, R., Kipfer, R., Peeters, F., Imboden D.M., Shimaraev M.N., 1997. Processes of deep-water renewal in Lake Baikal. *Limnol. Oceanogr.*, **42**: 841-855.
- Kolotilo, L.G. and Sherstyankin, P.P., 1985. *Tablitsy skorosti zvuka v vode ozera Baikal i popravki glubin, izmerennykh ekholotom. D221/k 641-T* (Tables of Sound Velocity in the Lake Baikal Water and Corrections of Depths Measured by Echo Sounder D221/k 641), Leningrad: TsVMB, (In Russian).
- Mamaev, O.I., 1987. On question about the thermal regime on Lake Baikal. *Dokl. Akad. Nauk SSSR*, **292**: 1477-1481. [In Russian]

- Rossolimo L.L. *Temperaturnyi rezhim ozera Baikal*. [The Temperature Regime on Lake Baikal]. Trudy Baikal'skoi limnologicheskoi stantsii, XYI, Publishing House of Akademii Nauk SSSR, 1957. 552 p.
- Sherstyankin P.P. O sezonnoi izmenchivosti pokazatelya oslableniya svetovogo izlucheniya na Baikale. [On Seasonal Changes of Attenuation Coefficient of Light Radiation on Baikal]. In *Krugovorot veshchestva i energii v vodoemakh. Gidrologiya i klimat. Listvenichnoe na Baikale: 1977*, pp. 171-175.
- Sherstyankin, P.P., Kuimova, L.N., and Potemkin, V.L. 1997. Basic Regularities of the Thermohaline Regime of the Lake Baikal Deep Zone on the Basis of T,S-Analysis. Interperiodica Publishing (Russia), Transactions (Doklady) of the Russian Academy of Sciences / Earth Science Sections ISSN 0012-484X, 1997, Vol.355A, July-August, No.6, Part 2. pp.922-926.
- Sherstyankin P.P., Kuimova L.N., Potemkin V.L. 1998. Determination of potential temperatura and density for deep fresh waters. *Journal of Lake Sciences*, Vol. 10, Suppl., pp.261-266, 1998. C4-2001-6-261-266 Copyright ©1998 by Science Press, Beijing. Printed in P. R. China.
- Sherstyankin P.P., Kuimova L.N., and V.L. Potemkin. 2001. Calculation of the Potential Temperature of Natural Waters. *Izvestia, Atmospheric and Ocean Physics*. **37**: 407-410.
- Sherstyankin P.P. and Kuimova L.N. 2002. Thermobaric Stability and Instability of Deep Natural Waters in Lake Baikal. *Doklady Earth Sciences*, Vol.385, No.5, pp. 604-608. Translated from Doklady Akademii Nauk, Vol. 385, No.2, 2002, pp. 247-251.
- Sherstyankin P.P., L. G. Kolotilo, Yu. F. Tarasyuk, L. N. Kuimova, V. G. Ivanov, and V. V. Blinov. 2002. Sound Velocity in Lake Baikal. *Doklady Earth Sciences* ISSN 1028-334X Vol. 386, No. 7, 2002 Part 2. Geochemistry, Geophysics, Oceanology, Geography p.799-803.
- Vereshchagin, G.Yu., 1927. Some data on the regime of the deep waters of Baikal in the area of Maritui. In *Tr. komissii po izucheniyu ozera Baikal, II*, pp. 77–138. [In Russian]
- Vereshchagin, G.Yu. 1936. Basic features of the vertical distribution of dynamics of the water masses in Baikal. In *Sbornik Acad. V.I.Vernadskomu k 50-letiyu nauchnoi i pedagogicheskoi deyatel'nosti*, Izdatel'stvo AN SSSR, 1207-1230. [In Russian]
- Weiss, R.F., Carmack, E.C., and Koropalov, V.M., 1991. Deep-water renewal and biological production in Lake Baikal. *Nature*, **349**: 665–669.

MEROMIXIS – THE EFFECT OF WIND AND RIVER INFLOW

John Little

Department of Civil and Environmental Engineering
Virginia Tech, Blacksburg, VA 24061, USA
[jcl@vt.edu]

Alfred Wüest

Limnological Research Center
EAWAG, CH-6047 Kastanienbaum, Switzerland
[wuest@eawag.ch]

Abstract

A model that simulates the salt accumulation cycle in Lake Baldegg, a eutrophic, hard-water lake in Central Switzerland, is assembled. The model is used to investigate the effect of wind and river inflow on meromixis. Average water column salinity data collected over a 15-year period are used to calculate salt fluxes as a function of time and depth. River inflow and outflow data collected over a 5-year period are used to determine net salt input, as well as the density of the influent river water as a function of time. The salt fluxes and influent river properties are incorporated into a one-dimensional, seiche-extended, k-epsilon model that has proven to be especially effective at predicting vertical turbulent diffusivity during stratified periods. Simulations using actual weather data reveal that salt water inflow induces and sustains meromixis, while high wind during the winter and early spring tends to eradicate meromixis. Simple turbulent kinetic energy calculations support these conclusions and highlight the strong influence of wind-induced seiche mixing.

Introduction and objectives

In holomictic lakes, and depending on the degree of primary productivity, the bottom water may experience seasonal deoxygenation. In meromictic lakes, the stagnant monomolimnion will usually remain deoxygenated as long as meromixis persists (Hutchinson, 1957). The extent to which meromixis prevails will be determined by primary productivity, meteorological conditions (especially wind and temperature), and river and groundwater inflows. Because the redox conditions of the bottom water have a profound effect on the biogeochemistry of the sediments, it would appear possible to deduce information about climate variability by examining the long-term historical sediment record (Gruber et al., 2000). The key needed to unlock these sediment records is a better understanding of the factors that induce or eradicate meromixis, thereby establishing the prevailing redox conditions in the water column.

Lake Baldegg is a small lake with a maximum depth of 65 m, a volume of 0.17 km³, a surface area of 5.2 km², and is characterized by high primary productivity and ineffective vertical mixing at large depths (Wehrli et al., 1997). Using the sediment record Niessen and Sturm (1987) reconstructed the history of anoxia in Lake Baldegg for the last century. Between 1960 and 1980 extensive summer anoxia developed in the hypolimnion with clear evidence of meromixis persisting for extended periods during these decades (Wehrli et al., 1997). Artificial mixing during winter and hypolimnetic oxygenation during summer were introduced in 1982 to maintain oxygenated conditions above 4 g m⁻³ in the

entire water column throughout the year (Wüest et al., 1992). The excellent data sets that were collected prior to and especially after the introduction of artificial aeration present an opportunity to develop a model for Lake Baldegg that simultaneously incorporates the effects of primary production, meteorology, net river inflow, and mixing in the water column, thereby simulating the conditions that control meromixis.

Our overall research goal is to develop a model that simulates the conditions in Lake Baldegg for a single representative year. Because the salt accumulation cycle is relatively complex, (Ramisch et al., 1999) we use salinity data to calculate salt fluxes that are incorporated into a 1-D hydrodynamic lake model (Goudsmit et al., 2001). This seich-extended k-epsilon model has proven to be especially effective at predicting vertical turbulent diffusivity during stratified periods and is therefore well suited for simulating the conditions surrounding meromixis. Once the model has been assembled and validated, it will be used to quantify the effect of wind and river inflow on meromixis.

Estimating salt fluxes

The following approach was taken to estimate salt fluxes in Lake Baldegg:

- monthly temperature and salinity profiles were available for a 16-year period;
- the change in salt content from one month to the next give the salt accumulation rate;
- a simple two-box approach is used during the stratified period, with average accumulation rates estimated for both epilimnion and hypolimnion;
- during the well-mixed winter months, average salt accumulation rates were estimated for the entire lake volume;
- monthly temperature, salinity, and flow rate data were also available for river inflow and outflow and these were used to determine the net salt load on the lake.

The average salt concentration in Lake Baldegg is shown in Figure 1 for the months of January (onset of well mixed conditions), April (beginning of summer stratification), and August (height of summer stratification). From January to April, salt is added to the lake in significant quantities. Following April, even though salt continues to be added to the epilimnion, the effect of primary production is to cause a significant decrease in near-surface salinity. The decrease continues through August, after which gradual deepening of the mixed layer eventually restores well-mixed conditions by January. The average salt concentration profiles for all the months of the year were integrated to obtain the total salt content of the lake as shown in Figure 2. For illustrative purposes, the data are normalized to the salt content of 62,000 tons at the beginning of the year, and the annual cycle is repeated for a second year. Also shown are similar data obtained for Lake Hallwil (maximum depth 48 m, volume 0.29 km³, surface area 9.9 km², initial salt content 83,000 tons), the lake immediately downstream of Lake Baldegg. The regular and remarkably similar salt cycle in both lakes support the observed trends shown in Figure 1. As will be shown in the following analysis, primary productivity during the summer months causes rapid removal of salt from the lake, while net river inflow recharges the salt at differing rates during the course of the year.

To investigate these trends in more detail, simple calculations are employed to deconvolute the data. During the well-mixed winter months, the salt balance over the entire lake is

$$\frac{\Delta S_t}{\Delta t} = RI - RO - NS$$

where S_t represents total salt content, t is time, RI is river inflow, RO is river outflow, and NS is net sedimentation. During the stratified summer months, the balance over the epilimnion is

$$\frac{\Delta S_e}{\Delta t} = RI - RO - GS$$

where S_e is salt content in the epilimnion and GS represents gross sedimentation. The balance for the hypolimnion is

$$\frac{\Delta S_h}{\Delta t} = R$$

where S_h is salt content in the hypolimnion and R is re-dissolution. Net river input (NRI) equals $RI - RO$. The data shown for Lake Baldegg in Figure 2, along with average monthly data for RI and RO , are used to calculate NS and NRI over the entire year, as well as GS and R during the summer. The results are shown in Figure 3. GS , the net removal of salt from the epilimnion, rises and then falls during the summer months, apparently reflecting the amount of sunlight available for algal growth. Redissolution by contrast, is very small. This accumulation of salt in the hypolimnion is either caused by the dissolution of calcite crystals as they sink through the hypolimnion, or by the dissolution of calcite that is present in the sediments. Either way, only a very small fraction of the salt removed from the epilimnion accumulates in the hypolimnetic water. Also, R should only get smaller during the winter when there are no crystals sinking through the hypolimnion. NS , the net removal of salt from the entire water column, reflects the GS calculated from the epilimnion data.

Incorporating salt fluxes in lake model

The following approach was taken to couple the salt fluxes with the seiche-extended k-epsilon model (Goudsmit et al., 2002) for Lake Baldegg:

- the k-epsilon model was previously calibrated for Lake Baldegg (Goudsmit et al., 2002), although salinity was not included in the model at that stage;
- an extensive meteorological data set obtained during 1995/96 was used for the baseline weather conditions;
- average monthly temperature, salinity, and flow rate data for river inflow were prescribed as input for the model;
- temperature and salinity were used to determine the density of the influent river water, and this was used to establish the depth to which the river water plunges in the lake (generally, the river mixes into the epilimnion during summer, but plunges into the lower hypolimnion during winter);
- average monthly flow rate data for river outflow were prescribed as withdrawal from the surface layer;
- gross sedimentation was simulated by removing the appropriate amount of salt from the epilimnion from April to September;
- redissolution was represented by adding the appropriate amount of salt to the hypolimnion from May to September;

- the simulation was started from an initial well-mixed condition in January and an iterative procedure was used to establish the depth to which the influent river water plunged over the course of the year;
- the simulation was repeated for a second year, using the final temperature and salt concentration at the end of the first-year as the initial condition for the second year – in effect, this produced a “steady-state” situation for the particular set of forcing conditions imposed by weather, river inflow and outflow, and salt fluxes induced by primary productivity.

The model-predicted salt concentration is shown in Figure 4 as a function of time and depth. This baseline simulation uses actual weather conditions from 1995. The lake begins the year in a weakly stratified condition. As salty river water enters the lake and sinks to the bottom, the salinity of the lower hypolimnion increases. However, despite the continuing influx of dense salty water from January through April, three strong wind events (in mid-January, mid-February, and again in late March) cause brief periods of complete mixing, as shown in Figure 4. In May, the river water is sufficiently warm such that it is less dense than that in the lake, and it enters and mixes into the epilimnion. Although this adds salt to the surface water, gross sedimentation between May and September removes a significant amount, causing an overall decrease in the surface salt concentration during the summer. During the stratified period, redissolution causes a modest increase in the salinity of the hypolimnion. From October onwards, there is no further gross sedimentation or redissolution, and net river inflow recharges the salt in the lake. The river adds to the surface water during October and November, dropping down somewhat during December with the deepening of the mixed layer.

A coarse sensitivity analysis showed that wind can have a very strong impact on the mixing of salt in the lake. To illustrate this, the baseline simulation is repeated, but the wind speed is reduced by 20% over the course of the entire year. Figure 5 shows that this modest decrease in wind speed has a significant impact, with the lake becoming permanently meromictic.

Table 1. Estimated Rates of Turbulent Kinetic Energy Consumption (–) and Production (+) and Comparison to River Inflow.

Process	W kg ⁻¹	Ratio
River Inflow	–9.0 × 10 ⁻¹⁰	1.0
Sediment Flux	–1.9 × 10 ⁻¹¹	0.1
BBL Dissipation	+1.0 × 10 ⁻⁹	1.1
Wind (1.5 m/s)	+1.3 × 10 ⁻¹⁰	0.1
Wind (6 m/s)	+8.1 × 10 ⁻⁹	9.0

As a check on the validity of the overall modeling approach, simple order-of-magnitude estimates were made of several processes that either consume or produce turbulent kinetic energy (TKE). River inflow and sediment flux both consume TKE due to the induced density gradient that suppresses mixing. Bottom boundary layer (BBL) dissipation and wind both add TKE. The estimated rate at which the various processes either consume or produce TKE is shown in Table 1, and compared to river inflow. The results are in general agreement with those from the model, suggesting that dense river inflow during the first few months of the year is crucial to both induce and sustain meromixis. BBL dissipation roughly balances the effect of river inflow, perhaps revealing why meromixis

in the past has been intermittent. Sediment flux is negligible, as is wind at the average wind speed of 1.5 m/s. However, wind speeds above 6 m/s are very effective at eradicating meromixis.

References

- Goudsmit, G.-H., Burchard, H., Peeters, F. and Wüest, A. 2002. Application of k - ϵ turbulence models to enclosed basins – the role of internal seiches. *Journal of Geophysical Research*. Vol. 107. No. C12. pp. 3230.
- Gruber, N., Wehrli, B. and Wüest, A. 2000. The role of biogeochemical cycling for the formation and preservation of varved sediments in Soppensee. *J. Paleolimnology*. Vol. 24. pp. 277-291.
- Hutchinson, G. E. 1957. *A Treatise on Limnology – Volume 1*. John Wiley & Sons, Inc. New York.
- Niessen, F. und Sturm, M. 1987. Die Sedimente des Baldeggersee (Schweiz) – Ablagerungsraum und Eutrophierungsentwicklung während der letzten 100 Jahre. *Arch. Hydrobiol.* Vol. 108. pp. 365-383.
- Ramisch, F., Dittrich, M., Mattenberger, C., Wehrli, B. and Wüest, A. 1999. Calcite dissolution in two deep eutrophic lakes. *Geochimica et Cosmochimica Acta*. Vol. 63. No. 19/20. pp. 3349-3356.
- Wehrli, B., Lotter, A. F., Schaller, T. and Sturm, M. 1997. High-resolution varve studies in Baldeggersee (Switzerland): Project overview and limnological background data. *Aquatic Sciences*. Vol. 59. pp. 285-294.
- Wüest, A., Brooks, N. H. and Imboden, D. M. 1992. Bubble plume modeling for lake restoration. *Water Resources Research*. Vol. 28. No. 12. pp. 3235-3250.

Figure 1. Average salt concentration profiles in Lake Baldegg

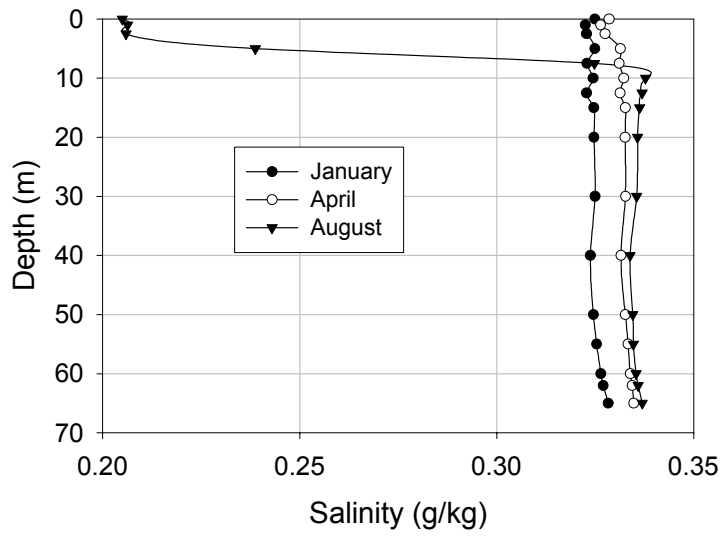


Figure 2. Normalized salt content in Lake Baldegg and Lake Hallwil. The average annual cycle is repeated for purposes of illustration.

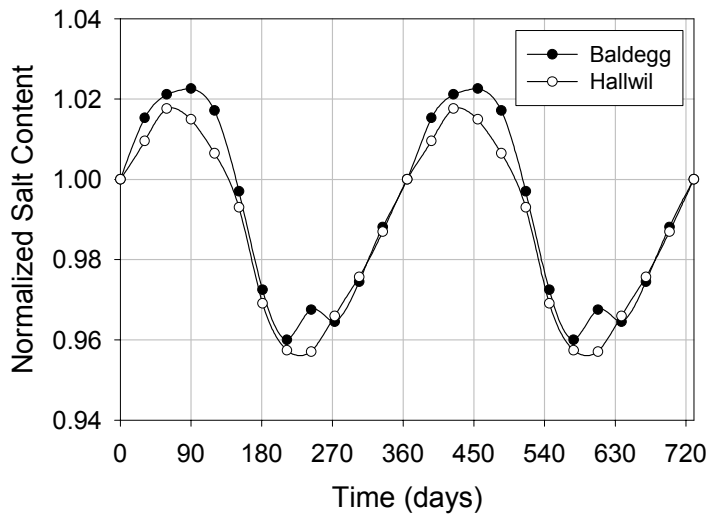
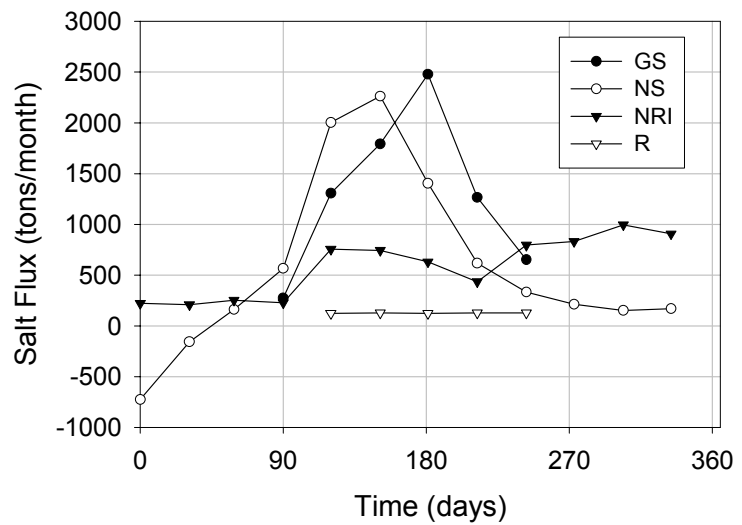


Figure 3. Average salt fluxes in Lake Baldegg



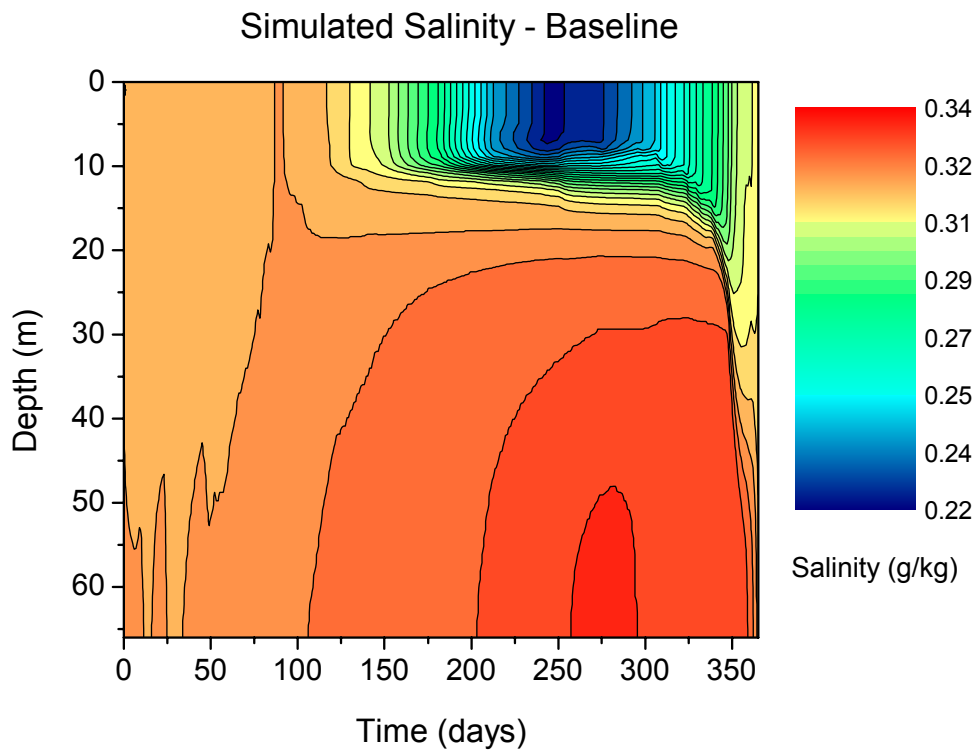


Figure 4. Predicted annual salt concentration contour plot using baseline weather conditions.

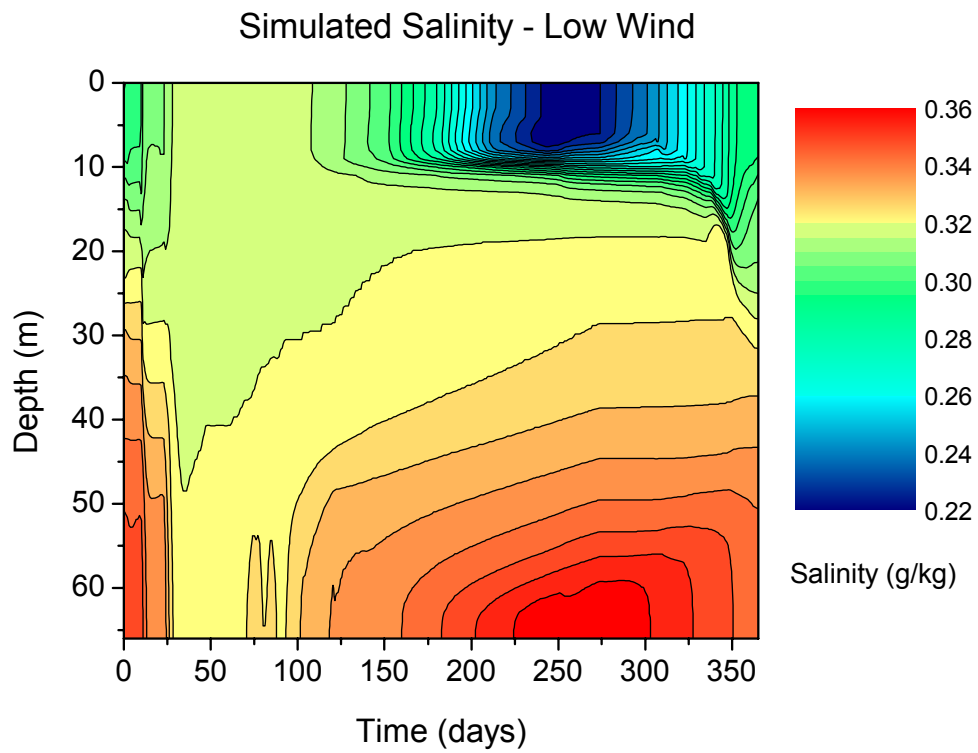


Figure 5. Predicted annual salt concentration contour plot using baseline weather conditions with wind speeds reduced by 20%.

The contribution of near-inertial waves to stratified turbulence and diapycnal mixing in Lake Baikal

Martin Schmid, André Masson, Michael Schurter, Alfred Wüest

EAWAG, Limnological Research Center, Seestrasse 79, CH-6047 Kastanienbaum

Yuri Parfenov

Irkutsk State University, Institute of Applied Physics, 664003 Irkutsk, Russia

Nick Granin

Limnological Institute of the Siberian Division of the Russian Academy of Sciences, P.O. Box 4199, Irkutsk 664033, Russia

Three moorings have been installed in Lake Baikal to measure time series of temperature and bottom currents and to collect sinking particles in sediment traps. The mooring at the site of the Baikal Neutrino Experiment (Balkanov et al. 2002), a few km off the northern shore of the south basin has been installed from March 1999 to March 2003 (NT mooring). The configuration of this mooring was changed from year to year. In the frame of the EU project CONTINENT (Continent, 2003) two additional moorings were installed in the center of the north (Baikal North Central mooring) and the south basin (Baikal South Central mooring). Temperature measurements are available from July 2001 to July 2002 for the BNC mooring, and from March 2001 to March/June 2002 for BSC mooring. Temperature time series were recorded with Vemco miniloggers and RBR TR-1000 temperature recorders at several depths throughout the water column. The time resolution was 10 minutes for the TR-1000 and 1 hour for the Vemco miniloggers. Simultaneously, velocity and direction of bottom currents were recorded every 30 minutes with Aanderaa current meters a few meters above the lake bottom of each mooring (NT mooring only until March 2001).

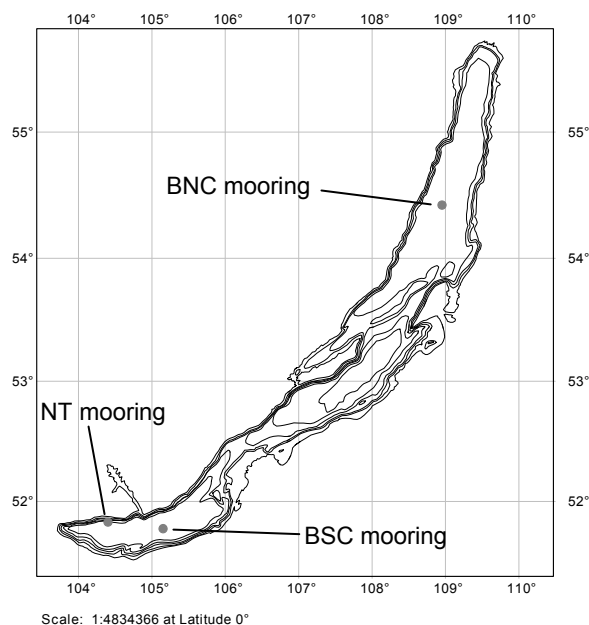


Figure 1: Positions of the three moorings installed in Lake Baikal.

During the ice-free period, strong near-inertial waves were regularly observed in the temperature time series from the top 200 m. Similar near-inertial waves were also observed as a dominant signal in the bottom currents. Figure 2 shows an example of a time series of the bottom currents observed at the BNC mooring.

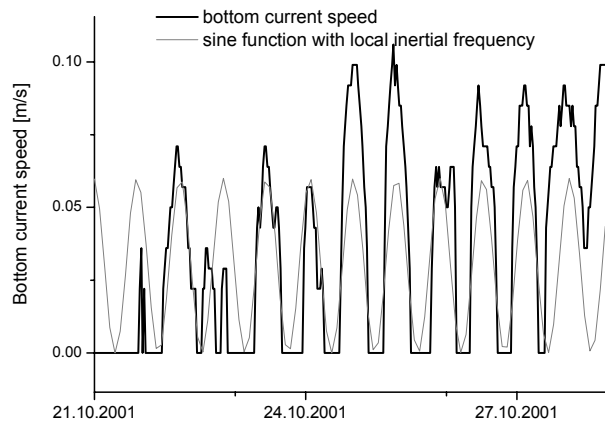


Figure 2: Observed bottom current speeds at the BNC mooring in October 2001 compared to the local inertial frequency.

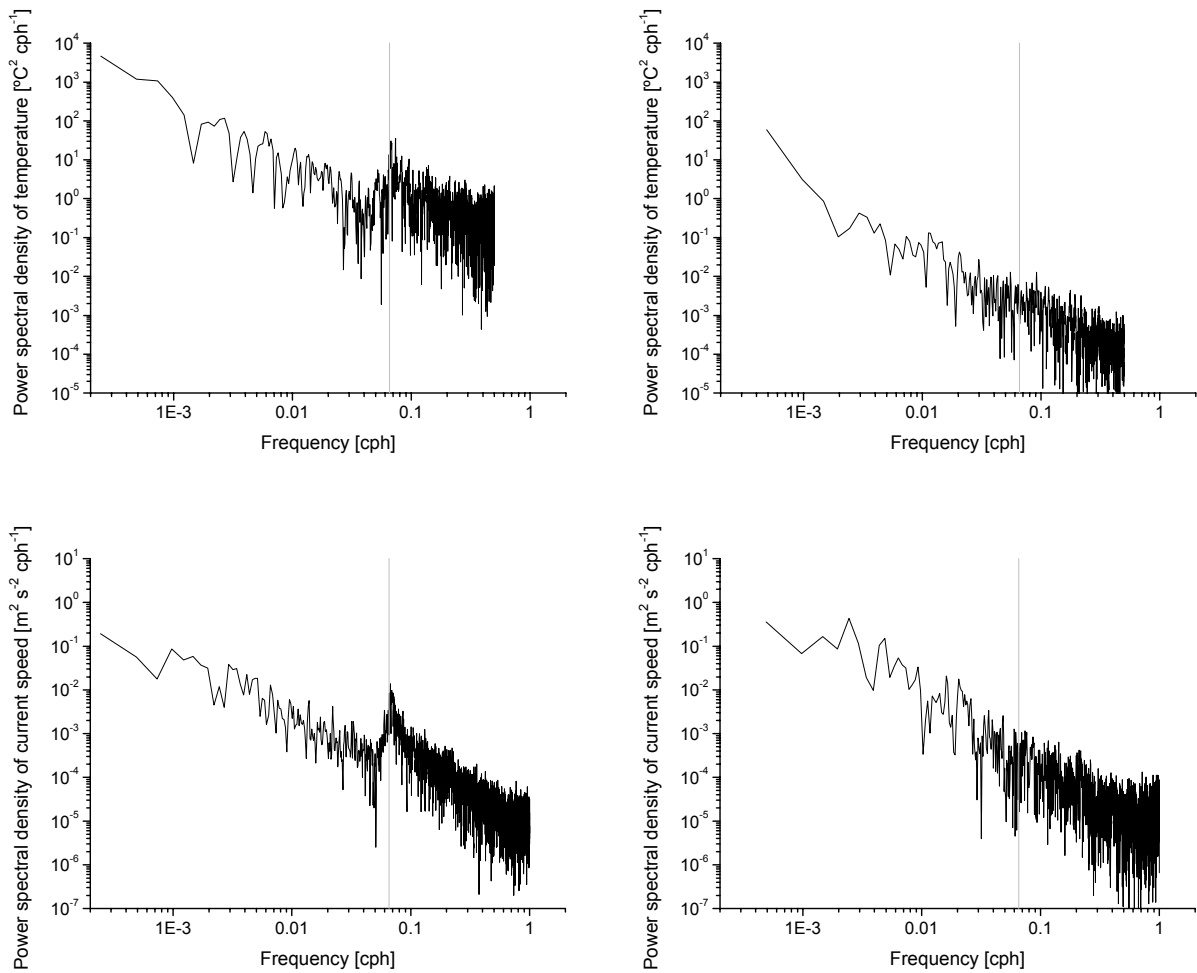


Figure 3: Power spectral densities of temperature at 16 m depth (above) and current speed at the bottom (below), observed at the BSC mooring during the ice free period from 1 June 2001 to 23 January 2002 (left) and during the ice covered period from 24 January to 30 April 2002 (right). The grey line shows the local inertial frequency. The comparison clearly demonstrates that the presence of the inertial waves is restricted to the ice-free period.

The power spectral densities of temperature and bottom current speed show strong peaks near the inertial frequency during the time when the lake surface is free, but both these peaks disappear during the ice-covered period (Figure 3). This indicates that the near-inertial oscillations observed in the temperature and in bottom currents receive their energy primarily from the wind at the lake surface. Similar observations have already been made in bottom current data collected in 1996/7 (Ravens et al. 2000).

A dominance of clockwise rotation would be expected in near-inertial currents on the northern hemisphere. Whereas at the BNC mooring the rotary spectra of the bottom current velocities are clearly dominated by clockwise rotation, this is not the case for the BSC mooring, where both rotational spectra show near-inertial peaks of very similar height (Fig. 4). This observation raises the question whether the transport of energy from wind to the bottom currents is different in the two basins. On the other hand the BSC currents reveal distinctive peaks at periods of c. 90 and 180 hours in the counter-clockwise spectrum. These could be related to the large-scale counter-clockwise circulation patterns observed in the basins (Shimaraev et al. 1994). The BSC mooring is located in the peripheral part of one of the observed large-scale gyres, whereas the BNC mooring is located in the central part of a gyre.

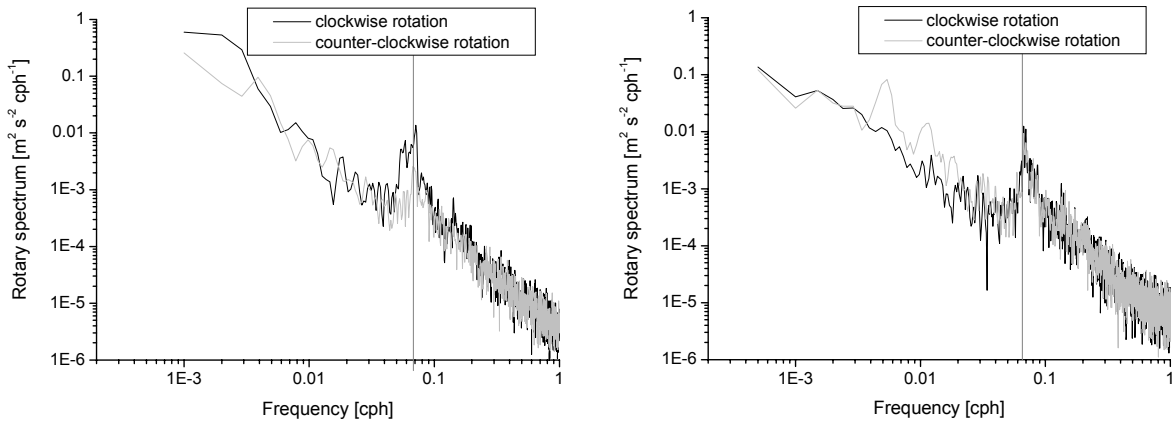


Figure 4: Rotary spectra of observed bottom current velocity at the BNC mooring from 5 July 2001 to 31 December 2001 (left), and at the BSC mooring from 1 June 2001 to 23 January 2002 (right).

The energy of near-inertial waves is known to propagate downwards in the ocean (Fu 1981) and to contribute about 30 - 50% to the energy of the turbulent mixing needed to keep up thermohaline circulation (Watanabe and Hibiya 2002). The direction of the group velocity and thus the energy propagation of internal waves depends on the relation between the local stability frequency N and the inertial frequency f . Figure 5 shows vertical profiles of the square of the stability frequency N^2 calculated from CTD profiles measured at the BSC and the BNC mooring in July 2002. The stability frequency is very low, in parts of the water column even lower than the local inertial frequency, whereas in the ocean the square of the stability frequency is generally between 10^{-7} and 10^{-5} s^{-2} . The angle α between the horizontal and the group velocity of internal waves with the frequency ω is given by

$$\tan \alpha = \sqrt{\frac{\omega^2 - f^2}{N^2 - \omega^2}}$$

This means that the low stability frequency in Lake Baikal leads to a steeper ray path of the internal waves than in the ocean. Consequently, the vertical transport should be more efficient in Lake Baikal.

The aims of the present study are (i) to investigate the structure of the different energy spectra of the temperature signals during the ice-free and the ice-covered periods and the time scales of the transition between the two different states, (ii) to discuss the mechanisms of the vertical transport of energy from the lake surface to the deep bottom currents by near-inertial waves, and (iii) to estimate the contribution of the near-inertial waves to diapycnal mixing in the water column.

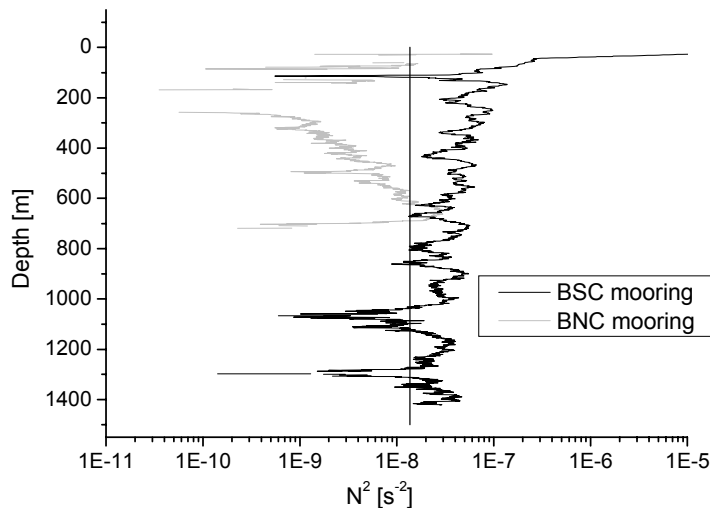


Figure 5: Vertical profiles of the square of the stability frequency, N^2 , calculated from CTD profiles measured at the BSC mooring on 5 July 2002 and at the BNC mooring on 10 July 2002. The vertical line is the square of the local inertial frequency f^2 .

References

- Balkanov V, Belolaptikov I, Budnev N, Bezrukov L, Chensky A, Danilchenko I, Dzhilkibaev Z, et al. (2002) BAIKAL experiment: status report. Nuclear Physics B - Proceedings Supplements 110:504-506
- Continent (2003), High-resolution CONTINENTAL paleoclimate record in Lake Baikal, EU-project, <http://icdp.gfz-potsdam.de/html/continent/html/index.html>
- Fu L-L (1981) Observations and models of inertial waves in the deep ocean. Reviews of Geophysics and Space Physics 19:141-170
- Ravens TM, Kocsis O, Wüest A, Granin N (2000) Small-scale turbulence and vertical mixing in Lake Baikal. Limnology and Oceanography 45:159-173
- Shimaraev MN, Verbolov VI, Granin N, Sherstayankin PP (1994) Physical limnology of Lake Baikal: a review. Baikal International Center of Ecological Research, Irkutsk, Okayama
- Watanabe M, Hibiya T (2002) Global estimates of the wind-induced energy flux to inertial motions in the surface mixed layer. Geophysical Research Letters 29:10.1029/2001GL014422

Observation of double diffusive convection in Lake Nyos, Cameroon

Martin Schmid, Andreas Lorke, Christian Dinkel, Alfred Wüest

EAWAG, Limnological Research Center, Seestrasse 79, CH-6047 Kastanienbaum

Gregory Tanyileke

Institute for Geological and Mining Research (IRGM), 4110 Yaoundé, Cameroon

Lake Nyos is a 208 m deep crater lake with a surface area of 1.58 km² in the north-western part of Cameroon. A sublacustrine source introduces warm, salty and CO₂-enriched water into the deepest layers of the lake (Nojiri et al. 1993; Evans et al. 1994; Kusakabe et al. 2000, Schmid et al. 2003). Due to the high CO₂ concentration, the source water is heavier than the hypolimnetic water and thus increases the stability of the water column. This is the main reason for the permanent stratification of the lake below a depth c. 50 m which is reached by seasonal convective mixing. In August 1986, a large CO₂ cloud erupted from the lake and asphyxiated more than 1700 people (Kling et al. 1987). Several processes have been proposed as the trigger of the eruption. In general, it is assumed that local supersaturation of CO₂ caused by a baroclinic dislocation of the water column triggered a self-amplifying plume within the water column (Evans et al., 1994). Since then the lake has been slowly recharging with CO₂. To prevent a new disaster, a plan for degassing the lake was developed and is currently in test (Halbwachs and Sabroux 2001; Halbwachs 2002). Without the degassing, a similar eruption could reoccur within decades.

A key characteristic of Lake Nyos is the permanent stratification of the water column which is upheld against the destratifying effect of the temperature by the high concentrations of CO₂ and dissolved solids. Such conditions, a so-called diffusive regime (Turner 1973), can lead to double-diffusive convective layers, if the stabilizing factor of salinity is not more than approximately 10 times as large as the destabilizing effect of temperature (Kelley et al. 2002). The susceptibility to double-diffusive convection increases as this so-called density ratio R_ρ decreases. Steps in vertical temperature and conductivity profiles caused by double-diffusive convection have been observed in several lakes with a diffusive-regime: Lake Vanda (Hoare 1966), Powell Lake (Osborn 1973), and Lake Kivu (Newman 1976). The present study shows for the first time the occurrence of double-diffusive convection in Lake Nyos and its importance for the vertical transport of heat and CO₂ in this system.

A set of 26 well-mixed convective layers with thicknesses of 0.2 - 2.2 m was observed in a CTD profile taken on 8 December 2002, distinctly separated by interfaces of strong gradients (Figure 1). Surprisingly, the double-diffusive staircases were only observed in December 2002 but not in November 2001. The 2001 profiles were vertically not as well resolved as the 2002 profile, but the presence of staircases, as prominently as in 2002, would have been clearly visible in the 2001 profiles. Consequently, the staircases must have developed during the time between the two CTD profiles. The temperatures observed at 62 m depth indicate that this happened at the end of March 2003.

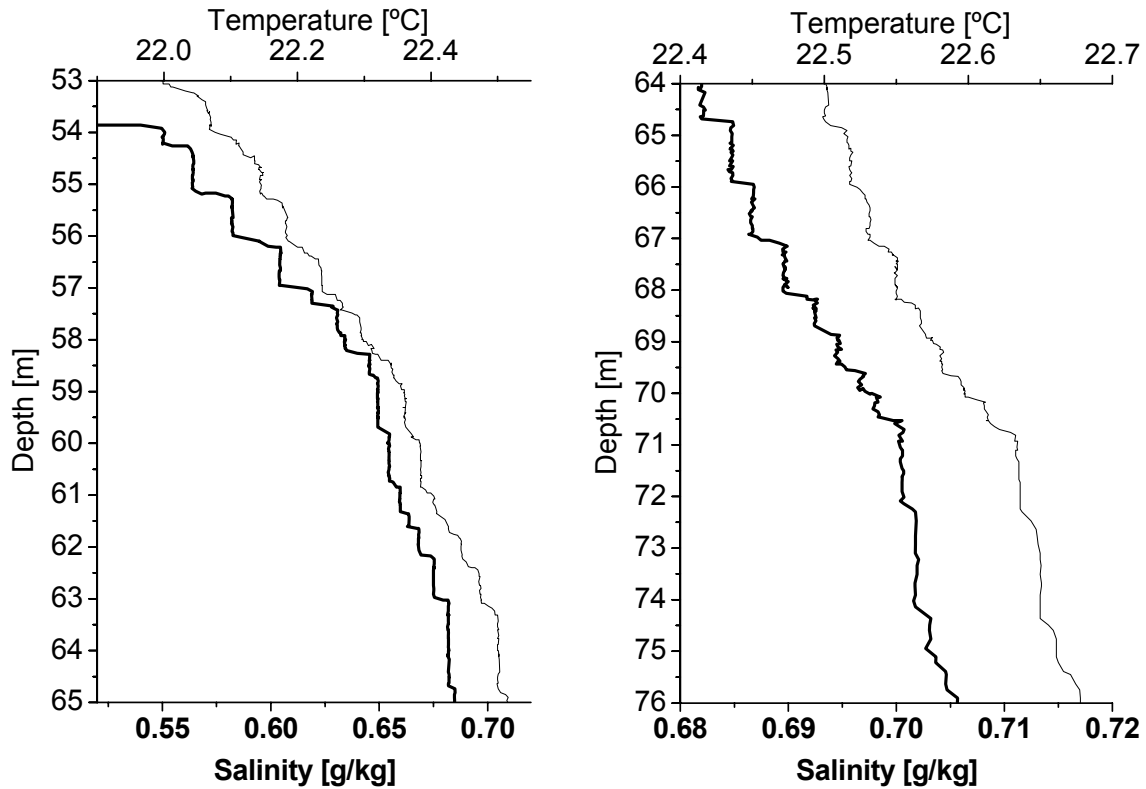


Figure 1: The 26 double-diffusive staircases observed in the salinity (thick lines) and temperature (thin lines) profiles in Lake Nyos in December 2002.

The temperature profile at 53 to 74 m depth in Lake Nyos, which had previously remained almost constant for more than 5 years, was strongly affected by the double-diffusive convection beginning in March 2002. At 62 m depth, the temperature decreased by 0.15 °C within 9 months. The heat flux caused by the double-diffusive convection in this layer ranged from 0.1 W m⁻² at the bottom to 0.6 W m⁻² at the top. The heat flux calculations based on the heat budget method and on the theory of double-diffusive convection yielded the same results within the uncertainty range (Figure 2). Together with the nearly linear decrease of temperature at 62 m depth, this indicates that the double-diffusive heat-flux was fairly constant throughout the observed time period.

The observed heat fluxes as well as the observed layer thicknesses are in good agreement with the values calculated based on the semi-empirical equation of Kelley (1990). The agreement is slightly worse with the 4/3 flux law of Turner (1973).

An estimation of the turbulent diffusivity below the chemocline produced by the internal seiche showed that without the double-diffusive convection the heat flux is most probably dominated by molecular heat diffusion. The apparent diffusivities caused by the double-diffusive convection are about one order of magnitude larger than the molecular heat diffusion coefficient. Consequently, we can conclude that the double diffusion has increased the heat flux by one order of magnitude and the heat flux at this depth has been dominated by double-diffusive convection.

The heat fluxes due to double-diffusive convection are similar to the heat input with the sublacustrine source at the bottom of the lake. Due to the low diffusivity in intermediate depth, the temperature increased at the bottom of the lake and decreased in the double-diffusive layer. The CO₂ fluxes caused by double diffusion are negligible compared to the input at the bottom of the lake.

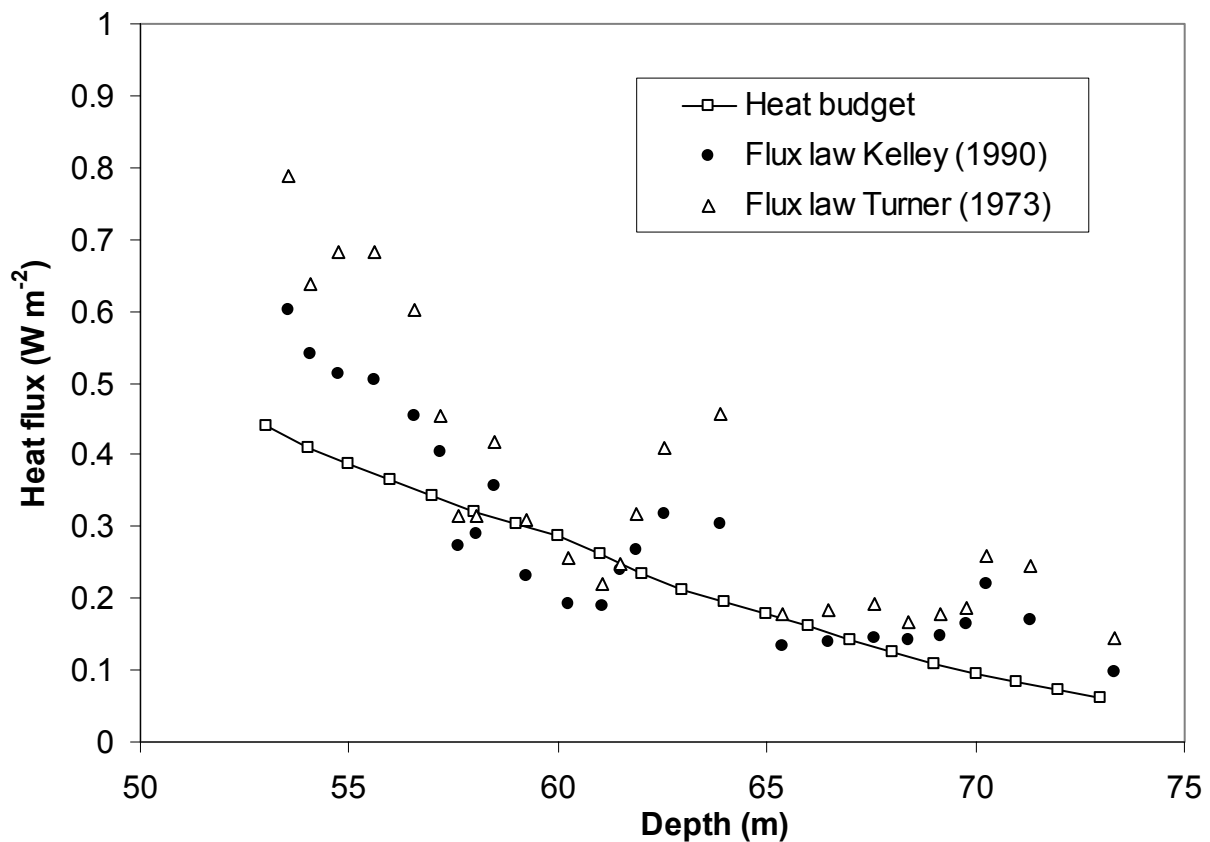


Figure 1: Upward heat fluxes in the double diffusive layer of Lake Nyos calculated for each observed staircase with the flux laws of Turner (1973) and Kelley (1990) and the heat budget method.

The uncertainties in the salt fluxes (including CO_2) are very large due to several reasons and conclusions based on these fluxes are rather speculative. However, the salt fluxes calculated with the salt budget method agree perfectly with the flux laws if we assume that the Fe^{2+} , transported to the surface by the degassing pipe, was dissolved in a 10 m thick layer below the chemocline. This is at least an indication that the iron was actually transported to and dissolved within this layer.

The current situation with the vertical divergence of the heat flux, i.e. the decreasing heat fluxes with depth, leads to an increase in the destabilizing temperature gradient in this layer, which is only to a small part equalized by the salt flux. If the temperature gradient continues to increase in this way, the entire double-diffusive layer could become unstable and a large mixed layer could be formed. If the rate of change of the temperature gradient continued as observed from March to December 2002, this would approximately happen after four years. This would however require a cooling of the mixed layer above the chemocline by almost 1°C to 21°C . With the current CO_2 concentrations in this layer, such a mixing would not be dangerous, but if the CO_2 concentration were near saturation, this process could lead to local supersaturation of CO_2 and subsequently to an eruption. This mechanism, even though it seems less probable than an internal wave caused by a landslide, should be added to the list of possible mechanisms that could have triggered the eruption in 1986.

References

- Evans WC, White LD, Tuttle ML, Kling GW, Tanyileke G, Michel RL (1994) Six years of change at Lake Nyos, Cameroon, yield clues to the past and cautions for the future. *Geochemical Journal* 28:139-162
- Halbwachs M (2002) Degassing Lake Nyos project. <http://perso.wanadoo.fr/mhalb/nyos/nyos.htm>
- Halbwachs M, Sabroux JC (2001) Removing CO₂ from Lake Nyos in Cameroon. *Science* 292:438-438
- Hoare RA (1966) Problem of heat transfer in Lake Vanda, a density stratified arctic lake. *Nature* 210:787-789
- Kelley DE (1990) Fluxes through diffusive staircases: a new formulation. *Journal of Geophysical Research* 95:3365-3371
- Kelley DE, Fernando HJS, Gargett AE, Tanny J, Oezsoy E (2002) The diffusive regime of double-diffusive convection. *Progress in Oceanography*: in press
- Kling GW, Clark MA, Compton HR, Devine JD, Evans WC, Humphrey AM, Koenigsberg EJ, Lockwood JP, Tuttle ML, Wagner GN (1987) The 1986 Lake Nyos gas disaster in Cameroon, West-Africa. *Science* 236:169-175
- Kusakabe M, Tanyileke GZ, McCord SA, Schladow SG (2000) Recent pH and CO₂ profiles at Lakes Nyos and Monoun, Cameroon: implications for the degassing strategy and its numerical simulation. *Journal of Volcanology and Geothermal Research* 97:241-260
- Newman FC (1976) Temperature steps in Lake Kivu: a bottom heated saline lake. *Journal of Physical Oceanography* 6:157-163
- Nojiri Y, Kusakabe M, Tietze K, Hirabayashi J, Sato H, Sano Y, Shinohara H, Njine T, Tanyileke G (1993) An estimate of CO₂ flux in Lake Nyos, Cameroon. *Limnology and Oceanography* 38:739-752
- Osborn TR (1973) Temperature microstructure in Powell Lake. *Journal of Physical Oceanography* 3:302-307
- Schmid M, Lorke A, Wüest A, Halbwachs M, Tanyileke G (2003) Development and sensitivity analysis of a model for assessing stratification and safety of Lake Nyos during artificial degassing. *Ocean Dynamics*: in press
- Turner JS (1973) *Buoyancy Effects in Fluids*. Cambridge University Press, Cambridge

3-D thermal structure of Lake Ladoga: a new approach and results

M.Naumenko, S.Karetnikov, V.Guzivaty

Institute of Limnology, Russian Academy of Sciences, Sevastyanov st., 9, 196105, St.-Petersburg, Russia;
E-mail: naumenko@limno.org.ru

Thematic databases serve as convenient store of the information and allow receiving a new knowledge on a natural object. Lake Ladoga, the biggest in Europe, has surface area 17700 km² and mean depth 47 m. The thermal database of Lake Ladoga comprises more than 170 thousand lines of water temperature values and the accompanying hydrophysical and meteorological elements fixed on coordinates and on time (Naumenko et al., 1998; 2000a). The database covers the period from 1897 to 2002 submitted on 75 years.

The aim of the study was to investigate three-dimensional thermal structure of Lake Ladoga on the basis of huge thermal database. For the first time we have got average long-term values of water temperature with decade step for all six morphometric zones from May to November. A new approach of using temporal approximation dependences for seasonal course of temperature and another elements permits to plot and analyze daily mean spatial distribution of ones.

A. Tikhomirov's (1982) knowledge about a thermal regime of Lake Ladoga has allowed revealing a thermal features of large dimictic lakes with the monthly temporal resolution.

The water temperatures and its main statistical characteristics on 8 horizons (0,5,10,20,30,40,50 and 100 m), since May 15 were calculated for each of Lake Ladoga various morphometric zones. The averaging period was 10 days with shifting on 5 days (Naumenko et al., 2000b). We have got a temporal variation of temperatures, their dispersions, vertical gradients of temperature and water density (Fig. 1).

Mean dates of water temperatures transition through 4 °C for various zones of lake on different depth are discussed. In coastal shallow area the front of a thermal bar passes till May 15. Within June surface display of the front passes through all zones of lake (Naumenko and Karetnikov, 2000). For water of other horizons, transition through 4°C occurs to delay on the average for a week on every 10 m. In spring period the determining factor in thermal evolution is the lake morphometry (Naumenko and Karetnikov, 2002).

The lower border of a thermocline was estimated by a vertical temperature gradient. The critical value was taken less than 0.02 °C/m. The thermocline in a surface water layer is formed just after passages of vernal thermal bar within June. The lower border of thermocline falls up to 60 - 80 m, depending on morphometric zones to September - October. Temperature dispersions become less than 1 on the same depth. We believe that it is the depth of seasonal variations.

The daily mean spatial distributions of water temperature on horizons 0, 20 and 50 m, temperature and humidity of air were calculated from May 15 to November (Naumenko et al., 2000c; d). Determination factor in most dependences was over 0.7. As example we show the spatial distribution of water temperature on Fig.2 for July 15 and August 15.

The daily mean spatial distribution temperature and humidity of air are shown on Fig. 3 a,b,c,d. Spatial isochrones of spring front of thermal bar surface display in Lake Ladoga is shown on Fig. 3 e. Duration of a «biological summer» is the period, when the water temperature exceeds 10°C. It varies from four months on Volkhov Bay to one month on northern deep areas (Fig. 3 f).

The spatial distribution of monthly transparency and cloudiness were calculated from May to October. The functional representations of Lake Ladoga seasonal course of water temperature, humidity and temperature of air will be useful for computer simulation of water – air interaction and heat exchange.

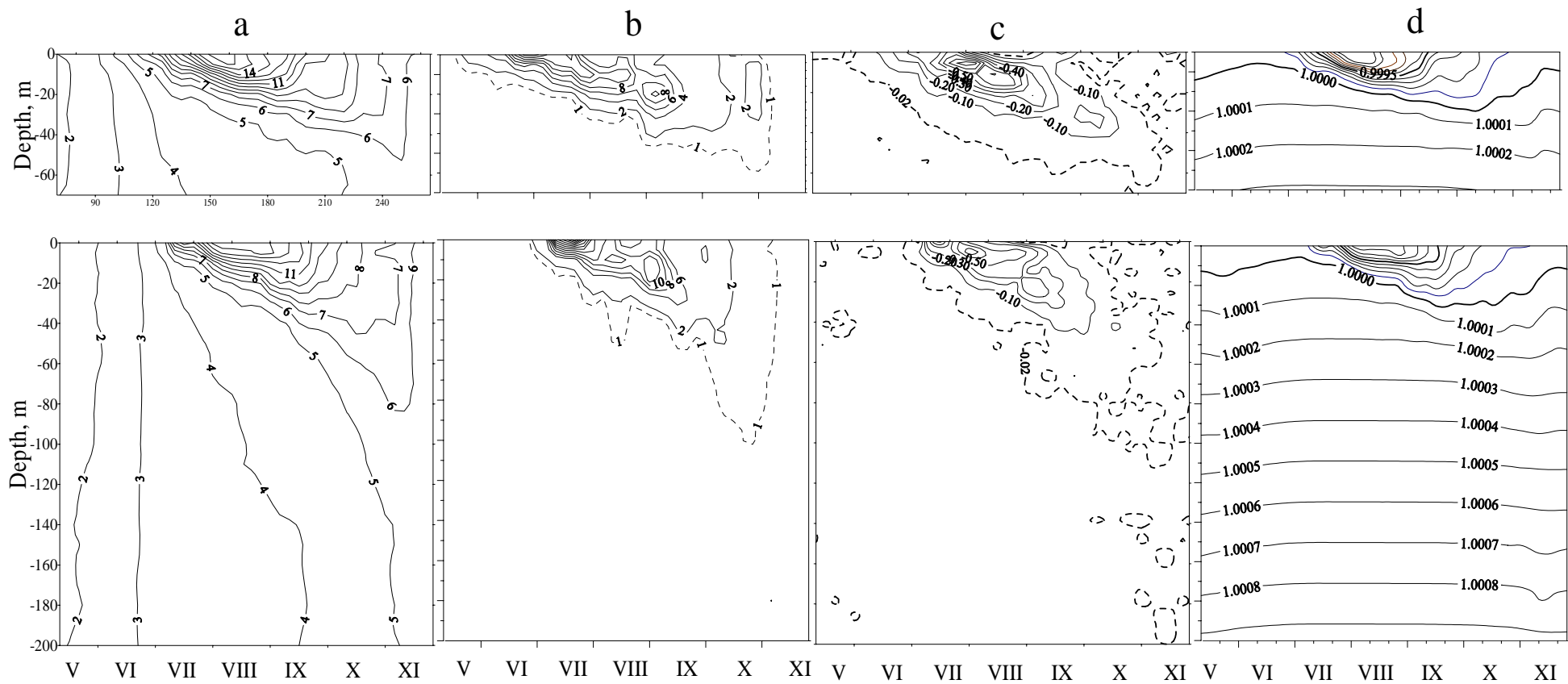


Fig.1. Seasonal evolution of water temperature (a), their dispersions (b), vertical gradients of temperature (c) and water density(d) for two morphometric zones (upper – for bottom depth 50-70 m, lower – for bottom depth more 140 m).

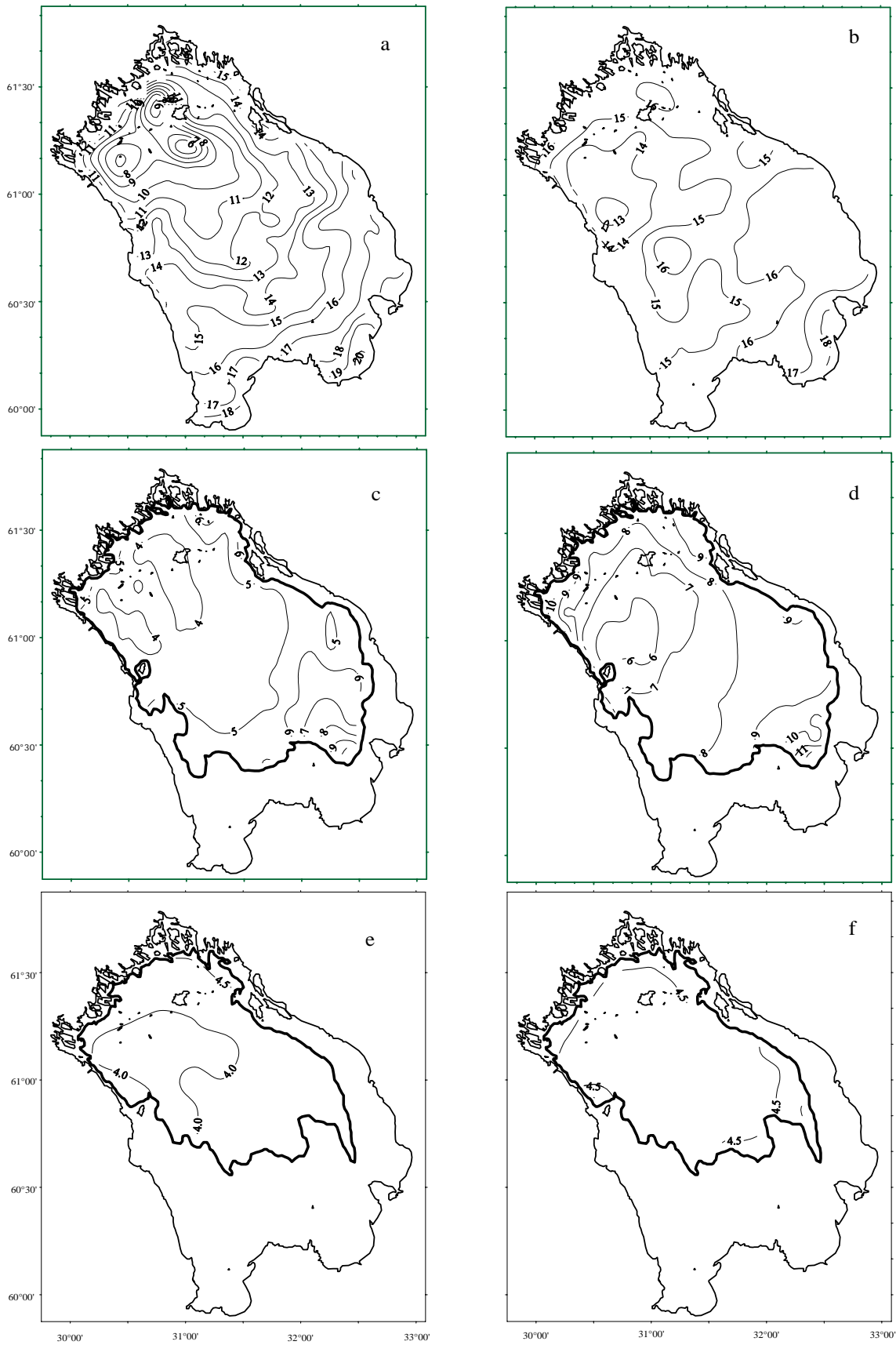


Fig. 2. Spatial distribution of water temperature on the surface (a,b), on 20 m (c,d), on 50 m (e,f) for July,15 (left) and August, 15 (right).

References

- Naumenko M, Karetnikov S., 2000. Determining role of spring thermal front on internal processes and water-air interaction in Lake Ladoga. *In Proc. of 5th workshop on physical processes in natural waters. 23-29 August 2000. Limnological Institute. Prep. №4. Irkutsk. p.16-19.*
- Naumenko M.A., Karetnikov S.G., 2002. Sezonnaya evolyutsiya prostranstvennogo raspredeleniya temperatury poverhnosti vody Ladozhskogo ozera v svyazi s ego morfometriei. *Doklady Akademii nauk*, **386**: 250-253. [Seasonal dynamics of spatial distribution of surface water temperature in Lake Ladoga in relation to the lake depth. In Russian]
- Naumenko M.A., Karetnikov S.G., Guzivaty V.V., 1998. Mean thermal pattern of Lake Ladoga: results of a database. *In Peltonen A., Huttula T. & Viljanen M. (eds). Proceedings of the workshop on numerical models - a case study of Lake Ladoga. Univ. of Joensuu. Publ. Karelian Institute. Working Papers. № 5, pp. 50-57.*
- Naumenko M, Guzivaty V., Karetnikov S., 2000a. Lake Ladoga thermal database-Institute of Limnology(IL). *In Huttula T., Peltonen A. & Filatov N. (eds). Hydrological monitoring and modelling of Lake Ladoga with recommendations for further research. University of Joensuu. Publ. of Karelian Institute. Working Papers. № 2, pp. 11-21.*
- Naumenko M, Guzivaty V., Karetnikov S. , 2000b. The thermal regions of Lake Ladoga. *In Peltonen A., Gronlund & Viljanen (eds). Proc. Third Int. Lake Ladoga Symp. 1999, University of Joensuu. Publ. of Karelian Institute. No.129. 2000. p.437-441.*
- Naumenko M, Guzivaty V., Karetnikov S. , 2000c. Spatial distribution of daily mean surface temperatures in Lake Ladoga from May to November. *In Peltonen A., Gronlund & Viljanen (eds). Proc. the Third Int. Lake Ladoga Symp.1999, University of Joensuu. Publ. of Karelian Institute. No. 129. 2000. p.442-447.*
- Naumenko M, Karetnikov S., Guzivaty V. , 2000d. Mean daily spatial surface temperature at Lake Ladoga: a new approach from thermal information-diagnostic system. *In Proc. 4th Int. Conf. on Integrating Geographic Information Systems (GIS) and Environmental Modeling (GIS/EM4) Sep.2-8, 2000. <http://www.colorado.edu/research/cires/banff/pubpapers/246/>.*
- Tikhomirov A.I., 1982. *Termika krupnykh ozer*. Nauka, Leningrad, 232 pp. [Thermal regime of large lakes. In Russian.]

Developing LANGMUIR-1 and LANGMUIR-2 – the databases for a study of Langmuir circulation

Sergey V. Ryzanin¹⁾, Peter Chu²⁾, Lev N. Karlin³⁾, Nikolay V. Kochkov¹⁾

¹⁾Institute of Limnology, Russian Academy of Sciences, Sevastyanova 9, St Petersburg, 196105, RF, Te./fax +7 812 3878020/3887327, E-mail: ryanzhin@peterlink.ru

²⁾Naval Postgraduate School, Dept. Oceanography, 1 Univ.Cir., Monterey, CA, 93943-5122, USA, Tel./fax +1 831 6563688/85, E-mail: pchu@nps.navy.mil

³⁾Russian State Hydrometeorologic University, Maloohhtinskii pr. 98, St Petersburg, 195196, RF, Tel./fax +7 812 4444163/4446090; E-mail: Klara@rshu.ru

Resulting from the atmosphere-lake (ocean) interaction, the Langmuir circulation (LC) is a system of coherent vortices producing strong mixing of the upper water layer. However, despite of its obvious significance, theoretical and experimental understanding of LC remains unsatisfactory. Moreover, no adequate parameterizations of LC mixing effects have been derived using, e.g., relatively simply accessed data on LC streak spacing (surface lateral distance between two neighbor lines of convergences) and gross hydrometeorological conditions. In addition, no reliable relationships for LC characteristics were obtained basing on the field data. One of the reasons is dispersion of field data on LC over the vast literature. Therefore, to advance LC studies and fill the above gaps two databases abbreviated as LANGMUIR-1 and LANGMUIR-2 were constructed.

LANGMUIR-1 database for relevant references was created in WinRM (Reference Manager for Windows; rm – file extension) format. The database having a size of approx. 400 Kb comprises more than 240 world references on LC publications including a couple of dozen PhD and MSc thesis and internal scientific reports. It also contains comments, abstracts, more than hundred key words for browsing and approx. 50 full electronic copies attached (Acrobat files). Available studies can be arbitrarily attributed to theoretical, field and laboratory ones (approx. 90, 140 and 10 publications respectively). Fig. 1 shows accumulated chronology of these studies starting from pioneer article (Langmuir 1938) to date. The slopes of corresponding curves are variable and several periods or stages could be indicated in dependence of prevailing theoretical explanation of LC or/and observation approach applied at a moment. In Fig. 1 they are summarized as OTC – organized thermal convection; EFI – Ekman flow instability; CLT – Craik-Leibovich theory; FLIP – field observations using r/p FLIP, and SAM – sonar acoustic field measurements. As seen from Fig. 1, despite of certain overlaps, each stage is characterized by increased number of publications. Seems Woodcock and Wyman (1947) and Tzikunov et al. (1950) initiated explanation of LC as resulted from OTC. Later, Faller (1962, 1963) to describe generation of LC pioneered EFI mechanism, initially applied to the atmospheric boundary layer. Both mechanisms looked attractive since satisfactorily described some principal LC features. However, later field data showed that OTC-mechanism does not explain generation of LC under hydrostatically stable condition and/or warming of the upper water layer. Similarly, EFI-mechanism provides much higher characteristic time of instability grows (hours) than it is observed for LC (minutes). In the middle of 70th Craik and Leibovich (1976) and Craik (1977) have suggested CLT. The theory latter developed in two modifications (CL-1 and CL-2), considers LC as resulted from non-linear interaction of shear flow in water and Stokes drift due to surface wind-waves. It should be noticed, however, that although CLT adequately describes main LC peculiarities, many problems and questions remain unsolved. Field studies of LC using merged SAM technique and steady floating research platform FLIP were initiated by Thorpe and Stubbs (1979) at Loch Ness and Weller et al. (1985) in Pacific respectively. Both approaches considerably enlarged knowledge on LC scales and structure and are currently in a progress.

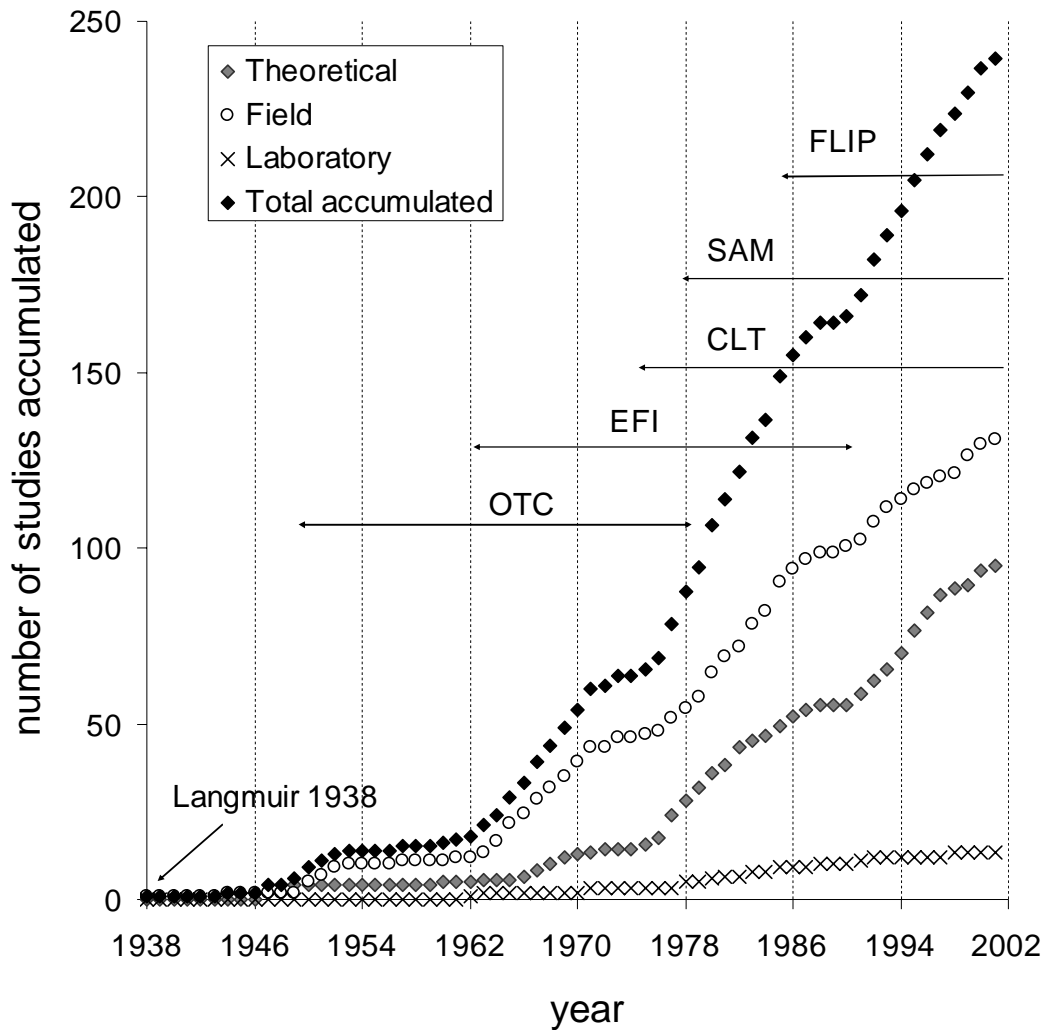


Fig. 1. Chronology of accumulated theoretical, field and laboratory studies of Langmuir circulation published from pioneer article (Langmuir 1938) to date. Approximate stages of theoretical and field studies are: OTC – organized thermal convection; EFI – Ekman flow instability; CLT – Craik-Leibovich theory; FLIP – observations using r/p FLIP; SAM – sonar acoustic measurements.

LANGMUIR-2 database. LC streak spacing is relatively simply and reliably measured LC characteristic. Relevant field measurements were carried out in western Atlantic, eastern Pacific (mainly off California), Gulf of Mexico, Sargasso, Nordic, Black, Baltic, Laptev, Wadden, White, and Bering Seas and such lakes as George (New York), Ontario, Huron, Oneida (New York), Mendota (Wisconsin), Lake-of-the-Wood (Canada/USA), Loch Ness (Scotland), Russian lakes Ladoga, Onega, Vuoksa, Punnus-jarvi (Russian Karelia), reservoirs Eglwys Nynydd (Wales, UK), Klyazma and Mozhaysk (Russia) and others. Brief review of some of these observations was given in (Ryanzhin 1994, 1999) and their geographical distribution is shown in Fig. 2. However, relevant field data remain dispersed over the vast literature accumulated in the above-described LANGMUIR-1 database. The LANGMUIR-2 database (4.4 Mb, Excel files) was developed to combine these dispersed data and study relationships for streak spacing. The database includes more than 1000 rows of records and comprises literature field data on original sets (sequences) of streak spacing and gross hydrometeorological and hydrographic conditions measured. The latter include geographical co-ordinates, salinity, wind speed, direction and surface stress, surface wind-waves characteristics, air temperature and humidity, surface heat and buoyancy fluxes, water and/or the upper mixed layer depth, thermocline breadth, water temperature profiles, buoyancy

frequency, etc. In addition, authors' published (Ryanzhin 1982, 1994, 1999) and unpublished data obtained from the Baltic and Black Seas, lakes Ladoga and Punnus-jarvi were included into LANGMUIR-2. The database contains originally measured spacing sets and statistical estimates (average, standard deviation, skewness, kurtosis, distribution function, mode and median of distribution, spectrum, etc.) already published, calculated or recalculated from literature by the authors.

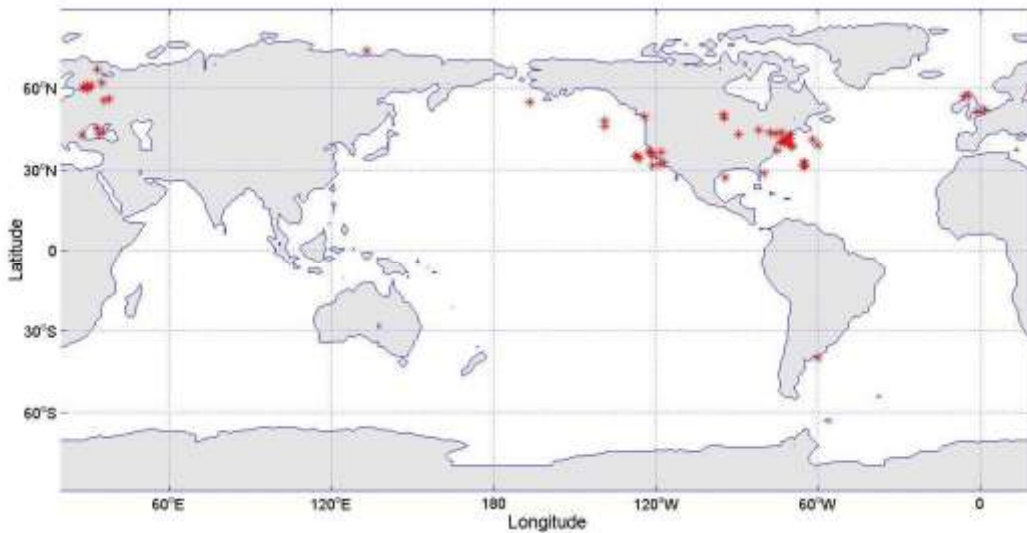


Fig. 2. Worldwide geographical distribution of field studies of LC streaks accumulated in LANGMUIR-2 database.

The study of SR, LK and NK was partly supported by Russian Foundation for Basic Research (grant 01-05-64049).

References

- Craik A.D.D. 1977. The generation of Langmuir circulations by an instability mechanism, *J. Fluid Mech.*, 81 (p2): 209-223, 1977.
- Craik A.D.D. and Leibovich S. 1976. A rational model for Langmuir circulations, *J. Fluid Mech.*, 73 (3): 401-426.
- Faller A.J. 1962. The instability of Ekman boundary layer flow and its application as a possible explanation of Langmuir circulation cells in the ocean, *J. Geophys. Res.*, 67 (9): 3556.
- Faller A.J. 1963. An experimental study of instability of the laminar Ekman boundary layer, *J. Fluid Mech.*, 15 (4): 560-576.
- Langmuir I. 1938. Surface motion of water induced by wind, *Science*, 87 (2250): 119-123.
- Ryanzhin S.V. 1982. Transverse dimensions of Langmuir circulation cells in a lake in the absence of a thermocline, *Izvest. Atmos. Oceanic Phys. (USSR)*, 18 (10): 814-820.
- Ryanzhin S.V. 1994. How do dispersions of Langmuir circulation spacings and their average values correlate? *Dokl. (Trans.) Acad. Sci. (Russia)*, 336 (5): 692-696 (In Russian; translated into English as: Relationship between the variance and the average transverse dimensions of Langmuir circulation cells, *Trans. Doklady-Russian Acad.Sci.: Earth Science Section*, 338 (7): 22-27
- Ryanzhin S.V. 1999. Langmuir circulation, In: (eds.) K.Ya.Kondratyev and N.N.Filatov, *Limnology and Remote Sensing: Contemporary Approach*, London-Berlin: Springer-Praxis, 90-98 pp.

Tzikunov V.A., Rzheplinskii G.V., and Brovikov I.S. 1950. On the lateral circulations in wind currents, *Trudy (Proc.) GOIN (Russia)*, 16 (28): 40-49 (in Russian).

Thorpe S.A. and Stubbs A.R. 1979. Bubbles in a freshwater lake, *Nature*, 279 (5712): 403-405.

Weller R.A., Dean P.Jr, Marra J., Price J.F., Francis E.A., and Boardman D.C. 1985. Three-dimensional flow in the upper ocean, *Science*, 227: 1552-1556.

Woodcock A.H. and Wyman J. 1947. Convective motion in air over the sea, *Ann. New York Acad. Sci.*, 48 (8): 749-776.

Selected statistics calculated for streak spacing of Langmuir circulation measured in natural waters

Sergey Ryzanin¹⁾, Peter Chu²⁾

¹⁾Institute of Limnology, Russian Academy of Sciences, Sevastyanova 9, St Petersburg, 196105, RF,
Tel./fax +7 812 3878020/3887327, E-mail: ryzanin@peterlink.ru

²⁾Naval Postgraduate School, Dept. Oceanography, 1 Univ.Cir., Monterey, CA, 93943-5122, USA,
Tel./fax +1 831 6563688/85, E-mail: pchu@nps.navy.mil

To memory of Prof. Alexander
Ivanovich Duvanin is dedicated

Introduction

Streak spacing L (lateral distance between two neighbor convergence lines at the surface) is the most reliably measured characteristic of Langmuir circulation (LC). However, in natural waters L values often reveal high spatial-temporal variability even under relatively steady gross hydrometeorological and hydrographic conditions (such as wind speed V and direction, wind-wave parameters, mixed layer or/and water depth, surface buoyancy flux, etc.). In addition, sometimes at least two distinguish scales marked with “main” (or “primary”) and “secondary” streaks as well as group structures consisting of different number of cells can be clearly seen in LC (Ryzanin 1982). As an example of spacing variability, Fig. 1 and 2 demonstrate set (sequence) and corresponding distribution of 124 streak spacing measured in Lake Ladoga (Russia) under water homogeneity and cooling. Therefore, to study variability of LC spacing an application of stochastic methods should be productive and relevant.

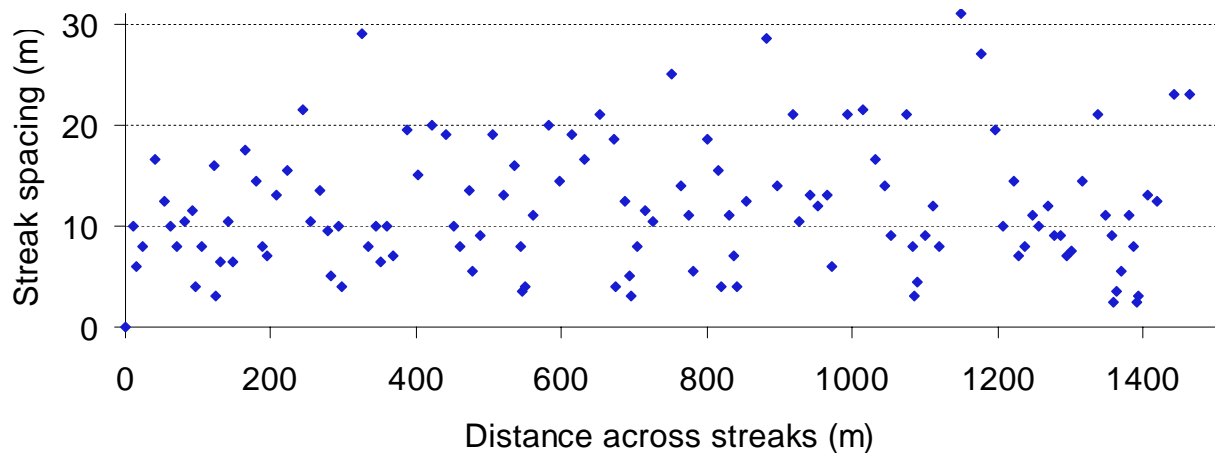


Fig. 1. Example of set (sequence) of 124 measured streak spacing. Set#18.1, Lake Ladoga, 1027-1037 8 Sep 1984, water depth 8.0-8.5m, bottom slope $1.4-2.1 \times 10^{-4}$, thermal homogeneity and cooling, wind speed $V=7.6\text{m/s}$, surface water and air temperature $T_w=12.8^\circ\text{C}$, $T_a=9.6^\circ\text{C}$, surface heat flux $Q=-14\text{W/m}^2$, wave height 0.6m and period 2.5 sec.

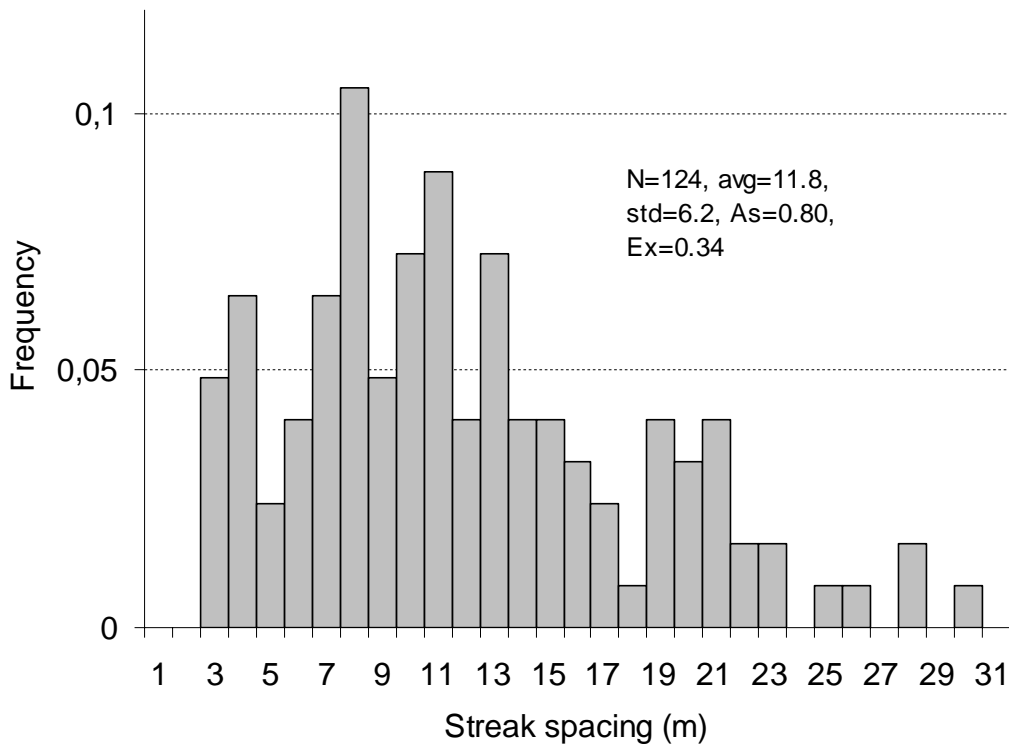


Fig. 2. Distribution of 124 LC streak spacing at Lake Ladoga shown in Fig. 1. Set#18.1, 1027-1037 8 Sep 1984, water depth 8.0-8.5m, bottom slope $1.4-2.1 \times 10^{-4}$, thermal homogeneity and cooling, wind speed $V=7.6\text{m/s}$, surface water and air temperature $T_w=12.8^\circ\text{C}$, $T_a=9.6^\circ\text{C}$ respectively, surface heat flux $Q=-14\text{W/m}^2$, wave height 0.6m and period 2.5 sec.

State-of-the-Art

Despite many workers measured streak spacing, only few statistical features were numerically established so far (see brief reviews Ryanzhin 1994; 1999). Kenney (1977) tested five sets of L (from 270 to 607 spacing each) measured at shallow water in Lake-of-the-Woods (Canada/USA). He concluded that their distribution to be lognormal with some deviation for both large and small L values "tails". Similar distribution suggests generation of surface convergences of LC at random times and locations on the surface. Latter, Csanady (1994) also suggested log-normality for LC spacing. Ryanzhin (1982) χ^2 -tested six sets of spacing (several hundred spacing each) obtained from off- and near- shore Lake Ladoga for uniform, normal, lognormal, Maxwell-, Raleigh- and γ -distributions. He concluded that Raleigh and γ - distributions gave the best fitting. It should be underlined, however, that all distributions of L published in (Myer 1969; Kenney 1977; Thorpe and Hall 1982; Ryanzhin 1982; see also Fig. 2) reveal both positive skewness (As) and kurtosis (Ex) values. Ryanzhin (1994) treated coefficient of variance $K_{var}=\text{std}/\text{avg}$ calculated from more than 150 sets of LC spacing obtained from Atlantic (McLeish 1968; Myer 1969), Lake-of-the-Woods (Kenney 1977), Loch Ness (Thorpe and Hall 1982), Baltic Sea (Dmitrieva and Ryanzhin 1976), Lake Ladoga (Ryanzhin 1982), Black Sea and Punnus-jarvi (author's unpublished). It was found that distribution of K_{var} varying from 0,34 (Black Sea, Lake-of-the-Woods) to 0,71 (Lake Ladoga) gives the mode $Mo=0,45$ and global average value $\text{avg}=0,51$. In addition, strong positive correlation ($0,85 \pm 0,05$) between avg and std was established as $\text{avg}=C_1 \cdot \text{std}$, where $C_1=0,54 \pm 0,06$ is calculated dimensionless regression coefficient. Similar strong regression at $C_1=0,50 \pm 0,03$ was

derived also for both dimensionless avg and std values when wind-wave length scale V^2/g was taken for scaling (Ryanzhin 1994; 1999).

Statistics calculated

Some new statistics calculated for *LC* spacing using relevant field data accumulated in LANGMUIR-2 database (Ryanzhin et al. 2003) are given below and shown in Fig. 3 and 4. First, updated distribution of K_{var} comparing with given in (Ryanzhin 1994, 1999), was calculated using additional data sets obtained from Atlantic (Ichiye et al. 1985), Pacific (Zedel and Farmer 1992), L.Huron (Csanady and Pade 1969), Lake Ladoga (unpublished). This distribution (Fig. 3) varying from 0,12 to 0,85 (Lake Ladoga) is characterized with average $avg=0,50$ and expressed mode $Mo=0,49$ values. Notice, that these estimates are close to those derived in (Ryanzhin 1994).

Values of skewness As and kurtosis Ex were calculated for 94 original sets of spacing measured in Lake Ladoga (Ryanzhin 1982; unpublished) under different hydrometeorological conditions. Original sets are similar to shown in Fig. 1. These data were expanded by adding with one and three pair of As and Ex values taken in Atlantic (Ichiye et al. 1985) and Pacific (Zedel and Farmer 1991) respectively. Then, distributions and corresponding statistics were calculated (Fig. 4). It should be underlined that no negative values of As and Ex were found. However, both statistics vary within wide ranges. For example, As values having $avg=1,90$ and $std=2,35$ vary from 0,23 to 13,97 (both extremes at Lake Ladoga). Distribution of As values reveals high positive skewness and kurtosis and demonstrates expressed mode at 1,05 (Fig. 4). Similar features are seen in distribution of Ex values (Fig. 4). However, in comparison with As , distribution of Ex demonstrates higher values of $avg=3,53$ and $std=4,19$ at lower skewness, kurtosis and range of variation (from 0,23 to 13,97; both extremes at Lake Ladoga). It should be pointed out that similar to As , distribution of Ex gives the mode close to 1 ($Mo=0,97$; Fig. 3).

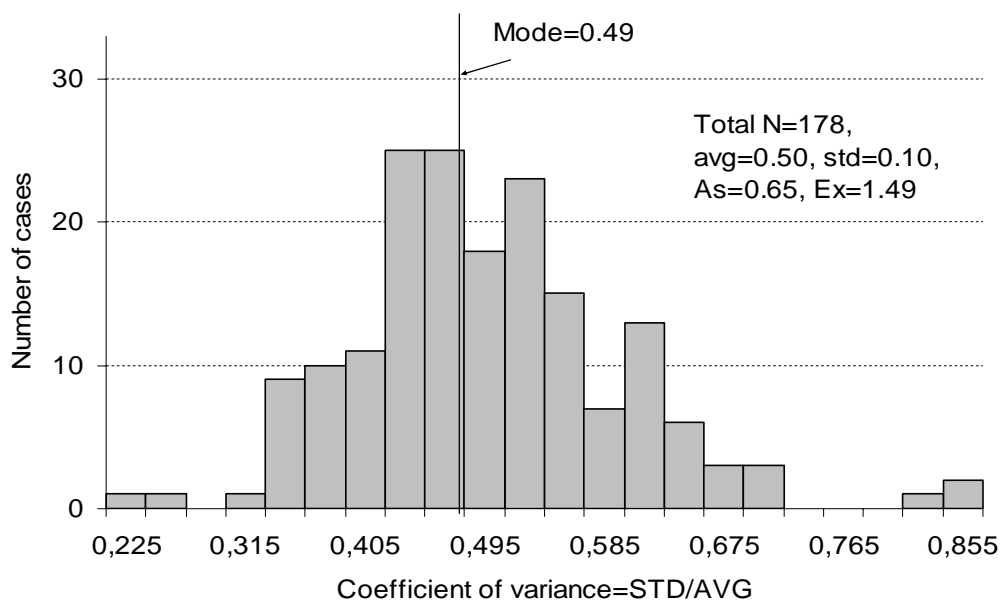


Figure 2. Distribution and corresponding statistics of variance coefficient $K_{var}=std/avg$ of *LC* spacing. N is total number of observations analyzed; avg , std , As , Ex and Mo is average, standard deviation, skewness, kurtosis and mode of distribution respectively. Original field data were obtained from Atlantic (McLeish 1968; Myer 1969; Ichiye et al. 1985), Pacific (Zedel and Farmer 1992), Gulf of Finland (Dmitrieva and Ryanzhin 1976), Black Sea (Ryanzhin 1994), Lake Huron (Csanady and Pade 1969), Lake Ladoga (Ryanzhin 1982; unpublished), Lake-of-the-Woods (Kenney 1977), Loch Ness (Thorpe and Hall 1982), Punnus-jarvi (Ryanzhin 1994).

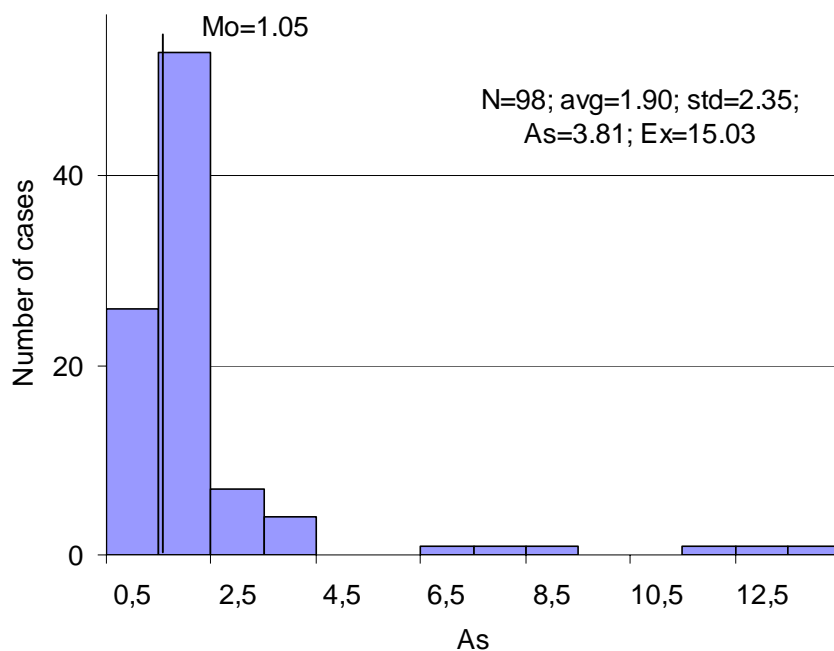
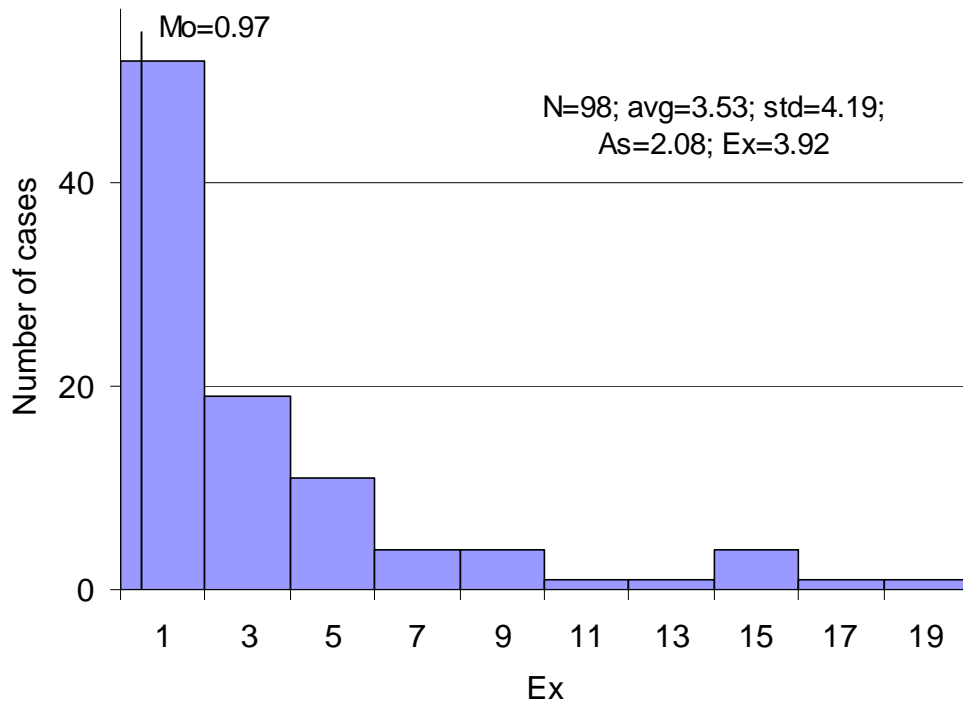


Figure 4. Distributions and corresponding statistics of kurtosis Ex and skewness As values for LC spacing. N is total number of observations analyzed; avg , std , As , Ex and Mo is average, standard deviation, skewness, kurtosis and mode of distributions respectively. Original field data were obtained from L.Ladoga (Ryanzhin 1982; unpublished), with addition of one value from Atlantic (Ichiye et al. 1985) and three values from Pacific (Zedel and Farmer 1991).

Conclusions

Thus, following conclusions can be formulated. First, despite of high variability of statistics calculated some dominating (mode) values can be seen in functions of distribution (0,49; 1,05 and

0,97 for K_{var} , A_s and E_x respectively). Second, since values of skewness and kurtosis widely vary, the application of functions of distribution with constant A_s and E_x values (such as Raleigh, Maxwell, etc.) to describe distribution of LC spacing looks at least highly restricted.

Acknowledgments

Professor Alexander Ivanovich Duvanin (Department of Oceanology, Moscow State University) passed us away in October 9, 2002. For a long time Prof. Duvanin endorsed, inspired and supported doctoral students and young scientists who wished to study LC. We dedicate the present study to his memory.

The study was partly supported (SR) by Russian Foundation for Basic Research (grant 01-05-64049).

References

- Csanady G.T. 1994. Vortex pair model of Langmuir circulation, *J. Marine Res.* 52 (4): 559-581.
- Csanady G.T. and Pade B. 1969. Windrow observations, Rept. Dynamics and Diffusion in the Great Lakes, Waterloo, Ontario: University Waterloo, Dept. Mech. Engin., 23-38.
- Dmitrieva A.A. and Ryanzhin S.V. 1976. Hydrometeorological conditions for occurrence of Langmuir circulation, *Vestnik Leningrad State University (USSR)* 18 (3): 110-117, (in Russian).
- Ichiye T., McGrath J.R., and Howard M. 1985. Some dynamic features of Langmuir circulation, *In* (eds.) Y.Toba and H.Mitsuyasu, *The Ocean Surface: Wave Breaking, Turbulent Mixing and Radio Probing*, Dordrecht, Reidel Publ., p. 479-486.
- Kenney B.C. 1977. *An Experimental Investigation of the Fluctuating Currents Responsible for the Generation of Windrows*, PhD thesis, Waterloo University, Waterloo, Ontario, 163 pp.
- McLeish W.L. 1968. On the mechanisms of wind-slick generation, *J. Deep-Sea Res.* 15 (4): 461-469.
- Myer G.E. 1969. A field study of Langmuir circulations, *In Proc. 12th Confer. Great Lakes Res.*, Ann Arbor, Michigan, 652-663.
- Ryanzhin S.V. 1982. Transverse dimensions of Langmuir circulation cells in a lake in the absence of a thermocline, *Izvest. Atmos. Oceanic Phys. (USSR)*, 18 (10): 814-820.
- Ryanzhin S.V. 1994. How do dispersions of Langmuir circulation spacings and their average values correlate? *Dokl. (Trans.) Acad. Sci. (Russia)*, 336 (5): 692-696 (In Russian; translated into English as: Relationship between the variance and the average transverse dimensions of Langmuir circulation cells, *Trans. Doklady-Russian Acad.Sci.: Earth Science Section*, 338 (7): 22-27
- Ryanzhin S.V. 1999. Langmuir circulation, *In* (eds.) K.Ya.Kondratyev and N.N.Filatov, *Limnology and Remote Sensing: Contemporary Approach*, London-Berlin: Springer-Praxis, 90-98 pp.
- Ryanzhin S.V., Chu P., Karlin L.N., Kochkov N.V. 2003. Developing LANGMUIR-1 and LANGMUIR-2 – the databases for a study of Langmuir circulation, (present Proceedings)
- Thorpe S.A. and Hall A.J. 1982. Observation of the thermal structure of Langmuir circulation, *J. Fluid Mech.* 114: 237-250.
- Zedel L. and Farmer D.M. 1991. Organized structures in subsurface bubble clouds: Langmuir circulation in the open ocean, *J. Geophys. Res.* 96 (D): 8889-8900.

The effect of the bottom boundary on diapycnal mixing

Alfred Wüest, Andreas Lorke and Michael Schurter

Applied Aquatic Ecology, Limnological Research Center, EAWAG, CH-6047 Kastanienbaum,
Switzerland

Abstract. Tracers released into the pelagic, stratified center of lakes, show that interior mixing – based on both mode-related internal shear and higher-frequency internal waves – is extremely weak. After horizontal spreading, the tracers “feel” the local bottom boundaries (BBL) and the basin-scale diapycnal (vertical) mixing increases by more than one order of magnitude. Balancing kinetic energy and dissipation reveals that the observed internal energetics and mixing can be explained by classical bottom friction of the basin-scale (seiches) or inertial currents alone, without relying on further processes. The assumption that the buoyancy flux is generated within the BBL and diffusively intrudes into the interior is compatible with the observed tracer residence time scale in the interior. Within enclosed water bodies of limited extent, the BBL structure is modified due to the strong periodicity (typically several hours to days) of the near-bottom currents. This Stokes solution-like behavior (of the oscillating currents) can also be expected to be important in estuaries and ocean subbasins, where the 12 and 24-hours periodicity is relevant. (This article is from the recent Aha Huliko’a 2003 workshop and published in the proceedings).

Introduction

The intensity and spatial structure of diapycnal diffusivity and upwelling are fundamental for abyssal renewal and ocean thermohaline stratification. In a steady-state ocean the stratification below the outcropping density surfaces is given by the competition between upwelling, $w \cdot \rho$, and the vertical diffusive flux, $-K \cdot \partial \rho / \partial z$ (Munk, 1966; Munk and Wunsch, 1998). Inverse modeling or fitting the Munk model to measured profiles of water properties provides estimates of diapycnal diffusivity in the range of the canonical value of $1 \text{ cm}^2 \text{ s}^{-1}$. It is important to realize that such tracers are averaging processes over the entire basin and therefore capture the large-scale property distributions.

In contrast, by using microstructure profilers we are able to observe turbulence and mixing directly, although only in the limited volume which is sampled by the profiler. Despite the large number of microstructure observations in the 70’s and 80’s (Osborn and Cox, 1972; Gregg and Sanford, 1988; Moum 1996), the canonical diffusivity has remained a puzzle: In fact, microstructure-based diffusivities were found to be $O(0.1 \text{ cm}^2 \text{ s}^{-1})$, which is an order of magnitude smaller than the canonical value (Gregg, 1987; Davis, 1994). This led to disputes over the potential of microstructure profilers to preferentially sense low-turbulence in the pelagic interior ocean, thus not being representative for basin-scale tracer diffusivity. In addition, the microstructure technique has been criticized for a number of methodological reasons.

This discrepancy urgently called in the late 80’s for the well-known validation experiments by Ledwell et al. (1993, 1995, 1998 and 2000). In addition, further comparison experiments were carried out in lakes (Wüest et al., 2000). In contrast to the ocean, lakes have several advantages: Enclosed water bodies of manageable basin-scales allow the balancing of several water properties (such as temperature, density or geochemical constituents). Due to their limited size, a number of processes, particularly the contribution of mixing in the bottom boundary layer (BBL), can be studied comparably easily.

This contribution summarizes some of the peculiarities of the BBL in lakes and specifically examines its contribution to (overall) basin-scale diapycnal mixing. We show that insights into the BBL processes are important prerequisites for understanding the mechanisms of turbulent diapycnal diffusivity in lakes. Specifics about stratification in lakes

The stratification in lakes

The seasonally stratified water body in lakes (called hypolimnion) is quite different from the interior of the ocean. The stratification of the upper lacustrine thermocline is stronger and suppresses turbulence more efficiently than in the ocean. Subsequently, turbulent mixing is weak and eddy length (Thorpe) scales are short (Lorke and Wüest, 2002). In contrast, the stratification in deep water is usually weaker than in the ocean, leading to diapycnal diffusivities as large as the canonical value. In general, the variability of the water column stability in lakes is huge and can reach up to nine orders of magnitude: $N^2 \approx 10^{-10}$ to 10^{-1} s^{-2} .

In particular, internal waves and basin-scale motions are omnipresent and usually forced by wind (Imberger, 1998). Although many mechanisms of forcing are possible, it is mainly the setup of the thermocline that couples wind momentum most efficiently into the lake interior. In general, the response of the thermocline to an imposed wind stress is a complex function of geometry, stratification and the temporal dynamics of the wind forcing. For simply-shaped and small-to-medium-sized lakes, modal-type responses are usually observed (Stevens & Imberger, 1996; Antenucci et al., 2000).

For diapycnal mixing, the currents, vertical displacements and associated shear related to internal (baroclinic) motions are most important. From the fact that about 3% of the wind energy flux from the atmosphere ends up in the hypolimnion (Wüest et al., 2000), we can roughly estimate the mechanical energy content in the stratified interior. The level of excitation is typically $\sim 1 \text{ J m}^{-3}$, corresponding to from several J m^{-2} in shallow lakes (Gloor et al., 2000) to almost 1000 J m^{-2} in the deepest lakes (Ravens et al., 2000). Given that typical energy residence time scales are days (shallow lakes) to ~ 1.5 months (deepest lakes), the dissipation rate ϵ of the internal energy is $\sim 10^{-8}$ (shallow lakes) to $\sim 10^{-10} \text{ W kg}^{-1}$ (deepest lakes). These energy transformation rates and the modes of decay of the mechanical energy are crucial for the stratification and mixing in the interior. An important observation is that most of the internal wave energy is contained in the basin-scale waves and currents (Imberger, 1998). Of those, the inertial currents and the seiche are the most important energy reservoirs (Wüest and Lorke, 2003).

In the following sections we demonstrate how these basin-scale currents affect diapycnal mixing in enclosed water bodies of limited extent.

Dominance of BBL versus interior mixing

The basin-scale currents contain much more shear in the BBL than in the interior. This is a well-known result from the analysis of the modal structure of the internal seiches (Fricker and Nepf, 2000). The cause of the unexpected level of apparent turbulent diffusivity in lakes, given the very large Richardson numbers in their thermoclines, has therefore remained unexplained (Imberger and Ivey, 1991).

Evidence for the dominance of BBL versus interior turbulence was provided by a series of tracer experiments in lakes and deep enclosed ocean sub-basins. Carefully designed experiments using Uranin, a fluorescent artificial tracer, released into the interior of the hypolimnion of Lake Alpnach (a medium-sized Swiss lake) clearly revealed the existence of two different types of mixing regimes: slow mixing ($K_z \approx 10^{-3} \text{ cm}^2 \text{ s}^{-1}$) within the stratified interior of the lake and enhanced mixing ($K_z \approx 10^{-1} \text{ cm}^2 \text{ s}^{-1}$) within the BBL of a few meters height (Goudsmit et al., 1997).

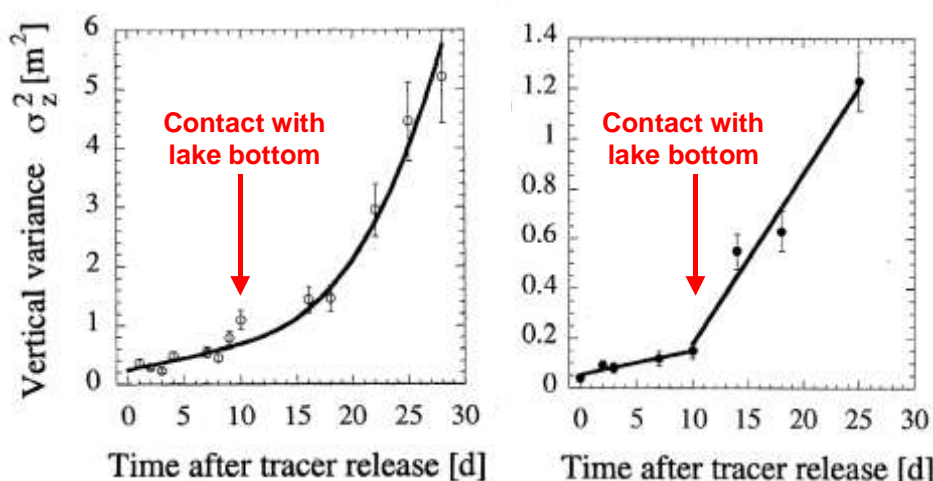


Figure 1. Two examples of vertical spreading of the dye tracer, released into the interior of the hypolimnion of Lake Alpnach in June 1995: After approximately ten days, the dye reached the BBL at the sides of the basin (arrows). The arrows indicate the drastic increase of the diffusion rate by at least a factor of ten caused by the transition from the interior to the entire basin (including the BBL). Details in Goudsmit et al. (1997).

The turbulent diffusivities inferred from the 2nd moment ($K = \frac{1}{2} \partial \sigma^2(t) / \partial t$) of the vertical tracer distribution agreed perfectly with diffusivity estimates based on heat budgeting, which was performed as a control (Goudsmit et al., 1997). These experiments proved that the basin-scale buoyancy flux [left side in Eq. (1)] can be interpreted as a superposition of mixing in the interior and mixing in the BBL (right side of Eq. (1)). Expressed by the Osborn (1980) relation

$$K_{\varepsilon}(z)N^2 = \gamma_{\text{mix}} \varepsilon(z) \quad (1)$$

implies that ε is the sum of interior and BBL energy dissipation per kg of water at the respective depth (γ_{mix} is the mixing efficiency ~ 0.15).

On a much larger scale, a comparison between microstructure and “naturally” occurring tracers (i.e., already available in the lake water) in Lake Baikal revealed, again, that the basin-scale diffusivity is a superposition of contributions from the interior and from the BBL. Whereas the interior turbulence dominates in the upper thermocline (large volume per sediment area), the BBL turbulence is superior in the deeper layers (large sediment area per water volume).

Experiments by Ledwell and Hickey (1995) and Ledwell and Bratkovich (1995) in deep enclosed sub-basins of limited size led to similar conclusions. Tracer inserted into the interior of the Santa Monica Basin and Santa Cruz Basin showed slow vertical spreading ($K_z \approx 0.25$ and $1 \text{ cm}^2 \text{ s}^{-1}$, respectively) as long as the tracer resided in the interior and increased by an order of magnitude to 1.3 and $10 \text{ cm}^2 \text{ s}^{-1}$, respectively, as the BBL became involved.

Enhanced mixing at the boundaries is manifested by the observation of well-mixed BBLs with typical heights of a few to dozens of meters in lakes (Fig. 2) and many dozens of meters in the ocean (Fig. 6). However, the near boundary stratification is not only determined by the generation of turbulent kinetic energy (TKE), but also by the rate of release of dissolved ions (salt) from the sediment surface (consumption of TKE). The ion flux from the sediment stems from the decomposition of organic matter, which is previously synthesized by primary production in the upper water column (Wüest and Gloor, 1998). For highly productive waters with low levels of kinetic energy, the redissolution of ions from the sediment can lead to strong density stratification within the BBL, which in turn suppresses turbulent mixing.

The overall effect of the two counteracting processes – turbulent mixing within the BBL and re-dissolution of ions – define the vertical extent of the well-mixed BBL. Conceptually, its height is related to a modified Monin-Obukhov length, which is determined by the generation of TKE and the buoyancy flux from the sediment ion flux.

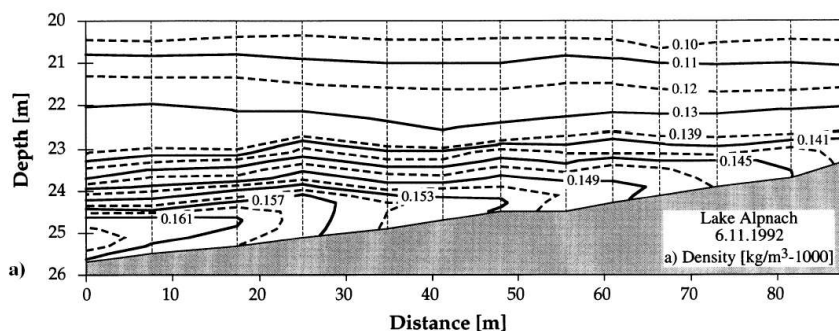


Fig. 2. A snapshot of the isopycnals, determined from eleven CTD casts (collected within a few minutes) in November 1992, in the stratified water column of Lake Alpnach (max depth: 34 m). In the lower section, the BBL is thicker and unstably stratified (Peeters et al., 1997)

Oscillatory boundary layers and straining-induced mixing

Usually, it is assumed that the balance between shear production and dissipation of TKE in the BBL is in a “quasi” steady-state with the forcing currents, which leads to the well-known logarithmic velocity structure and the *law-of-the-wall* dissipation profile. However, in lakes this

balance is mostly unjustified for two reasons: Firstly, in low-energetic systems the turbulence can fade, especially under the mentioned ion flux from the sediment. Secondly and more importantly, due to a pronounced periodic forcing, resulting from basin-scale internal currents (seiches), the structure and dynamics of a turbulent BBL can deviate significantly from the steady-state *law-of-the-wall*. Measurements and k- ϵ turbulence modeling of Lorke et al. (2002) in Lake Alpnach - for a seiching period of 24 hours - showed that the *law-of-the-wall* scaling is restricted to the lowest 0.5 m from the sediment. Above, Stokes' solution for an oscillatory boundary layer applies, leading to a distinct maximum of the current speed at a height of a few meters above the bottom (Figure 3). In this particular case of Lake Alpnach, the divergence of TKE resulted in a phase lag between the current velocity and the turbulent dissipation of 1.5 hours. Because the phase lag and the profile distortion have been shown to also depend on the energy level (Baumert and Radach, 1992; Mellor, 2002), it is expected that the effect of the periodicity is reduced for tidal flows.

Straining-induced convection can be an additional source of TKE, whenever the isopycnals are not parallel to the local bottom. An exemplification of this mechanism is tidal straining in the regions of freshwater influence (Simpson, 1997). There, the isopycnals are nearly vertical on average and the depth-varying and oscillating tidal currents create alternating stable and unstable stratification, resulting in periods of strong and weak turbulent mixing (Rippeth et al., 2001; Fig. 4a).

An angle between the current velocity and the isopycnal surfaces can also occur above a sloping bottom (Fig. 2) or in the presence of baroclinic motions (Fig. 3) or by a combination of both (Figure 4). This can result in straining-induced convection analogous to tidal straining, as described above (Fig. 4a). The data shown in Figures 2 and 3 were measured independently in the same lake, and both Figures unambiguously reveal the unstable stratification within the BBL. The convective layer is restricted to depth intervals with strong vertical gradients of the current speed, and hence to the vertical extent of the BBL (Fig. 3). During the reversed currents, the opposite effect will stabilize the stratification and thereby suppress turbulent mixing.

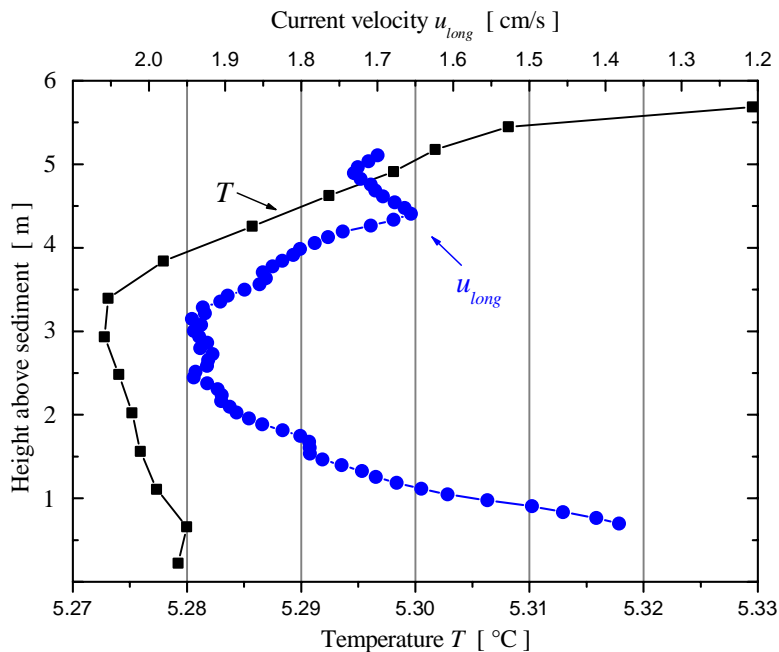


Fig. 3. The Stokes' solution-type current profile within a few meters above the sediment with the characteristic maximum at 3 m. The temperature reveals the straining-induced instability in the BBL (Figure 4b). Details in Lorke et al. (2002).

Interior intrusions from sloping bottoms

So far we have convincingly shown - and this is manifested by CTD profiles again and again - that turbulent mixing in stratified lakes is enhanced above the sediment (MacIntyre et al., 1999).

As Fig. 2 indicates, subsequent well-mixed BBLs build-up not only in the deepest layers, but also along the slopes. This is most relevant for the diapycnal fluxes. One of the key questions is therefore an intrinsic one: “How is the enhanced mixing in the BBL communicated into the interior of the stratified water, and how effective is the turbulence in the BBL for the overall basin-scale buoyancy flux?”

The buoyancy flux provides an option for relating the turbulence in the BBL to basin-scale diffusivity. Balancing the buoyancy flux, generated by intrusions of BBL water into the interior [left side of (2)], with the basin-scale buoyancy flux [right side of (2)] leads to:

$$g \cdot \langle w' \Delta \rho / \rho \rangle = K \cdot N^2 \quad (2)$$

The rate of water intrusion (expressed as upwelling velocity $w' = Q_{ex} \cdot A^{-1}$; symbols in Fig. 5) is subsequently $w' = K \cdot N^2 \cdot (g \cdot \Delta \rho / \rho)^{-1}$, where K ($\sim 0.035 \text{ cm}^2 \text{ s}^{-1}$) and N^2 ($\sim 4.5 \cdot 10^{-4} \text{ s}^{-2}$) are the basin-scale diapycnal diffusivity and stability, respectively, $g = 9.81 \text{ m s}^{-2}$ and $\Delta \rho / \rho$ ($\sim 10 \cdot 10^{-6}$; Figure 2) is the horizontal density step through the BBL. This “tertiary circulation” (Garrett, 1991) corresponds to an upwelling in the interior with $w' \approx 1.4 \text{ m d}^{-1}$ for the values given in parentheses, which are representative for this discussed case of Lake Alpnach (Fig. 5; Wüest et al., 2000). As the stratified volume of the lake has a mean depth of 18 m, the residence time of the interior water in the hypolimnion ($V_{Interior}$) is therefore $18 \text{ m} / w' = 13 \text{ days}$. The residence time in the BBL volume is much shorter, since V_{BBL} is a small part of the entire hypolimnion. Assuming a BBL thickness of 1 m (Figure 2) yields a volume ratio of 1/18. Correspondingly, the residence time in V_{BBL} is only $13 \text{ d} / 18 = 17 \text{ hours}$.

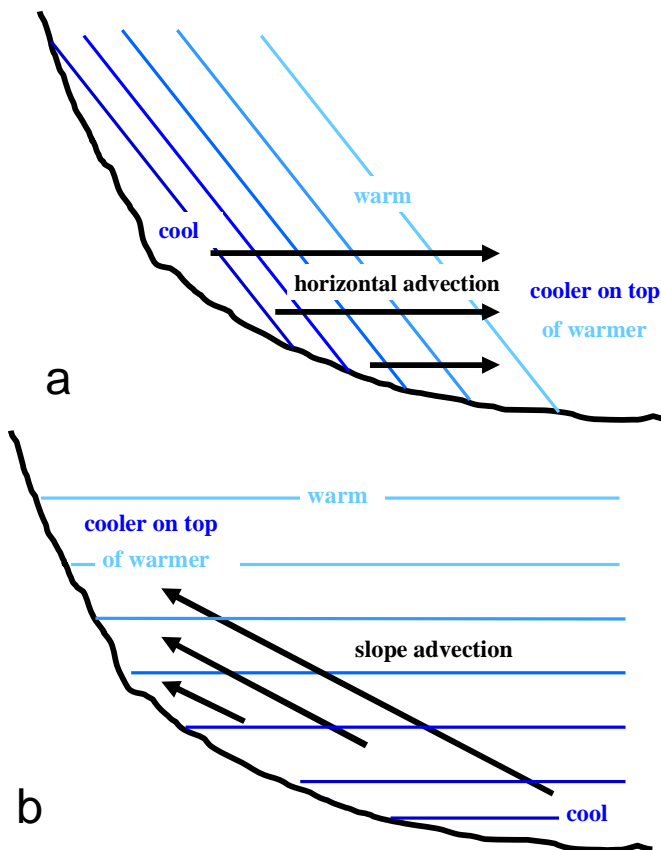


Fig. 4. Schematics of two generation mechanisms for straining-induced instabilities by moving cooler water on top of warmer water: (a) Tilted isopycnals in a vertical current structure and (b) Horizontal isopycnals in an upslope parallel current. The case (b) is the relevant mechanism for the instable BBLs of Figs. 2 and 3.

This time scale is indeed approximately the period of the dominant seiche (second vertical mode) and close to the residence time scale of the kinetic energy in the stratified volume (Gloor et al., 2000). This indicates that during basically every seiche period, the well-mixed layer of Fig. 2 is newly formed during the phase of maximum currents, whereas the density difference can readjust (by releasing water into the interior) while the motion comes to a halt at the seiche's maximum dislocation.

These estimates are quite consistent with the observations by Gloor et al. (2000), who concluded that the height of the BBL is not only dependent on the forcing (currents) but also on the rate of intrusions. If the BBL water were not to intrude, the BBL would become significantly higher. In fact, in the deepest layer, where there is no volume to intrude into, the thickness is indeed larger (~4 m; Gloor et al., 2000).

Another consistency check is provided by the TKE balance performed for the hypolimnion of Lake Alpnach. Again, comparing the total buoyancy flux of the hypolimnion (i.e., the vertical integral of eq. (2)) with the total dissipation in the BBL allows the determination of a system mixing efficiency, by applying equation (1) in its integral form. As detailed in Wüest et al (2000), the system mixing efficiency is about 0.15 (close to the expected maximum of 0.2: Osborn, 1980; Ivey and Imberger, 1991), again indicating that the BBL water is mixed with a high effectiveness (Garrett, 1991). If the BBL water were to reside for long, BBL-mixing would work on water which is already well mixed and therefore we would expect reduced effectiveness (Garrett, 1990, 1991).

In summary: The water in the hypolimnion of Lake Alpnach resides on average for ~13 days in the interior (experiencing hardly any turbulent mixing; Fig. 1) before becoming entrapped in the BBL, where it is exposed to ~300-times more intense mixing (Goudsmit et al., 1997). The water resides in the BBL for a seiche period (~17 hours) before it is again released into the interior. The fact that it took the tracer, after its interior release, indeed about two weeks to reach the BBL (Fig. 1) is a strongly consistent argument.

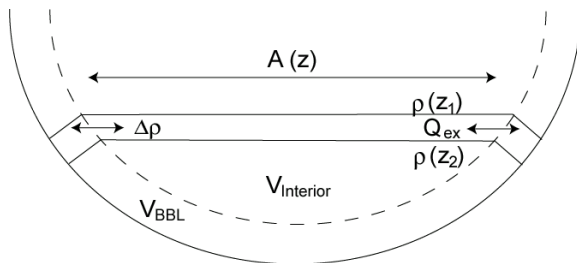


Fig. 5. Schematics of the water exchange Q_{ex} between the BBL and the interior. $\Delta\rho = \rho(z_2) - \rho(z_1)$ is the horizontal density difference between BBL and interior water (Figure 2). $A(z)$ is the cross sectional surface at depth z

Ledwell's deep ocean basins

Unfortunately, the data from the Santa Monica Basin (Ledwell and Hickey, 1995) and the Santa Cruz Basin (Ledwell and Bratkovich, 1995) are not detailed enough in the lateral dimension to perform the same estimates of the residence time scales. If we assume a density difference $\Delta\rho/\rho \approx 1 \cdot 10^{-6}$ between the interior and the well-mixed BBL (Fig. 6), we obtain an approximate time scale of one month for the Santa Monica Basin ($N^2 \approx 3.7 \cdot 10^{-6} \text{ s}^{-2}$; $K_z \approx 1.3 \text{ cm}^2 \text{ s}^{-1}$) and one year for the Santa Cruz Basin ($N^2 \approx 1.2 \cdot 10^{-7} \text{ s}^{-2}$; $K_z \approx 10 \text{ cm}^2 \text{ s}^{-1}$). These values are not inconsistent with the above observations, although the temporal development is not fully resolved. Ledwell and Hickey (1995) conclude that a residence time of at least four days would be required in order to mix 30 m high BBLs in the Santa Monica Basin (Fig. 6). Using the same buoyancy balance, we estimate a consistent value for the residence time scale of about 7 days.

Conclusions

Diapycnal tracer experiments reveal that turbulence in stratified lakes mainly occurs close to the bottom boundary. The turbulence level is according to classical BBL friction and does not call for other processes, such as internal wave breaking (Thorpe, 2001). The observations of the tracer and kinetic energy residence time scales, as well as the observed mixing efficiency, support the hypothesis that the BBL-generated buoyancy flux is transported into the interior of the stratified water by well-mixed layer intrusions. The observations by Ledwell in deep ocean basins are not inconsistent with this conclusion.

Acknowledgments

We would like to thank Arkady Terzhevik, Northern Water Problems Institute, Russ.Acad. Sci., Petrozavodsk, Russia for the possibility to give this talk. We also acknowledge the support of Michelle Stubbs with the proper usage of the English language. This work has been supported by EAWAG and by several grants from the Swiss National Science Foundation – the latest being 2000-067091.01.

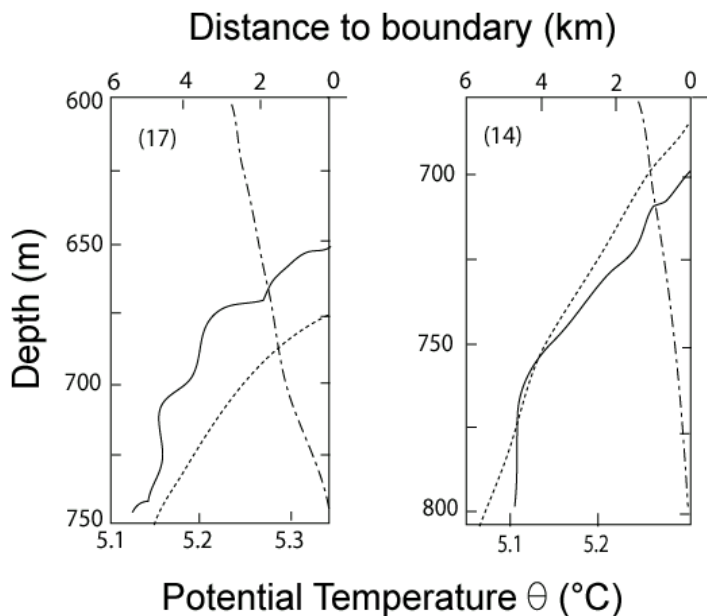


Fig. 6. Two examples of the horizontal temperature structure in the Santa Monica Basin during the SF₆ tracer experiment: The profile collected in the boundary area (solid line), is compared the profile from the interior (dotted line). Note the heights of the well-mixed layers. Details in Ledwell and Hickey (1995)

References

- Antenucci JP, Imberger J, Saggio A., Seasonal evolution of the basin-scale internal wave field in a large stratified lake. *Limnol. Oceanogr.* 45:1621–38. 2000.
- Baumert, H., and G. Radach, Hysteresis of Turbulent Kinetic Energy in Nonrotational Tidal Flows: A Model Study. *J. Geophys. Res.* 97: 3,669 – 3,677. 1992.
- Fricker, P.D., and H.M. Nepf, Bathymetry, stratification, and internal seiche structure. *J. Geophys. Res.* 105: 14,237 – 14,251. 2000.
- Davis, R. E., Diapycnal mixing in the ocean: the Osborn-Cox model, *J. Phys. Oceanogr.*, 24, 2560 – 2576, 1994.
- Garrett, C., The role of secondary circulation in boundary mixing, *J. Geophys. Res.*, 95, 3181 - 3188, 1990.
- Garrett, C., Marginal mixing theories, *Atmosphere Ocean*, 29, 313 - 339, 1991.
- Gloor, M., A. Wüest, and D. M. Imboden, Dynamics of mixed bottom boundary layers and its implications for diapycnal transport in a stratified, natural water basin, *J. Geophys. Res.*, 105, 8629 – 8646, 2000.
- Goudsmit, G.-H., F. Peeters, M. Gloor, and A. Wüest, Boundary versus internal mixing in stratified natural waters, *J. Geophys. Res.*, 102, 27,903 – 27,914, 1997.
- Gregg, M. C., Diapycnal mixing in the thermocline: A review, *J. Geophys. Res.*, 92, 5249 – 5286, 1987.

- Gregg, M. C., and T. B. Sanford, The dependence of turbulent dissipation on stratification in a diffusively stable thermocline, *J. Geophys. Res.*, 93, 12'381 – 12'392, 1988.
- Imberger, J., and G.N. Ivey, On the Nature of Turbulence in a Stratified Fluid. Part II: Application to Lakes. *J. Phys. Oceanogr.* 21: 659 - 680. 1991.
- Imberger, J. 1998. Flux paths in a stratified lake: A review, p. 1-18. In J. Imberger, [eds.]. *Physical Processes in Lakes and Oceans*. American Geophysical Union.
- Ivey, G.N., and J. Imberger, On the nature of turbulence in a stratified fluid. Part I: The energetics of mixing, *J. Phys. Oceanogr.*, 21, 650 - 659, 1991.
- Ledwell, J. R., A. J. Watson, and C. S. Law, Evidence for slow mixing across the pycnocline from an open-ocean tracer-release experiment, *Nature*, 364, 701 –703, 1993.
- Ledwell, J. R., and A. Bratkovich, A tracer study of mixing in the Santa Cruz basin, *J. Geophys. Res.*, 100, 20,681 – 20,704, 1995.
- Ledwell, J. R., and B. M. Hickey, Evidence for enhanced boundary mixing in the Santa Monica basin, *J. Geophys. Res.*, 100, 20,665–20,679, 1995.
- Ledwell, J. R., A. J. Watson, and C. S. Law, Mixing of a tracer in the pycnocline, *J. Geophys. Res.*, 103, 21,499–21,529, 1998.
- Ledwell, J. R., E. T. Montgomery, K. L. Polzin, L. C. St-Laurent, R. W. Schmitt, and J. M. Toole, Evidence for enhanced mixing over rough topography in the abyssal ocean, *Nature*, 403, 179 – 182, 2000.
- Lorke A. and Wüest, A., The probability density of displacement and overturning length scales under diverse stratification. *J. Geophys. Res.* 107, doi: 10.1029/2001JC001154, 2002.
- MacIntyre, S., K.M. Flynn, R. Jellison, and J.R. Romero.. Boundary mixing and nutrient fluxes in Mono Lake, California. *Limnol. Oceanogr.* 44: 512 - 529. 1999.
- Mellor, G., Oscillatory bottom boundary layers, *J. Phys. Oceanogr.*, 32, 3075 – 3088. 2002.
- Moum, J. N., Efficiency of mixing in the main thermocline, *J. Geophys. Res.*, 101, 12,057 – 12,069. 1996.
- Munk, W. H., Abyssal recipes, *Deep-Sea Res.*, 13, 707 –730. 1966.
- Munk, W. H., and C. Wunsch, Abyssal recipes II: energetics of tidal and wind mixing, *Deep-Sea Res.*, 45. 1998.
- Osborn, T. R., Estimates of the local rate of vertical diffusion from dissipation measurements, *J. Phys. Oceanogr.*, 10, 83 – 89. 1980.
- Osborn, T. R., and C. S. Cox, Oceanic fine structure, *Geophys. Fluid Dyn.*, 3, 321 – 345. 1972.
- Ravens, T. M., O. Kocsis, N. Granin, and A. Wüest, Small-scale turbulence and vertical mixing in Lake Baikal, *Limnol. Oceanogr.*, 45, 159 – 173. 2000.
- Rippeth, T.P., N.R. Fisher, and J.H. Simpson, The cycle of turbulent dissipation in the presence of tidal straining. *J. Phys. Oceanogr.* 31, 2458 - 2471. 2001.
- Simpson, J.H. 1Physical processes in the ROFI regime. *J.Mar. Syst.* 12, 3 - 15. 1997.
- Stevens CL, Imberger J., The initial response of a stratified lake to surface shear stress. *J. Fluid Mech.* 312:39 – 66. 1996.
- Thorpe, S. A., On the reflection of internal wave groups from sloping topography, *J. Phys. Oceanogr.*, 31, 3121 – 3126, 2001.
- Wüest, A., and M. Gloor, Bottom boundary mixing: The role of near-sediment density stratification, 54, 464 – 480. 1998.
- Wüest, A., G. Piepke, and D. C. Van Senden, Turbulent kinetic energy balance as a tool for estimating vertical diffusivity in wind-forced stratified waters, *Limnol. Oceanogr.*, 45, 1388 – 1400. 2000.
- Wüest, A., N. Granin, O. Kocsis, T. M. Ravens, M. Schurter, and M. Sturm, Deep mixing in Lake Baikal - low replacement and high turbulence, in *International conference on stratified Flow*, pp. 425–430, Vancouver. 2000b.
- Wüest, A. and Lorke, A., Small-Scale Hydrodynamics in Lakes. *Ann. Rev. Fluid Mech.* 35: 373 - 412. 2003.

The Seasonal Ice Cycle in Lake Pääjärvi, Southern Finland

Matti Leppäranta

Division of Geophysics, University of Helsinki; Finland, E-mail: Matti.Lepparanta@phnet.fi

Lake Pääjärvi is a meso-oligotrophic lake, with surface area 13 km² and mean depth 15 m. It freezes every winter for five months, and the ice cover is static with maximum annual thickness of 30–80 cm. Ice research programme has been ongoing there since 1993 for the stratigraphy and crystal structure of the ice, snow on ice, and impurities (Leppäranta and Kosloff 2000; Leppäranta et al. 2003b). A new thermodynamic model has been developed for the growth and melting of ice, including snow metamorphosis with snow-ice formation.

Ice Structure and Growth

Ice sampling has been made in March at time of the maximum ice thickness. In 1997-1999, the stratigraphy was as follows (Table 1).

Table 1

Date	Total ice, cm	Snow-ice, cm	Snow, cm - g·cm ⁻³
1997, March 19	37	11	0/-
1998, March 27	52	10	5 - 0.33
1999, March 23	53	23	18 - 0,25

The ice sheet had a two-layer structure: granular snow-ice on top and columnar or macro-grained congelation ice below. The grain size of snow-ice was 1-5 mm, and the congelation ice crystals had dimensions from 2 cm to more than 10 cm. The total ice thickness was 37-43 cm, with snow-ice portion 20-40%. Snow is an insulator for congelation ice growth and producer for snow-ice growth. In 1999, the snowfall was exceptionally large, and the snow thickness was 50-80 cm in the surrounding land area. Also then snow-ice had sub-structure: 13 to 18 cm from the top there was a slush layer, which remained unfrozen for at least one month. The maximum ice thickness since 1993 has been 80 cm (year 2003).

A thermodynamic model has been developed for the evolution of the ice thickness including snow metamorphosis and snow-ice formation reproducing well the observed cycle from the initial ice formation to the final melting. This model, originally designed for a coastal site of the Baltic Sea (Saloranta, 2000), includes the classical congelation ice model based on the heat conduction law. For the snow treatment, the model takes into account compaction, which reduces the insulation capability of snow, slush formation from flooding or snowmelt, and snow-ice formation from the freezing of slush. First results have been given by Uusikivi (2001).

Impurities

Lake ice impurities consist of gas bubbles, liquid solution, and solid particles or sediments. They are stored in the ice sheet, possibly transported due to drifting of ice, and re-introduced into the water body when the ice melts. In 1997–1999, the following results were obtained (Table 2).

Table 2

Medium	Conductivity, $\mu\text{S}\cdot\text{cm}^{-1}$ [25 °C]	Dissolved matter, $\text{mg}\cdot\text{l}^{-1}$	pH	Sediment content, $\text{mg}\cdot\text{l}^{-1}$ /organic %
Ice	13.0±5.6	14.3±5.5	6.7	2.1±0.5/36
Snow	16.5±7.8	15.0±5.7	-	4.2±3.4/38
Water	108.0±5.2	64.0±30.6	6.6	3.7±4.2/40

The ice, snow and water concentrations were for dissolved matter $DM_I \sim DM_S \ll DM_W$ and for sediments $SM_I \sim SM_S \sim SM_W$, with the organic proportion of 35 – 40%. Both were similar in ice and snow, is likely due to the major role of atmospheric fallout as the source of impurities. Average metal concentration levels in the ice were: Al and Fe – 100 $\mu\text{g/l}$, Zn – 30 $\mu\text{g/l}$, Cu, Mn and Ni – 5 $\mu\text{g/l}$, and Cd – 0.5 $\mu\text{g/l}$. The levels were within the factor of 0.5 – 2 from those in water or snow, apart from cadmium, which was much higher in ice. Nutrient levels in ice were usually the following: Total-P – 2 $\mu\text{g/l}$, Total-N – 250 $\mu\text{g/l}$, SO_4 and Ca – 2 mg/l, Cl – 1 mg/l, and Mg, K and Na – 0.3 mg/l. The levels were much lower, by one order of magnitude, than in water and very close to those in snow, except much higher nitrogen level in snow. The storage and later release of impurities may become an important ecological factor especially for the load of harmful substances. This load is released to lake water within one month in spring, and its influence depends on the stratification of the water column. If there is a thin stable surface layer a heavy load may result.

A field programme on the optical properties of ice was initiated in winter 2000 (Leppäranta et al., 2003a). The attenuation of light inside ice depends on the ice structure and optically active impurities, in particular yellow substance and chlorophyll.

Final Remarks

In winter 2003, a new automatic station was deployed in Lake Pääjärvi to monitor the water/ice/snow – air heat exchange, radiation balance, and the temperature and solar radiation in ice and snow. Further model development focuses on snow-ice growth, solar radiation transfer, and coupling to a temperature model of the lake water body for realistic heat flux and stratification. A good ice model also aids to improve water body models since ice is not only a passive boundary condition for them but influences the stratification by filtering the solar radiation.

Acknowledgements

I acknowledge financial support (2003 –) from the European Commission's Environment and Sustainable Development Programme under contract EVK1-CT-2002-00121 (CLIME).

References

- Leppäranta, M. and P. Kosloff, 2000. The structure and thickness of Lake Pääjärvi ice. *Geophysica* 36, 233-248.
- Leppäranta, M., A. Reinart, H. Arst, A. Erm, L. Sipelgas and M. Hussainov, 2003a. Investigation of ice and water properties and under-ice light fields in fresh and brackish water bodies. *Nordic Hydrology*, in press.
- Leppäranta, M., M. Tikkanen and J. Virkanen, 2003b. Observations of ice impurities in some Finnish lakes. In *Proc. Estonian Acad. Sci. Chemistry*, in press.
- Saloranta, T., 2000. Modeling the evolution of snow, snow ice and ice in the Baltic Sea, *Tellus*, 52A, 93-108.
- Uusikivi, J., 2001. *Evolution of ice conditions in Lake Pääjärvi in winter 1999/2000*. MSc. Thesis, Division of Geophysics, University of Helsinki.

Motions in ice-covered lakes

Michail Petrov, Arkady Terzhevnik, Roman Zdorovenov and Galina Zdorovenova

Northern Water Problems Institute, Karelian Scientific Centre, Russian Academy of Sciences,
Petrozavodsk, Russia; E-mail: ark@nwpi.krc.karelia.ru

Measurements

The water motions in the ice-covered Lake Vendyurskoe, Russia, have been studied in 1994-2002 winters. The measurements were performed at different locations along cross-sections 4 and 6 (Fig. 1). They have been done at different depths with registration intervals from seconds to several minutes. Period of measurements lasted from one hour to several days. The high-resolution acoustic current meter (ACM) and drag wire current meter (DWCM) were developed (Glinsky, 1998); also, a sensitive water level meter WLR5 AANDERAA was used. In winter 1995-1996, three experiments with simultaneous registrations of currents, fluctuations of ice cover, wind velocity, and air pressure were performed. For that case, special devices were developed (Malm et al., 1997). All data received and preliminary results were published in (Malm et al., 1996; 1997).

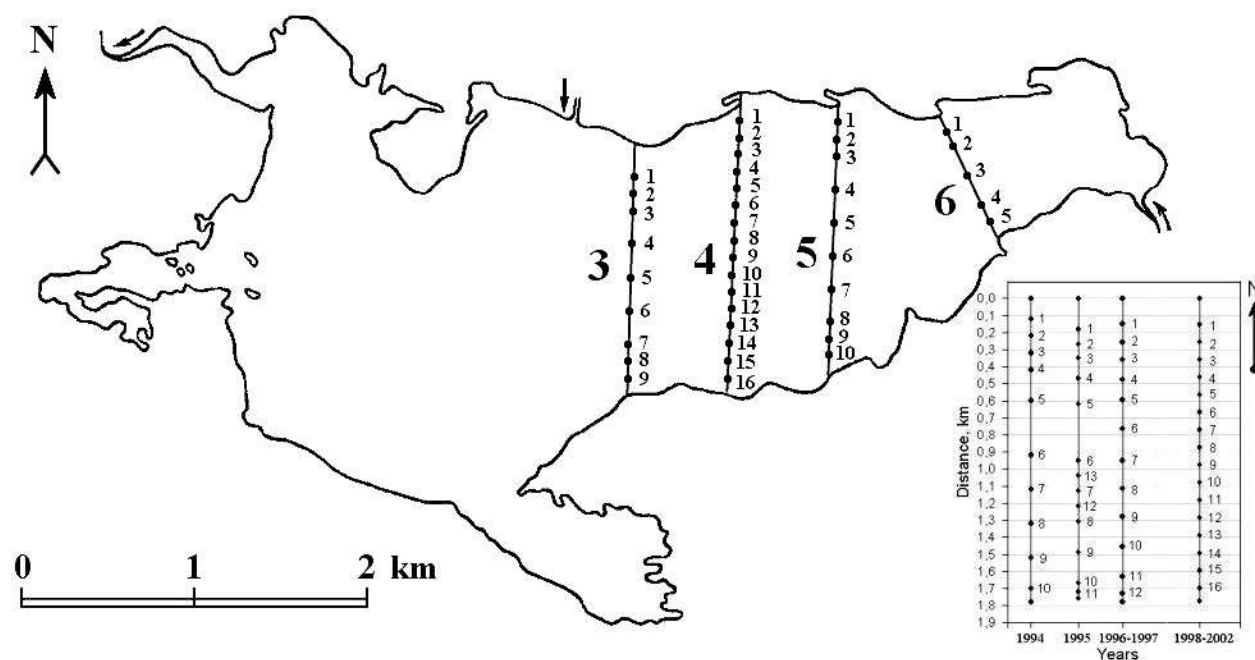


Fig. 1. Location of observational stations in Lake Vendyurskoe.

Currents

According to observational data, motions in the lake exist during the whole ice-covered period. Progressive vector diagrams and spectral Fourier analysis (FFT) allow distinguishing the periodic components. One of them, which dominates nearly in all samplings, is equal to 26-29 min, others to 16-17, 5-6 and 3-4 min. The estimates with use of the Merian formula show that they well correspond to theoretical periods of longitudinal and transverse seiches in Lake Vendyurskoe (Malm et al., 1996). It is worth to note that oscillations with a period of 26-28 min that corresponds to that of the first longitudinal mode are present always, independently from wind conditions over the lake. Their energy usually dominates over other fluctuations. Sometimes, oscillations with a period of 6 min, which we identify as a period of the first transverse mode, were dominant. Maximal velocities of the longitudinal component of currents in the central part of the lake are in range from fractions to $18 \text{ mm}\cdot\text{s}^{-1}$. With a wind increase, high-frequency

oscillations with a period from several seconds to several minutes appear. An example of DWCM registrations is shown in Fig. 2.

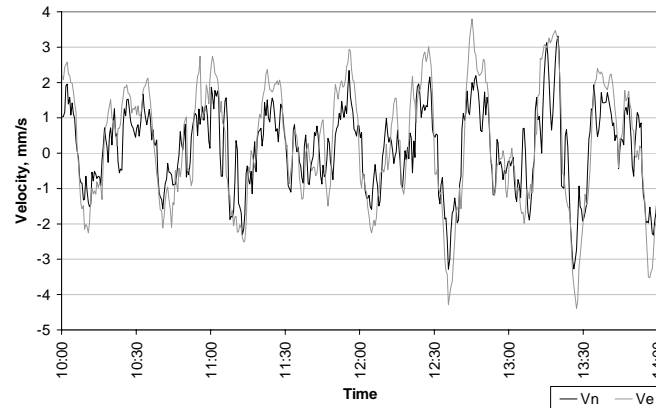


Fig. 2. Longitudinal (V_e) and transverse (V_n) components of currents registered with DWCM at st. 6-3 (22.8.03.1995, 10:00 – 14:00 MSK, depth 2 m).

As seen from Fig. 2, a non-sinusoidal asymmetrical shape is typical for curves. Along with the first longitudinal mode, the high-frequency components are present. Analysis of samplings received shows that asymmetry of oscillation periods and certain irregularity of the period duration is observed even for the first longitudinal mode. During windy weather, dispersion of high-frequency fluctuations grows and becomes comparable to that of low-frequency fluctuations both for the longitudinal and transverse components of currents. To our opinion, the facts that point out on inharmoniousness oscillations are quite important for understanding a physical nature of observed motions.

Along with oscillating motions, average currents were observed. As a residual transport, they can be seen on progressive vector diagrams and on scatter-plots. Analysis of long registrations of currents (from tens of hours to several days) shows that a significant variability of velocity and direction exists. Figure 3 can be used as an example. During 12 hours, instantaneous values of current velocities increased for more than one order of magnitude, with average values 5 times higher. The main input into observed variability is contributed by the first longitudinal mode of seiche-like oscillations and by appearance of high-frequency motions during the process intensification.

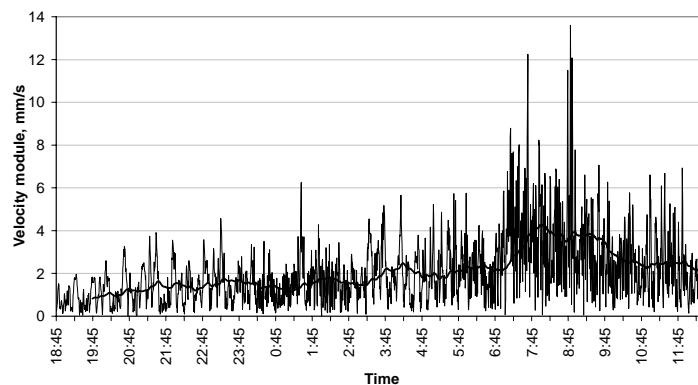


Fig. 3. Velocity of currents registered at st. 6-3, 12-13.02.1995. The 1-hour linear trend was used to estimate average values.

Kinetic energy may increase from time to time for more than one order of magnitude (Fig. 4). During intensification of oscillatory motions, a fraction of high-frequency components

increased also. These observations show that oscillatory motions are a strong source of energy for the development of water movements in the ice-covered lake.

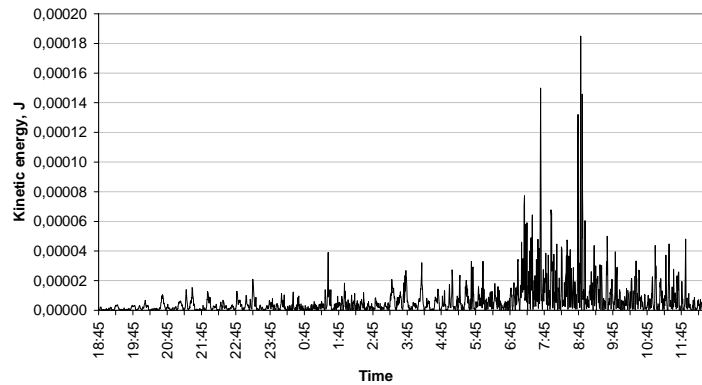


Fig. 4. Kinetic energy of currents. Station 6-3, 12-13.02.1995, depth 2 m.

On a progressive vector diagram that represents data observed on 12-13 February 1995, two different patterns of motions can be distinguished (Fig. 5). In time, they correspond to aforementioned cases. At transition from weak to intense oscillations, the direction of the average transport changes.

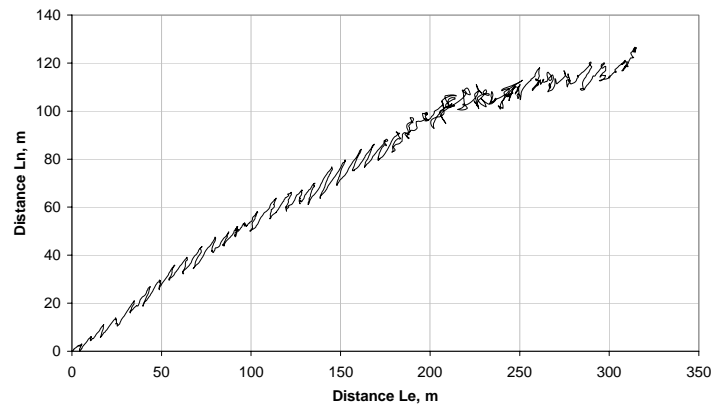


Fig. 5. Progressive vector diagram of currents registered at st. 6-3, 18:45:08 12.02.1995 to 12:34:08 13.02.1995, depth 2 m.

While fluctuating motions had small amplitude, the oscillations typical for the first longitudinal mode with a small fraction of high-frequency motions were mostly present (Fig. 6, left panel). A propagation line of motions had a shape of a saw-tooth wave. After oscillations intensified, a trajectory became loop-like, having a quasi-chaotic character (Fig. 6, right panel). It is seen that the average transfer for each period of the first-mode fluctuations depends on their amplitude.

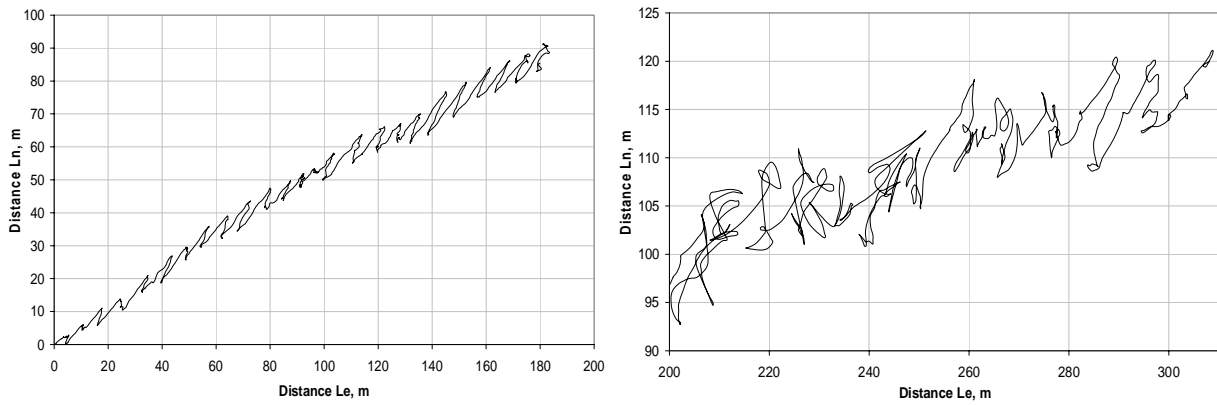


Fig. 6. Trajectory of motions at st. 6-3 during the period of weak (from 18:45:38 12.02 to 05:48:38 13.02.1995), left panel; and strong oscillations (5:48:38-11:56:38, 13.02.1995), right panel.

The scatter plots well illustrate the character of oscillating motions (Fig. 7). As seen, directions of the average transfer change. A position of the scattering field centres also indicates the existence of the residual transfer. During abovementioned periods, this transfer was greater at time of high fluctuations despite the fact that fraction of transverse components increased, and trajectories had a loop-like shape.

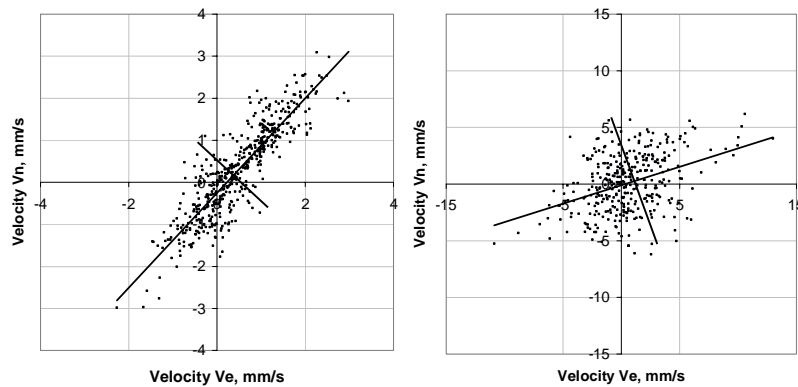


Fig. 7. Scatter plots for components of currents registered at st. 6-3, depth 2 m, during the period of weak oscillations (from 18:45:08 to 22:57:38, 12.02.1995, 500 values in total), left panel; and during the period of intense seiche development (from 06:17:38 to 10:37:38 13.02.1995; 500 values in total), right panel.

The diagram shows that during the period of weak seiches the unilateral transfer was mainly observed (the density function has only one maximum) with a direction +45 degrees, *viz.* longitudinal. After seiches intensified, the role of the transverse component increased, and the second maximum appeared, with direction -60 degrees. As a result, a direction of residual transfer shifted, and a stream function looked loop-like. An increase of the effect of transverse motions is also evidenced by results from FFT, by progressive vector diagrams and ratios of the velocity components.

During winter, the vertical stratification of ice-covered lakes changes significantly. We calculated variations of the Brunt-Väisälä frequency to estimate a potential input of internal oscillations. The calculated periods are in the range of tens to hundreds of minutes that coincides with a general frequency spectrum of motions in Lake Vendyurskoe.

Seiches

During the ice-covered period, a direct wind impact on the water surface is excluded. Nevertheless, the oscillating water motions were registered throughout the whole period of measurements. Bengtsson (1996) assumes that the wind stress initiates vertical displacements of the ice cover, which in turn generate seiches in ice-covered lakes. Malm *et al.* (1997) suggest that the pressure drops in the wind field effect the ice cover and can generate the drops in levels of the ice and water surface. The transient fields of atmospheric pressure, slowly moving over the lake, can contain wave numbers and frequencies appropriate for the resonance interaction with modes of surface and internal waves (Phillips, 1997). It likely results in the formation of seiche-like water movements.

According to the generally accepted concepts, the seiches are considered as linear standing waves characterized by time reversible (sinusoidal) movements of small amplitude, with residual currents and mixing absent. In reality, the process is more complicated as irregularity is typical for bottom topography of natural reservoirs. This leads to the wave refraction and interaction of movements of different modes, which likely cause non-harmonic fluctuations. A deviation from the sinusoidal character and/or inharmoniousness testify to the presence of the progressive waves. Theoretical studies on transformation of standing waves to progressive have been started rather recently (Hill, 2003).

In order to distinguish main mechanisms of generation of the seiche-like movements in ice-covered Lake Vendyurskoe, three experiments were performed in March 1996. They included simultaneous registrations of currents, fluctuations of ice cover level, wind velocity and direction, horizontal gradients of atmospheric pressure (Fig. 8). Measurements of currents were performed at the fixed depth (2.2 m) with use of DWCM and at different depths with use of ACM at st. 6-3 during 23-36 March, 1996. At stations 2-4 and 6-3, two meters were positioned to register the horizontal gradient of atmospheric pressure along the lake.

From spectral densities calculated for the ice-cover and currents, it was found that the main period of their fluctuations is equal to 26.9 min, which coincides with that of the first longitudinal mode seiche. A phase shift between fluctuations of mentioned parameters estimated from the cross-correlation analysis (correlation coefficient 0.8) is equal to the quarter of period and well corresponds with theory of seiches. According to the joint analysis of data on wind velocity, vertical displacements of the ice cover and currents, several frequency bands with corresponding periods from minutes to hours can be distinguished (coherence values up to 0.9).

Longitudinal oscillations of the first mode ice-cover displacements, atmospheric pressure differences and wind stress estimates were compared. Within time of observations, three well pronounced periods of seiche-like fluctuations of currents can be marked, which correspond to those with a coinciding increase of the wind stress. The registered atmospheric pressure differences varied in the range of 0.01-0.1 mbar. In two of three cases, the well expressed variations of the atmospheric pressure preceded the increased oscillations of the ice cover and of currents. As seen in Fig. 8, the atmospheric pressure differences have a strongly oscillating character. If these oscillations include a frequency that corresponds to the seiche period, i.e. close to the state of the resonance for wave motions, an increase of the vertical displacements of the ice cover may be expected.

The scale estimates for maximal velocities of seiche currents can be received from a simple relation between potential and kinetic energy in a standing wave. From the Merian formula, it is easy to get a relation binding a maximal water level (H) and a velocity of seiche currents (V),

$$V = H \sqrt{g / D}$$

where g is gravitational acceleration; D is a mean lake depth. The estimates of the maximal velocities of the seiche currents coincide with observed values.

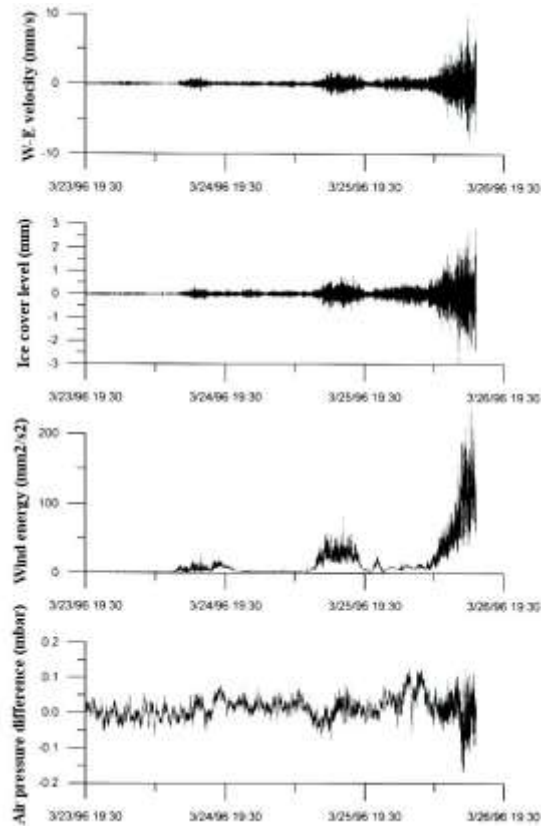


Fig. 8. W-E current velocity and ice cover level fluctuations, air pressure difference along the main axis of the lake (air pressure difference between stations 6-3 and 2-4), and wind stress (square of wind velocity) registered at station 6-3 on 23-26 March (time interval of registrations 30 s).

Fig. 9 shows a relation between velocities of currents and wind taken as residuals averaged over the 5-min period. Though a certain scatter exists, the scattergram evidences a strong dependence. Thus, we can assume that wind is the most likely cause for generation of oscillating water motions.

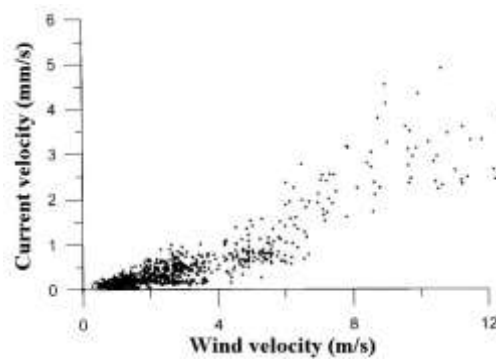


Fig. 9. Standard deviation values of current velocity fluctuations and wind velocity, averaged over 5-min period(23-26 March,t station 6-3).

Residual currents

In addition to the long registrations of instantaneous values of velocity components, we also performed measurements of residual (average) currents along two cross-sections using ACM and a specially developed approach [see Appendix A in (Malm et al., 1996)]. The length of

registrations at each location depth was approximately equal to the maximal period of the first longitudinal seiche mode, i.e. 30 min. To eliminate a possible error due to the zero drift, ACM was turned around once. From values registered, means were estimated for further calculations of the velocity and direction of currents.

Observational data indicate that velocity of residual currents decrease in time throughout the lake, and this is a common feature for all years of observations. Maximal velocities, up to $10 \text{ mm}\cdot\text{s}^{-1}$, are observed over the deep part of the lake during the first 6-7 weeks after the ice cover formation. In late March – early April, velocities are minimal, up to fraction of $\text{mm}\cdot\text{s}^{-1}$.

At all locations of observations, maximal velocities were registered at the depths of 2-3 m, being equal to $10 \text{ mm}\cdot\text{s}^{-1}$ in the central part of cross-sections and to several $\text{mm}\cdot\text{s}^{-1}$ in the near-shore area. Notice that a mean depth of Lake Vendyurskoe is about 6 m, thus maximal currents are related to the half-mean depth. In both directions from this depth, velocities decrease, being equal to fraction of $\text{mm}\cdot\text{s}^{-1}$ near the solid boundaries. In most cases, residual currents in the central part of cross-sections are directed to the east, i.e. along the longitudinal axis of the lake. Along the southern coast, currents are directed to the west, and along the opposite coast to the east, rarely to the west or offshore. Such a picture can be considered as quasi-stationary.

Yet, observations indicate that residual currents may change quite fast. Analysis of long registrations of currents and progressive vector diagrams show that residual currents can vary in tens of minutes. This fact leads to the conclusion that estimates of average currents based on momentary data should be considered rather carefully. Figure 10 represents a progressive vector diagram from data registered near the northern shore (st. 4-2). For the short time (the length of registrations was one hour), a transverse residual transfer changed its direction to longitudinal.

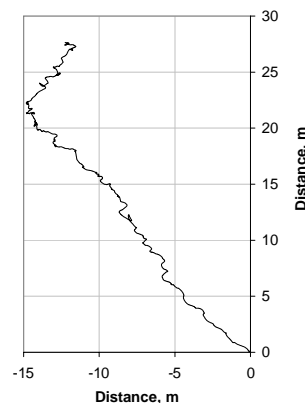


Fig. 10. Trajectory of motions at st. 4-2 (15:54 – 16:40, 18.03.1995).

Acknowledgements

This work has been partially supported by European Commission, project INTAS-97-0734.

References

- Bengtsson L., 1996. Mixing in ice covered lakes. *Hydrobiologia*, **322**:91-97.
- Glinsky A., 1998. Current meters for measurement of low-speed velocities in ice covered lakes. *Limnol. Oceanogr.*, **43**: 1661-1668.
- Hill D., 2003. Transient and Steady-State Amplitudes of Forced Waves in Rectangular Basins. Accepted in *Physics of Fluids*.
- Malm J., Terzhevik A., Bengtsson L., Boyarinov P., Glinsky A., Palshin N., and Petrov M., (1996). A Field Study of Thermo- and Hydrodynamics in Three Small Karelian Lakes during Winter 1994/1995. Report 3197, Department of Water Resources Engineering, Lund Institute of Technology, Lund University, Sweden. 220 p.

- Malm J., Terzhevik A., Bengtsson L., Boyarinov P., Glinsky A., Palshin N., and Petrov M., (1997). Temperature and Hydrodynamics in Lake Vendurskoe during Winter 1996/1997. Report 3213, Department of Water Resources Engineering, Lund Institute of Technology, Lund University, Sweden.
- Malm J., Terzhevik A., Bengtsson L., Boyarinov P., Glinsky A., Palshin N., and Petrov M., 1998. A field study on currents in a shallow ice-covered lake. *Limnol. Oceanogr.*, **43**: 1669-1679.
- Phillips O.M., 1997. *The dynamics of the upper ocean*. 2nd Edition, Cambridge University Press.

Thermal structure of shallow lakes in early winter

Michail Petrov, Arkady Terzhevnik, Roman Zdorovenov and Galina Zdorovenova

Northern Water Problems Institute, Karelian Scientific Centre, Russian Academy of Sciences,
Petrozavodsk, Russia; E-mail: ark@nwpi.krc.karelia.ru

For several years, the development of the thermal structure during winter was registered in Lake Vendyurskoe (Russia) with use of thermistor chains and accidental surveys at different locations (Malm et al. 1996; 1997; Terzhevnik et al. 2000). Usually, the thermistor chains (with a time interval of registrations equal to 3 hours) were installed before the ice cover formation and raised after the ice break, thus data cover the whole ice-covered period. Devices used in the surveys and their accuracy are described in (Malm et al., 1996). Numbers of stations mentioned hereinafter correspond to Fig. 1 shown in (Petrov et al., 2003, see this volume).

The date of the ice cover formation differs from year to year, and therefore we introduce a new time scale in terms of days of the ice cover existence that allows directly comparing evolution of the thermal structure described by data from different seasons.

As soon as the lake is isolated from atmosphere, warming due to the heat transfer from bottom sediments starts, with a sharp increase of water temperature in bottom layers (Fig. 1). Usually, the under-ice warming starts under different conditions from year to year (amount of heat gained during the open-water period, stability of the ice cover existence, etc.), thus the thermal structure development may differ (Table 1). Nevertheless, many features of the seasonal development of the thermal structure are similar from year to year. The temperature wave gradually propagates from the bottom upwards, and the vertical temperature profile, being homogenous at the beginning, becomes stratified in its lower part, which quickly grows in time. For the deep part of the lake, in thirty days the upper boundary of the stratified part of the profile reaches a 3-m depth. At shallower locations, the lake may become fully stratified to the same time. As seen from the Table, rate of warming in bottom layers gradually decreases, and this feature is typical for all years of observations.

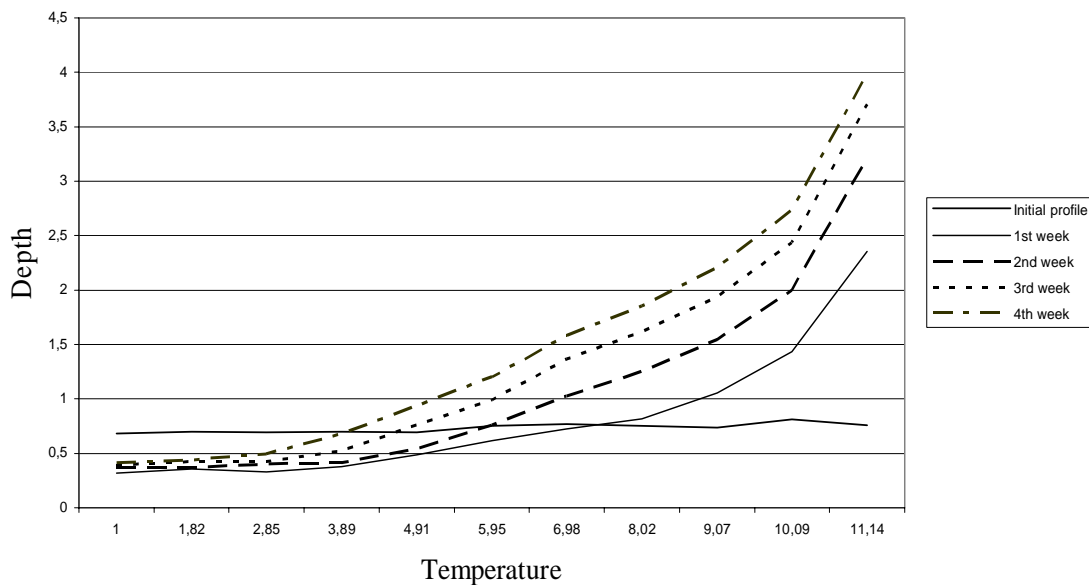


Fig. 1. Development of the vertical thermal structure in Lake Vendyurskoe during first four weeks of the ice cover existence (data from thermistor chains, winter 1995-1996).

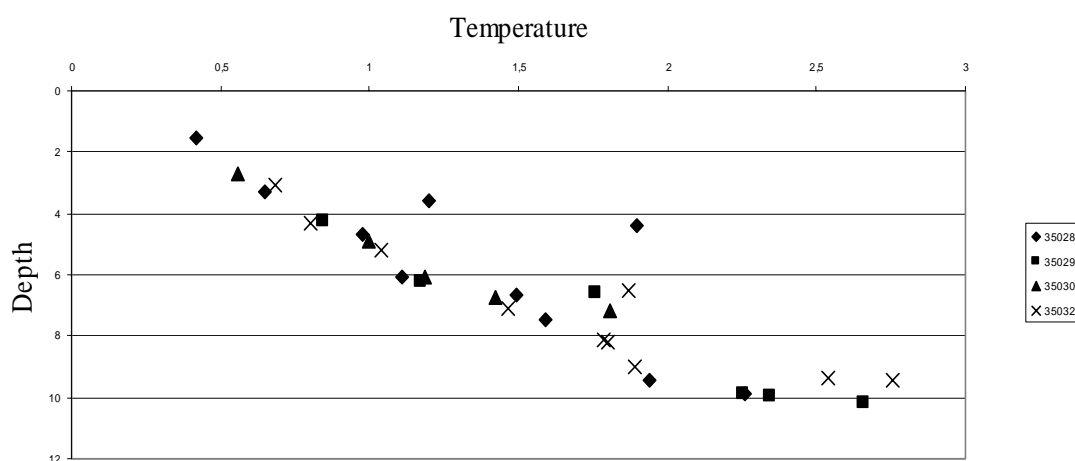
Table 1

Temperatures of upper (TUD) and bottom (TBD) depths and lower depth of the mixed layer (DML) estimated from thermistor chain data

Winter, date of ice cover formation	TUD, °C		TBD, °C		DML, m	
	deep	shallow	deep	shallow	deep	shallow
1994-1995, 07.11.94	0.65	-	1.44	-	*	-
1 st week	0.81	-	2.45	-	*	-
2 nd week	0.90	-	3.07	-	*	-
3 rd week	0.96	-	3.46	-	*	-
4 th week	0.93	-	3.73	-	*	-
1995-1996, 06.11.95	0.68	0.81	0.76	0.95	~11	~6.5
1 st week	0.32	0.42	2.36	2.79	~4	~4.5
2 nd week	0.37	0.41	3.29	3.33	~4	absent
3 rd week	0.39	0.37	3.75	3.44	~3	absent
4 th week	0.41	0.38	4.08	3.52	3	absent
1996-1997, 11.12.96	0.72	-	0.86	-	~9	-
1 st week	0.51	-	1.71	-	~5	-
2 nd week	0.55	-	2.22	-	~5	-
3 rd week	0.51	-	2.57	-	~4	-
4 th week	0.56	-	2.80	-	~3	-
1999-2000, 14.11.99	0.93	0.78	0.85	0.73	~11	6.5~
1 st week	0.59	0.41	2.14	1.07	~6	~5.5
2 nd week	0.60	0.41	2.80	1.27	~5	~3.5
3 rd week	0.64	0.45	3.20	1.41	~4.5	~3.5
4 th week	0.64	0.46	3.49	1.58	~4.5	~2.5

*The mixed layer was not observed.

The distribution of bottom temperatures versus the depth differs in time (Fig. 2). At the beginning of the ice-covered period, they seemingly “remember” the history of strong mixing and currents typical for the open-water period in late autumn – early winter, which is characterized by a certain scatter of values (Fig. 2a). In a month, the distribution has a more ordered species (Fig. 2b).



a)

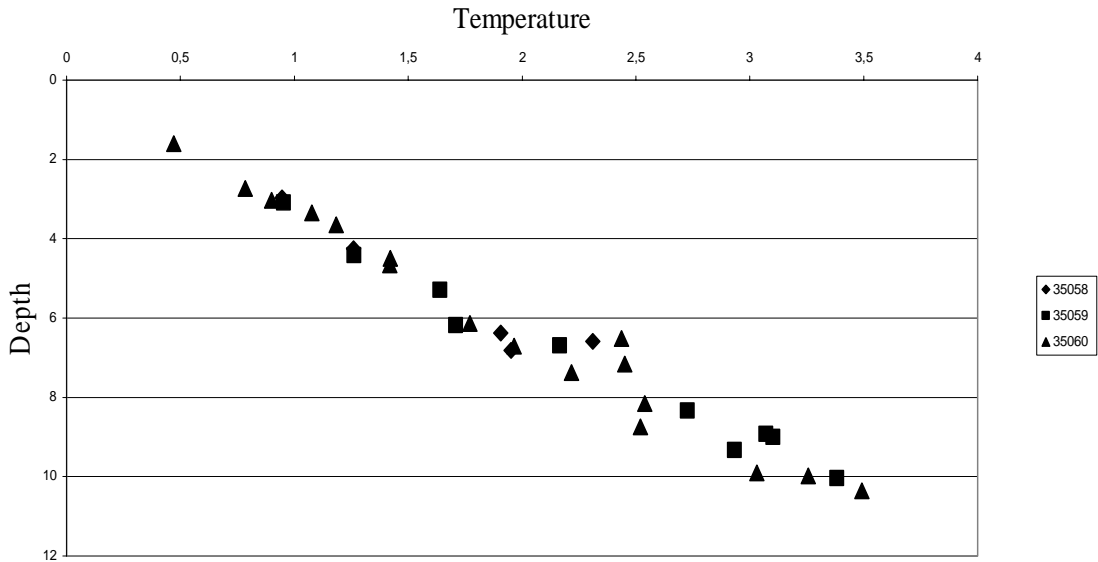


Fig. 2. Bottom temperatures vs. depth in Lake Vendyurskoe: a) in November and b) in December 1995.

The effective coefficient of thermal conductivity, λ_{eff} , can be estimated from the relation binding a linear scale of deformation of the temperature profile with time, during which this deformation takes place,

$$\lambda_{eff} = \frac{(D-h)^2}{t_*},$$

where D is depth; h thickness of a mixed layer; t_* is length of the considered period. According to the estimates based on observational data from different seasons, λ_{eff} varies through the range of $2-2.5 \cdot 10^{-5} \text{ m} \cdot \text{s}^{-2}$. It is worth to notice that heat during early winter propagates much faster than expected on a molecular level. Estimates of the effective coefficients of thermal conductivity for different layers are several times, sometimes up to one order of magnitude, higher than molecular one.

The heat content (HC) of a water column can be considered as a parameter that integrally describes the history of main events during the ice-covered period. The HC values were calculated with use of data from thermistor chains. After removing the seasonal trend from calculated values, the temporal distribution of residuals shows that the vertical thermal structure experiences a quite strong variability (Fig. 3). Using the FFT-analysis, we calculated the spectral densities and estimated the periods that correspond to the main frequencies present in the patterns received (see Table 2, Fig. 4). Remarkably, all spectra are very similar in shape. Most of periods distinguished are close in their length to synoptical variability.

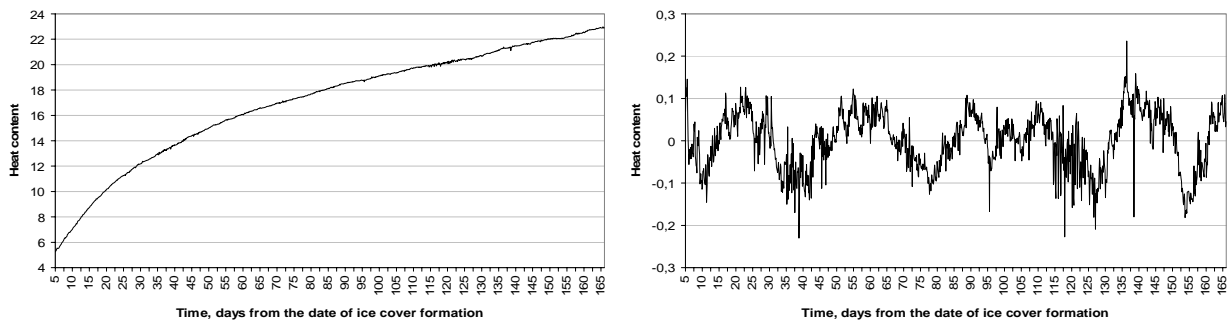


Fig. 3. The seasonal course of heat content and residuals after removing the seasonal trend by the 6-power polynomial (st. 4-7, 11.11.1995, 0:00:00 to 19.04.1996, 21:00, time interval of registrations 3 h).

Table 2

Main periods (days) of fluctuations in the heat content course for different years

Years	Section	Station	Period, days					
1994-1995	4	6	29	-	9	5.9	4.5	3.7
1995-1996	4	7	41	13	7.8	-	-	-
1995-1996	4	3	30.5	12.7	7.8	-	4.4	3.7
1996-1997	4	7	32.8	10.6	8	5.5	4	2.7
1996-1997	4	11	31.3	9.7	-	5.8	-	-
1998-1999	4	11	31	10.7	-	6.1	4.8	3.9
1998-1999	4	9	23	12	7.9	6.3	-	3.7
1999-2000	4	9	33.8	12.5	8.3	5.5	4	2.9
1999-2000	4	11	-	14.8	-	-	-	3.7
1999-2000	4	14	-	17	-	-	-	3.7
2002-2003	4	3	20.3	-	-	-	-	3.1

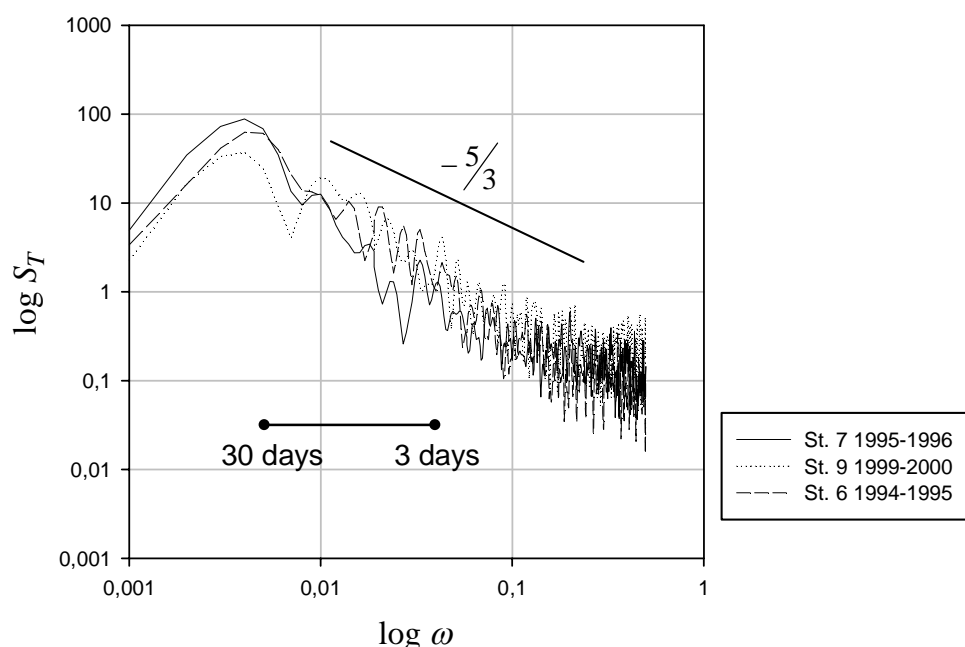


Fig. 4. Spectral densities calculated on the basis of heat content residuals.

Discussion

From our analysis, it follows that (1) heat content of the water column increases rapidly during first 30-45 days, and after that the changes become smaller throughout the season until under-ice penetrative convection starts, e.g. see Figs. 7-9, 12 in (Malm et al., 1997); (2) transport of heat from bottom layers in early weeks is faster than molecular transfer would provide.

Taking into account the abovementioned results and some conclusions from (Petrov et al., 2003, see this volume), we assume that the main mechanisms controlling the development of the thermal structure in ice-covered lakes are vertical heat transfer and a wide spectrum of motions generated by wind impact on the ice cover, which intensify heat transport in bottom layers. Fig. 5 presents the vertical distribution of standard deviation values calculated with use of thermistor chain data received with 1-hour time interval of registrations. As seen, the highest variability takes place in the bottom layers.

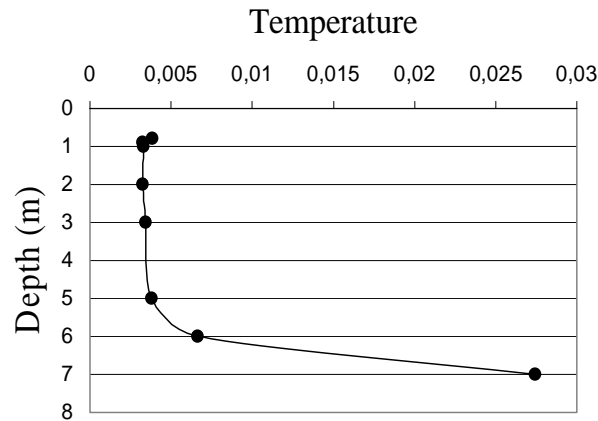


Fig. 5. Vertical distribution of standard deviation values (thermistor chain data from st. 4-3, 24.12.02-12.03.03; time interval of registrations 1 h).

Acknowledgements

This work has been partially supported by European Commission, project INTAS-97-0734.

References

- Bengtsson L., Malm J., Terzhevik A., Petrov M., Boyarinov P., Glinsky A., Palshin N., 1995, *A field study of thermo- and hydrodynamics in a small Karelian lake during late winter 1994*. Department of Water Resources Engineering, Institute of Technology, University of Lund, Report 3185. Lund, 72 p.
- Malm J., Terzhevik A., Bengtsson L., Boyarinov P., Glinsky A., Palshin N., Petrov M., 1996, *A field study of thermo- and hydrodynamics in three small Karelian lakes during winter 1994/1995*. Department of Water Resources Engineering, Institute of Technology, University of Lund, Report 3197. Lund, 220 p.
- Malm J., Terzhevik A., Bengtsson L., Boyarinov P., Glinsky A., Palshin N., Petrov M., 1997, *Temperature and hydrodynamics in Lake Vendyurskoe during winter 1995/1996*. Department of Water Resources Engineering, Institute of Technology, University of Lund, Report 3113. Lund, 205 p.
- Terzhevik A. Yu., Boyarinov P. M., Filatov N. N., Mitrokhov A. V., Palshin N. I., Petrov M. P., Jonas T., Schurter M., Maher O. Ali, 2000. Field study of winter hydrodynamics in Lake Vendyurskoe (Russia), Abstract sent to Physical Processes in Natural Waters, 5th Workshop, 110-113, Irkutsk, Russia.

Thermal Structure and Heat Exchange in Ice-Water Column-Sediment System

Sergey D. Golosov¹, Ilia S. Zverev¹ and Arkady Yu. Terzhevik²

¹Institute of Limnology, Russ. Acad. Sci., 196105 St. Petersburg, RUSSIA; E-mail: sergey_golosov@mail.ru

²Northern Water Problems Institute, Karelian Scientific Centre, Russ. Acad. Sci., Petrozavodsk, RUSSIA; E-mail: ark@nwpi.krc.karelia.ru

The numerous observational data on the thermal regime of the ice-covered lakes (Kuzmenko, 1976, 1984; Bengtsson et al., 1995; Malm et.al., 1997) show that redistribution of the heat storage between the bottom sediment and water takes place during winter, which may last for five-six months. It results in a so-called effect of the under-ice lake warming. Fig. 1 presents observational data on the vertical distribution of the water temperature in Lake Vendyurskoe (Russia) in November 1995 – April 1996 (Malm et.al. 1997), which demonstrate the mentioned effect. Below, a one-dimensional model that describes specifics of heat transfer in an ice-covered lake is discussed.

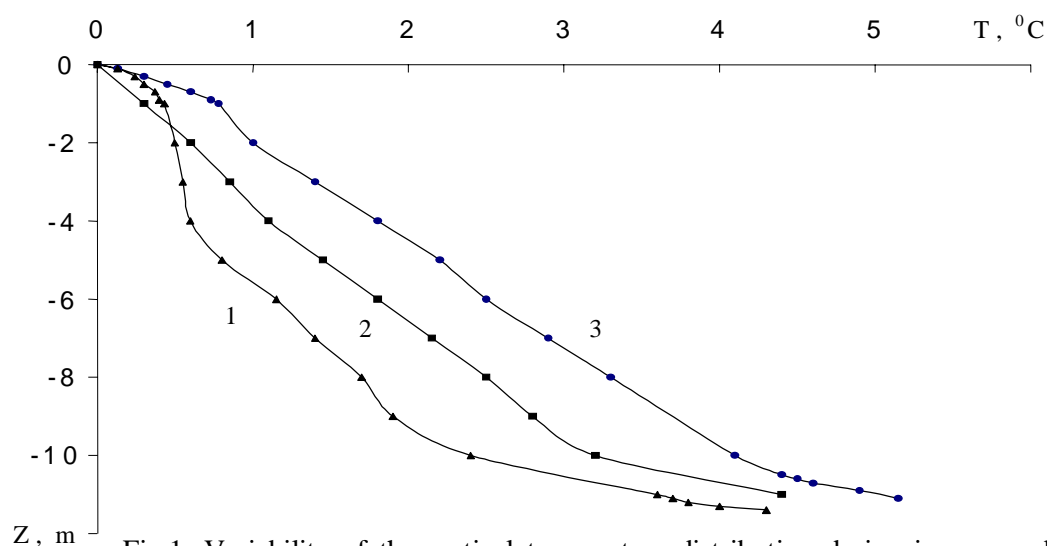


Fig.1. Variability of the vertical temperature distribution during ice-covered period in Lake Vendyurskoye: 1 – November 1995, 2 – December 1995, 3 – March 1996 (data from Malm et.al. 1997).

Model description

Figure 2 schematically represents a vertical thermal structure of the system ‘ice-water-bottom sediment’ in absence of snow on the ice surface. In adopted notations, the vertical co-ordinate axis is directed from the ice surface ($z=0$) towards the lower boundary of the active layer of bottom sediment ($z=L$) where the temperature is equal to T_L ; l stands for ice thickness, the upper boundary of which has a temperature T_s ; the temperature of the lower boundary of ice ($z=l$) during the whole ice-covered period equals to that of water freezing, $T_f = 0^\circ\text{C}$. In the very vicinity from the lower boundary of ice, a thin layer ($\delta-l$) is located, within which heat transfer is accomplished on a molecular level; D is a water-bottom interface with temperature T_D .

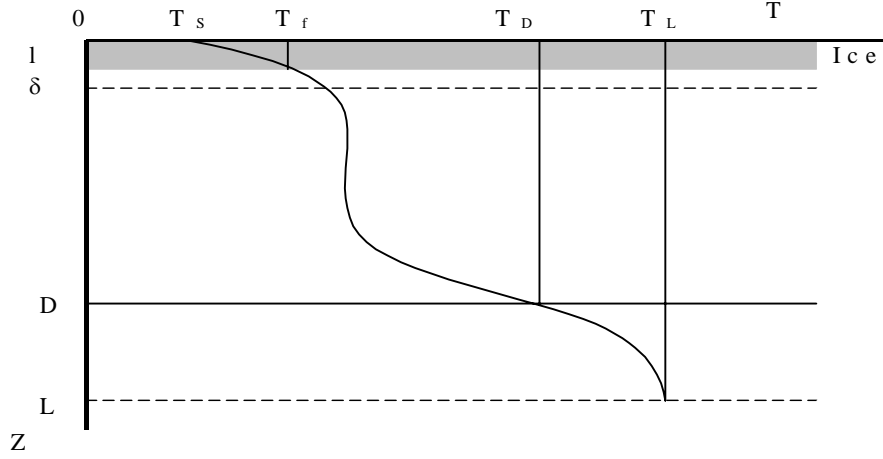


Fig 2. Schematic representation of the vertical temperature profile in an “ice-water column-sediments” system.

Equation of heat conductivity for the considered domain $0 \leq z \leq L$ is,

$$\frac{\partial T}{\partial t} = - \frac{\partial Q}{\partial z} \quad (1)$$

where t is time; z is depth; T is water temperature; Q is vertical kinematic heat flux.

Let us present the vertical temperature profile in the considered domain as the following parametric concept,

$$T(z) = \begin{cases} T_S - (T_S - T_f) f_1\left(\frac{z}{l}\right) & \text{at } 0 \leq z \leq l \\ T_f + (T_D - T_f) f_2\left(\frac{z-l}{D-l}\right) & \text{at } l \leq z \leq D \\ T_D + (T_L - T_D) f_3\left(\frac{z-D}{L-D}\right) & \text{at } D \leq z \leq L \end{cases} \quad (2)$$

Dimensionless functions $f_1(\xi_1)$, $f_2(\xi_2)$ and $f_3(\xi_3)$, where $\xi_1 = (z/l)$, $\xi_2 = (z-l)/(D-l)$ and $\xi_3 = (z-D)/(L-D)$ are dimensionless depths, describe the vertical temperature distribution in ice, water and bottom sediments, respectively, and satisfy the obvious boundary conditions,

$$f_1(0) = f_2(0) = f_3(0) = 0; f_1(1) = f_2(1) = f_3(1) = 1; f_3'(1) = 0. \quad (3)$$

The last condition (3) for the function $f_3(\xi_3)$ follows from definition of the active layer of bottom sediments, according to which the vertical temperature gradient for $z = L$ is close to zero. From here, we consider only a problem of joint evolution of temperature profiles in water and sediments, described by the second and third equations in (2).

Let us integrate Eq. (1) with respect to z twice, first from l to D using the second equation in (2), then from D to L using the third equation in (2). As a result, we obtain the following differential equations,

$$\frac{dT_D}{dt} (D - L) \alpha_2 = -Q_D + Q_l + T_D \alpha_2 \frac{dl}{dt} - T_D (D - L) \frac{d\alpha_2}{dt} \quad (4)$$

$$\frac{dT_D}{dt} (L - D) (1 - \alpha_3) + (T_L - T_D) (L - D) \frac{d\alpha_3}{dt} = Q_D \quad (5)$$

$$\alpha_2 = \int_0^1 f_2(\xi_2) d\xi_2; \quad \alpha_3 = \int_0^1 f_3(\xi_3) d\xi_3.$$

Eqs. (4) and (5) include five unknown parameters: bottom temperature T_D ; heat fluxes Q_D and Q_I through water-bottom and water-ice interfaces, respectively; and also parameters α_2 and α_3 , which are integrals accordingly from functions $f_2(\xi_2)$ and $f_3(\xi_3)$. To calculate the development of ice thickness, any of numerous models describing the interaction between a lake and atmosphere can be used (e.g. Patterson and Hamblin 1998; Romyantsev *et al.* 1986). Notice that derivatives from integral parameters α_2 and α_3 belonging to Eqs. (4) and (5) describe redistribution of heat between water and bottom sediments. To enclose our system of equations, we need three additional relations.

According to (3), the function $f_2(\xi_2)$ has two time-constant boundary conditions, $f_2(0) = 0$ and $f_2(1) = 1$, which are insufficient to define its time dependence. In a framework of the one-dimensional model, it is impossible to set a boundary condition on the lower boundary of ice for the derivative of the desired function as the thickness of the “molecular” layer and the temperature gradient within it are not determined. Nevertheless, a time-dependent boundary condition for the derivative of function $f_2(\xi_2)$ can be set up at the interface water-sediment ($\xi_2=1$). Usually, the upper layer of bottom sediments has high porosity (~95%) and saturation (90-95%). This allows considering its heat-conducting capacity close to that of bottom water. In such a case, the heat flux through the water-sediment interface can be written as,

$$\lambda_{eff} \frac{dT_w}{dz} = Q_D, \quad (6)$$

where λ_{eff} is effective thermal conductivity in water, dT_w/dz is the vertical temperature gradient in the vicinity of bottom. Taking into account the second equation in (2), Eq. (6) can be re-written as,

$$-\lambda_{eff} \frac{T_D}{D-l} \frac{df_2}{d\xi_2} = Q_D \quad \text{at } \xi_2 = 1. \quad (7)$$

The value of λ_{eff} can be estimated from the relation binding a linear scale of deformation of the temperature profile with time, during which this deformation takes place,

$$\lambda_{eff} = \frac{(D-l)^2}{t_*}, \quad (8)$$

where t_* is length of the ice-covered period. Thus, the function $f_2(\xi_2)$ has three boundary conditions,

$$f_2(0) = 0; f_2(1) = 1, f_2'(1) = A, \quad \text{where } A = \frac{Q_D(D-l)}{\lambda_{eff} T_D} \quad (9)$$

The last condition in (9) defines variability of $f_2(\xi_2)$ in time. According to (9), $f_2(\xi_2)$ can be expressed as a second-degree polynomial with time-dependent coefficients,

$$f_2(\xi_2) = (2-A)\xi_2 + (A-1)\xi_2^2. \quad (10)$$

According to (3), $f_3(\xi_3)$ has three boundary conditions that are not dependent on time, $f_3(0)=0$, $f_3(1)=1$, $f_3'(1)=1$. To describe time dependence of function $f_3(\xi_3)$, we need additional boundary condition analogous to the last condition in (9). By repeating considerations led to (6) and taking into account the third equation in (2), the fourth boundary condition can be written as,

$$\lambda_{eff} \frac{(T_L - T_D)}{(L-D)} \frac{df_3}{d\xi_3} = Q_D \quad \text{at } \xi_3 = 0. \quad (11)$$

This boundary condition, in much the same as (7), defines variability of $f_3(\xi_3)$ in time. According to (3) and (11), a desired function can be expressed as a third-degree polynomial with time-dependent coefficients,

$$f_3(\xi_3) = B\xi_3 + (3 - 2B)\xi_3^2 + (B - 2)\xi_3^3, \text{ where } B = \frac{Q_D(L - D)}{\lambda_{eff}(T_L - T_D)} \quad (12)$$

Verification of formulae (10) and (12) was performed with use of data from (Malm *et al.* 1997), see Fig. 3. Curves 1 and 2 correspond to the vertical temperature profiles in November 1995 and March 1996, respectively. Apparently, the profile 2 corresponds to the higher heat content in the lake. Moreover, the temperature distribution described by the curve 2 is tended to linear that complies with a regime of quasi-stationary heat conduction and is confirmed by observational data. Curves 3 and 4 correspond to the temperature profiles in bottom sediments (November 1995 and March 1996, respectively). Curve 4 represents the lesser heat content of bottom sediments, compared to the initial (curve 3). The temperature profile in bottom sediments also is tended to the linear type, i.e. to the temperature distribution that agrees with quasi-stationary heat conduction.

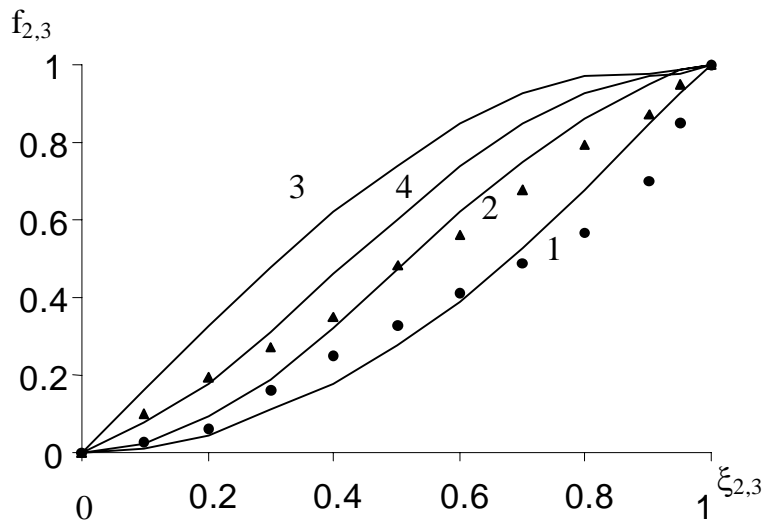


Fig. 3. Dimensionless temperature profiles during the ice-covered period. Lines 1 and 2 represent modelled profiles in water column of Lake Vendyurskoe in November 1995 and March 1996, respectively; lines 3 and 4 are those for the lake sediments. Symbols mark the temperature profiles measured in a lake water column in November (circles) and in March (triangles).

Finally, the last closure equation for (4)-(5) can be easily received in the following way. Let us write the expression for the heat flux from water to the lower ice boundary as,

$$Q_l = -\lambda_{eff} \left. \frac{dT}{dz} \right|_{z=l}, \quad (13)$$

or, with respect to the second equation in (2) and also to the expression (10),

$$Q_l = -\lambda_{eff} \frac{T_D}{(D - l)} (2 - A). \quad (14)$$

Thus, the system of equations (4), (5), (10), (12) and (14) is closed and represents a simple model describing evolution of heat distribution between bottom sediments and water during the ice-covered period.

Conclusions

Comparison of calculations of Q_D and Q_I in Lake Krasnoe performed for the ice-covered period in 1974 with observational data from Lake Vendyurskoe in 1996 (Malm et al. 1997) is of special interest (Fig. 4). It allows making the following conclusions on specific features of the thermal regime in ice-covered lakes.

1. In early winter, heat penetration from bottom sediments several times exceeds the heat outflow through the ice that results in under-ice heating of lakes.
2. Despite the fact that calculations were performed for Lake Krasnoe in 1974 and measurements in Lake Vendyurskoe in 1996, a qualitative character of variability of those heat fluxes in time is similar. Moreover, Lake Vendyurskoe is located about 500 km northward from Lake Krasnoe, and their thermal conditions are different. Difference in location reflects in different values of the heat flux through the water-sediment interface, namely in Lake Krasnoe it is higher. The latter can be explained by the higher heat content of bottom sediments before the ice formation.
3. Equality of the water-ice heat flux in both lakes evidences that the development of the ice cover in freshwater reservoirs proceeds similar from one to another.
4. To the end of March, all vertical heat fluxes become practically equal that means presence of the quasi-stationary heat conduction regime.

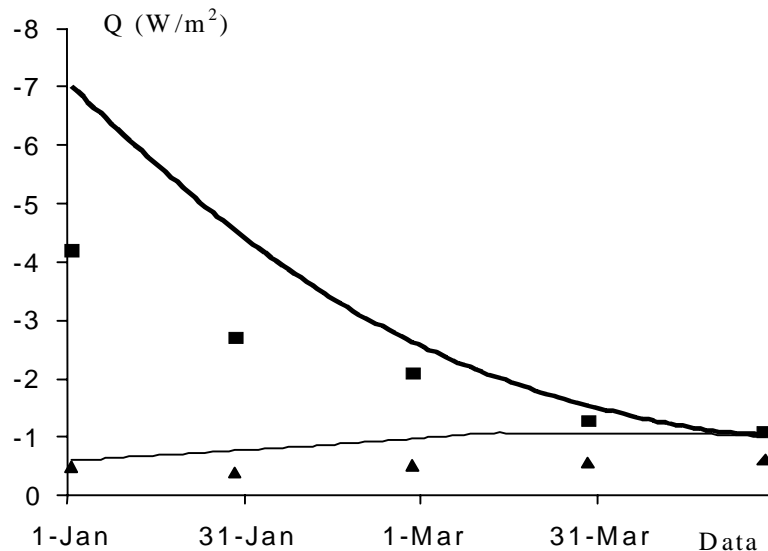


Fig. 4. Heat fluxes across the water-sediment (Q_D) and water-ice (Q_I) interfaces in lakes Krasnoye (lines) and Vendyurskoe (symbols). Solid and thin lines represent the values of Q_D and Q_I respectively calculated for Lake Krasnoe (1974), filled squares and triangles are the same heat fluxes evaluated from measurements in Lake Vendyurskoe (Malm *et al.* 1997).

Acknowledgements

This work has been performed in a framework of the project INTAS-97-0734.

References

- Bengtsson L., Malm J., Terzhevik A., Petrov M., Boyarinov P., Glinsky A., Palshin N., 1995, *A field study of thermo- and hydrodynamics in a small Karelian Lake during late winter*. Sweden, Lund Univ., Rep. № 3185, 72 p.
- Kuzmenko L.G. 1976, Thermal regime of lake water column and sediments. In *Biological productivity of Lake Krasnoye*. Leningrad, "Nauka" Publishing House, p. 18-36 (in Russian).

- Kuzmenko L.G. 1984, The seasonal structure of lakes thermal states. In *The features of water quality formation in lakes of different types at Karelian Isthmuth*. Leningrad, "Nauka" Publ. House, pp. 45-60 (in Russian).
- Malm J., Terzhevik A., Bengtsson L., Boyarinov P., Glinsky A., Palshin N., Petrov M., 1997, *Temperature and hydrodynamics in Lake Vendyurskoe during winter 1995/1996*. Sweden, Lund Univ., Rep. № 3213, 203 p.
- Patterson J.C., Hamblin P.F. 1988, Thermal simulation of a lake with winter ice cover. *Limnol. Oceanogr.* 33, pp. 323-338.
- Rumyantsev V.A., Razumov E.V., Zilitinkevich S.S. 1986, *Parameterized model of seasonal temperature changes in a lake (application to the problem of Lake Sevan)*, Leningrad, Institute of Limnology RAS, 74 p. (in Russian).

Measuring water storage with high resolution pressure sensors in a small lake

Bertram Boehrer¹ and Stephanie Kastner^{1,2}

¹Umweltforschungszentrum; Germany

²Friedrich Schiller Universität Jena, Germany

E-mail: boehrer@gm.ufz.de

Precipitation and evaporation as well as all other inflows and water losses can be important for the development of the stratification in the lake. All methods of measuring precipitation on lakes are connected with problems as are assumptions about the losses due to evaporation, especially on small lakes, where wind conditions can be highly variable in space.

We show the results of measuring the water storage with several high resolution pressure sensors in the small mining lake RL111, which prove that the accuracy lies in the range of $1 \text{ kg} \cdot \text{m}^{-2}$ which corresponds to 1 mm of water column. This is better than one can manage from measurements of the water level, considering that thermal expansion is biasing those data.

Temperature Profile in Lake Bottom Sediments: An Analytical Self-Similar Solution

Dmitrii V. Mironov,^{1†} Sergej D. Golosov² and Ilya S. Zverev²

¹ German Weather Service, Offenbach am Main, Germany

² Institute of Limnology, Russian Academy of Sciences, St. Petersburg, Russia

Abstract

The vertical temperature structure of bottom sediments in lakes is discussed. Observations indicate that the temperature profile in the bottom sediments has the form of a thermal wave. The wave starts at the water-sediment interface and propagates downward as the lake water and the bottom sediments are heated during spring and summer. When heating ceases and cooling sets in, a new wave starts at the water-sediment interface and propagates downward as the lake water and the sediments are cooled over autumn and winter. Although the temperature in the thermally active layer of bottom sediments varies considerably with time, a characteristic *shape* of the temperature-depth curve remains approximately the same. Based on this observational evidence, a two-layer parametric representation of the temperature profile in lake bottom sediments was proposed. In this note, a theoretical explanation for the observed self-similarity of the temperature profile is offered. Assuming a travelling wave-type behaviour of the temperature profile in bottom sediments, an analytical solution to the heat transfer equation is found. This solution is compared with data from measurements in a number of lakes and in a laboratory tank.

1 Introduction

A distinctive feature of most shallow lakes, ponds and other natural and man-made reservoirs is a strong thermal interaction between the water body and the bottom sediments. A sizable portion of the heat received from the atmosphere during spring and summer is accumulated in the thermally active upper layer of bottom sediments. This heat is then returned back to the water column during autumn and winter, leading to a hysteresis-like behaviour of the seasonal temperature cycle of the water column-bottom sediment system.

A straightforward approach to describe the vertical temperature structure of bottom sediments is to use the equation of heat transfer with a priori knowledge of the thermal diffusivity of sediments (see Gu and Stefan 1990, Fang and Stefan 1996, 1998, and references therein). The major shortcoming of this straightforward approach is that the thermal diffusivity is strongly dependent on the composition of the sediments and on the amount of organic matter they contain and therefore it is rarely well known.

Golosov and Kreiman (1992) proposed an alternative way of describing the vertical temperature structure of bottom sediments. Their approach is based on a two-layer self-similar parametric representation of the evolving temperature profile in the sediments that is conceptually similar to a parametric representation of the temperature profile in the upper mixed layer and the seasonal thermocline in the ocean (Kitaigorodskii and Miropolsky 1970). Using empirical polynomial approximations of the temperature-depth curve, a computationally-efficient bulk model for calculating the temperature structure of bottom sediments and the heat flux through the water-sediment interface was developed (Golosov et al. 1998). The concept of self-similarity

[†]Corresponding author: Deutscher Wetterdienst, Referat FE14, Frankfurter Str. 135, D-63067 Offenbach am Main, Germany. E-mail: dmitrii.mironov@dwd.de

of the temperature profile in bottom sediments rests on empirical evidence and has received no theoretical explanation so far. In the present note, a plausible theoretical explanation for the observed self-similarity is offered in terms of the travelling wave-type solution to the heat transfer equation.

2 Background

Observations suggest (a summary of observational studies is given by Ryzanin 1997) that the temperature profile in bottom sediments has the form of a thermal wave. Typical temperature profiles in the lake bottom sediments are illustrated schematically in Fig. 1. The wave starts at the water-sediment interface $z = D$ and propagates downward as the lake water and the bottom sediments are heated during spring and summer. When heating ceases and cooling sets in, a new thermal wave starts at $z = D$. It propagates downward as the lake water and the sediments are cooled during autumn and winter, thus closing the annual cycle. The layer $D \leq z \leq L$, where seasonal temperature changes take place, is the thermally active layer of bottom sediments. Below the level $z = L$ the temperature changes are negligibly small. Importantly, a characteristic *shape* of the temperature-depth curve remains approximately the same, although the temperature at different depths varies considerably with time. Motivated by this empirical evidence, a two-layer self-similar parametric representation of the temperature profile in the bottom sediments was proposed by Golosov and Kreiman (1992) and further developed by Golosov et al. (1998). The expression of Golosov et al. (1998) reads

$$\theta(z, t) = \begin{cases} \theta_D(t) + [\theta_H(t) - \theta_D(t)]\Theta(\zeta) & \text{at } D \leq z \leq H(t) \\ \theta_H(t) + [\theta_L - \theta_H(t)]\vartheta(\xi) & \text{at } H(t) \leq z \leq L. \end{cases} \quad (1)$$

Here, t is time, $\theta(z, t)$ is the temperature, θ_L is the (constant) temperature at the outer edge $z = L$ of the thermally active layer of the sediments, $\theta_D(t)$ is the temperature at the water-sediment interface, $\theta_H(t)$ is the temperature at the depth $H(t)$ penetrated by the wave, and $\Theta \equiv [\theta(z, t) - \theta_D(t)]/[\theta_H(t) - \theta_D(t)]$ and $\vartheta \equiv [\theta(z, t) - \theta_H(t)]/[\theta_L - \theta_H(t)]$ are dimensionless universal functions of dimensionless depths $\zeta \equiv [z - D]/[H(t) - D]$ and $\xi \equiv [z - H(t)]/[L - H(t)]$, respectively. These functions, often referred to as shape functions, are universal in the sense that they are independent of time, although the temperature and the depth penetrated by the wave are time dependent. Using empirical polynomial approximations of $\Theta(\zeta)$ and $\vartheta(\xi)$, Golosov et al. (1998) developed a simple procedure for calculating the heat flux through the water-sediment interface. Simulations of the seasonal cycle of temperature in the bottom sediments of several lakes using this procedure showed a satisfactory agreement with observations (Golosov et al. 1998, Kondratiev et al. 1998).

Notice that the temperature profile below the level $z = H$ penetrated by the thermal wave does not remain “frozen”. Some temperature changes do occur at $z > H$ through molecular heat conductivity due to the non-linearity of the initial temperature profile. These changes are, however, very slow as compared to the temperature changes in the layer $D \leq z \leq H$. A model of the vertical temperature structure of bottom sediments, where $\partial\theta/\partial t = 0$ at $z > H$, i.e. the point $(z = H, \theta = \theta_H)$ slides down the initial temperature profile, was considered by Golosov and Kreiman (1992). Here, no consideration is given to the temperature distribution at $z > H$. We focus attention on the layer $D \leq z \leq H$ where major temperature changes take place.

There is a close analogy between the self-similarity of the temperature profile in bottom sediments and the self-similarity of the temperature profile in the upper mixed layer and in the seasonal thermocline in the ocean and lakes. Using the mixed-layer temperature θ_s and its depth

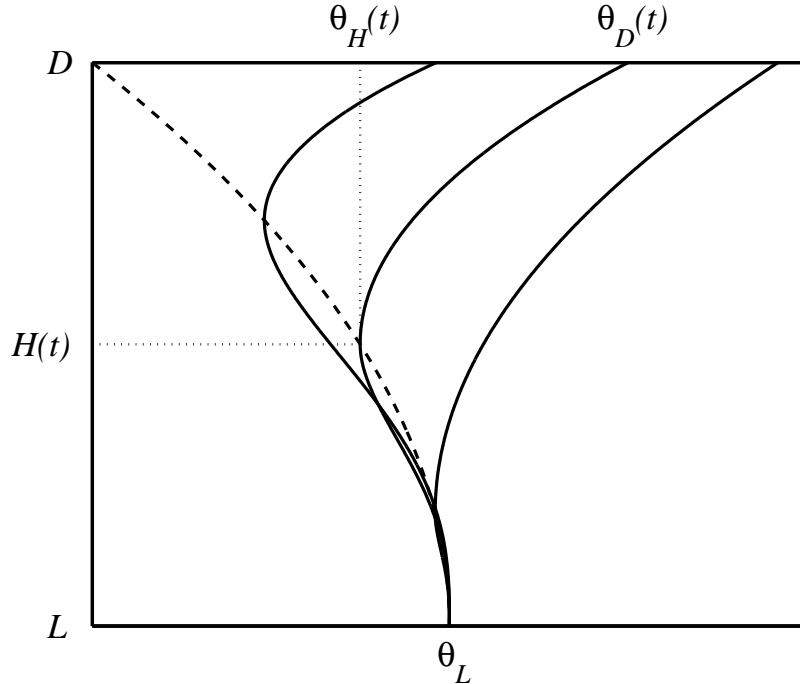


Figure 1: Schematic representation of the temperature profiles in bottom sediments during the period of heating. Dashed curve shows the initial temperature profile, i.e. the profile developed towards the end of the previous period of cooling. The profiles during the period of cooling are mirror images of the profiles during the period of heating.

h , the mixed layer concept can be expressed as $\theta(z, t)/\theta_s(t) = \Phi_{ML}[z/h(t)]$, where a dimensionless universal function Φ_{ML} is simply a constant equal to one. The concept of the temperature uniform mixed layer has been extensively used in geophysical fluid dynamics over several decades. Its natural extension is the concept of self-similarity of the temperature profile in the thermocline. It was put forward by Kitaigorodskii and Miropolsky (1970) to describe the vertical temperature structure of the oceanic seasonal thermocline. The essence of the concept is that the dimensionless temperature profile in the thermocline can be parameterized through a universal function of dimensionless depth, using the temperature difference $\Delta\theta$ across the thermocline and its thickness Δh as appropriate scales of temperature and depth, respectively. That is

$$\frac{\theta_s(t) - \theta(z, t)}{\Delta\theta(t)} = \Phi_T \left[\frac{z - h(t)}{\Delta h(t)} \right] \quad \text{at } h(t) \leq z \leq h(t) + \Delta h(t), \quad (2)$$

where a dimensionless function Φ_T , the shape function, is not merely a constant, as is the case with Φ_{ML} in the mixed layer, but a more sophisticated function of dimensionless depth. Notice that in small-to-medium depth reservoirs, the thermocline is pressed against the bottom. The abyssal quiescent layer is usually absent so that $\Delta\theta = \theta_s - \theta_D$ and $\Delta h = D - h$.

The concept of self-similarity of the temperature profile in the thermocline received support through observational (e.g. Filyushkin and Miropolsky 1981, Mälkki and Tamsalu 1985, Zilitinkevich 1991) and laboratory (e.g. Linden 1975, Wyatt 1978) studies. It proved to be a useful phenomenological alternative to a rigorous theory of turbulent heat transfer in strongly stable stratification characteristic of the thermocline. The concept has been successfully applied to model the oceanic seasonal thermocline (e.g. Kitaigorodskii and Miropolsky 1970, Arsenyev and Felzenbaum 1977, Filyushkin and Miropolsky 1981), the temperature inversion capping the

atmospheric convectively mixed layer (e.g. Deardorff 1979, Fedorovich and Mironov 1995) and seasonal temperature changes in fresh-water lakes (e.g. Zilitinkevich 1991, Mironov et al. 1991).

A plausible theoretical explanation for the observed self-similarity of the temperature profile in the thermocline was provided in case of the mixed-layer deepening, $dh/dt > 0$ (Barenblatt 1978, Turner 1978, Shapiro 1980, Zilitinkevich et al. 1988, Zilitinkevich and Mironov 1992, Kirillin 2001). Introducing a vertical co-ordinate moving with the mixed layer-thermocline interface and assuming constant temperatures at the upper and lower boundaries of the thermocline, these authors considered a travelling wave-type solution to the heat transfer equation,

$$\frac{\partial \theta}{\partial t} = \frac{\partial}{\partial z} K \frac{\partial \theta}{\partial z}, \quad (3)$$

where K is the temperature diffusivity that was either assumed to be constant, or was taken to be dependent on the temperature (density) stratification in the thermocline. The travelling wave-type analytical solutions to Eq. (3) proved to be fairly similar to empirical polynomial approximations of $(\theta_s - \theta)/\Delta\theta$ versus $(z - h)/\Delta h$ curve. We note that in case of the mixed-layer stationary state or retreat, $dh/dt \leq 0$, no theoretical explanation for the observed self-similarity of the temperature profile in the thermocline has been provided so far. The self-similarity at $dh/dt \leq 0$ should, therefore, be considered as purely phenomenological.

The thermal wave in the bottom sediments propagates downward both over the period of heating and over the period of cooling, so that $dH/dt > 0$. It is then tempting to find an analytical travelling wave-type solution to the heat transfer equation that would provide a theoretical explanation for the observed self-similarity of the temperature profile in bottom sediments. Such solution is presented in the next section.

3 Analytical Solution

Consider the simplest case of constant temperature diffusivity K of the bottom sediments. Introducing dimensionless variables $\Theta \equiv (\theta - \theta_D)/(\theta_H - \theta_D)$ and $\zeta \equiv (z - D)/(H - D)$, the equation of heat transfer (3) takes the form

$$\frac{d^2 \Theta}{d\zeta^2} + E\zeta \frac{d\Theta}{d\zeta} - (\Pi_D - \Pi_H)\Theta = -\Pi_D, \quad (4)$$

where $E = K^{-1}(H - D)dH/dt$ is the dimensionless rate of propagation of the thermal wave, and $\Pi_D = K^{-1}(\theta_D - \theta_H)^{-1}(H - D)^2 d\theta_D/dt$ and $\Pi_H = K^{-1}(\theta_D - \theta_H)^{-1}(H - D)^2 d\theta_H/dt$ are the dimensionless time-rates-of-change of the temperature at the water-sediment interface $z = D$ and at the depth $z = H$ penetrated by the wave, respectively.

Taking E , Π_D and Π_H to be constant (restrictions these assumptions impose on the feasibility of the results are discussed in the next section), Eq. (4) subject to the boundary conditions $\Theta(0) = 0$ and $\Theta(1) = 1$ has an analytical solution in the form

$$\Theta = \frac{\Pi_D}{\Pi_D - \Pi_H} \times \left(1 + \frac{\exp(-E\zeta^2/4)}{\zeta^{1/2}} \left\{ P \left[\frac{W_{p,1/4}(E/2)}{M_{p,1/4}(E/2)} M_{p,1/4}(E\zeta^2/2) - W_{p,1/4}(E\zeta^2/2) \right] - \frac{\Pi_H}{\Pi_D} \exp(E/4) \right\} \right), \quad (5)$$

where $P = 2^{1/4}\pi^{-1/2}E^{-1/4}\Gamma[(2E + \Pi_D - \Pi_H)/2E]$, $p = -[2(\Pi_D - \Pi_H) + E]/4E$, Γ is the Gamma function, and M and W are the Whittaker functions (Abramowitz and Stegun 1964, Chapter 13). The solution (5) describes a family of temperature-depth curves where the shape of the curve depends upon E , Π_D and Π_H .

4 Comparison with Data

In Fig. 2, the analytical solution (5) is compared with data from measurements in Lake Krasnoe, ca. 80 km north of St. Petersburg, Russia (Kuzmenko 1976, 1984), in Lake Velen, southern Sweden (Thanderz 1973) and in Lake Mendota, Wisconsin, USA (Birge et al. 1927), and with data from laboratory experiments (Golosoov et al. 1998).

Measurements of temperature in the bottom sediments of Lake Krasnoe were taken during the period from 1972 to 1985 at a number of stations with the water depth ranging from 3 m to 10 m. Measurements were taken with a slow-response temperature probe mounted on the tip of a thin metal rod. The rod was plunged into the sediment to position the probe at various depths where readings were taken. The spacing between the depths of measurements was from 0.25 m to 0.5 m, with the uppermost reading taken at the water-sediment interface and the lowermost reading 3–4 m beneath the interface. The temperature profiles were recorded three times a month when the lake was free of ice and once a month during the period of ice cover. The profiles selected for comparison with analytical results were taken at stations with the water depth of 10 m and 3 m. The data shown in Fig. 2 were taken during 1976, 1983 and 1980 and are representative of anomalously cold, of anomalously warm, and of climatologically mean weather conditions, respectively. Measurements in Lake Velen were performed during February – September 1971 at the station with the water depth of 11.5 m; details are given in Thanderz (1973). The temperature profiles shown in Fig. 2 are taken from temperature-depth plots. Also presented in Fig. 2 are data from the pioneering paper of Birge et al. (1927). These authors were apparently the first to consider the temperature distribution in lake bottom sediments based on measurements in Lake Mendota. Measurements were performed during the period from 1916 to 1921 at a number of stations with the water depth ranging from 8 m to 23.5 m.

Laboratory data on the temperature distribution in bottom sediments are taken from Golosoov et al. (1998). Experiments were performed in a rectangular tank 50 cm × 20 cm in cross-section, filled with 5 cm of water and 10 cm of sediment. Silt and sand were used as the working media. Heating of the sediment was accomplished by circulating warm water through the tank. The water temperature was controlled with a thermostat. Cooling of the sediment was achieved by adding ice to the system to keep the water temperature close to the freezing point. Temperature records were obtained with a thermistor chain. The chain has 7 thermistors with 1.5 cm spacing, the uppermost sensor being at the water-sediment interface. An experiment with the silt consisted of a period of heating over 1.75 hours, followed by a period of cooling over 1 hour. An experiment with the sand consisted of a period of heating over 1 hour. The temperature profiles were recorded at 5 to 10 minute intervals.

As we have mentioned in the previous section, the analytical solution (5) is conditioned by a constant dimensionless propagation rate of the thermal wave, $E = K^{-1}(H - D)dH/dt$, and constant time-rates-of-change of the temperatures at the water-sediment interface and at the depth penetrated by the wave, $\Pi_D = K^{-1}(\theta_D - \theta_H)^{-1}(H - D)^2 d\theta_D/dt$ and $\Pi_H = K^{-1}(\theta_D - \theta_H)^{-1}(H - D)^2 d\theta_H/dt$, respectively. In case E , Π_D and Π_H are not constant but vary slowly with time, the self-similarity of the temperature profile in bottom sediments is approximate. If these parameters undergo fast changes, no self-similarity is expected. The condition $E = const$ implies that the depth penetrated by the thermal wave grows as $H - D = (2EKt)^{1/2}$. This 1/2 power law is consistent with empirical and laboratory data (see Golosoov et al. 1998), except at the initial stage and at the final stage of the development of the thermal wave. We therefore excluded from the analysis the temperature profiles with H close to D and H close to L . The conditions $\Pi_D = const$ and $\Pi_H = const$ imply that $\theta_D/\theta_* = \Pi_D(\Pi_D - \Pi_H)^{-1}(t/t_*)^{(\Pi_D - \Pi_H)/2E}$ and $\theta_H/\theta_* = \Pi_H(\Pi_D - \Pi_H)^{-1}(t/t_*)^{(\Pi_D - \Pi_H)/2E}$, where θ_* and t_* are the temperature and time

scales. These power laws (that obey initial conditions $\theta_H = \theta_D = 0$ at $t = 0$) describe a broad spectrum of time dependencies of θ_D and θ_H and therefore impose rather mild restrictions on the feasibility of analytical results.

Following Golosov et al. (1998), the depth $z = H$ penetrated by the wave is determined from the measured temperature profiles as the level of zero vertical temperature gradient. As this is not the only conceivable way to determine H , some uncertainty may be introduced. It is likely to be small, however, considering that the temperature changes below the level of zero temperature gradient are small for the majority of profiles used for the analysis. The dimensionless parameters E , Π_D and Π_H are estimated from the measured temperature profiles, using finite-difference approximations of time derivatives of H , θ_D and θ_H . We find that the values $E = 1$, $\Pi_D = 2$ and $\Pi_H = 1$ and $E = 2$, $\Pi_D = 4$ and $\Pi_H = 2$ cover for the most part the range of conditions characteristic of the lakes and of the laboratory experiments considered in the present study. Theoretical curves plotted in Fig. 2 correspond to three different combinations of the dimensionless parameters: $E = 1$, $\Pi_D = 2$ and $\Pi_H = 1$; $E = 1.5$, $\Pi_D = 3$ and $\Pi_H = 1.5$; and $E = 2$, $\Pi_D = 4$ and $\Pi_H = 2$. As Fig. 2 suggests, the analytical results are in good agreement with observational and laboratory data. On the average, the curve that corresponds to $E = 1.5$, $\Pi_D = 3$ and $\Pi_H = 1.5$ gives the best fit to the data. The scatter of data is substantial, however.

Also shown in Fig. 2 is a phenomenological approximation of $\Theta(\zeta)$ proposed by Golosov et al. (1998), using a geometrical approach. These authors expressed Θ as a polynomial in ζ and invoked boundary conditions to specify the polynomial coefficients. The conditions $\Theta(0) = 0$ and $\Theta(1) = 1$ follow from the definition of Θ and ζ . The third condition is the zero temperature gradient at the depth penetrated by the thermal wave, that is $d\Theta(1)/d\zeta = 0$. The resulting expression is the second-order polynomial

$$\Theta = 2\zeta - \zeta^2, \quad (6)$$

which is the simplest polynomial that satisfies a minimum set of constraints. As seen from Fig. 2, the polynomial (6) lies in the region bounded by the upper and the lower analytical curves. By and large it slightly underestimates the data.

5 Conclusions

The vertical temperature profile in bottom sediments in lakes, ponds and other natural and man-made reservoirs was observed to be self-similar, having the form of a thermal wave that propagates from the water-sediment interface downward. The self-similarity means that, although the temperature in the thermally active upper layer of bottom sediments varies considerably with time, a characteristic shape of the temperature-depth curve remains approximately the same.

A theoretical explanation for the observed self-similarity of the temperature profile in bottom sediments is offered. Assuming a travelling wave-type behaviour of the temperature profile, an analytical solution to the heat transfer equation is found. This solution compares favourably with data from measurements in a number of lakes and with data from laboratory experiments. The analytical solution, Eq. (5), appears to be fairly similar to a phenomenological polynomial approximation of the temperature profile, Eq. (6), developed on the basis of empirical data.

Acknowledgments. We are grateful to Evgeni Sulkovsky for his painstaking effort in performing laboratory experiments, to Lyudmila Kuzmenko for providing data from measurements in Lake Krasnoe, and to Erdmann Heise for useful comments. The work was partially supported by the European Commissions through the project INTAS-01-2132 ‘‘Representation of Lakes in Numerical Models for Environmental Applications’’.

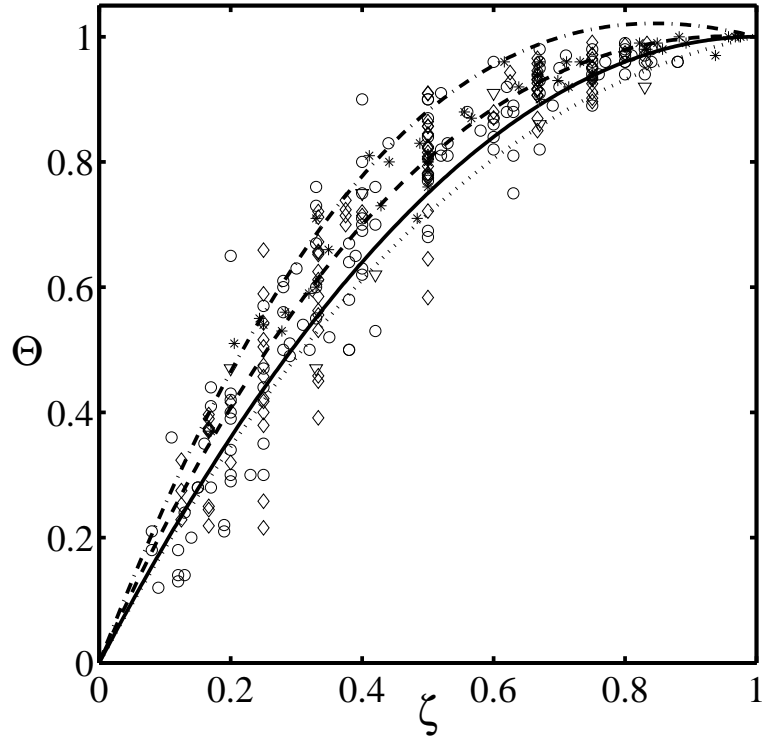


Figure 2: Dimensionless temperature $\Theta \equiv (\theta - \theta_D)/(\theta_H - \theta_D)$ as a function of dimensionless depths $\zeta \equiv (z - D)/(H - D)$. Open symbols show data from measurements in Lake Krasnoe (circles), in Lake Velen (triangles), and in Lake Mendota (diamonds). Asterisks show data from laboratory experiments. Solid curve shows a phenomenological approximation (6). Other curves show the travelling wave-type analytical solution (5) with different values of dimensionless parameters E , Π_D and Π_H : $E = 1$, $\Pi_D = 2$ and $\Pi_H = 1$, dotted curve; $E = 1.5$, $\Pi_D = 3$ and $\Pi_H = 1.5$, dashed curve; and $E = 2$, $\Pi_D = 4$ and $\Pi_H = 2$, dot-dashed curve.

References

- Abramowitz, M., and I. A. Stegun, 1964: *Handbook of Mathematical Functions*. National Bureau of Standards, Applied Mathematics Series 55.
- Arsenyev, S. A., and A. I. Felzenbaum, 1977: Integral model of the active ocean layer. *Izv. Akad. Nauk SSSR. Fizika Atmosfery i Okeana*, **13**, 1034–1043.
- Barenblatt, G. I., 1978: On the self-similar distribution of temperature and salinity in the upper thermocline. *Izv. Akad. Nauk SSSR. Fizika Atmosfery i Okeana*, **14**, 1160–1166.
- Birge, E. A., C. Juday, and H. W. March, 1927: The temperature of the bottom deposits of Lake Mendota. *Trans. Wiscon. Acad. Sci.*, **23**, 187–231.
- Deardorff, J. W., 1979: Prediction of convective mixed-layer entrainment for realistic capping inversion structure. *J. Atmos. Sci.*, **36**, 424–436.
- Fang, X., and H. G. Stefan, 1996: Dynamics of heat exchange between sediment and water in a lake. *Water Resour. Res.*, **32**, 1719–1727.
- Fang, X., and H. G. Stefan, 1998: Temperature variability in lake sediments. *Water Resour. Res.*, **34**, 717–729.

- Fedorovich, E. E., and D. V. Mironov, 1995: A model for shear-free convective boundary layer with parameterized capping inversion structure. *J. Atmos. Sci.*, **52**, 83–95.
- Filyushkin, B. N., and Yu. Z. Miropolsky, 1981: Seasonal variability of the upper thermocline and self-similarity of temperature profiles. *Okeanologia*, **21**, 416–424.
- Golosov, S. D., and K. D. Kreiman, 1992: Heat exchange and thermal structure within “water-sediments” system. *Vodnye Resursy (Water Resources)*, **6**, 92–97.
- Golosov, S., I. Zverev, and A. Terzhevik, 1998: Modelling Thermal Structure and Heat Interaction between a Water Column and Bottom Sediments. *Report No. 3220 [LUTVDG/(TVVR-3220) 1-41(1998)]*, Dept. of Water Resources Engineering, Inst. of Technology, Univ. of Lund, Lund, Sweden, 41 pp.
- Gu, R., and H. G. Stefan, 1990: Year-round temperature simulation of cold climate lakes. *Cold Regions Sci. Technol.*, **18**, 147–160, 1990.
- Kirillin, G., 2001: On self-similarity of thermocline in shallow lakes. *Proc. of the 6th Workshop on Physical Processes in Natural Waters*, X. Casamitjana, Ed., University of Girona, Girona, Spain, 221–225.
- Kitaigorodskii, S. A., and Yu. Z. Miropolsky, 1970: On the theory of the open ocean active layer. *Izv. Akad. Nauk SSSR. Fizika Atmosfery i Okeana*, **6**, 178–188.
- Kondratiev, S. A., S. D. Golosov, K. D. Kreiman, and N. V. Ignatieva, 1998: Modelling hydrological processes and mass transfer in a watershed-lake system. *Vodnye Resursy (Water Resources)*, **25**, 571–580.
- Kuzmenko, L. G., 1976: Thermal regime of the water column and bottom sediments in a lake. *Biological Productivity of Lake Krasnoe and Conditions of Its Formation*, I. N. Andronikova and K. A. Mokievskii, Eds., Nauka Publishing House, Leningrad, 18–36.
- Kuzmenko, L. G., 1984: Seasonal thermal structure of lakes. *Features of the Water Quality of Lakes of Karelian Isthmus*, I. N. Andronikova and K. A. Mokievskii, Eds., Nauka Publishing House, Leningrad, 45–60.
- Linden, P. F., 1975: The deepening of a mixed layer in a stratified fluid. *J. Fluid Mech.*, **71**, 385–405.
- Mälkki, P., and R. E. Tamsalu, 1985: Physical Features of the Baltic Sea. *Finnish Marine Research*, No. 252, Helsinki, 110 pp.
- Mironov, D. V., S. D. Golosov, S. S. Zilitinkevich, K. D. Kreiman, and A. Yu. Terzhevik, 1991: Seasonal changes of temperature and mixing conditions in a lake. *Modelling Air-Lake Interaction. Physical Background*, S. S. Zilitinkevich, Ed., Springer-Verlag, Berlin, etc., 74–90.
- Ryanzhin, S. V., 1997: *Thermophysical Properties of Lake Sediments and Water-Sediments Heat Interaction*. Report No. 3214, Dept. of Water Resources Engineering, Inst. of Technology, Univ. of Lund, Lund, Sweden, 95 pp.
- Shapiro, G. I., 1980: Effect of fluctuations in the turbulent entrainment layer on the heat and mass transfer in the upper thermocline. *Izv. Akad. Nauk SSSR. Fizika Atmosfery i Okeana*, **16**, 433–436.
- Thanderz, L., 1973: Heat budget studies. *Dynamic Studies in Lake Velen*, M. Falkenmark, Ed., NFR (Swedish Natural Science Research Council), Intern. Hydrol. Decade, Report 31, 51–78.
- Turner, J. S., 1978: The temperature profile below the surface mixed layer. *Ocean Modeling*, No. 11, 6–8.
- Wyatt, L. R., 1978: Mixed layer development in an annular tank. *Ocean Modeling*, No. 17, 6–8.
- Zilitinkevich, S. S., 1991: *Turbulent Penetrative Convection*. Avebury Technical, Aldershot, 179 pp.
- Zilitinkevich, S. S., K. D. Kreiman, and A. I. Felzenbaum, 1988: Turbulence, heat exchange and self-similarity of the temperature profile in a thermocline. *Dokl. Akad. Nauk SSSR.*, **300**, 1226–1230.
- Zilitinkevich, S. S., and D. V. Mironov, 1992: Theoretical model of the thermocline in a freshwater basin. *J. Phys. Oceanogr.*, **22**, 988–996.

Study of physical processes in coastal zone for detecting anthropogenic impact by means of remote sensing

Valery G. Bondur¹ and Nikolai N. Filatov²

¹ Scientific-educational center “Aerokosmos” of Moscow State University of Geodesy and Cartography, Moscow,

² Northern Water Problems Institute, Petrozavodsk, Russia;
E-mail: nfilatov@nwpi.karelia.ru

A complex study of physical processes in the coastal zone for detecting anthropogenic impact on coastal waters by means of remote sensing was performed in the shelf zone of Oahu Island, Hawaii in August-September 2002 (Bondur, Vinogradov et al, 2003). Using observational data from the buoy stations, analysis of surface and internal waves, turbulence, microstructure, currents and tides was done.

Materials and methods of investigations

Several buoy stations were installed for registrations, i.e. two buoy stations on the shelf zone on depths ~60 m for measuring currents with use of ADCP, one buoy station with Aanderaa thermistor chain, three buoy stations to measure surface waves (Sullivan, Dayananda, 1996; Oceanit, 2003). Also, measurements of turbulence, microstructure, temperature fields, salinity and conductivity using sondes (MSS) were performed from the boat board (Gibson et al, 2003). A methodology for detecting submerged outfall, wastewaters and to determine their shape and size with use of high-resolution remote sensing data from satellites Ikonos-2 and QuickBird was developed.

Currents

A variability of currents was analyzed in the time scales varying from several minutes up to 36 hours, i.e. from the Vaisial-Brendt's frequency to the local inertial period. 3D progressive vector diagrams of currents observed at the stations B2 and B4 for various depths were calculated. These diagrams enabled to determine trajectories of water masses. An along-shore flow having direction of 220° (i.e. SW) is dominant at the depths of 10, 30 and 60 m with quasi-wave fluctuations of current fields in the southwest – southeast directions.

At the station located in the proximity of the diffuser, the components V_e and V_n at all the depths are mainly affected by semidiurnal tidal oscillations. It should be also pointed out that the oscillations of amplitudes of velocities at all the levels are practically synchronous.

Vector-Algebraic Method for Analyzing ocean currents

The data on velocities of currents collected in September 2002 within the framework of the project was processed with use of analysis of vector time series. At present, due to lack of uniform generally accepted technique of analysis of time series, data processing for currents is performed on the basis of substitution of velocity vector: projections of velocity vector to Cartesian axis (component method); complex-valued method that represents complex number, its real and imaginary members being equal to the projections of velocity vector to Cartesian axis; method of rotary-components (see Mooers, 1973; Gonella, 1972). In this work, the advanced vectorial-algebraic method developed by Rozhkov et al. (1983) was applied. The most general model of the ocean currents is their representation in a form of non-stationary non-homogeneous vectorial stochastic functions with values in Euclidean space (see Limnology and Remote sensing, 1999).

As the main probability characteristics of current velocities we assume expectation vector V , correlation tensor determined as an expectation of tensor product of vectors and also spectral

density tensors determined through one- and two-fold Fourier's transformation of the correlation function. Functions $S_V(\bullet)$ characterize distribution by the frequencies of oscillations of current velocities and give a quantitative measure of intensity of such oscillations and their orientation in the accepted system of coordinates and changes in time. The abovementioned probability characteristics are invariant by the method of determination, and do not depend on the choice of a system of coordinates. The properties of the tensor-functions $K_V(\bullet)$, and so the process $V(t)$ properties may be most completely opened through the set of invariant scalar functions; characterize by correspondingly interrelation of collinear and orthogonal components (or their Fourier's function) of the vectorial process. Central problems of processing and analysis of natural data are formulation of the estimation rule and determination of the measure of proximity of estimate to the probability characteristic.

Time series analysis of vector currents in the experiment allows us establishing the dominance of tidal semidiurnal phenomena ($\omega \sim 0.5 \text{ rad}\cdot\text{h}^{-1}$), there were also detected small diurnal ($\omega \sim 0.26 \text{ rad}\cdot\text{h}^{-1}$), long-period ($\omega < 0.1 \text{ rad}\cdot\text{h}^{-1}$) and 6 hour ($\omega \sim 1 \text{ rad}\cdot\text{h}^{-1}$) fluctuations. Diurnal fluctuations of currents in upper layers (0-10 m) are caused by diurnal variations of meteorological parameters. Analysis of high-frequency spectral bands of horizontal and vertical components of current vector has shown that the short-period internal waves also have turbulent motions of diverse genesis. The tidal ellipse at the upper level has a greater anisotropy compared to that observed at the depth more than 30 m. In relatively high-frequency spectral band of currents ($\omega \geq 1.0 \text{ rad}\cdot\text{h}^{-1}$) any noticeable fluctuations of velocities were not observed. Thus, as our analysis of the rotation indicator shows, in low-frequency range the rotation was clockwise (inertial oscillations) while the tidal component rotating counter-clockwise at all depths. The rotation of vector of currents with semidiurnal period is explained by the tendency of direction of the main current to the zone of steep depth gradient. Oscillations of currents in the upper layers with diurnal recurrence (September, depths of 0-30 m) could be caused by diurnal changes of meteorological parameters.

Water temperature distributions and internal waves

Water salinity and temperatures data were collected at five stations with use of CTD "Seabird" and MSS sondes. Investigations of salinity near the diffuser show complicated vertical profiles of salinity, which are most probably caused by the intrusion of wastewater discharged from the diffuser. The Aanderaa thermistor chain data enable estimating the temperature variability at station B2 at depths of 18-60 m. Sampled data on the temperature have allowed evaluating the density spectrum of internal gravity-inertial waves in temporal ranges varying from local inertial band ($\omega \approx f$) to short-term intervals of ~ 15 minutes typical for the Brunt-Väisälä local frequency. Data of analysis clearly shows that there is a strong correlation between the seawater temperature changes registered at the 60-m depth and regular ascending and descending of the oceanic level caused by the tidal forces. It should be noted that the phase of high water (tide) corresponds to an increase of water temperature at depths of 30-60 m. Under these conditions, the thermocline is descending down to deeper levels. Spectral analysis of water temperature shows, that the maximum in spectra is observed at the frequency of semidiurnal oscillations ($\omega \sim 0,5 \text{ rad}\cdot\text{h}^{-1}$) were detected together with several small maxima (the temporal scales varying from 3 to 12 hours). Those spectra reveal the existence of harmonics corresponding to the groups of internal waves having random phases and amplitudes.

The "fast" temperature variations observed above the diffuser, have the major impact on the sewages' surfacing and on the level of pollution concentration in the water area. Sharp changes of temperature and current velocities are possibly related to the internal waves caused by the tidal waves colliding steep coasts. Studies of internal waves were carried out through the analysis of changing isotherm depths. The spectrum of internal waves (see Fig. 1) has the main maximum at

the tidal frequency ($\omega \sim 0.5 \text{ rad}\cdot\text{h}^{-1}$), as well as minor maxima in high frequency range ($\omega / 1 \text{ rad}\cdot\text{h}^{-1}$) caused by short-period internal waves. On the base of data on the depth of 25°C isotherm there was constructed a frequency-temporal spectrum $S(\omega, t)$ built by means of calculating the spectra of internal waves for several time spans belonging to the observation period non stationary spectra of internal waves for different time intervals. These spectra composed for these five time intervals determine the energy distribution at temporal scales varying from diurnal ones to the scales corresponding to the local Brunt-Väisälä frequency $N(z)$. These figures demonstrate essential variability of spectra in time. Generally, the presence of maxima at tidal semidiurnal frequency ($\omega \sim 0.5 \text{ rad}\cdot\text{h}^{-1}$) is observed there. When the energy of semidiurnal tidal waves reaches its maximum, there are no significant maxima in the high frequency ($\omega/0.5 \text{ rad}\cdot\text{h}^{-1}$) spectral range [see Fig. 1 (a)]. When the amplitude of tidal waves decreases in this spectral band, there are observed higher frequency maxima corresponding to 6 and 3 hours. In the high frequency spectral range, there were not detected any important periodic fluctuations, and the slope of the spectrum of internal was proportional to $\omega \sim n^2$ what is typical of internal oceanic waves.

Presence of predominant semidiurnal tidal internal waves with average amplitude of 8 m and diurnal oscillations of considerably smaller amplitudes was also detected. Descending of the thermocline causes intensive internal waves of the lowest mode of 30 m amplitude that could lead to the ascent of discharged sewages to the near-surface level. Spectral analysis of water temperatures time series and temperature fields has allowed us detecting rapid changes of temperature above the diffuser (caused by internal waves, which appear when the tidal waves collide with the steep coast). That leads to the ascending of sewages and to an increase of concentration of pollutants in the water area.

Turbulence and microstructure

Comprehensive measurements of microstructures and turbulence realized by Prof. C. Gibson (Gibson et al., 2003) during the experiment have shown that the discharge jet velocity is a source of strongly active, local turbulence in the immediate diffuser area. Diluted effluent forms a rising, buoyancy driven turbulent plume that is trapped below the sea surface, forming partially fossilized turbulence microstructure patches. The patches are convected by the local currents.

This process of turbulence fossilization and re-generation is repeated along the vertical and stops by wave breaking at the surface, which interferes with the surface wave field. This generates the surface wave field anomalies detected by remote sensing methods. The observed phenomena were caused by other physical mechanisms of interaction at surface and internal waves (Bondur and Grebenuk, 2001).

Surface waves

To determine spectra of surface heaving in the water area of the Mamala Bay, there were used three wave buoys (wave recorders), namely two Directional Waveriders buoys and the Trident Directional Wave buoy. Processing of in-situ measurements enabled to determine parameters describing relevant wave processes observed at those stations and namely, $S(\omega, \theta)$ and $S(\omega)$. An analysis of these spectra $S(\omega)$ observed at the stations was carried out in the spectrum band of $0,157 \leq \omega \leq 3,644 \text{ sec}^{-1}$, i.e. in the band of gravitational waves. They have at least three apparent spectral maximums at the following frequencies: $\omega_{\max 1} \approx 0,41 \text{ s}^{-1}$, $\omega_{\max 2} \approx 0,69 \text{ s}^{-1}$, $\omega_{\max 3} \approx 1,57 \text{ s}^{-1}$. That allows supposing existence of three systems of waves in the water area studied that seriously complicates the analysis of wave processes. Spatial periods of wind driven sea surface heaving could be determined with the help of empirical evaluation of the heaving spectra. For example, use of Pearson-Moskovitz method gives the values of spatial periods varying from 10 m to 55 m. That allows guessing that the wave field observed in the region was affected by two systems of swell waves having average lengths $\lambda \sim 370 \text{ m}$ and $\lambda \sim 130 \text{ m}$, as well as by the system of wind

driven waves ($\lambda \sim 25$ m). Spectral density $S(\omega)$ of swell waves of $\lambda^{(1)}_{\max} \approx 370$ m were in 5,8 times greater than that of $\lambda^{(2)}_{\max} \approx 130$ m and about in 22,5 times greater than the value of $S(\omega)$ for wind driven waves. Spectral maxima are clearly seen in the frequency-oriented $S(\omega, \theta)$ spectra enables to determine trends of propagation of selected wave groups and their dynamics.

The values of wave lengths for detected spectral maxima coincide with those derived from “Ikonos-2” imagery spatial spectra $S(k_x, k_y)$ in the range of registered scales.

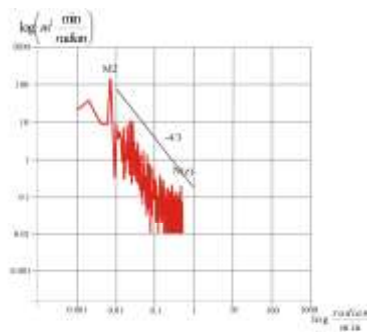


Fig. 4.27. Spectrum of internal waves (25°C isotherm) for the period of September 1-6, 2002, Mensala Bay, station 02

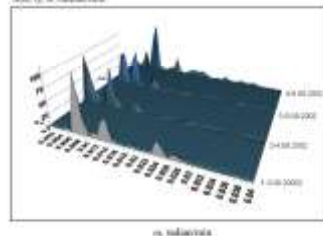


Fig. 4.28. Time-and-frequency spectra of internal waves (25°C isotherm depth) at the station 02

Fig. 1. Spectra of internal waves (calculated from values of the 25°C-isotherm depth)

Summary

The experiment shows main features of oceanographic parameters in the coastal zone. Physical backgrounds for the Detection of Anthropogenic Impact on the Littoral Waters (coastal zone) by remote sensing methods were developed. Various methods, including uncontrollable classification, color-coding, calculation of ratios of band signals and filtration were used for the processing of multi-spectral “Ikonos-2” and ISS imagery taken during the period of our sub-satellite experiments and for the processing of multi-spectral “Ikonos-2” images.

A complex analysis of zones of the sea heaving anomalies highlighted with use of spatial spectra of satellite imagery and the anomalies in the near-surface layers observed in multi-spectral images, and the results of sub-satellite measurements have shown good correlation. Contact measurements of current fields, turbidity, salinity and biological parameters distribution confirm presence of southwest and southeast lobes in zones of anomalies propagation detected at the processing of remotely sensed data. Main harmonics detected in spectra of satellite images were also detected in frequency spectra, measured in the vicinity of the outfall system.

Complex analysis of space data and also hydrophysical and hydrobiological data obtained during *in situ* experiments and spatial spectral processing of “Ikonos-2” images and archival “QuickBird” imagery has allowed us detecting the regions of superficial anomalies caused by deep outfall system of sewage waters, and to determine their shape and size. Some of the anomalous formations studied had a butterfly-shaped form with southwest (214-224°) extending at about 10 km and having southeast lobes of 6 - 7 km length propagating in the directions of 147-152° (see Fig. 2 a). This

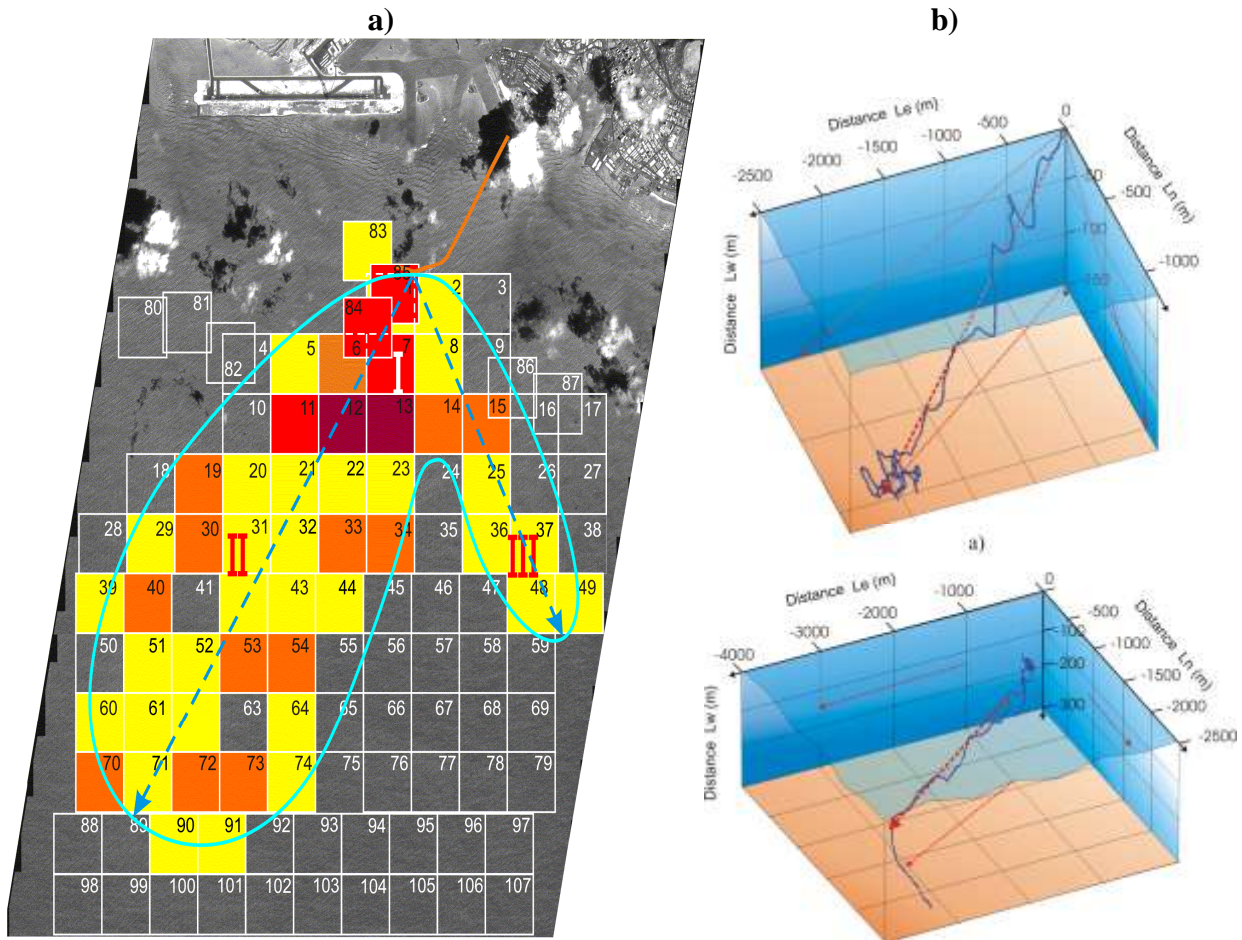


Fig. 2. a) Satellite data analysis from IKONOS-2 satellite panchromatic image, 1 m resolution in September 2002. The green boundary line is the outline of the waste field outlining the range of surface wave anomalies. The thick red line is the waste water submerge diffuser pipe coming from the Honolulu is in red at the top of the picture. Intensively of anomaly of manifestation of polluted waters show by colour; b) 3-D progressive-vector diagram at the station B2 near diffuser 2.09.02 and 6.09.02.

An analysis of 3D progressive-vector diagrams of currents (Fig. 2 b) are showed well agreement with propagation of superficial manifestations of the deep plume obtained by satellite imagery processing (Fig. 2 a).

References

- Bondur V.G., Vinogradov M.E., Dolotov U.S., Filatov N.N. at al., 2003. Final Report "Remote Sensing of Anthropogenic Influence caused by submerged sewers on ecosystems of Littoral Waters with use of space methods". Information Systems and Scientific Capacious Technologies, Moscow, 238 p.
- Patrick K. Sullivan, Dayananda Vithanage. Ocean outfall performance as a function of density gradient variations from internal waves. Hawaii Water Environmental Association 18th Annual Conference, 1996, 11p.
- Oceanit. Groundtruthing Measurements Data Report, Honolulu, March 2003, 26 p.
- Gibson C. H., P.T. Leung, F. Wolk, and H. Prantke, 2003. Interpretative Report of Microstructure Measurements conducted at the Sand Island Outfall., UCSD, San Diego, March 103 p.p.
- Moers C, 1973. A technique for analysis of pair complex-valued time series. *Deep-Sea Res.*, **20**: 1129-1141.

- Gonella J., 1972 A rotary-component method for analyzing meteorological and oceanographic vector time series. *Deep-Sea Res.*, **19**: 833-846.
- Rozhkov V.A., A.P., Belishev and Yu.P. Klevantcov Ju. P., 1983. *Vector analysis of ocean currents*. L.. 264 p. [In Russian]ю
- Kondratyev K. and N. Filatov (Eds.), 1999. *Limnology and Remote sensing*. Springer-Praxis. London. 412 p.
- Bondur, V. and G. Grebenuk, 2001. Remote sensing indications of anthropogenic impacts on sea waters by submerge outfalls: modeling and experiments. *J. Investigations of Earth from Space*. **6**: 49-67.

Differentiation of Suspended Bottom Deposits by Tidal Waves in Shallow Water

V. N. Zyryanov

Institute of Water Problems, Russian Academy of Sciences, Moscow, Russia;

E-mail: zyryanov@aqua.laser.ru

The problem of transport of suspended bottom deposits in a tidal flow in shallow water is an important component of the integrated problem associated with the dynamics of the coastal zone. The transport of a suspended admixture and associated lithodynamic processes occurring in shallow water are primarily defined by the joint action of tidal currents and wind waves. The transport of suspended matter by wind waves has been studied for a long time, whereas the problem of bottom transformation under the influence of tidal currents is at the initial stage of research. Interest in this problem has grown in relation to the problems of developing new gas deposits in the arctic seas.

The asymmetry of a tidal wave in shallow water is an important factor determining the process of suspended matter transport in the tidal flow when tidal flows are stronger but less prolonged than the ebb flows. An attempt is made in (Aubrey and Speer, 1983) to apply precisely this asymmetry to explain nonzero residual transport of suspended matter in the onshore direction.

Nevertheless, tidal asymmetry is not the only reason for residual transport. As was shown in (Postma, 1961), residual transport of suspended matter in the onshore direction is also induced by a symmetric tidal wave with a decreasing onshore direction.

At present, the two most extreme time scales, corresponding to quasi-stationary (riverine) flows and rapidly oscillating motions (wind waves), have been studied extensively while investigating the problem of suspended matter transport. Tidal flows fall in the middle of these time scales and are not related to either the first or the second type.

This work deals with the study of the peculiarities of suspended matter transport and evolution of a solitary sand macroform in the shallow zone of a tidal sea.

Residual tidal transport of water or, as it is sometimes called, residual tidal circulation (RTC) is a quasi-stationary component of the velocity of the currents in a tidal sea, which appears as a result of averaging the velocity over the period of the tidal wave. The residual tidal circulation has significantly smaller velocities as compared to the tidal current, but nevertheless, these residual currents together with the wind and gradient currents have precisely the main influence on the formation of the temperature and salinity fields and on the distribution of admixtures in a tidal sea. This is one of the reasons why so much attention is being paid to the investigation of tidal residual currents.

It is especially important to know the properties of residual tidal currents in the coastal zones of tidal seas, where pollution and admixtures are mainly transported by the continental runoff.

Sea floor transformation by tidal waves was studied in a semi-infinite channel using theoretical and experimental methods within a gradient-viscous model of tidal flow in shallow water with a depth less than the thickness of the Stokes layer

$$h < h_{st} = \sqrt{AT},$$

where A is the vertical turbulence viscosity and T is the period of a tidal wave (Zyryanov and Reshetkov, 1999). The results of laboratory experiments confirm the formation of inverse dunes in the tidal flow.

A new hydrodynamic effect: formation of a residual alongshore current by tides in a shallow water, when the water depth h becomes less than the thickness of the Stokes layer was described in (Zyryanov and Reshetkov, 1999). It is also shown that a residual tidal transport (RTT) of water

is formed to the right of the direction of the main tidal wave in the coastal region of the sea with supercritical depths $h < h_{st}$. Thus, the coast is on the left side of the residual current. The maximum velocities of the residual tidal transport are reached at the marine boundary of the zone of supercritical depths, and they can be as large as $1-2 \text{ cm}\cdot\text{s}^{-1}$. The results of a laboratory experiment confirming the theoretical results are presented.

Formulation of the problem

On the basis of experimental studies of the tidal currents in shallow water (Debol'skii et al., 1984) and other theoretical works (Zyryanov and Leibo, 1985; Zyryanov and Muzylev, 1988; Zyryanov, 1995), we found that the flow in long gravity waves is characterized by a gradient-viscous regime and the pressure gradient is balanced by the turbulent friction stress in the equation of momentum conservation under the condition that the depth is less than the thickness of the Stokes layer. The depth $h < h_{st}$ is called the supercritical depth (Zyryanov and Leibo, 1985). The sufficient condition for the existence of the gradient-viscous regime is the supercritical depth h and low Froude number

$$Fr = U^2 / gh \ll 1$$

(Zyryanov and Muzylev, 1988; Zyryanov, 1995). The value of the depth for a semidiurnal tidal wave is equal to 12-17 m if the value of the turbulent exchange coefficient characteristic of shallow-water tidal estuaries is $A \sim 102 \text{ cm}^2 \cdot \text{s}^{-1}$ (Debol'skii et al., 1984).

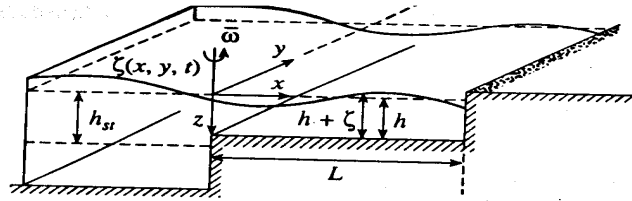


Fig.1. Scheme for the formulation of the problem.

We shall consider before the problem under the assumption of a semi-infinite coastal zone with a constant depth h , which is less than the critical depth for the given tidal wave with a period T (Fig. 1). The width of the zone is assumed to be much greater than its depth and much less than the external Rossby radius of deformation; thus, we can neglect the Coriolis acceleration in the first order of the approximation. Let us choose the axes of the left-hand Cartesian coordinate system in the following way: X-axis in the direction of the propagation of the front of the tidal wave, Y-axis parallel to the front of the wave, and Z-axis directed vertically downwards (Fig. 1). The origin of the coordinate system is at the non-disturbed surface of the sea, at the marine edge of the shallow-water zone. We use the gradient-viscous approximation, then, taking into account the Coriolis force for the homogeneous fluid, we shall have the following system of dynamic equations:

$$\frac{\partial}{\partial z} \left[A(x, y, z, t) \frac{\partial U}{\partial z} \right] + fV = \frac{1}{\rho_0} \frac{\partial p}{\partial x} \quad (1)$$

$$\frac{\partial}{\partial z} \left[A(x, y, z, t) \frac{\partial V}{\partial z} \right] - fU = \frac{1}{\rho_0} \frac{\partial p}{\partial y} \quad (2)$$

$$g\rho_0 = \frac{\partial p}{\partial z}, \quad (3)$$

$$\frac{\partial U}{\partial x} + \frac{\partial V}{\partial y} + \frac{\partial W}{\partial z} = 0, \quad (4)$$

$$\frac{\partial S}{\partial t} + U \frac{\partial S}{\partial x} + V \frac{\partial S}{\partial y} + (W + \omega_0) \frac{\partial S}{\partial z} = k_x \frac{\partial^2 S}{\partial x^2} + k_y \frac{\partial^2 S}{\partial y^2} + k_z \frac{\partial^2 S}{\partial z^2} \quad (5)$$

where $A(x, y, z, t)$ is the kinematic coefficient of vertical turbulent exchange, which is assumed constant $A(x, y, z, t) = A = \text{const}$; U , V and W are the horizontal and vertical components of the velocity vector, respectively; f is the Coriolis parameter, ρ_0 is the fluid density; p is the pressure in the fluid; $S(x, y, z, t)$ is the concentration of suspension; ω_0 is the fall velocity of the particles in the suspension and bottom deposits; and k_x , k_y and k_z are horizontal and vertical coefficients of suspension diffusion, respectively, which are assumed to be constant.

Let us designate the elevation of the free surface as $\zeta(x, y, t)$ then, the total depth will be equal to

$$H(x, y, t) = h(x, y, t) + \zeta(x, y, t).$$

The boundary conditions are the following:

at the free surface of the fluid, $z = -\zeta(x, y, t)$

$$\text{a zero wind: } A \frac{\partial U}{\partial z} = A \frac{\partial V}{\partial z} = 0, \quad (6)$$

$$\text{the kinematic condition: } W \Big|_{z=-\zeta} = -\frac{\partial \zeta}{\partial t} + \left(U \frac{\partial \zeta}{\partial x} + V \frac{\partial \zeta}{\partial y} \right) \Big|_{z=-\zeta} \quad (7)$$

$$\text{zero suspension transport is } \left[k_z \frac{\partial S}{\partial z} - (W + \omega_0) S \right] \Big|_{z=-\zeta} = 0; \quad (8)$$

at the bottom $z = h(x, y, t)$:

$$\text{the nonslip condition for the fluid is } U \Big|_{z=h} = V \Big|_{z=h} = W \Big|_{z=h} = 0; \quad (9)$$

$$\text{the suspension transport from the bottom is } k_z \frac{\partial S}{\partial z} \Big|_{z=h} = \frac{f + |f|}{2}, \quad (10)$$

where

$$f = |\zeta_x| \frac{Rg(h + \zeta)}{U_e^2} - R$$

is the function of the source of solid admixture, ζ_x is the slope of the surface; R is an empirical coefficient ($R=0.0086 \text{ kg m}^{-2} \text{ s}^{-1}$); U_e is the critical value of the dynamic velocity; when

$$U_*^2 = |\zeta_x| g(h + \zeta) \geq U_e^2,$$

tidal currents erode the bottom, and when

$$U_*^2 = |\zeta_x| g(h + \zeta) < U_e^2$$

there is no erosion and suspension is not transport into water. Condition (10) describes this pulse regime (Zyryanov and Reshetkov, 1999).

A tidal harmonic wave with period equal to T propagating from the deep water region ($x < 0$) along the normal to the marine boundary of the shallow-water area would generate a level displacement at the boundary of the shallow water (see Fig. 1):

$$\zeta(0, y, t) = \zeta^0 \sin(\omega t), \quad \omega = 2\pi/T \quad (11)$$

The gradient-viscous regime of the dynamics of tidal waves in shallow water of supercritical depth is described by a parabolic equation for the level [10]:

$$\frac{\partial \zeta}{\partial t} = \frac{g}{3A} \nabla \cdot [(h + \zeta)^3 \nabla \zeta] + \frac{2gf}{15A^2} \nabla \times [(h + \zeta)^5 \nabla \zeta], \quad (12)$$

where

$$\nabla = \left(\frac{\partial}{\partial x}, \frac{\partial}{\partial y} \right), \quad (\cdot), (\times)$$

are the scalar and vector products, respectively.

Solution of equation (12) with boundary condition (11) and the condition of wave attenuation at infinity for $x \rightarrow \infty$ in neglecting the Coriolis parameter in the first order approximation was obtained in (Zyryanov and Muzylev, 1988) using decomposition of the level into an asymptotic series with respect to a small parameter $\varepsilon = \zeta^0/h$:

$$\zeta = -h\varepsilon e^{-kx} \sin(\omega t - kx) - h\varepsilon^2 \left[\frac{3}{4}(1 - e^{-2kx}) + \frac{3}{2}e^{-2kx} \cos(2\omega t - 2kx) - \frac{3}{2}e^{-\sqrt{2}kx} \cos(2\omega t - \sqrt{2}kx) \right] + O(\varepsilon^2) \quad (13)$$

where k is found from the dispersion relation

$$k = k_0 \left(1 - \frac{9}{8}\varepsilon^2 + \dots \right), \quad k_0 = \sqrt{\frac{3\omega A}{2gh^3}} \quad (14)$$

The stationary part of the solution of (13)

$$\frac{3}{4}h\varepsilon^2(1 - e^{-2kx})$$

describes nonlinear level pumping (Zyryanov and Leibo, 1985; Zyryanov and Muzylev, 1988; Zyryanov, 1995). One can easily see from (1), (2), and (3) that the velocity profile will be parabolic in neglecting the Coriolis parameter.

Equation (5) will have the form

$$\omega_0 \frac{\partial S}{\partial z} = k_z \frac{\partial^2 S}{\partial z^2} \quad (15)$$

The solution of the equation (15) with boundary conditions (8), (10) is given by the expression

$$S(x, z, t) = \frac{f + |f|}{2\omega_0} \exp\left[\frac{\omega_0}{k_z}(z - h)\right] \quad (16)$$

Variation of the transport of suspended admixture

$$q(t) = \int_0^{h+\zeta} U S dz$$

calculated using relations (13), (14), and (16) during a tidal cycle for point $x = 6$ km with the depth of the channel $h = 5$ m at the value of $\zeta_0 = 0.5$ m in (11), is shown in Fig. 2. The integral of this transport over the period

$$I = \int_0^T q(t) dt$$

is positive. This means that there is an onshore residual suspension transport at each point of the shallow zone. Its value decreases approximately exponentially with the distance from the sea boundary of zone (Fig. 3). From this follows an important conclusion: in the case of non-deficit erosion of the bottom, deposits of sediments would occur over the entire zone of eroding velocities. The closer the point to the sea boundary of a zone l , the more intensive is the process. With a decrease in depth, this process decreases due to reducing the depth and consequently the decrease in tidal velocities.

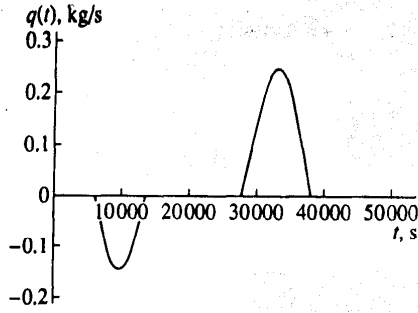


Fig. 2. Tidal evolution of the integral transport of suspension $q(t) = \int_0^{h+\zeta} USdz$ at the point $x = 6$ km of a semi-infinite channel when the values of the parameters are $\omega_0 = 1.5$ cm/s, $A = 0.01$ m²/s, $R = 0.0086$ kg m⁻² s⁻¹, $U_e = 0.041$ m/s, $\epsilon = 0.1$, $h = 5$ m, and $\zeta = 0.5$ m.

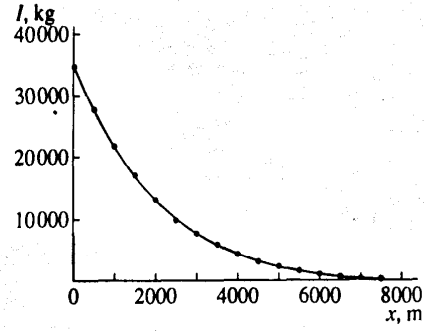


Fig. 3. Variation of residual integral transport of suspension $I = \int_0^T q(t)dt$ along the channel. The parameters are the same as in Fig. 2.

For each sediment fraction the critical distance from a sea boundary of a shallow zone exists farther with a tidal wave cannot transfer this fraction. In the first order approximation by ϵ it may be expressed by the inequality

$$x_i \leq -\frac{1}{k} \ln \left[\frac{(U_e^{(i)})^2}{\sqrt{2\zeta_0} k g h} \right]$$

It is apparent that the regime of bottom transformation described above is valid under the condition of equivalent erosion of the bottom at each point of the channel. This, however, is rarely encountered in practice. Finite (localized) forms of bottom sediments in the form of sand ridges located on a weakly eroded floor are usually observed in reality. Deficit zones would appear at the edges of these forms and the process of bottom transformation would be more complicated.

We emphasize that the existence of a nonzero average over the tidal period onshore transport of suspended particles in the tidal current is confirmed by the results of some field measurements.

Dynamics of finite bottom forms

The process of formation and transportation of localized bottom ridges under the influence of the tidal current was studied using the methods of numerical and laboratory modeling. The Cauchy problem for the equation of bottom deformation with account for relations (13) and (16) was solved in the first case. The initial form of the ridge was specified in the numerical experiment in the form of a part of a parabola with a height of 0.5 m and a length of $L = 10$ km, located on the non-eroded floor of the channel with a depth of $h = 5$ m. The results of numerical solution are shown in Fig. 4, where one can see that the symmetric ridge was transformed into a dune under the influence of the tidal wave. Its left (sea side) slope becomes steeper, and the right slope becomes flatter. At the same time, the dune slowly moves in the onshore direction. The displacement of the left boundary of the ridge during a time of $t=7T$ was equal to 0.8 km, the displacement of the right boundary was equal 3.6 km.

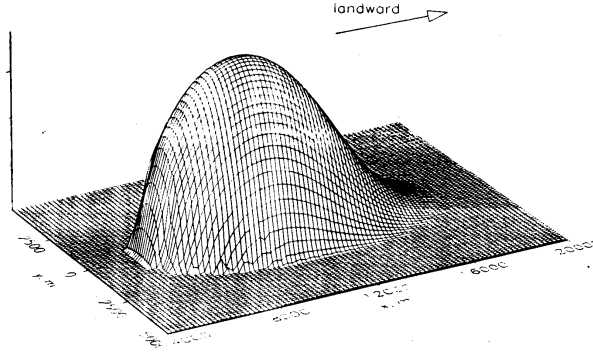


Fig. 4. The result of the numerical experiment. Formation of an inverse dune.

Residual water and suspended admixture transport

To find the solution when the width of supercritical depth is finite, we shall use the same approach as in (Postma, 1961) and seek the solution of equation (16) in the form of an asymptotic series with respect to $\varepsilon = \zeta^0/h$. Averaging equation (16) over the period of the tide and taking into account condition (15), we obtain

$$\frac{g}{3A} \left\langle (h + \zeta)^3 \frac{\partial \zeta}{\partial x} \right\rangle = 0, \quad (17)$$

where

$$\langle \phi \rangle = \frac{1}{T} \int_0^T \phi dt.$$

We can see that the expression (17) is the invariant, that is, the integral transport normal to the coast, averaged over the period, is equal to zero. Now, applying the averaging operation to the component of the integral transport along the coast S_y , we obtain the expression for the residual alongshore water transport:

$$\langle S_y \rangle = \frac{2gf}{15A^2} \left\langle (h + \zeta)^5 \frac{\partial \zeta}{\partial x} \right\rangle. \quad (18)$$

Finally, we shall obtain the expression for residual alongshore transport

$$\langle S_y \rangle = \frac{2gf h^6 \varepsilon^2}{15A^2 L} \frac{d}{dx} (\tilde{f} \tilde{f}^*), \quad (19)$$

where asterisk means complex conjugation and

$$\tilde{f} = \frac{\cosh[\tau(x-1)]}{\cosh(\tau)}, \quad \tau = (2\alpha)^{-1/2}(1+i), \quad \alpha = \frac{gh^3}{3AL^2\omega}, \quad (20)$$

i is the imaginary unit.

The distribution of the residual transport for several values of L including the infinite width of the shallow-water zone is shown in Fig. 5. One can see that when $L > 50$ km, we can practically use the approximation for the infinite width of the shallow-water zone. Residual alongshore water transport is formed in the zone of supercritical depths in the negative direction by Y . The latter means that, if we look in the direction of the residual current, the coast would always be on the left. This remarkable theoretical result was obtained for the first time for the case of the infinite width of the shallow-water zone in paper (Zyryanov, 1995) and had experimental confirmation in paper (Zyryanov and Reshetkov, 1999).

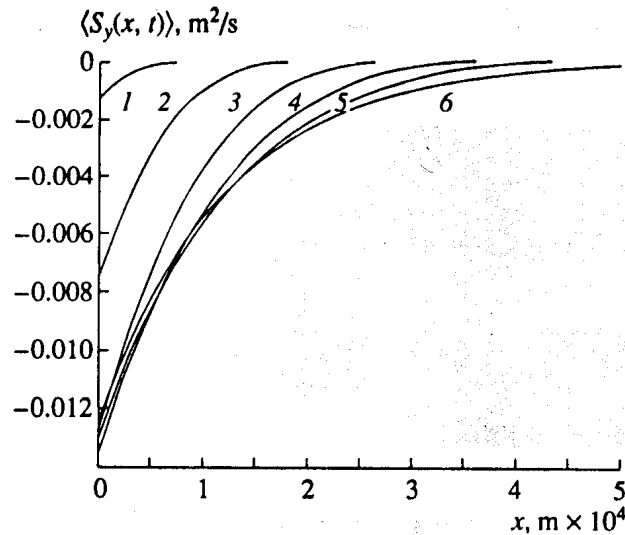


Fig.5. Graphs of the integral transport of the residual longshore water and suspended admixture transport for different values of the shallow-water zone with a width of L : (1) – 10 km; (2) – 20 km; (3) – 30 km; (4) – 40 km; (5) – 50 km, and (6) – ∞ . The values of the parameters are: $h = 5$ m, $A = 0.01$ m²/s, $f = 1.32 \cdot 10^{-4}$, $\varepsilon = 0.1$

Discussion of the results

As was shown above, the average transport of suspended particles in the tidal flow in shallow water over the tidal period is nonzero and directed onshore. Its values decrease with the growth in the distance from the boundary of the shallow water area with the sea. It is interesting that, unlike the transport of suspended matter, the fluid transport average over the tidal period at any point of the channel is zero (Zyryanov and Muzylev, 1988). The latter means that there is a nonzero residual Stokes velocity in the tidal wave.

The results of numerical calculations showed that under the influence of a tidal wave a solitary sand macroform is transformed into an asymmetric dune. Its slope closest to the shore becomes flatter and the distant one (offshore) becomes steeper. The macroform moves in the onshore direction. Macroforms of the dune and antidune types are well known in river flows. The dune is oriented with its steep ("lee") slope in the direction of the suspended matter transport; the antidune, on the contrary, is oriented against the transport of sediments. Both macroforms move in the direction of their steep slope; that is, the dune moves in the direction of the sediment transport, and the antidune moves against the transport.

A new type of a macroform, an inverse dune was generated, which is an antidune by its form, because it is oriented with its steep slope against the residual transport of the suspended matter, and a dune by its motion. The results of the laboratory experiments confirmed the correctness of the theoretical results.

The transport of deposits is one of the least studied problems of the hydrodynamics of the shallow zone in tidal seas. It was shown in (Antsyferov and Arutyunyan, 1992) that to calculate the transport of deposits by tidal currents it is possible to use the methods for stationary flows averaging the displace period. The latter means that the displacement of the particles should occur along the line of the wave propagation. The result obtained in this work indicates that for finely dispersed suspension, which remains in the suspended condition during the entire tidal cycle, the residual displacement by tidal current would occur not along the line of the tidal wave propagation but over a normal to that direction.

So, differentiation of suspended bottom deposits by tidal waves in shallow water on fractions takes place not only along the direction of a tidal wave propagation but also in the angle 90° to the right from the direction of wave propagation.

In conclusion, we emphasize that the mechanism of residual transport formation described in the article is caused by viscous effects in the shallow-water zone of a tidal sea. When the depths are significantly greater than the thickness of the Stokes layer h_{St} viscous effects would not be significant, and the residual water transport would be generated mainly due to the nonlinear motion of the fluid and correspondingly due to the evolution of the potential vorticity (Garreau and Maze, 1992). It was, however, correctly noted in (Huthnance, 1993) that we have to account for viscosity even in the deep-water zones in order to avoid, for example, zero values of the residual Lagrangian water transport along closed geostrophic contours. As was shown in (Zyryanov, 1995), nonlinear terms of the equation of momentum conservation in the Stokes layer $h < h_{St}$ have an order of $(h/h_{St})^2$ as compared to viscous ones. From this it follows that in the region of supercritical depths $h < h_{St}$, the non-viscous mechanism would be weaker in the formation of the residual transport than the viscous one at least by a factor of $(h/h_{St})^2$.

The result obtained is also interesting because it points to the formation of the residual tidal circulation in bays and inlets in the band of supercritical depths, which goes around the basin of a bay in an anticyclonic way, whereas around the islands located in the zone it goes in a cyclonic way.

References

- Antsyferov, S.M. and Arutyunyan, G.E., 1992. Studies of Displacement of the Sediment Suspended by a Tidal Flow, *In* Proektirovanie, stroitel'svo i ekspluatatsiya morskikhportovykh sooruzhenii (Design, Construction, and Exploitation of Marine Port Arrangements), Moscow: Soyuzmorniiproekt, 1992, pp. 12-26. [In Russian]
- Aubrey, D.G. and Speer, P.E., 1983. *Sediment Transport in a Tidal Inlet*. Woods Hole Oceanogr. Inst., *Tech. Rep.*, WHO 1-83-20.
- Debol'skii, V.K., Zyryanov, V.N., and Mordasov, M.A., 1984. On the Turbulent Exchange in a Tidal Mouth under the Presence of an Ice Cover, *In* Dinamika i termika rek i vodokhranilishch (Dynamics and Thermal Conditions of Rivers and Reservoirs), Moscow: Nauka, 1984, pp. 279-290. [In Russian]
- Garreau, P. and Maze, R., 1992. Tidal Rectification and Mass Transport over a Shelf Break. A Barotropic Frictionless Model, *J. Phys. Oceanogr.*, **22**: 719-731.
- Huthnance, J.M., 1993. Tidal Rectification and Mass-Transport over a Shelf Break: A Barotropic Frictionless Model. Comments, *J. Phys. Oceanogr.*, **23**: 1893.
- Muzylev, S.V., Lifshits, V.Kh., Petrov, M.P., and Titov, V.S., Variability of Hydrophysical Parameters in a Shallow-Water Estuary in Winter, *In* Gidrofizicheskie protsessy v rekakh i vodokhranilishchakh (Hydrophysical Processes in Rivers and Reservoirs), Moscow: Nauka, pp. 237-246. [In Russian]
- Postma, H., 1961. Transport and Accumulation of Suspended Matter in the Dutch Wadden Sea, *Neth. J. Sea Res.*, **I**: 148-190.
- Zyryanov, V.N. and Leibo, A.B., 1985. Evolution of a Tidal Wave in a River Mouth Covered with Ice, *In* Gidrofizicheskie protsessy v rekakh i vodokhranilishchakh (Hydrophysical Processes in Rivers and Reservoirs), Moscow: Nauka, pp. 246-257. [In Russian]
- Zyryanov, V.N. and Muzylev, S.V., 1988. Nonlinear Sea-Level Pumping by Tides in a Shallow Sea, *Dokl. Akad. Nauk SSSR*, **298**: 454-458. [In Russian]
- Zyryanov, V.N., 1995. *Topograficheskie vikhri v dinamike morskikh techenii* (Topographic Eddies in the Dynamics of Marine Currents), Moscow: Inst. Vodnykh Problem Ross. Akad. Nauk. [In Russian]
- Zyryanov, V.N. and Reshetkov, A.B., 1998. Sediment Transport and Sea Floor Transformation by Tidal Waves in Shallow Water. *Oceanology*, **38**: 679-686.
- Zyryanov, V.N. and Reshetkov, A.B., 1999. Residual Water Transport by Longshore Tidal Currents along the Coast in Shallow Water. *Oceanology*, **39**: 296-305.

Numerical model of the thermal bar and its ecological consequences in a river-dominated lake

Paul R. Holland, Anthony Kay and Vincenzo Botte

*Department of Mathematical Sciences, Loughborough University,
Loughborough, Leicestershire, LE11 3TU, United Kingdom*

1 Introduction

There have been numerous theoretical and experimental studies of thermal bars formed in lakes when radiative heating or cooling causes the surface temperature to pass through the temperature of maximum density ($T_{md} \approx 4^\circ\text{C}$). Less attention has been paid to the riverine thermal bar, which appears when a lake and an inflowing river have temperatures on opposite sides of T_{md} . The only source of field data on the latter phenomenon appears to be from an experimental campaign in Kamloops Lake in the 1970's (Carmack, 1979; Carmack et al., 1979), while the only theoretical study has been that by Holland et al. (2001) (hereafter HKB) who used a greatly simplified numerical model for a deep lake. The first aim of the present work is to produce a more realistic model of the hydrodynamics of the riverine thermal bar, using the shallower ($< 200\text{m}$) bathymetry of Kamloops Lake which will allow more accurate representation of physical processes with the same computational resources.

It is well established that the presence of a thermal bar can have a profound effect on the distribution of dissolved or suspended matter, in two ways: firstly, the double-cell circulation can lead to a concentration of floating matter due to surface convergence and an impediment to mixing of effluent from the shoreline into the deeper parts of the lake; secondly, the thermal bar is a boundary between regions of stable and unstable stratification, with vertical mixing being hindered in the stable region. In particular, plankton and the nutrients on which they feed will be subject to these effects. An experimental study of plankton distributions in Lake Baikal was performed by Likhoshway et al. (1996) and their results were qualitatively reproduced in a computational study by Botte & Kay (2000). The second aim of the present work is to extend the computational results to the case of a riverine thermal bar, using firstly the same simple plankton population model used by Botte & Kay (2000), and then comparing with a more sophisticated ecological model.

2 The mathematical models

The hydrodynamical model is based on Navier-Stokes equations for flow in three dimensions, including all components of planetary rotation. However, the model is two-dimensional in the sense that all variables are assumed to be independent of the alongshore coordinate; this simplification is subject to the criticism that Kamloops Lake is rather narrow, but will nevertheless allow an assessment of the effects of coriolis forces even though the lake geometry will not be fully represented. The horizontal eddy viscosity is set to a constant value, while

the vertical eddy viscosity is constant in unstable conditions but decreases with increasing stability in stable stratification. Water densities are calculated from the equation of state of Chen & Millero (1986).

Scalar quantities (temperature, salinity and components of the ecological model) are governed by convection-diffusion equations, with eddy diffusivities set equal to the corresponding eddy viscosities. The equations for ecological components also include source/sink terms, representing the processes of photosynthesis, grazing and mortality, but formulated differently in the models of Franks et al. (1986) and of Parker (1991), hereafter referred to as models F and P, respectively. In particular, model P includes a detritus (D) component in addition to the nutrients, phytoplankton and zooplankton (N - P - Z) of model F; photosynthesis is dependent on light levels, and hence on depth, but model P also includes the effects of diurnal variations and self-shading by plankton; all processes are temperature-dependent in model P, but this factor is ignored in model F.

The computational domain includes a sloping river delta down to a maximum depth of 150 m. Boundary conditions include a surface heat flux of $170\text{W}\cdot\text{m}^{-2}$ as well as the usual hydrodynamic conditions at solid boundaries and the free surface. The lake is initially at 2.4°C and the river at 3.6°C , and the river is subsequently warmed at $0.2^\circ\text{C}\cdot\text{day}^{-1}$, conditions which approximate those measured in Kamloops Lake during Spring 1975. The lake is assumed initially to be in its nutrient-rich, low-biomass, Winter condition, with N - P - Z (- D) = 4-1-1(-1) mmol N m^{-3} . The ecological components in the river are taken to remain constant, at values equal to the initial conditions in the lake.

Full details of all the hydrodynamical and ecological model equations and initial and boundary conditions are given by Holland et al. (2003).

3 Results: Hydrodynamics

A thermal bar forms on day 3 of the simulation and for the next few days its circulation is confined to a region within 2 km of the river mouth, with a strong plume descending towards the lake bed (figure 1(a)). Any river-borne materials entering the lake at this stage would thus be conveyed towards the bed and could be expected to have a long residence time in the lake but minimal influence on biological processes in the euphotic zone. However, as the river temperature continues to rise, the river water becomes lighter than the lake water and forms a surface gravity current which extends across the lake until mixing has created sufficient water of maximum density to produce a descending thermal bar plume (figure 1(b)). This configuration allows river-borne materials to have a much greater influence on the euphotic zone, and constitutes an intermediate stage in the succession towards the Summer condition in which river water remains close to the lake surface from inflow to outflow.

Sensitivity analyses have been performed with regard to features of the present model that were omitted from the earlier model by HKB. Firstly, compared to a simulation in which the only heat input to the lake is from the river, the inclusion of a surface heat flux hastens the progression from boundary plume to surface overflow: by warming the lake towards the temperature of maximum density, it increases the density contrast between lake and river water and so strengthens the surface gravity current. Secondly, replacing the sloping delta

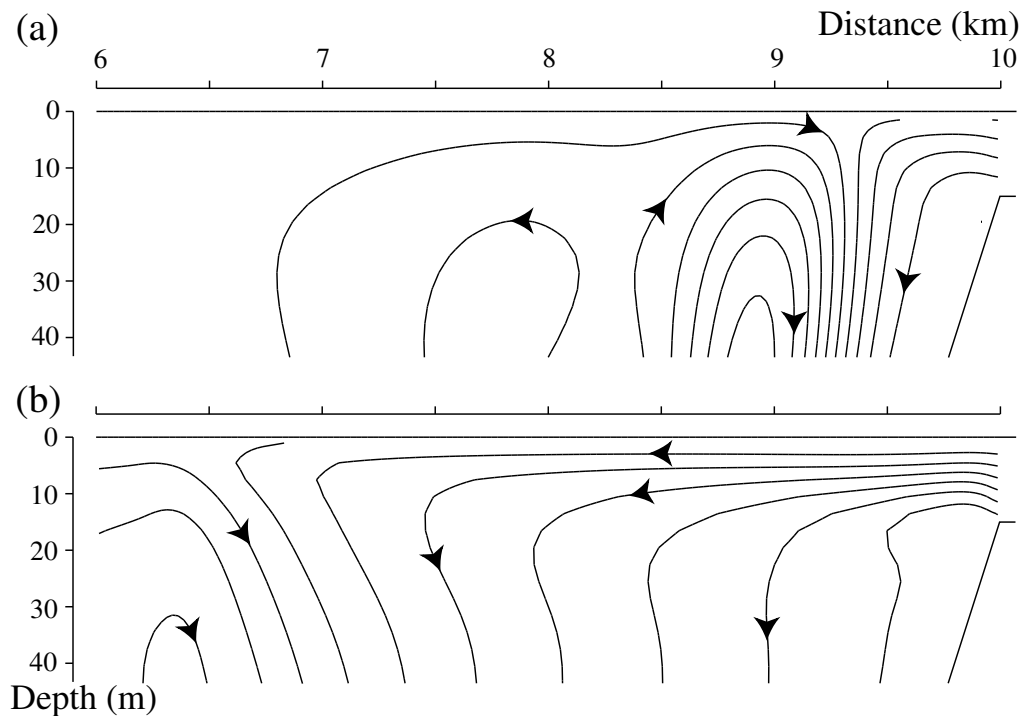


Figure 1: Progression of the flow-field at different stages of the simulation: (a) 8 days, (b) 24 days. The river inflow is on the right.

with a vertical boundary as used by HKB has very little effect on the behaviour of the thermal bar. Finally, the inclusion of the coriolis force is found to be the most important of the model refinements in the present study: in a non-rotating frame the thermal bar constantly accelerates, due to a strong return flow initially retarding its progress whereas in the later stages the gravity current propels it offshore; the effect of coriolis force is to weaken these flow components by turning them parallel to the thermal bar, thus smoothing its progress to a nearly constant speed.

4 Results: Plankton Ecology

Using ecological model F in conjunction with the hydrodynamical model yields the results illustrated in figure 2. A phytoplankton bloom has appeared at the location of the thermal bar within 16 days, accompanied by significant nutrient depletion and a small rise in the zooplankton population. At this stage the converging flow at the thermal bar appears to be the dominant influence on the plankton ecology. However, at 24 days a double bloom structure has appeared, with the outer bloom still located at the thermal bar (compare figure 1(b), which is on a different scale), but with an inner bloom which is found to be where the stability is at a maximum, preventing downward diffusion of nutrients and plankton. The dip in phytoplankton levels between the two blooms is clearly attributable to a combination of nutrient depletion and grazing by zooplankton.

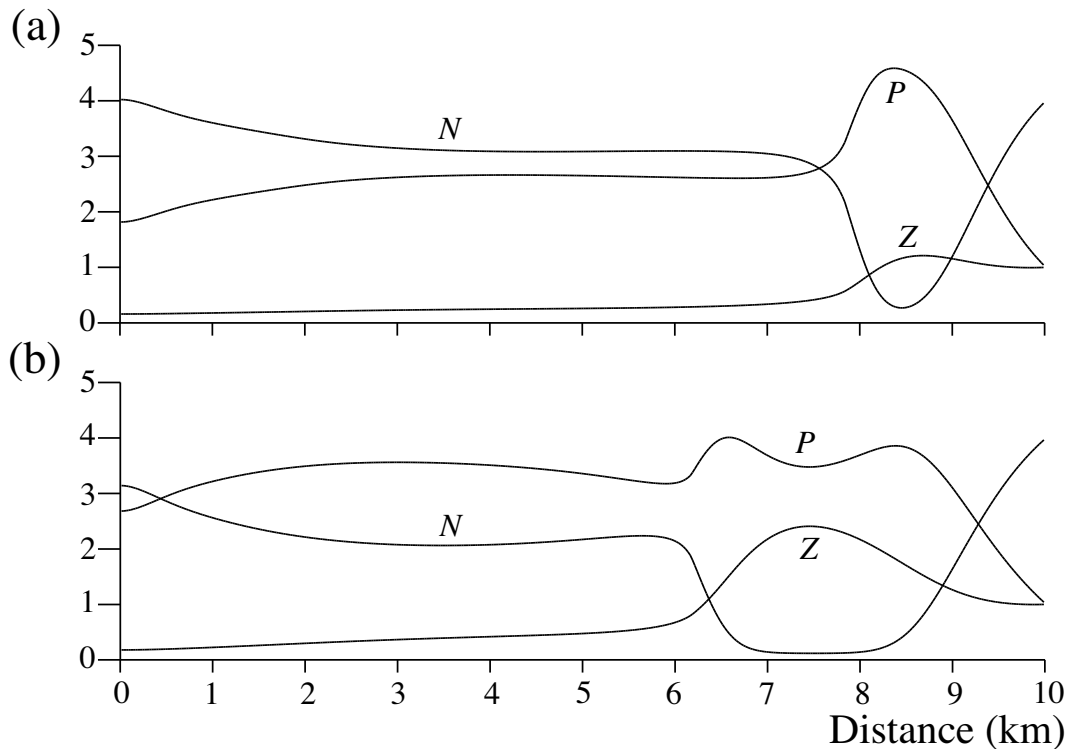


Figure 2: Horizontal profiles of all ecological components at 5m depth, using model F: (a) 16 days, (b) 24 days.

These findings do not concur with the experimental observations of St. John et al. (1976), who found a much steadier development of plankton populations in Kamloops Lake; in particular, there was no evidence of a double bloom structure ever appearing. There are several factors omitted from model F which would tend to moderate the plankton productivity: these include temperature-dependence, self-shading and the presence of a detritus component (which delays the recycling of dead plankton into the nutrient pool), all of which are included in model P. Some results from a simulation using model P are shown in figure 3, in which the intense double bloom of figure 2 (b) is replaced by a more modest phytoplankton bloom located in the stable region inshore of the thermal bar. This in turn results in only a partial depletion of nutrients and is insufficient to support any significant growth of zooplankton at this stage. Sensitivity analyses show that these differences are principally due to the temperature-dependence in model P, which leads to a general decrease in the rates of all biological interactions due to the cool temperatures in Spring, and also combines with stability effects to shift the bloom towards the warmer river water. Self-shading also has a significant effect in reducing phytoplankton growth.

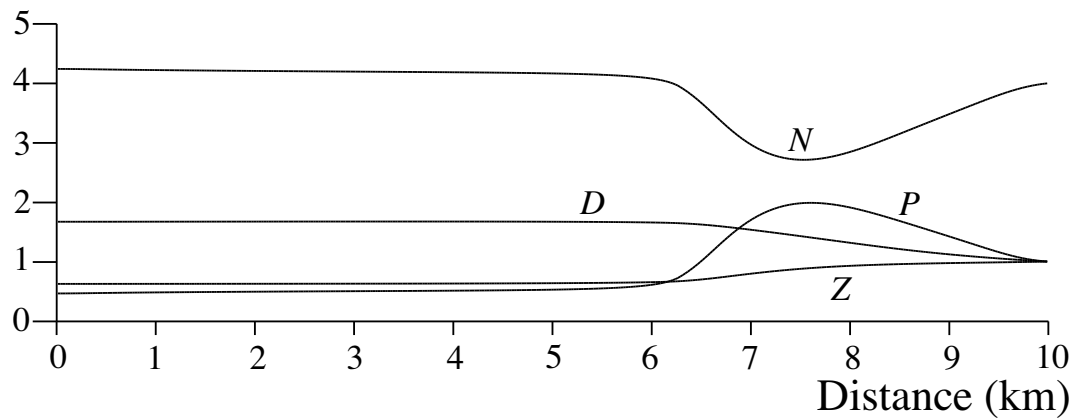


Figure 3: Horizontal profiles of all components at 5m depth, using model P, at 24 days.

References

- Botte, V. and Kay, A., 2000. A numerical study of plankton population dynamics in a deep lake during the passage of the Spring thermal bar. *J. Mar. Sys.*, 26:367-386.
- Carmack, E.C., 1979. Combined influence of inflow and lake temperatures on spring circulation in a riverine lake. *J. Phys. Oceanogr.*, 9:422-434.
- Carmack, E.C., Gray, C.B.J., Pharo, C.H., and Daley, R.J., 1979. Importance of lake-river interaction on seasonal patterns in the general circulation of Kamloops Lake, British Columbia. *Limnol. Oceanogr.*, 24:634-644.
- Chen, C.T.A. and Millero, F.J., 1986. Precise thermodynamic properties for natural waters covering only the limnological range. *Limnol. Oceanogr.*, 31:657-662.
- Franks, P.J.S., Wroblewski, J.S., and Flierl, G.R., 1986. Behaviour of a simple plankton model with food-level acclimation by herbivores. *Mar. Biol.*, 91:121-129.
- Holland, P.R., Kay, A., and Botte, V., 2001. A numerical study of the dynamics of the riverine thermal bar in a deep lake. *Environmental Fluid Mechanics*, 1: 311-332.
- Holland, P.R., Kay, A., and Botte, V., 2003. Numerical modelling of the thermal bar and its ecological consequences in a river-dominated lake. Submitted to *J. Mar. Sys.*
- Likhoshway, Y.V., Kuzmina, A.Ye., Potyemkina, T.G., Potyemkin, V.L., and Shimaraev, M.N., 1996. The distribution of diatoms near a thermal bar in Lake Baikal. *J. Great Lakes Res.*, 22:5-14.
- Parker, R.A., 1991. Eddy diffusion of phytoplankton and nutrients: estimating coefficients from simulated and observed vertical distributions. *J. Plankton Res.*, 13:815-830.
- St. John, B.E., Carmack, E.C., Daley, R.J., Gray, C.B.J. and Pharo, C.H., 1976. The Limnology of Kamloops Lake, British Columbia. Inland Waters Directorate, Vancouver, B.C., Canada.

Radiative damping of convection near the maximum density temperature: a specific mixing regime in ice-covered lakes.

Georgiy Kirillin,

Institute of Freshwater Ecology and Inland Fisheries, Berlin, Germany

kirillin@igb-berlin.de

Arkady Terzhevik

Northern Water Problems Institute, Petrozavodsk, Russia

ark@nwpi.krc.karelia.ru

1 Introduction

The effect of sub-surface heating in ice-covered lakes by penetrating solar radiation has been repeatedly reported in literature starting from early studies (Freiherr, 1905; Birge, 1910). The fact that radiative heating destabilizes the water column and leads to convective mixing, has attracted attention of researchers more recently Farmer (1975); Kelley (1997); Mironov *et al.* (2002). Generally, the convective mixing process proceeds until the temperature of the mixed layer (ML) achieves the maximum density value and the water column becomes fully mixed vertically. If the ice cover does not disappear by this, a thin “conduction” layer (CL) stays at the surface, where the temperature increases sharply from the melting point T_0 to the maximum density temperature T_m . From this moment, the penetrating radiation depresses convection and stable temperature stratification develops in the bulk of water column, whereas the heat flux from water to ice results in upward decrease of the temperature near the surface. As a result, a local temperature maximum is formed in the upper part of the water column, and the layer above it, with temperatures exceeding T_m , becomes gravitationally unstable. Formation of these unstable temperature structures in ice-covered lakes was reported in literature earlier (Barnes & Hobbie, 1960; Hill, 1967; Rigler, 1978). Most of authors referred the absence of thermal convection in this case to the effect of small salt concentrations existing in lakes. Here we analyze in some detail the main mechanisms governing the vertical temperature structure when solar radiation warms the water column up above T_m .

2 Observations

Temperature data were obtained during April 1999 in Lake Vendyurskoe, North-West Russia, by means of precise CTD measurements. The synoptical situation was characterized in this period by sudden oncoming of a strong anticyclone in the middle of the month. As a result, an unusually large amount of solar radiation penetrated the ice within few days and caused the water body to get heated up to the 4°C under ice. Subsequent changes in the temperature structure are recovered in

the south-north temperature cross-section of the April, 24 (Fig. 1). A layered, horizontally quasi-homogeneous structure is clearly distinguished in the figure. The strongly stratified CL adjoining the ice cover from below proceeds into a warm layer with temperatures exceeding 5 °C. The layer occupies depths between 0.5 and 1.0 metres under ice; the bulk of water below corresponds to the ML that has the maximum density temperature T_m except the near-bottom part, where inverse thermal stratification develops on account of the salt inflow from sediments (the latter effect was described by Kirillin *et al.* (2001)). The most of the warm water overlaying the ML displays no evident convection though the stratification is unstable here. Only in the northern part of the lake (right side in the Fig. 1), a new mixed layer develops under the ice cover. Since the cross-sectioning took the period from 17:00 to 20:00 LMT, this effect has a rather temporal character: last measurements were performed after sunset when the stabilizing radiation flux disappeared.

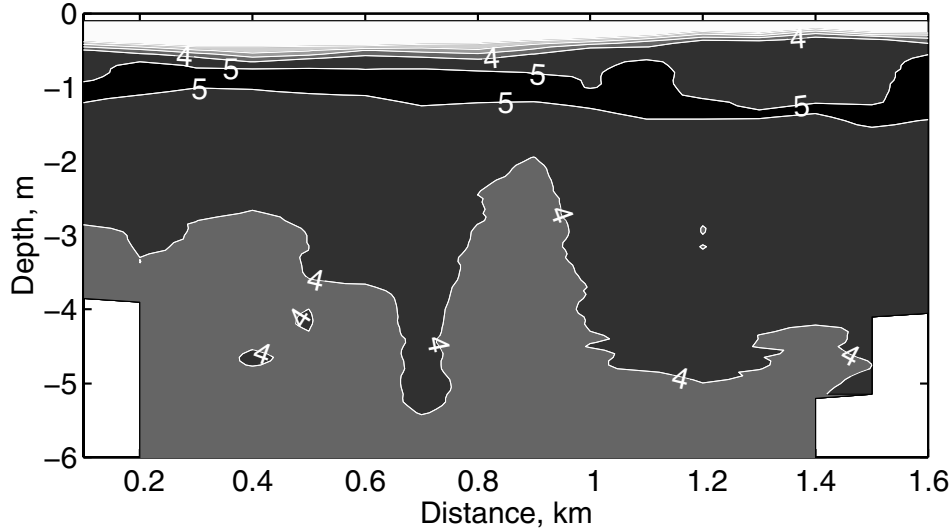


Figure 1: Temperature cross-section CS-4 (south-north), 24 Apr. 1999, Lake Vendyurskoe. Depth is measured from the ice surface. The distance between stations is about 100m.

3 Conduction-radiation model

If no convection develops during solar heating, the balance between radiation absorption and molecular heat transfer determines the heat budget of the water column:

$$\frac{\partial T(z, t)}{\partial t} - \kappa \frac{\partial^2 T(z, t)}{\partial z^2} = -\frac{d}{dz} I_0 \exp(-\gamma z), \quad (1)$$

with boundary conditions,

$$T(0, t) = 0, \quad T(\infty, t) = T_m, \quad T(z, 0) = \phi(z). \quad (2)$$

Here, I_0 is the amount of the radiation penetrating the ice normalized by density and specific heat of water; γ is the extinction coefficient, assumed to be uniform in the whole daylight spectrum; $\kappa \approx 1.4 \cdot 10^{-7} \text{ m}^2 \cdot \text{s}^{-1}$ is kinematic heat conductivity. The initial temperature profile $\phi(z)$ can be

presented in the form:

$$\phi(z) = \begin{cases} I_0 \kappa \gamma (1 - e^{-\gamma z}) (1 - z/\delta) + T_m z/\delta & \text{at } 0 < z < \delta \\ T_m & \text{at } z > \delta \end{cases}, \quad (3)$$

which corresponds to a steady-state solution of the heat transfer equation within the CL with the rest of the water column being completely mixed (Mironov *et al.*, 2002). If the solar heat flux I_0 is constant in time, the solution of (1)-(3) can be written as:

$$\begin{aligned} T(z, t) = & \\ & \left\{ T_m - \frac{I_0}{\kappa \gamma} \right\} \left\{ \tilde{z} + \frac{1}{2} [\operatorname{erfc}_1(x) - \operatorname{erfc}_1(y)] \right\} \tilde{\delta}^{-1} + \\ & \frac{1}{2} \frac{I_0}{\kappa \gamma} \left\{ \tilde{\delta}^{-1} e^{-\gamma \delta} \left([\operatorname{erf}(x) + \operatorname{erf}(y)] \tilde{z} + [e^{-x^2} - e^{-y^2}] \pi^{-1/2} \right) \right. \\ & \left. + e^{\tilde{\gamma}^2 - \gamma z} \operatorname{erfc}(y + \tilde{\gamma}) - e^{\tilde{\gamma}^2 + \gamma z} \operatorname{erfc}(x + \tilde{\gamma}) - 2e^{-\gamma z} + 2 \right\}, \quad (4) \end{aligned}$$

where

$$\tilde{z} = z/\sqrt{4\kappa t} \quad \tilde{\delta} = \delta/\sqrt{4\kappa t} \quad \tilde{\gamma} = \gamma\sqrt{\kappa t} \quad x = (\delta + z)/\sqrt{4\kappa t} \quad y = (\delta - z)/\sqrt{4\kappa t}.$$

Here, erf, erfc and erfc_1 are the error function, the complimentary error function and the first order iterative complimentary error function (see e.g. Carslaw & Jaeger, 1959), correspondingly. The agreement of this simple model with observations is surprisingly good (Fig. 2). For simulation of the Lake Vendyurskoe case (Fig. 2A), the value $I_0 = 1.8 \cdot 10^{-5} \text{ } ^\circ\text{C} \cdot \text{m} \cdot \text{s}^{-1}$ was adopted, achieved by averaging the radiation measurements performed during 24 April directly under ice. The value $\gamma = 2 \text{ m}^{-1}$ was used here based on the average value for Lake Vendyurskoe. Under these conditions, the model predicts the shape of the temperature profile practically identical to that observed in the nature. According to the model, the warm bulge in the upper part of the water column reaches that of the observed temperature profile in 24 hours. The daylight duration at the time of measurements (about 16 hours) is in some inconsistency with the modeling result, if we assume the warm layer to be completely destroyed during the nighttime. Nevertheless, the model supports the diurnal character of temporal scales, and the underestimation of the heating rate can be ascribed to the assumption of constant I_0 .

Similar example of radiatively-driven heating under ice cover was described by Barnes & Hobbie (1960). Authors reported few temperature profiles taken with time intervals about fortnight in the ice-covered Lake Peters, Alaska. The last profile on 08 July 1959 reveals the warm bulge similar to that observed in Lake Vendyurskoe. The lake is deep (about 45 m), clear ($\gamma \approx 0.3 \text{ m}^{-1}$), and is located in higher latitudes, gaining large amount of solar radiation per day in summer. Application of (4) with $I_0 = 0.85 \cdot 10^{-5} \text{ } ^\circ\text{C} \cdot \text{m} \cdot \text{s}^{-1}$ [the value extrapolated from estimations given by Barnes & Hobbie (1960)] again results in a fair agreement with the observed shape of the temperature profile (Fig. 2B). Two distinctive features appear here in comparison with the Lake Vendyurskoe case. First, the ML temperature corresponds to $3.6 \text{ } ^\circ\text{C}$ that is lower than the typical maximum density value for fresh waters. However, no convection appears during subsequent heating of upper layers, and the mixed layer extends to the lake's bottom. This behavior indicates that the mixed layer rests at the maximum density temperature, whose low value could be conditioned by small quantities of dissolved salts. The second distinction consists in essentially larger time scales: according to the model, the warm bulge gains the observed temperature maximum in 6 days. It means that the

observed warm layer could not be of diurnal nature, but exists for sufficiently longer periods. If we take into account that the profile was taken in the middle of the polar summer, when the radiative flux does not disappear during nighttime, it is reasonable to associate the persistent warm layer with continuous radiative heating.

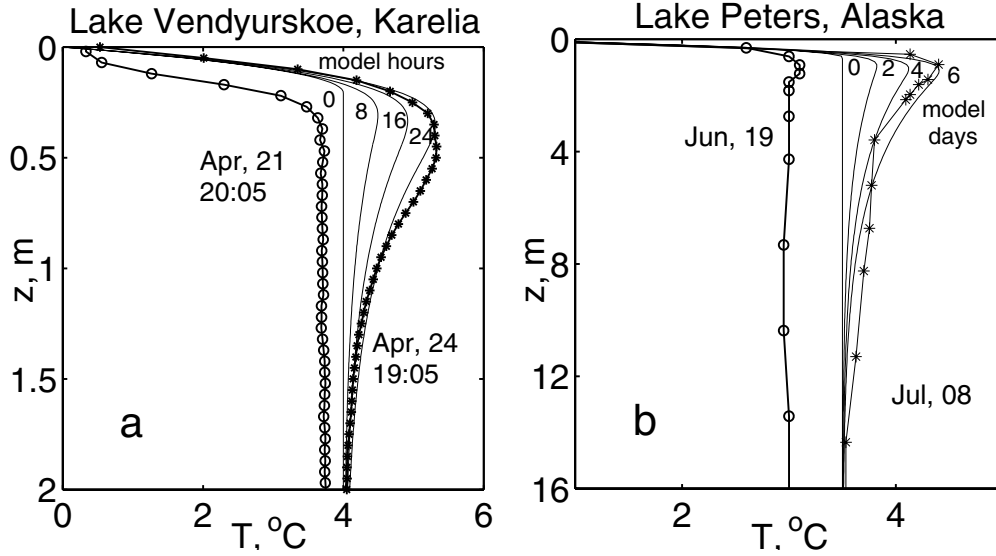


Figure 2: Vertical temperature profiles in Lake Vendyurskoe (a) and Lake Peters (b). Circles: the last measured profiles before the ML temperature achieved T_m . Asterisks: observed profiles with $T > T_m$. Lines: model predictions.

4 Discussion and conclusions

A thin gravitationally unstable layer presents in upper part of the observed and modeled temperature profiles, where temperature increases with depth from T_m to its maximum T_{max} . Assuming the thickness of this layer and the density jump $\rho(T_{max}) - \rho(T_m)$ to be appropriate length and density scales, the Rayleigh number reaches $6 \cdot 10^6$ in Lake Vendyurskoe and $2 \cdot 10^8$ in Lake Peters that is much higher than the critical values for the convection onset. At the same time, the good agreement of the observed temperature profiles with those resulting from the simple absorption-conduction equilibrium (Eq.4) demonstrates no significant convective mixing during the warm layer development.

Motivated by the evidence of fresh water inflow from melting ice, previous studies (Barnes & Hobbie, 1960; Hill, 1967) referred formation of this permanently unstable temperature gradient to the vertical flux of dissolved salts. However, there are many geophysical examples of similar permanently unstable thermal structures, which are not necessarily connected with salt flux but caused rather by the stabilizing effect of radiative heat transfer only. They include, among others, the well-known "cool skin" effect in the upper ocean layer (Soloviev & Vershinskii, 1982), the lifted temperature minimum (so-called Ramdas-effect) in the atmospheric boundary layer (Vasudeva Murthy *et al.*, 1993) and the super-adiabatic layer in convective zones of stars (Böhm-Vitense, 1992; Abbet *et al.*, 1997). In all these situations, radiation increases the critical value of the Rayleigh number and delays transition to the convective regime by altering the basic state temperature profile and/or by radiative damping, which suppresses small-scale temperature perturbations.

Indeed, the situation in ice-covered lakes differs from the Rayleigh-Bénard problem in some significant moments. It makes the results of the Rayleigh's classical linear stability analysis inapplicable here. Firstly, the density profile is sufficiently non-linear in this case. Vertical density gradient turns to zero at the bottom of the unstable layer, where the temperature maximum presents. It also disappears at the upper boundary, where temperature achieves its maximum density value $T = T_m$. The major density variation is in the center of the layer thus decreasing the effective length scale for convection. Christophorides & Davis (1970) considered the linear stability problem for radiating fluid and demonstrated that the resulting non-linearity of the initial density profile leads to increase of critical values of the Rayleigh number Ra_c . In addition, the unstable layer is bounded by stable fluid in this case instead of rigid plates in the Rayleigh-Bénard problem. In general case, absence of solid boundaries facilitates the onset of convection and decreases Ra_c (Veronis, 1963). However, the numerical analysis of Whitehead & Chen (1970) has shown that strong stable stratification in the adjacent fluid follows in values of Ra_c much higher than that for non-slip rigid boundaries. The explanation lies in the energy pumping into the stable regions, resulting in a restraining mechanism for convection. Another mechanism that should be taken into account is continuous, vertically inhomogeneous radiative heating of the layer. If we assume that convection starts, the upward convective heat transport will be reduced by radiation as long as upper layers absorb more heat than warmer fluid below. The recent work of Verevchkin & Startsev (2000) has demonstrated this effect in the oceanic cool skin formation by means of numerical modeling. The authors have shown that convection changes abruptly into steady-state regime with low mixing intensity at $I_0/Q_0 > 2$, where Q_0 is the negative destabilizing heat flux at the surface and I_0 is the surface value of radiative flux. As the ratio I_0/Q_0 increases, the convection becomes less intense, occupies thinner layer and finally disappears. If we take the heat flux from water to ice as the upper estimation for Q_0 , the ratio I_0/Q_0 exceeds 4 in both lakes, so one should expect strong depression of convective motions. Notice that I_0 , as it was chosen by Verevchkin & Startsev (2000), is not a relevant scale for the stabilizing radiation flux. Indeed, in asymptotic case of transparent fluid, I_0 can be as high as infinity without any influence on stability. The simplest estimation for the stabilizing radiative heat flux in a convective layer can be achieved in assumption of vertical temperature homogeneity. Then, the radiation scale takes the form $(I_1 + I_2)/2 - I_m$, where I_1 and I_2 are radiation values at boundaries of unstable layer and I_m is the mean value across it. Note, that the same scale describes the mixing intensity at temperatures lower than T_m that was proven by large eddy simulations and microstructure measurements under ice (Mironov *et al.*, 2002). A more detailed analysis of this regime is the subject for oncoming research. Apart from being a rare natural example of radiatively driven instability with many useful analogies in planetary and stellar physics, the regime can significantly influence the ice melting rate and biological conditions in polar and temperate lakes.

Acknowledgements

This work was partially supported by the EU-Project INTAS 97-0734.

References

- Abbet, W. P., Beaver, M., B., Davis, D., Georgobiani, Rathbun, P., & Stern, R. F. 1997. Solar Convection: Comparison of Numerical Simulations and Mixing-Length Theory. *Astrophys. J.*, **480**, 395–399.

- Barnes, D. F., & Hobbie, J. E. 1960. Rate of Melting at the Bottom of Floating Ice. *US Geol. Serv. Profess. Papers*, **400**, B392–B394.
- Birge, E. A. 1910. The Apparent Sinking of Ice in Lakes. *Science*, **32**, 81–82.
- Böhm-Vitense, Erika. 1992. *Introduction to Stellar Astrophysics 3: Stellar Structure and Evolution*. Cambridge Univ. Press. 301 pp., ISBN 0521344042.
- Carlslaw, H. S., & Jaeger, C. S. 1959. *Conduction of Heat in Solids*. 2nd edn. New York: Oxford University Press.
- Christophorides, C., & Davis, S. H. 1970. Thermal Instability with Radiative Transfer. *Phys. Fluids*, **13**, 222–226.
- Farmer, D. M. 1975. Penetrative Convection in the Absence of Mean Shear. *Q. J. R. Meteorol. Soc.*, **101**, 869–891.
- Freiherr, Otto. 1905. *Die Physicalische Eigenschaften der Seen*. Braunschweig: F. Vieweg und Sohn. 120 pp.
- Hill, H. 1967. A Note on Temperatures and Water Conditions Beneath Lake Ice in Spring. *Limnol. Oceanogr.*, **12**, 550–552.
- Kelley, D. E. 1997. Convection in Ice-Covered Lakes: Effects on Algal Suspension. *J. Plankton Res.*, **19**, 1859–1880.
- Kirillin, G., Mironov, D., & Terzhevik, A. 2001. Radiatively-Driven Spring Convection in Ice-Covered Lakes: The Effect of Salt Concentration. *Pages 199–203 of: Casamitjana, X. (ed), Proc. 6th International Workshop on Physical Processes in Natural Waters*. Spain: University of Girona.
- Mironov, D., Terzhevik, A., Kirillin, G., Jonas, T., Malm, J., & Farmer, D. 2002. Radiatively-Driven Convection in Ice-Covered Lakes: Observations, Scaling and Mixed-Layer Model. *J. Geophys. Res.*, **107**(C4), 1–16.
- Rigler, F., H. 1978. Limnology in the High Arctic: A Case Study of Char Lake. *Verh. Internat. Ver. Limnol.*, **20**, 127–140.
- Soloviev, A.V., & Vershinskii, N.V. 1982. The vertical structure of the thin surface layer of the ocean under conditions of low wind speed. *Deep Sea Res.*, **29**, 1437–1449.
- Vasudeva Murthy, A. S., Srinivasan, J., & Narasimha, R. 1993. A Theory of the Lifted Temperature Minimum on Calm Clear Nights. *Phil. Trans. R. Soc. Lond. A*, **344**, 183–206.
- Verevochkin, Yu. G., & Startsev, S. A. 2000. Numerical Simulation of Convection and Heat Transfer in Water Absorbing Solar Radiation. *J. Fluid Mech.*, **421**, 293–305.
- Veronis, G. 1963. Penetrative Convection. *Astrophys. J.*, **137**(2), 641–662.
- Whitehead, J., A., & Chen, M. M. 1970. Thermal Instability and Convection of a Thin Fluid Layer Bounded by a Stably Stratified Region. *J. Fluid Mech.*, **40**, 549–576.

Lake Baikal as Source and Receptor of Perturbations in the Region: Numerical Study

E.A. Tsvetova

Institute of Computational Mathematics and Mathematical Geophysics SD RAS

630090, Novosibirsk, Russia

e-mail E.Tsvetova@ommgp.sccc.ru

Lake Baikal is considered as a part of the climatic and ecological system of the region. A set of numerical models is developed for simulation of various problems of the atmosphere and the lake. There are models of two system levels. The models that describe the processes in the climatic system and its parts form the first basic level. These are the models of hydrothermodynamics and transport of pollutants in the atmosphere and water, and models of direct interaction of various media. The second system level is formed by the models and methods for solving optimization problems of control, planning, and ecological design using the basic-level models.

Estimating the role of Lake Baikal as source and receptor of perturbations in circulation and quality of the atmosphere is one of the goals of the study and the focus of the presentation.

1. Lake Baikal as source of perturbations in hydrological cycle.

The propagation of perturbations in the humidity field in the regional atmosphere is considered assuming that the perturbations are caused by evaporation from the lake surface. The task is derived from two facts. The lake is a climate-generating factor in the southern part of East Siberia and water vapour is one of the active elements of hydrological cycle. The variations in humidity fields influence on atmospheric radiation. Besides, they define, to a large extent, the processes of transformation, and wet and diffusive deposition of pollutants. Hence, the variations of humidity can serve as indicator of the lake's influence on the large number of processes that define as climatic as ecological state of the region.

A regional atmospheric model ($95^{\circ} - 115^{\circ} W$; $47,5^{\circ} - 60^{\circ} N$) [1] is used in the study. Following the principle of decomposition we divide the domain into two parts in vertical (the free atmosphere and the boundary layer) and introduce the hybrid coordinate system, which allows one to combine the advantages of isobaric coordinates in upper part and the conveniences of the σ -coordinates following the Earth relief.

In the 3D domain, the model solves the continuity equation, the momentum equations and transport equations for scalars. The hydrological cycle describes the transformation of 3 components: water vapour, cloud water and rain water.

The scenario approach is used. As we are interested in long time intervals, the background atmospheric circulation, presented by the Reanalysis data [2], is assimilated in the model with the help of the data assimilation procedure [3].

In the scenarios, the surface of Lake Baikal is considered to be the source of disturbances in hydrological cycle of atmospheric circulation due to evaporation of water vapour. As it is prescribed by the hydrological cycle, cloud water and rain water are generated and precipitation takes place if the mixing ratio of water vapour exceeds the saturation-mixing ratio at atmospheric temperature.

Some numerical scenarios were produced. Two fragments of the August 2000 scenario are presented here. Spreading the perturbations in the water vapour field at the surface level (relative units) is shown in Fig.1 and 2.

3 8.2000 17: 0

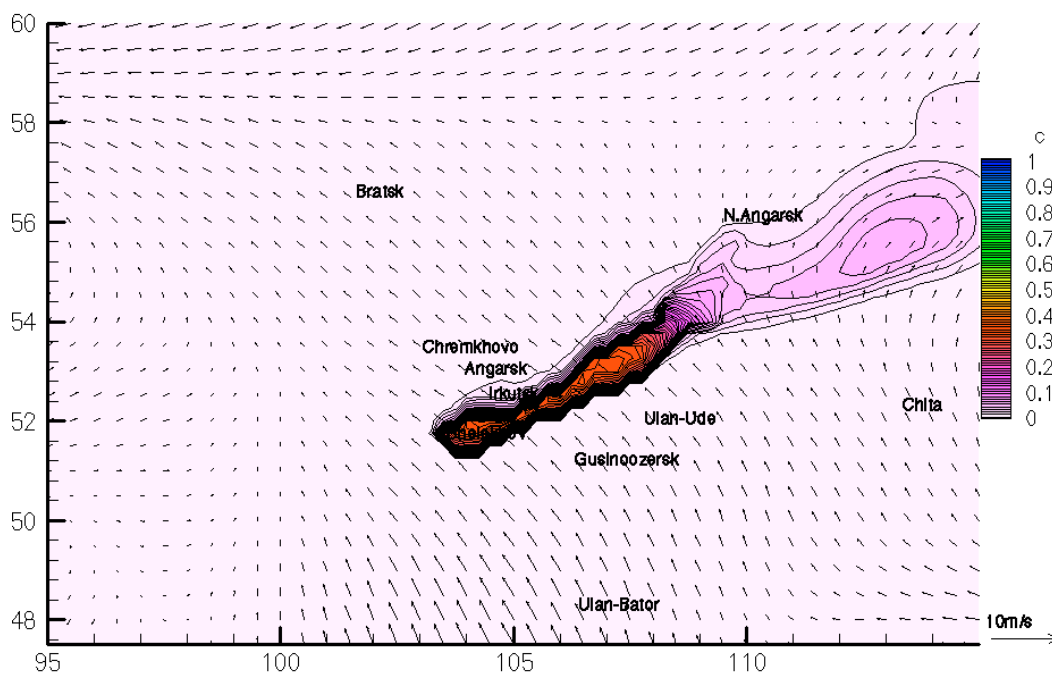


Fig.1. Wind velocities and variations of water vapour in the surface layer (07/08/2000, 14:00)

7 8.2000 14: 0

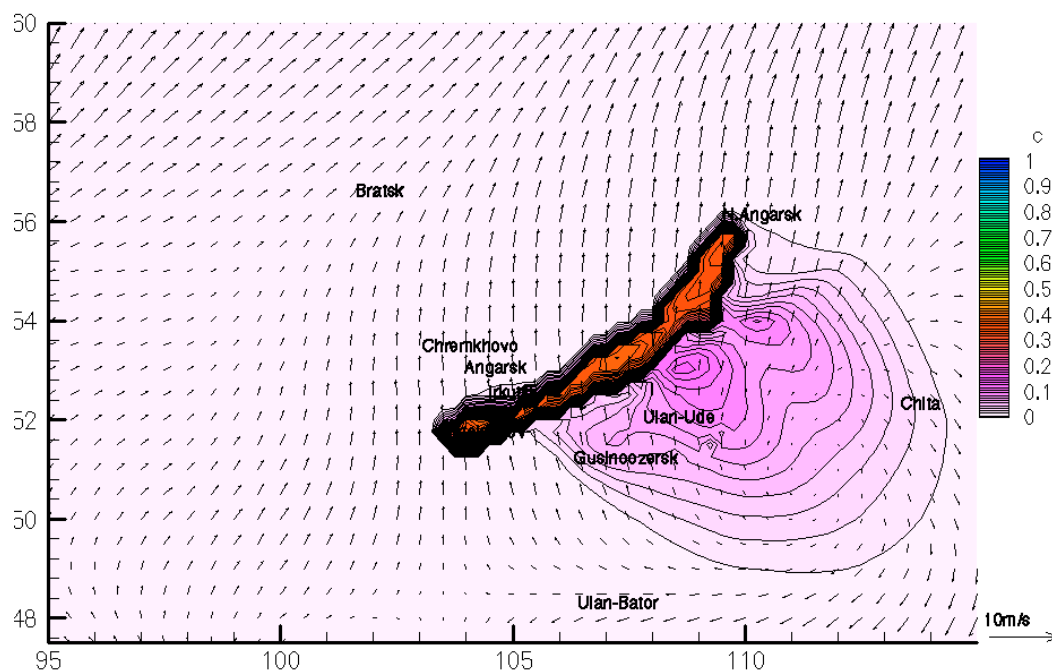


Fig.2. Wind velocities and variations of water vapour in the surface layer (07/08/2000, 14:00)

The analysis of the fields in dynamics provides the support for the view that the lake forms the specific Baikal's meso-climates in the structure of the regional circulation. The

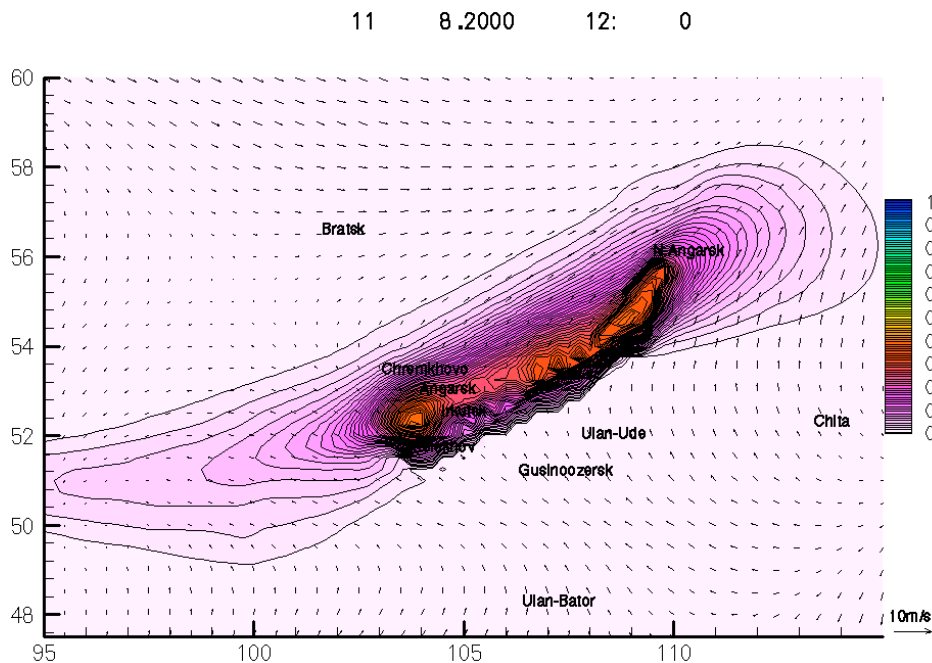
scales of the meso-climates are clearly recognized from the time and space behavior of the water vapour fields.

2. Lake Baikal as receptor of pollution (inverse problems)

The goal of inverse modeling is to learn to what extent the lake (and other territories in the region) is vulnerable with respect to anthropogenic loads and estimate the degree of ecological risk for the lake to be polluted by the acting and potentially possible new sources.

The statement of the inverse problems for lake studies have been discussed in [4]. With the help of inverse problems, the sensitivity function (SF) for the quality functional has been calculated. In this particular case, the functional describes the quality of the atmosphere in the surface layer over Lake Baikal. Here we present the SF with respect to the variations of the power of sources, placed both in the region and outside. The hydrodynamics of the same August scenario was taken in the run.

The SF is the 4D space-time dependent construction. The 2D cross-sections of SF (relative units) are shown in Fig.3,4. The values of SF show which part of the amount emission from the sources placed at the surface layer in the region can reach the lake. The more value of SF at a point, the higher danger has the source located at this point. This is true both for the acting and potentially possible sources. That is why the knowledge of SF for each area can be useful for planning of industrial activity and environmental design.



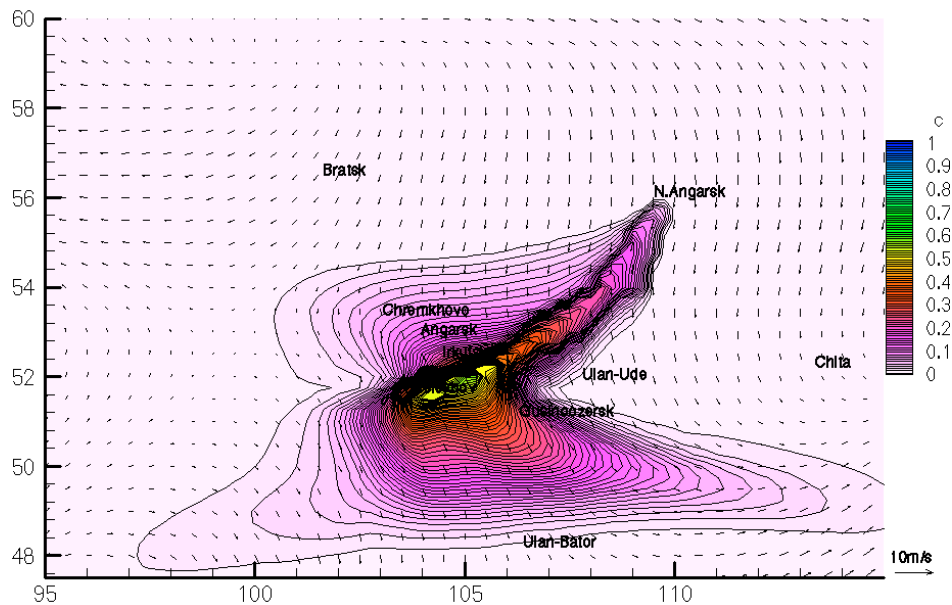


Fig. 4. Sensitivity function in the surface layer (22/08/2000, 7:00)

Concluding remarks

Thus, forming a concept of studying the climatic and environmental changes in Lake Baikal, we need to scale the range of interaction between the lake and the atmosphere. To this goal, some specific scenarios were made. The combination of the forward and inverse techniques was applied, providing additional possibilities for getting the roots of the problems concerning interconnections of the natural and anthropogenic factors in the climatic system.

Acknowledgements. The work is supported by the Russian Foundation of Basic Research (grant 01-05-65313) and Integration Grant 03-131 of SD RAS.

References.

1. V.V. Penenko, E.A. Tsvetova, Mathematical models for the study of interactions in the system Lake Baikal-atmosphere of the region. *Journal of Applied Mechanics and Technical Physics*, 1999, Vol.40, No.2, 308-316.
2. Kalney E., Ranamitsu M., Kistler R., et al., The NCEP / NCAR 40-year Reanalysis Project. // *Bull. Amer. Meteor. Soc.* 1996, V.77. P. 437-471.
3. V. Penenko and E. Tsvetova, Variational fast data assimilation algorithms. In: *Research Activities in Atmospheric and Oceanic Modeling. 2002 WGNE Blue Book Web Site* <http://www.cmc.ec.gc.ca/rpn/wgne> 01-48.
4. E. Tsvetova. Application of inverse modeling to lake studies. *The 4-th Workshop on Physical Processes in Natural Waters*, 1999, Tallinn, EMI Report Series, N 10, 39-43.

Response of a small stratified lake to a sudden midsummer change in weather conditions: 3-D simulation

E.A. Tsvetova

Institute of Computational Mathematics and Mathematical Geophysics, Novosibirsk, Russia

E. Bäuerle

Limnological Institute, University of Constance, Germany

A three-dimensional numerical model is applied for simulation of currents, temperature and salinity distributions in a residual mining lake (Lake Goitsche, Germany) which is in the process of continuous filling. The prediction of the inorganic chemistry requires the investigation of the quality of the inflowing ground water and the assessment of reactive geochemical inventories of the overburden sediments (e.g. acidity and acid neutralizing capacity). Hydrodynamic modeling on a diurnal time scale is needed to predict the evolution of the stratification in the lake during the filling process. A special task will be the simulation of the exchange of heat and mass between the various sub-basins of the topographically complex lake.

In order to test the numerical algorithm we run the model for a 3- week period in June/July 2000, when an extraordinary change in the weather took place changing the vertical structure of the lake in a spectacular way. It was the question whether the three-dimensional model is able to reproduce the response of the lake to the strong meteorological forcing.

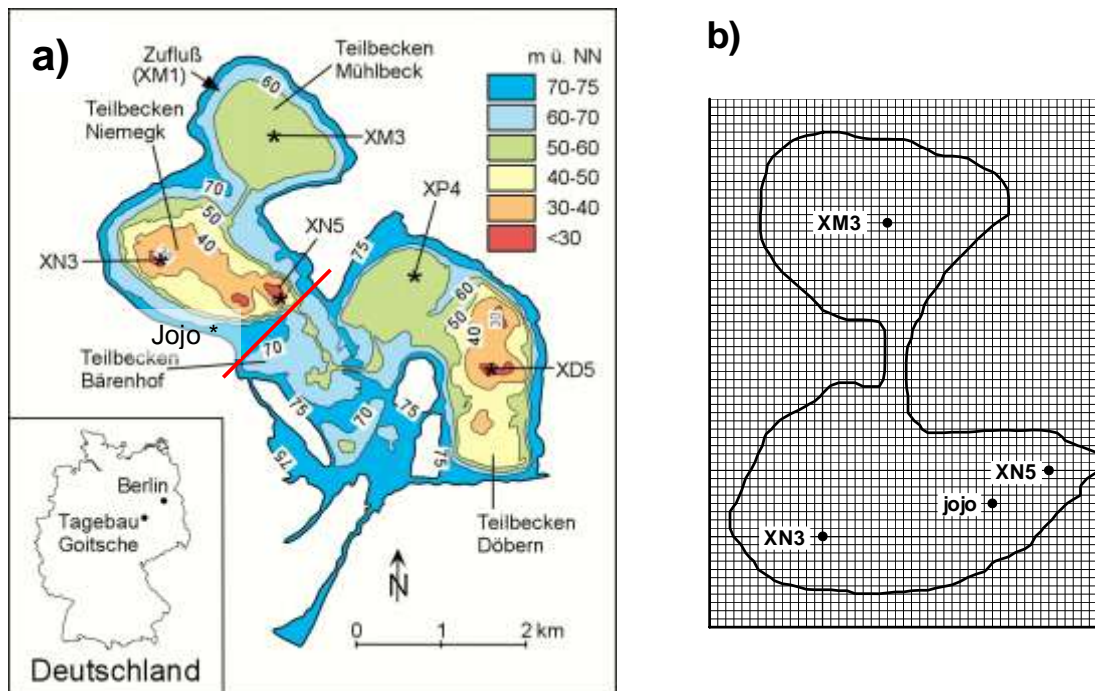


Fig.1 a): Map of Lake Goitsche with depth contour lines and measuring stations. The actual depth at June/July 2000 was 61 m asl. The final water level will be 75 m asl. The full drawn bar marks the south-eastern boundary of the numerical model. With 61 m asl, the connecting channel between the 2 sub-basins (Mühlbeck and Niemegek, respectively) has a depth of only 3 m; b): The contour line of 61 m asl and the (rotated) numerical grid on the sub-basins Mühlbeck and Niemegek of Lake Goitsche ($\Delta x = \Delta y = 50$ m). Positions of grid points where results are presented are marked by dots.

The numerical model

A modification of the three-dimensional numerical model [2] is applied to simulate the currents and the density distribution in the residual mining lake in a state of still low water level. The sub-basins of the lake are well separated from one another. The non-linear model assumes the pressure to be hydrostatic and the Coriolis parameter to be a constant. The model is driven by the fluxes of momentum and heat at the water surface. The incoming short wave solar radiation is absorbed in the near-surface layers of the water column according to the turbidity of the water. The mixing processes are parameterized by a hypothesis based on the gradient Richardson number [3]. The model is started from rest with an initial distribution of temperature and salinity deduced from measurements in the individual basins.

The spatial differentials are approximated by finite differences with grid distances of 50 m in the horizontal and 0.5 m in the vertical, resulting in 46 x 56 x 72 points in the x, y, z directions, respectively. A splitting technique is applied for construction of the numerical algorithm in time. The scheme of each time interval is symmetrized with respect to the center of the interval [4]. The splitting stages correspond to the physical processes of transport-diffusion and adjustment of the scalar and vector fields [4].

The simulation of a sudden weather change

We have chosen a period of 3 weeks in June/July 2000 with an extreme change of the weather: starting at 20 June, 00:00 h, with measured profiles of temperature and salinity, the model is driven by observed meteorological data, namely wind speed and wind direction, incoming solar radiation, air temperature and humidity (taken every 10 minutes). Involving the modeled surface temperature to calculate the long wave radiation of the water surface completes the heat balance at the surface. The boundary conditions are given constant for 10 minutes, whereas the basic time

of the model is 30 sec.

High air temperature (33 °C at noon, 20 °C at midnight) and low winds (less than 5 m/s) characterize the first 3 days of the simulation period. Within 2 days the temperature drops to less than 15 °C during the day and 10°C during the night. A strong wind with maxima around noon developed and continued to blow for several days from WNW. Afterwards, the air temperature increased a little bit, solar radiation was highly variable and winds abated. At 06 July, however, accompanied by strong winds (up to 10 m/s), another depression in temperature and solar radiation commenced.

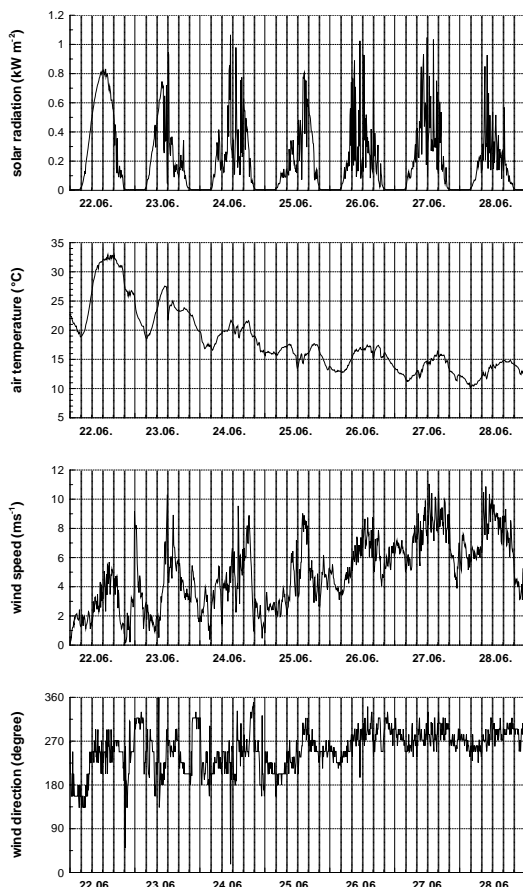


Fig.2: An extract of the meteorological time series, beginning at day 3 of the simulation, showing the change in the weather.

The lake's response

A first impression of the near-surface variations in temperature in response to the meteorological conditions at the water surface is given by the time series of isotherms which are depicted for 10 days periods beginning at 20 June (Fig. 3a) and 30 June (Fig. 3b), respectively. During the strong warming at the beginning of the first period the second, shallow thermocline is built up in addition to the already existing thermocline below 6 m. With the onset of the strong winds that upper thermocline is eroded. It takes about 3 days until the base of the well-mixed near-surface layer has reached the level of the "old" thermocline. With further deepening of the upper mixed layer the thermocline gets extremely sharp. The temperature of the mixed layer is decreasing continuously from 24°C (at 23 June) to 17°C (at 30 June). The process of upper layer mixing is accompanied by internal wave activity, which apparently exhibits second order vertical modality.

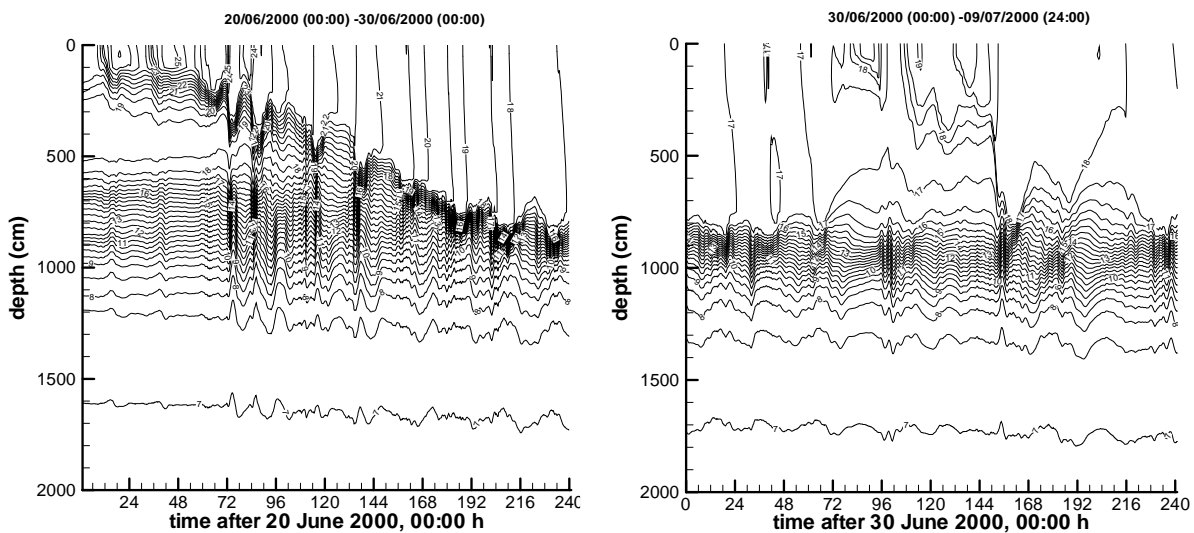


Fig.3a,b: Calculated isotherms as a function of depth and time for the uppermost 20 m at the jojo station.

The most impressive event of the period from 30 June to 09 July 2000 (see Fig.3b) is the vigorous mixing at 06 July in response to the storm which peaks at noon with wind velocities up to 10 m/s. Again, it is seen that most of the induced internal waves show second order vertical structure.

Comparison with observations

From the vertical temperature profiles which were gathered at 3-hour intervals at the jojo station (see Fig.1) we extracted the values at 0.7 m depth in order to compare with the above results of the numerical calculations. From Fig.4 we infer that there is a 4-day gap in the jojo data during the period of strong heating. However, the model bridges that episode in a very convincing manner.

Based on the vertical distributions of temperature which (among other parameters) were gained by 3-hourly profiling at the jojo station (see Fig.1) it is possible to confirm the sharpening of the thermocline which happened around 26 June (see Fig.3a and Fig.5b). As can be seen by comparing the thin drawn profiles of the sound with the thick drawn profiles of the numerical calculations the model follows the observations very well.

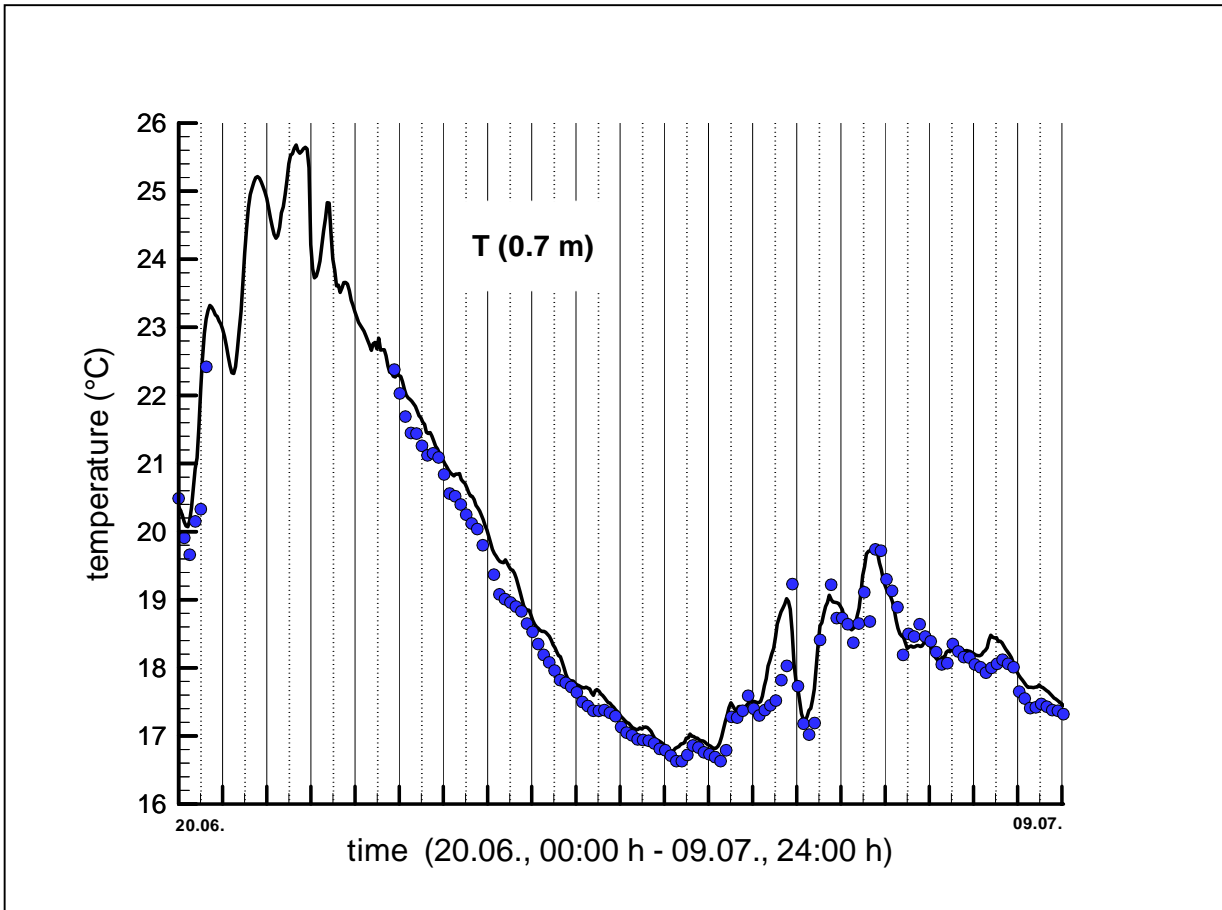


Fig.4: Comparison of temperatures measured 3-hourly by the vertical profiling sound (dots) with the values calculated in 0.7 m depth by the numerical model (line). No data are available from day 2 to day 5 of the simulation period.

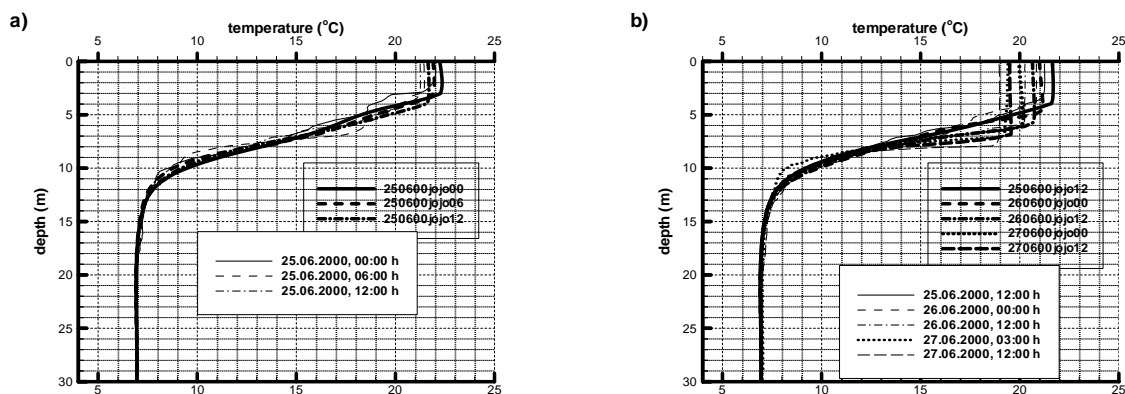


Fig.5a,b: Vertical profiles of temperature measured (thin) and calculated (thick) at the jojo station a) at the first half of 25.06.2000, b) from 25.06.2000, 12:00 h to 27.06.2000, 12:00 h.

Finally, we want to point out the horizontal differences, which emerge in cases of strong wind forcing. In Fig.5c we compare the vertical temperature profiles from selected positions of the numerical grid, which coincide with positions of the real lake where measurements were

undertaken (at the jojo station 3-hourly, at XN5 and XN3 bi-weekly or less). It is obvious that the thermocline is wider at the upwind position (XN3) than at the downwind stations (jojo and XN5, respectively) because of the upwelling which takes place at the upwind side of the lake. However, due to the small horizontal extent of the basin together with the strong stratification, even with those strong winds, which occurred during the period of under consideration, the base of the thermocline remains nearly horizontal.

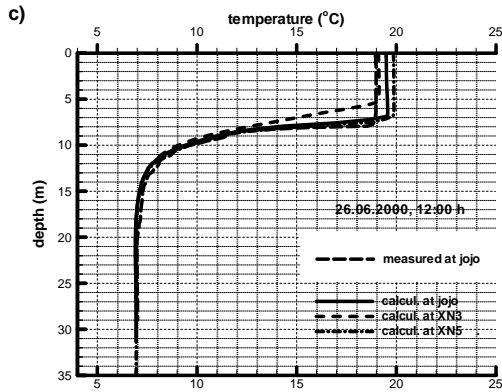


Fig.5c: Vertical profiles of temperature at different positions of the sub-basin Niemeck (see Fig.1). Measurements (longdashed line) are from the jojo station

Conclusions

The 3D model proves most satisfactory in simulating the observed mixing of the near-surface layers and the development of a sharp thermocline due to strong wind-forcing and vertical convection. The next step will be to model the convective heat exchange between the sub-basins of the filled lake and the resulting density-driven exchange flow over the separating sill and through the connecting channel.

Acknowledgements

The results are the part of the report ordered by the LMBV mbH (Lausitzer und Mitteldeutsche Bergbauverwaltungsgesellschaft) and the German Ministry for Education and Research (contract 02 WB 9983/3) in co-operation with the UFZ Leipzig-Halle (Department of Inland Water Research, Magdeburg). The authors thank Betram Boehrer and Martin Schultze for providing measurement data.

References

- Tsvetova, E. and Bäuerle, E., 2001. A numerical study of mass and heat exchange in a small artificial lake with complex topography. *In Proc. 3rd Internat. Symp. Environmental Hydraulics, Tempe, AZ, Dec. 5-8, p. 1-6.*
- Tsvetova, E., 1999. Mathematical modeling of Lake Baikal hydrodynamics. *Hydrobiologia*, 407: 310-320.
- Marchuk, G.I., Kochergin, V.P., Klimok, V.I. and Sukhorukov, V.A., 1977. On the dynamics of the ocean surface mixed layer. *J. Phys. Oceanogr.*, 7: 865-875.
- Marchuk, G.I. Sarkisyan, 1988. *Mathematical modeling of oceanic circulation*. Moscow, Publishing House Nauka, 301 p. [In Russian]

Parameterization of Lakes in Numerical Models for Environmental Applications

*Dmitrii Mironov,^{1†} Georgy Kirillin,² Erdmann Heise,¹
Sergej Golosov,³ Arkady Terzhevik⁴ and Ilya Zverev³*

¹ German Weather Service, Offenbach am Main, Germany

² Institute of Water Ecology and Inland Fisheries, Berlin, Germany

³ Institute of Limnology, Russian Academy of Sciences, St. Petersburg, Russia

⁴ Northern Water Problems Institute, Russian Academy of Sciences, Petrozavodsk, Russia

1 The Problem

Lakes significantly affect the structure of the atmospheric surface layer and therefore the surface fluxes of heat, water vapour and momentum. This effect has not been systematically studied so far and is poorly understood. In most numerical weather prediction (NWP), climate modelling and other numerical prediction systems for environmental applications, the effect of lakes is either entirely ignored or is parameterized very crudely. A physically sound model is required to predict the lake surface temperature and the effect of lakes on the structure and transport properties of the atmospheric surface layer. Apart from being physically sound, a lake model must meet stringent requirements of computational economy.

The problem is twofold. For one thing, the interaction of the atmosphere with the underlying surface is strongly dependent on the surface temperature and its time-rate-of-change. It is common for NWP systems to assume that the water surface temperature can be kept constant over the forecast period. The assumption is to some extent justified for seas and deep lakes. It is doubtful for small-to-medium size relatively shallow lakes, where the short-term variations of the surface temperature (with a period of several hours to one day) reach several degrees. At present, a large number of such lakes are indistinguishable sub-grid scale features. These lakes will become resolved scale features as the horizontal resolution is increased. In numerical prediction systems with coarser resolution, many small-to-medium size lakes remain sub-grid scale features. However, the presence of these lakes cannot be ignored due to their aggregate effect on the grid-scale surface fluxes.

Another important aspect of the problem is that lakes strongly modify the structure and the transport properties of the atmospheric surface layer. A major outstanding question is the parameterization of the roughness of the water surface with respect to wind and to scalar quantities, such as potential temperature and specific humidity. This second aspect of the problem is beyond the scope of the present paper.

In the present paper, a lake model capable of predicting the surface temperature in lakes of various depths on time scales from a few hours to a year is presented. The model is based on a two-layer parameterization of the temperature profile, where the structure of the stratified layer between the upper mixed layer and the basin bottom, the lake thermocline, is described using the concept of self-similarity of the evolving temperature profile. The same concept is used to describe the interaction of the water column with bottom sediments and the evolution of the ice and snow cover. This approach, that is based on what could be called “verifiable empiricism” but

[†]Corresponding author address: Deutscher Wetterdienst, Abteilung Meteorologische Analyse und Modellierung, Referat FE14, Frankfurter Str. 135, D-63067 Offenbach am Main, Germany. Phone: +49-69-8062 2705, fax: +49-69-8062 3721. E-mail: Dmitrii.Mironov@dwd.de

still incorporates much of the essential physics, offers a very good compromise between physical realism and computational economy.

2 Basic Concept

The concept of self-similarity of the temperature profile $T(z, t)$ in the thermocline was put forward by Kitaigorodskii and Miropolsky (1970) to describe the vertical temperature structure of the oceanic seasonal thermocline. The essence of the concept is that the dimensionless temperature profile in the thermocline can be fairly accurately parameterized through a universal function of dimensionless depth, that is

$$\frac{T_m(t) - T(z, t)}{\Delta T(t)} = \Phi_T(\zeta) \quad \text{at } h(t) \leq z \leq h(t) + \Delta h(t). \quad (1)$$

Here, t is time, z is depth, $T_m(t)$ is the temperature of the upper mixed layer of depth $h(t)$, $\Delta T(t) = T_m(t) - T_b(t)$ is the temperature difference across the thermocline of depth $\Delta h(t)$, $T_b(t)$ is the temperature at the bottom of the thermocline, and $\Phi_T \equiv [T_m(t) - T(z, t)] / \Delta T(t)$ is a dimensionless function of dimensionless depth $\zeta \equiv [z - h(t)] / \Delta h(t)$ that satisfies the boundary conditions $\Phi_T(0) = 0$ and $\Phi_T(1) = 1$. The temperature profile given by Eq. (1) is illustrated in Fig. 1.

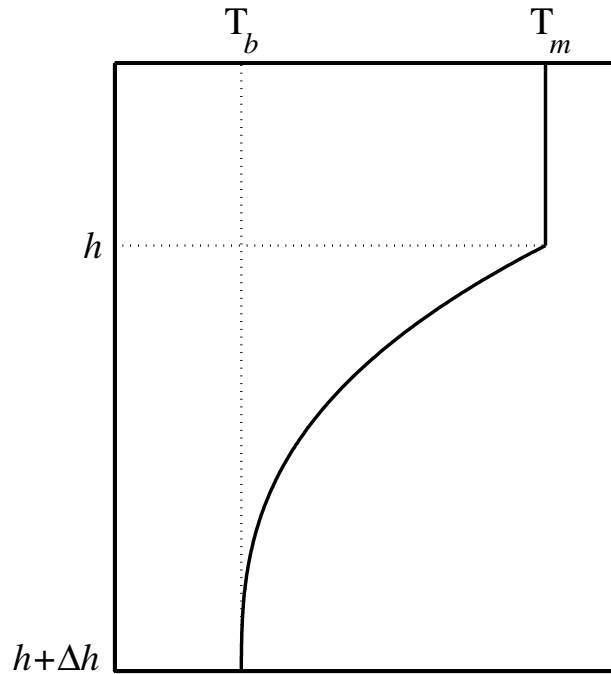


Figure 1: Schematic representation of the temperature profile in the upper mixed layer and in the thermocline. See text for notation.

The idea of self-similarity of the temperature profile in the thermocline can be traced back to the famous work of Munk and Anderson (1948). The following quotation (Munk and Anderson 1948, p. 276) is a qualitative statement of the idea: “. . . the upper layers are stirred until an almost homogeneous layer is formed, bounded beneath by a region of marked temperature gradient, the

thermocline. . . . If the wind increases in intensity the thermocline moves downward, but the characteristic *shape* of the temperature-depth curve remains essentially unchanged.” (Original authors’ *italic.*)

The concept of self-similarity of the temperature profile in the thermocline can be viewed as a natural extension of the concept of the temperature uniform mixed layer that has been successfully used in geophysical fluid dynamics over several decades. Using the mixed-layer temperature $T_m(t)$ and its depth $h(t)$ as appropriate scales, the mixed-layer concept is expressed as $T(z,t)/T_m(t) = \vartheta[z/h(t)]$, where a dimensionless function ϑ is simply a constant equal to one. The use of ΔT and Δh as appropriate scales of temperature and depth, respectively, in the thermocline leads to Eq. (1), where Φ_T is not merely a constant but a more sophisticated function of ζ .

The concept of self-similarity of the temperature profile in the thermocline received support through laboratory (e.g. Linden 1975, Wyatt 1978) and observational (e.g. Miropolsky et al. 1970, Efimov and Tsarenko 1980, Filyushkin and Miropolsky 1981, Mälkki and Tamsalu 1985, Zilitinkevich 1991) studies. A plausible theoretical explanation for the observed self-similarity of the temperature profile in the thermocline was offered in the case of mixed-layer deepening, $dh/dt > 0$ (e.g. Barenblatt 1978, Turner 1978, Zilitinkevich et al. 1988, Zilitinkevich and Mironov 1992). Introducing a vertical co-ordinate moving with the mixed layer-thermocline interface and invoking one or the other closure model to specify the eddy heat conductivity in the thermocline, these authors obtained travelling-wave type solutions to the heat transfer equation. These solutions proved to be fairly similar to empirical polynomial approximations of the $\Phi_T(\zeta)$ curve obtained on the basis of empirical data. In the case of mixed-layer stationary state or retreat, $dh/dt \leq 0$, no theoretical explanation for the self-similarity of the temperature profile has been offered so far. The self-similarity at $dh/dt \leq 0$ is based on empirical evidence only and should therefore be considered phenomenological.

A distinctive feature of shallow lakes is a strong thermal interaction between the water body and the bottom sediments. A sizable portion of the heat received from the atmosphere during spring and summer can be accumulated in the thermally active upper layer of bottom sediments. This heat is then returned back to the water column during autumn and winter, leading to a hysteresis-like behaviour of the seasonal temperature cycle of the water column-bottom sediment system. A straightforward approach to describe the evolution of the thermal structure of bottom sediments is to use the equation of heat transfer with a priori knowledge of the thermal diffusivity of sediments. A shortcoming of this straightforward approach is that the thermal diffusivity is strongly dependent on the composition of the sediments and is, therefore, rarely well known. Golosov and Kreiman (1992) proposed an alternative way of describing the vertical temperature structure of bottom sediments. It is based on a two-layer parametric representation of the temperature profile in the bottom sediments that is conceptually similar to a parametric representation of the temperature profile in the thermocline. Then, the use of the integral heat budget of the thermally active layer of bottom sediments yields a model where the thermal diffusivity of sediments is no longer needed.

Many lakes are frozen over a considerable part of the year so that the atmosphere does not directly communicate with the lake water. The atmosphere-lake interaction occurs through the air-ice or, if snow is present, through the air-snow interface. An ice-snow model is therefore required to predict the surface temperature. Use of sophisticated ice models with rheology is a standard practice in climate modelling where the integration is performed over many decades. For NWP and related applications, a sophisticated dynamic-thermodynamic ice model is not required (and most often cannot be afforded because of the high computation cost). A simplified thermodynamic model is usually sufficient. Again, the approach based on a parametric representation (assumed shape) of the temperature profile within ice and snow and on the integral heat budgets of the ice and snow layers offers a good compromise between physical realism and computational economy.

Notice that the assumption about the shape of the temperature profile within the ice, the simplest of which is the linear profile, is either explicit or implicit in many ice models developed to date. A model of ice growth based on a linear temperature distribution was proposed by Stefan as early as 1891.

The concept of self-similarity of the evolving temperature profile has found use in modelling geophysical flows. Computationally-efficient models have been developed and successfully applied to simulate the evolution of the mixed layer and seasonal thermocline in the ocean (e.g. Kitaigorodskii and Miropolsky 1970, Arsenyev and Felzenbaum 1977, Filyushkin and Miropolsky 1981) and of the atmospheric convectively mixed layer capped by a temperature inversion (e.g. Deardorff 1979, Fedorovich and Mironov 1995). Models of the seasonal cycle of temperature and mixing in medium-depth fresh-water lakes, based on the self-similar representation of the evolving temperature profile, have been developed and successfully applied by Zilitinkevich and Rumyantsev (1990), Zilitinkevich (1991), Mironov et al. (1991) and Golosov et al. (1998). A first attempt has been made to apply the above self-similarity concept to shallow lakes and to consider short-term (diurnal) variations of temperature and mixing conditions (Kirillin 2001). As different from the ocean and the atmosphere, where the thermocline (capping inversion) is underlain (overlain) by a deep stably or neutrally stratified quiescent layer, the above lake models assume a two-layer temperature structure, where the thermocline extends from the bottom of the mixed layer down to the basin bottom. This assumption is fair for most lakes, except for very deep lakes such as Lake Baikal.

3 The Lake Model

In this section, we present a very brief description of a lake model based on a self-similar representation of the temperature profile in the water column, in the bottom sediments and in the ice and snow (a detailed description of the model is given by Mironov 2003). The same basic concept is used to describe the temperature structure of the four media in question (snow, ice, water and sediment). The result is a computationally efficient lake model that incorporates much of the essential physics. The model proposed by Mironov et al. (1991) was taken as a starting point.

The lake model is based on the two-layer parameterization of the vertical temperature profile given by Eq. (1), where the thermocline is assumed to extend from the outer edge of the mixed layer, $z = h$, down to the lake bottom, $z = h + \Delta h = D$. According to Eq. (1), the evolving temperature profile is characterized by three time-dependent parameters, namely, the mixed-layer depth $h(t)$, its temperature $T_m(t)$, and the bottom temperature $T_b(t)$. These quantities are related to each other and to the mean temperature of the water column, $\bar{T}(t) \equiv D^{-1} \int_0^D T(z, t) dz$, through $\bar{T} = T_m - C_T(1 - h/D)(T_m - T_b)$. The quantity $C_T = \int_0^1 \Phi_T(\zeta) d\zeta$ is the so-called shape factor. We notice at once that, although the function $\Phi_T(\zeta)$ is useful in that it provides a continuous temperature profile through the water column, its exact shape is not required in our model. It is not Φ_T per se, but the shape factor C_T that enters the resulting equations.

The evolution equations for the above time-dependent quantities are developed by using the integral, or bulk, approach. The volumetric character of the short-wave radiation heating is accounted for. Integrating the heat transfer equation over the water column, i.e. from $z = 0$ to $z = D$, yields the equation for the mean temperature $\bar{T}(t)$. Integrating the heat transfer equation over the mixed layer, i.e. from $z = 0$ to $z = h$, yields the equation for the mixed-layer temperature $T_m(t)$. The equation for the bottom temperature depends on the mixed layer state. During the mixed layer stationary state or retreat, $dh/dt \leq 0$, the bottom temperature is kept unchanged, $dT_b/dt = 0$. During the mixed layer deepening, $dh/dt > 0$, the equation for $T_b(t)$ is obtained by means of double integration of the equation of heat transfer over the thermocline with due regard for the parame-

terization (1) (i.e. the integration is first performed over z' from h to $z > h$, and the result is then integrated over z from h to D). To this end, we use the idea of Filyushkin and Miropolsky (1981) that, in case of the mixed layer deepening, not only the profile of temperature but also the profile of the vertical turbulent heat flux in the thermocline can be represented in a self-similar form. This idea has received support through observational studies (Filyushkin and Miropolsky 1981, Tamsalu et al. 1997). Furthermore, the self-similarity of the vertical profile of the heat flux is suggested by an analytical travelling-wave type solution to the heat transfer equation.

The evolution equation for the mixed-layer depth is developed in a usual way, on the basis of the turbulence kinetic energy equation integrated over the mixed layer. Convective deepening of the mixed layer is described by the entrainment equation. It incorporates the Zilitinkevich (1975) spin-up correction term that prevents an unduly fast growth of $h(t)$ when the mixed-layer is shallow. The entrainment equation is also capable of predicting the equilibrium depth of a convectively mixed layer, where convective motions are driven by surface cooling, whereas the volumetric radiation heating tends to arrest the mixed layer deepening (Mironov and Karlin 1989). The depth of the wind-mixed layer is computed from a relaxation-type equation, where a multi-limit boundary-layer formulation proposed by Zilitinkevich and Mironov (1996) is used to compute the equilibrium mixed-layer depth.

A two-layer parameterization proposed by Golosov and Kreiman (1992) and further developed by Golosov et al. (1998) is used to predict the vertical structure of the thermally-active upper layer of bottom sediments and the heat flux through the water-sediment interface. Observations suggest that the temperature profile in the bottom sediments has the form of a travelling thermal wave. The wave starts at the water-sediment interface and propagates downward as the lake water and the bottom sediments are heated during spring and summer. When heating ceases and cooling sets in, a new wave starts at the water-sediment interface. It propagates downward as the lake water and the sediments are cooled during autumn and winter, thus closing the annual cycle. Importantly, a characteristic *shape* of the temperature-depth curve remains approximately the same. Using a two-layer parameterization proposed by Golosov et al. (1998), the evolving temperature profile in the sediments is described by two time-dependent parameters, namely, the depth $H_b(t)$ penetrated by the thermal wave and the temperature $T_H(t)$ at this depth. The evolution equations for these quantities are derived by integrating the heat transfer equation over z from the lake bottom $z = D$ to the depth $z = H_b$ penetrated by the thermal wave, and from $z = H_b$ to the depth $z = L$ of the thermally active layer of bottom sediments (at $z > L$, the seasonal temperature changes are negligible). The problem is closed by the diagnostic relation for the bottom heat flux. Importantly, the resulting equations do not incorporate the thermal diffusivity of sediments, a quantity that is rarely known to a satisfactory degree of precision.

An ice-snow model is developed, using a parametric representation (assumed shape) of the evolving temperature profile within ice and snow. That is, the basic concept is the same as the concept of self-similarity of the thermocline. Using the assumed shape of the temperature profile, the heat transfer equation is integrated over depth from the lower side to the upper side of the ice to yield the equation of the heat budget of the ice layer. The evolution equation for the ice thickness is developed by considering the heat budget of the ice slab with due regard for the heat release/consumption caused by the ice accretion/ablation. The result is an ice model that consists of two ordinary differential equations for the two time-dependent quantities, namely, the temperature $T_i(t)$ at the upper side of the ice and the ice thickness $H_i(t)$. The snow model is developed in a similar way except that the rate of snow accumulation is not computed within the snow model but is assumed to be a known time-dependent quantity that is provided by the driving atmospheric model or is known from observations. The result is two ordinary differential equations for the two time-dependent quantities, namely, the temperature $T_s(t)$ at the upper side of the snow and the

snow thickness $H_s(t)$.

Finally, we end up with a system of ordinary differential equations for several time-dependent quantities. These are the mean temperature of the water column, the mixed-layer temperature and its depth, the temperature at the lake bottom, the temperature at the bottom of the upper layer of bottom sediments penetrated by the thermal wave, and the depth of this layer. In case the lake is covered by ice and snow, four additional quantities are computed, namely, the temperatures at the air-snow and snow-ice interfaces, the snow depth and the ice depth. This system of differential equations is supplemented by a number of algebraic (or transcendental) equations for diagnostic quantities, such as the heat flux through the lake bottom and the heat flux through the ice-snow interface. Optionally, some modules can be switched off, e.g. the snow module or the bottom-sediment module. The lake model includes a number of thermodynamic parameters. These are taken to be constant except for the snow density and the snow heat conductivity that are functions of the snow depth.

The lake model described above contains a number of dimensionless constants and empirical parameters. Most of them are estimated with a fair degree of confidence. It must be emphasised that the empirical constants and parameters of the lake model are not application-specific. That is, once they have been estimated, using independent empirical and numerical data, they should not be re-evaluated when the model is applied to a particular lake. In this way we avoid “re-tuning” of the model, a procedure that may improve an agreement with a limited amount of data and is sometimes justified. This procedure should, however, be considered as a bad practice and must be avoided whenever possible as it greatly reduces the predictive capacity of a physical model (Randall and Wielicki 1997).

Apart from the optical characteristics of lake water, the only lake-specific parameters are the lake depth, the depth of the thermally active layer of bottom sediments and the temperature at this depth. These parameters should be estimated only once for each lake, using observational data or empirical recipes. In a similar way, the temperature at the bottom of the thermally active soil layer and the depth of this layer are estimated once and then used in an NWP system as two-dimensional external parameter arrays.

4 First Results

The lake model described above is being extensively tested and further developed. First results are exemplified by Figs. 2 and 3. These figures compare the modeled and measured mixed-layer temperature, bottom temperature and mixed-layer depth in Müggelsee (“See” is German for “lake”), a fresh-water lake located near Berlin, Germany. The lake covers an area of 7.3 km². Its average depth is 4.8 m, and the maximum depth is 8 m. The thermal regime of Müggelsee is characterized by a pronounced seasonal temperature cycle. In spite of a comparatively low depth of the lake, it is not always mixed down to the bottom. The thermocline exists over appreciable lengths of time from late spring through early autumn.

The temperature measurements shown in Figs. 2 and 3 are taken at the station where the depth to the bottom is $D = 7$ m. The lake model is forced by the observed incident radiation flux. The upward long-wave radiation flux is computed through the Stefan-Boltzmann law. The fluxes of sensible and latent heat are computed, using data from the surface-layer meteorological measurements and the atmospheric surface-layer parameterization scheme described in Mironov (1991). The model time step is 24 h.

As seen from Figs. 2 and 3, the simulated mixed-layer temperature and bottom temperature show an overall satisfactory agreement with observations. The model tends to slightly overestimate the bottom temperature, suggesting that the lake thermocline is somewhat too diffusive. Work is

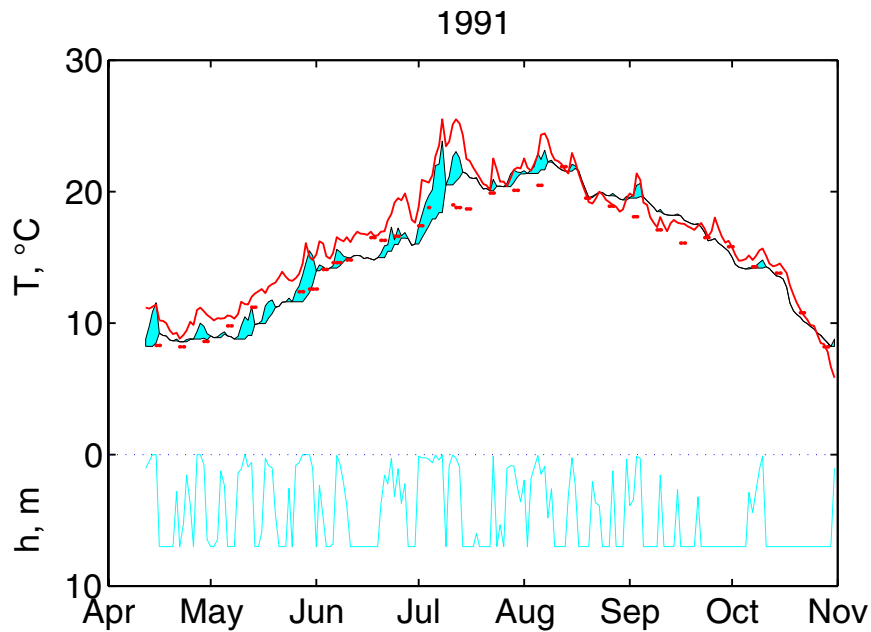


Figure 2: The evolution of the temperature structure in Müggelsee during April – November 1991. Heavy solid curve shows the observed mixed-layer temperature. Dots show the observed bottom temperature. Thin solid curves show the mixed-layer temperature (upper curve) and the bottom temperature (lower curve) computed with the lake model. Shaded areas mark the periods of stable density stratification in the lake thermocline, i.e. when the lake is not mixed down to the bottom. The computed mixed-layer depth is shown by thin solid line in the lower part of the plot.

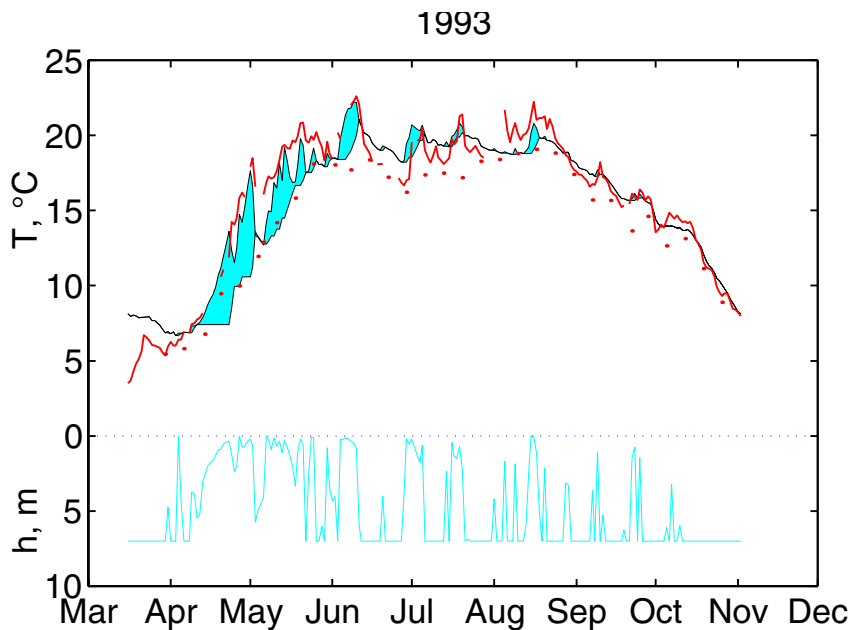


Figure 3: The same as in Fig. 2, but for the period March – December 1993.

underway to cure the trouble. Further numerical experiments are performed to test the ability of the proposed lake model to simulate short-term (diurnal) variations of the temperature structure.

5 Conclusions

We have presented a lake model suitable to predict the vertical temperature structure in lakes of various depth. The model is based on a two-layer parameterization of the temperature profile, where the structure of the stratified layer between the upper mixed layer and the basin bottom, the lake thermocline, is described using the concept of self-similarity of the evolving temperature profile. The same concept is used to describe the interaction of the water column with bottom sediments and the evolution of the ice and snow cover.

The proposed lake model is intended for use, first of all, in the NWP and climate modelling systems as a module to predict the water surface temperature. Apart from NWP and climate modelling, practical applications, where simple parameterized models are favoured over more accurate but more sophisticated models (e.g. second-order turbulence closures), include modelling aquatic ecosystems. For ecological modelling, a sophisticated physical module is most often not required because of insufficient knowledge of chemistry and biology.

Acknowledgements

The work was supported by the EU Commissions through the project INTAS-01-2132.

References

- Arsenyev, S. A., and A. I. Felzenbaum, 1977: Integral model of the active ocean layer. *Izv. Akad. Nauk SSSR. Fizika Atmosfery i Okeana*, **13**, 1034–1043.
- Barenblatt, G. I., 1978: On the self-similar distribution of temperature and salinity in the upper thermocline. *Izv. Akad. Nauk SSSR. Fizika Atmosfery i Okeana*, **14**, 1160–1166.
- Deardorff, J. W., 1979: Prediction of convective mixed-layer entrainment for realistic capping inversion structure. *J. Atmos. Sci.*, **36**, 424–436.
- Efimov, S. S., and V. M. Tsarenko, 1980: On a self-similarity of the temperature distribution in the upper thermocline. *Izv. Akad. Nauk SSSR. Fizika Atmosfery i Okeana*, **16**, 620–627.
- Fedorovich, E. E., and D. V. Mironov, 1995: A model for shear-free convective boundary layer with parameterized capping inversion structure. *J. Atmos. Sci.*, **52**, 83–95.
- Filyushkin, B. N., and Yu. Z. Miropolsky, 1981: Seasonal variability of the upper thermocline and self-similarity of temperature profiles. *Okeanologia*, **21**, 416–424.
- Golosov, S. D., and K. D. Kreiman, 1992: Heat exchange and thermal structure within “water-sediments” system. *Water Resources (Vodnye Resursy)*, **6**, 92–97.
- Golosov, S., I. Zverev, and A. Terzhevik, 1998: *Modelling Thermal Structure and Heat Interaction between a Water Column and Bottom Sediments*. Report No. 3220, Dept. of Water Resources Engineering, Inst. of Technology, Univ. of Lund, Lund, Sweden, 41 pp.
- Kirillin, G., 2001: On self-similarity of thermocline in shallow lakes. *Proc. 6th Workshop on Physical Processes in Natural Waters*, X. Casamitjana, Ed., University of Girona, Girona, Spain, 221–225.
- Kitaigorodskii, S. A., and Yu. Z. Miropolsky, 1970: On the theory of the open ocean active layer. *Izv. Akad. Nauk SSSR. Fizika Atmosfery i Okeana*, **6**, 178–188.

- Linden, P. F., 1975: The deepening of a mixed layer in a stratified fluid. *J. Fluid Mech.*, **71**, 385–405.
- Mälkki, P., and R. E. Tamsalu, 1985: Physical Features of the Baltic Sea. *Finnish Marine Research*, No. 252, Helsinki, 110 pp.
- Mironov, D. V., 1991: Air-water interaction parameters over lakes. *Modelling Air-Lake Interaction. Physical Background*, S. S. Zilitinkevich, Ed., Springer-Verlag, Berlin, etc., 50–62.
- Mironov, D. V., 2003: Parameterization of lakes in numerical weather prediction. Part 1: Description of a lake model. In preparation.
- Mironov, D. V., S. D. Golosov, S. S. Zilitinkevich, K. D. Kreiman, and A. Yu. Terzhevik, 1991: Seasonal changes of temperature and mixing conditions in a lake. *Modelling Air-Lake Interaction. Physical Background*, S. S. Zilitinkevich, Ed., Springer-Verlag, Berlin, etc., 74–90.
- Mironov, D. V., and L. N. Karlin, 1989: Penetrative convection due to surface cooling with vertically distributed heating. *Dokl. Akad. Nauk SSSR.*, **309**, 1336–1340.
- Miropolsky, Yu. Z., B. N. Filyushkin, and P. P. Chernyshkov, 1970: On the parametric description of temperature profiles in the active ocean layer. *Okeanologia*, **10**, 1101–1107.
- Munk, W. H., and E. R. Anderson, 1948: Notes on a theory of the thermocline. *J. Marine Res.*, **7**, 276–295.
- Randall, D. A., and B. A. Wielicki, 1997: Measurements, models, and hypotheses in the atmospheric sciences. *Bull. Amer. Met. Soc.*, **78**, 399–406.
- Stefan, J., 1891: Ueber die Theorie der Eisbildung, insbesondere über die Eisbildung im Polarmeere. *Ann. Phys.*, **42**, 269–286.
- Tamsalu, R., P. Mälkki, and K. Myrberg, 1997: Self-similarity concept in marine system modelling. *Geophysica*, **33**, 51–68.
- Turner, J. S., 1978: The temperature profile below the surface mixed layer. *Ocean Modeling*, No. 11, 6–8.
- Wyatt, L. R., 1978: Mixed layer development in an annular tank. *Ocean Modeling*, No. 17, 6–8.
- Zilitinkevich, S. S., 1975: Comments on “A Model for the Dynamics of the Inversion Above a Convective Boundary Layer”. *J. Atmos. Sci.*, **32**, 991–992.
- Zilitinkevich, S. S., 1991: *Turbulent Penetrative Convection*. Avebury Technical, Aldershot, 179 pp.
- Zilitinkevich, S. S., K. D. Kreiman, and A. I. Felzenbaum, 1988: Turbulence, heat exchange and self-similarity of the temperature profile in a thermocline. *Dokl. Akad. Nauk SSSR.*, **300**, 1226–1230.
- Zilitinkevich, S. S., and D. V. Mironov, 1992: Theoretical model of the thermocline in a freshwater basin. *J. Phys. Oceanogr.*, **22**, 988–996.
- Zilitinkevich, S. S., and D. V. Mironov, 1996: A multi-limit formulation for the equilibrium depth of a stably stratified boundary layer. *Boundary-Layer Meteorol.*, **81**, 325–351.
- Zilitinkevich, S. S., and V. A. Romyantsev, 1990: A parameterized model of the seasonal temperature changes in lakes. *Environmental Software*, **5**, 12–25.

Modelling of the shallow lake response to climate variability

Georgiy Kirillin

Institute for Freshwater Ecology and Inland Fisheries, Berlin, Germany

`kirillin@igb-berlin.de`

1 Introduction

Physical processes of heat and mass exchange are of great importance for lake ecosystems and incorporate, at the same time, a lot of feedbacks that makes it difficult to uncover the response of lakes to climatic changes. Existing climatic trends call for elaboration of criteria relating the seasonal stratification regime to the external conditions variability. Some of small lakes are stratified continuously during the summer heating period as long as surface temperatures are higher than 4°C (so-called *dimictic* lakes), other become full-mixed repeatedly during the summer on account of winds and convection, i.e. have the *polymictic* character. Climatic changes in the atmospheric influence can potentially lead to switching between the regimes in a certain lake that will alternate all interactions within the lake's ecosystem and, possibly, completely replace an existing ecosystem by another one. Answering the question about the lake regime dependence on external forcing needs adequate description of the process of turbulent mixing in stratified fluids. Existing methods of its description are based on introducing of different degree of empiricism into the problem. Even the probably most developed and widely used in applications two-equation turbulence models (so-called $k\text{-}\epsilon$ and Mellor-Yamada level 2.5 models) do not offer a universal scheme of accounting of non-local mixing in stratified media. At the same time, these models are complicated enough mathematically that makes application of such a model to a large number of lakes on climatic scales a time-consuming task with questionable results. Implementation of a parameterised bulk model based on the hypothesis of self-similarity of the thermocline is considered below as the physically sound and computationally efficient alternative for using in climatic studies. The vertical density structure of a lake can be represented in a bulk manner as having two-layered structure with a well-mixed upper layer. In order to obtain a reasonable compromise between physical realism and computational economy, the concept of self-similarity of the temperature profile in the thermocline can be applied to the stratified layer below the upper mixed layer. The concept was put forward by [Kitaigorodski and Miropolski, 1970] and implies that the dimensionless temperature profile in the thermocline can be fairly accurately parameterised through a “universal” function of dimensionless depth, where the temperature difference across the thermocline and its thickness are used as relevant scaling parameters (Fig. 1). The idea has received further support through the observational studies [Mälkki and Tamsalu, 1985]. A plausible theoretical explanation for the observed self-similarity was offered in case of deepening of the upper mixed layer [Turner, 1978; Kirillin, 2002]. A number of computationally-efficient parameterised models have been developed based on the self-similar representation of the temperature profile and successfully applied to simulate the seasonal thermocline in the ocean [Filyushkin and Miropol'skij, 1981] and the rise of the inversion capping convectively mixed layer in the atmosphere [Deardorff, 1979; Fedorovich and Mironov, 1995].

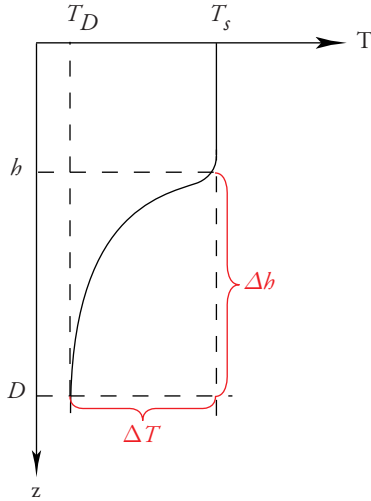


Figure 1: The model representation of the vertical temperature profile in a lake. Here, T_s is the mixed layer temperature, T_D is the temperature at lake's bottom, and h is the mixed layer depth. Dimensionless coordinates are build as $\zeta = (z-h)/\Delta h$, $\vartheta = [T(z)-T_D]/\Delta T$. The function $\vartheta(\zeta)$ is assumed to have a quasi-universal character in all lakes.

2 Materials and methods

The concept of the thermocline self-similarity is used in the model T_{EMIX} of the seasonal cycle of temperature and mixing in freshwater lakes [Mironov et al., 1991]. The model makes use of the two-layer parametric representation of the vertical temperature structure. The upper layer is treated as well-mixed and vertically homogeneous. The structure of the lower stably-stratified layer, the lake thermocline, is parameterised using a polynomial self-similar representation of the temperature profile $\vartheta(\zeta)$ (see Fig. 1). After integrating of the original partial differential equations of heat and energy transfer over each layer the problem diminishes to a system of ordinary differential equations describing evolution of parameters T_s , T_D and h . The mixed layer depth h is computed from the prognostic entrainment equation for convective mixed layer deepening, and from the diagnostic equilibrium boundary-layer depth formulation in conditions of wind mixing against the stabilising surface buoyancy flux. In this sense, the model belongs to the family of bulk models. The distinguishing feature of the present model is the fully parameterised representation of the vertical temperature profile that results in robust and computationally efficient algorithm, avoiding usage of purely known “constants” and conserving physical soundness. In previous studies, the model T_{EMIX} was successfully applied to simulation of thermal regime of Lakes Ladoga and Sevan as well as of small Karelian lakes in North-Western Russia. Here, we test the model on observational data from shallow Lake Müggelsee, located in Berlin, Germany. Prognostic calculations of the temperature variability in the lake have been performed for the next 55 years based on climatic scenarios of the Potsdam Institute for Climate Impact Research (PIK). Short analysis of the modelled shallow lake response to climatic changes is given below.

3 Results and discussion

3.1 Model validation

The model validation was performed on 17 years observational data from shallow polymictic Lake Müggelsee [Kirillin, 2001; Kirillin, 2002]. The model performance was also compared with results of k- ϵ modelling for the same lake (Fig. 2).

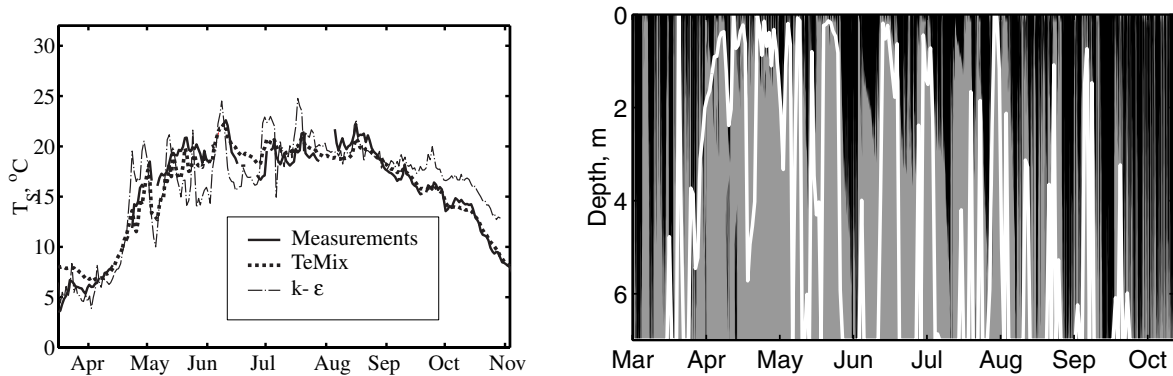


Figure 2: Examples of lake temperature and stratification calculation. Lake Müggelsee, 1993. Left: Surface temperature evolution observed in the lake (solid line), that predicted by T_{eMix} (dotted line) and by the $k-\epsilon$ model (dash-dotted line). Right: Mixed layer depth calculated with T_{eMix} (white line) versus regions of strong mixing ($TKE \geq 10^{-5} \text{ m}^2/\text{s}^2$) predicted by $k-\epsilon$ model (black filled areas).

The numerical code for $k-\epsilon$ modelling was used, developed by the GOTM project team [Burchard et al.]. The model T_{eMix} has demonstrated good abilities in reproduction of the temperature evolution in the lake as well as in prediction of the mixed layer depth and in modelling the polymictic behaviour of the lake. The values of model parameters T_s , T_D and h are in good agreement with those observed in Lake Müggelsee and are close to results of $k-\epsilon$ modelling, being achieved at essentially lower computational costs. It makes the model an attractive tool for climate-related studies, where series of long-term calculations for various external conditions are required.

3.2 Model simulations with climatic scenarios

Modelling of Lake Müggelsee response to the expected climatic changes in the next half-century was performed using atmospheric forcing from regional climatic scenarios for River Elbe basin. The scenarios were developed by the Potsdam Institute for Climate Impact Research (PIK) in frames of the “GLOWA-Elbe” project (Integrated Analysis of the Impacts of the Environment and Society in the Elbe River Basin). They include 100 climatic realizations with daily averaged meteorological values (solar radiation, air temperature, wind, air humidity etc.) covering the time span 2001-2055. Direct usage of these values in the model input has allowed distinguishing some trends in the temperature and mixing regime of the lake, related to climate changes (Fig. 3). In the figure, modelling results are shown for one of the typical climatic scenarios. The yearly averaged water temperatures increase on about 1.5°C in 50 years that coincides with increasing in the mean air temperature (1.4°C) envisaged in the scenario. It is the consequent result of the polymictic character of Lake Müggelsee: on sufficiently large time scales, the lake can be considered as a completely mixed water body, reacting instantaneously to the air temperature variations. More complicated, time-delayed response should be expected in dimictic lakes, where meteorological conditions during the short periods of spring and autumn overturns determine to a great extend the heat storage in a lake during the whole year.

Another noteworthy result consists in the shift of the summer temperature maximum to later dates. The model predicts the lag about one month (from mid-July to mid-August) through the calculation period. It results also in essentially higher autumn water temperatures and shorter ice-

covered periods, whereas the temperature dynamics during the spring and the early summer does not change significantly. Such an alteration in the seasonal temperature cycle can impact biological communities in a lake and should be taken into account when considering ecological interactions in climatic context.

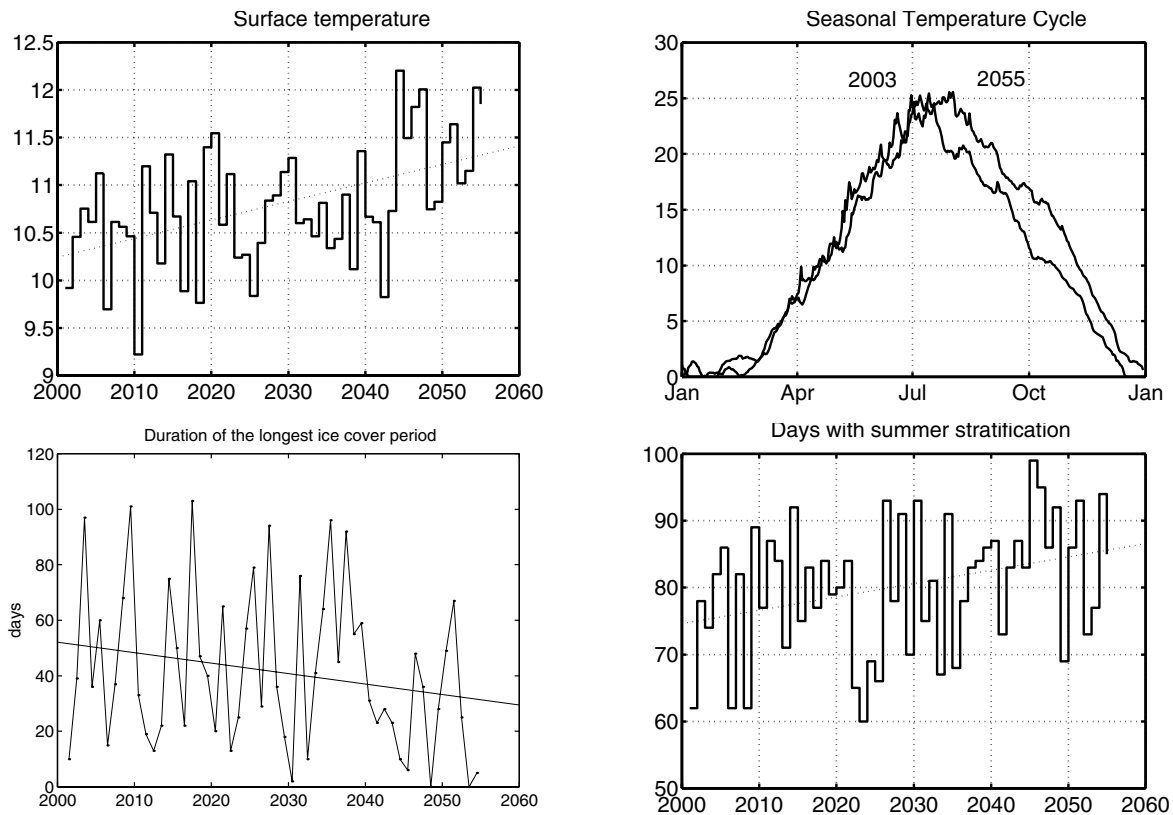


Figure 3: Examples of lake temperature and stratification calculation with meteorology input from a PIK climatic scenario. Lake Müggelsee, 2001-2055. From left-top to right-bottom: yearly averaged surface temperature evolution; seasonal temperature cycle in 2003 and 2055; duration of the longest ice cover period in year; number of days with vertical temperature stratification occurrence in summer.

The overall effect of the expected climatic changes on the vertical mixing regime consists in increased number of stratification events in the lake. The period of vertical stratification in the lake is about 20% longer in 2055 than in the beginning of calculations. It can be expected that the same climatic scenario can lead to switching from polymictic to dimictic regime in a certain lake, which would differ in morphometry or geographical location from that, modelled here.

4 Conclusions

Bulk modelling of thermal regime in a lake based on the concept of thermocline self-similarity gives reliable results at low computational costs and represents an attractive tool for lake-related environmental applications. This conclusion is also approved by comparison of the model performance with that of the $k-\epsilon$ model and by model tests on observations in a shallow polymictic lake. Model calculations with meteorological input from climatic scenarios show, in addition to the mean temperature increase, a time shift in seasonal temperature cycle and decreasing of the vertical mixing intensity in summer. The results are of great importance for analysis of the lake ecosystem response to the climate variability. The modelled changes in the

mixing intensity imply a possibility of mixing regime transition in a lake from polymictic to the dimictic one. Oncoming research should uncover the conditions of such a transition including meteorological forcing and the lake morphometry. A comprehensive study of climatic variations in lakes stipulates incorporation of the heat exchange with lake sediments and of the realistic model for ice dynamics into the model algorithm.

Acknowledgements

This study was partially founded by the German Ministry of Education and Research within the Project GLOWA-Elbe "Integral analysis of the consequences of global change on the environment and the society within the Elbe catchment". Useful contacts with the EU-Project INTAS-2132 "Representation of lakes in numerical models for environmental applications" are gratefully acknowledged.

References

- Burchard, H., Bolding, K., and Villarreal, M. R. GOTM, a General Ocean Turbulence Model. User manual. Available at <http://www.gotm.net>.
- Deardorff, J. W. 1979. Prediction of convective mixed-layer layer entrainment for realistic capping inversion structure. *J. Atmos. Sci.* 36:424-436.
- Fedorovich, E. E. and Mironov, D. V. 1995. A model for a shear-free convective boundary layer with parameterised capping inversion structure. *J. Atmos. Sci.* 52:83-95.
- Filyushkin, B. N. and Miropol'skij, Y. Z. 1981. Seasonal variability of the upper thermocline and self-similarity of temperature profiles. *Okeanologiya* 21:416-424. in russian.
- Kirillin, G. 2001. On self-similarity of thermocline in shallow lakes. In X. Casamitjana (ed.), Proc. 6th International Workshop on Physical Processes in Natural Waters, pp. 221-225, Spain. University of Girona.
- Kirillin, G. 2002. Modelling of the Vertical Heat Exchange in Shallow Lakes. PhD thesis, Humboldt-Universität, Berlin.
- Kitaigorodski, S. A. and Miropolski, Y. Z. 1970. On the theory of the open ocean active layer. *Izv. Akad. Nauk SSSR. Fizika Atmosfery i Okeana* 6:178-188.
- Mälkki, P. and Tamsalu, R. 1985. Physical features of the Baltic sea. *Finn. Mar. Res.* . 110 pp.
- Mironov, D. V., Golosov, S. D., Zilitinkevich, S. S., Kreiman, K. D., and Terzhevik, A. Y. 1991. Seasonal changes of temperature and mixing conditions in a lake, pp. 74-90. In S. S. Zilitinkevich (ed.), Modelling Air-Lake Interaction. Physical Background. Springer-Verlag, Berlin.
- Turner, J. S. 1978. The temperature profile below the surface mixed layer. *Ocean Model.* 11:6-8.

A comparison of several turbulent closure schemes in 1-D lake models

V. Podsechin

Pirkanmaa Regional Environment Centre, POB 297, 33101 Tampere, Finland

Introduction

The system of one-dimensional equations of transient boundary layers neglect horizontal variations of hydro-physical parameters and describe temporal and spatial dynamics of velocity, water temperature and salinity in vertical direction. They are popular in studies of upper mixed boundary layer in oceans or climate change effects on thermal regime in lakes. The main reasons are small computational requirements and a possibility to integrate for long periods of time. Detailed description of main assumptions and equations can be found, for example, in Svensson (1986) and Kochergin and Timchenko (1987). Main physical processes included in this type of models are rotational effects of Earth and vertical mixing due to turbulent diffusion. In some cases horizontal pressure gradients are also included. Well-known examples of these models are PROBE (Svensson, 1986, 1998), DYRESM (Imberger and Patterson, 1981). Several turbulent closure schemes common in this type of applications: constant two-layer, classical zero order formula and κ - ε model are compared in this study using simple hypothetical test case of constant wind forcing.

Materials and methods

The development of currents under the Southerly wind at a constant speed of 5 ms⁻¹ was simulated. To simplify the problem thermal stratification and salinity effects were excluded from the consideration. Thus the influence of different turbulent closure schemes on vertical profiles of currents can be seen more clearly.

A “classical model” of turbulence is based on the mixing length hypothesis, the vertical eddy viscosity is written in the following form (Benqué et al, 1982):

$$\nu(z) = l^2 \sqrt{\left(\frac{\partial u}{\partial z}\right)^2 + \left(\frac{\partial v}{\partial z}\right)^2}, \quad (1)$$

where $l = k \cdot z$, for $z < \Delta$, $l = k \cdot \Delta$ for $z \geq \Delta$, where $\Delta = \alpha \cdot H$, $k \approx 0.4$ is von Karman constant, $\alpha = 0.2$, H is the total depth, u and v are x and y velocity components, z is the vertical coordinate positive upward.

In a two-layer constant turbulence model the following values were used for the upper layer $\nu_1 = 1.33 \cdot 10^{-3}$ and $\nu_2 = 1 \cdot 10^{-4}$ m² s⁻¹ for the bottom layer.

For brevity details of κ - ε model are not presented here, they can be found for example in Svensson (1998). The PROBE was used to simulate the response of water column with a depth of 50 m to the Southerly wind at a constant speed of 5 ms⁻¹. The Coriolis parameter was equal to $1.26 \cdot 10^{-4}$ s⁻¹. This corresponds approximately to the central part of Lake Ladoga. The model was integrated for 720 hours with integration time step of 600 s.

Results and discussion

Calculated vertical profiles are shown in Figure 1. The “classical” model and two-layer constant model produce results close to Ekman spiral. It is known from observations and analytical studies (Madsen, 1977) that fully developed Ekman spiral has never been observed in reality. The simulated currents using κ - ε closure scheme are closer to observations.

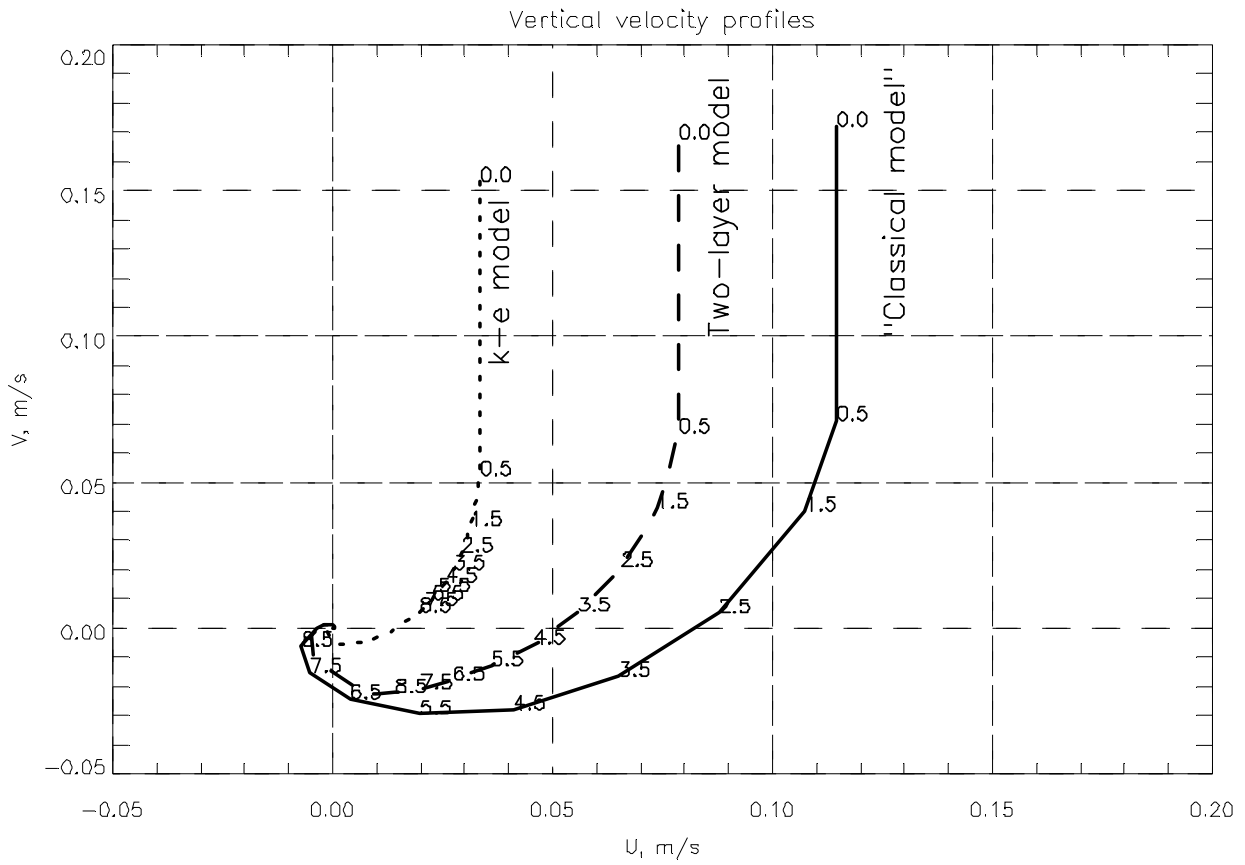


Fig.1. Calculated vertical velocity profiles under constant Southerly wind 5 m s^{-1} . Numbers note distance from surface in meters.

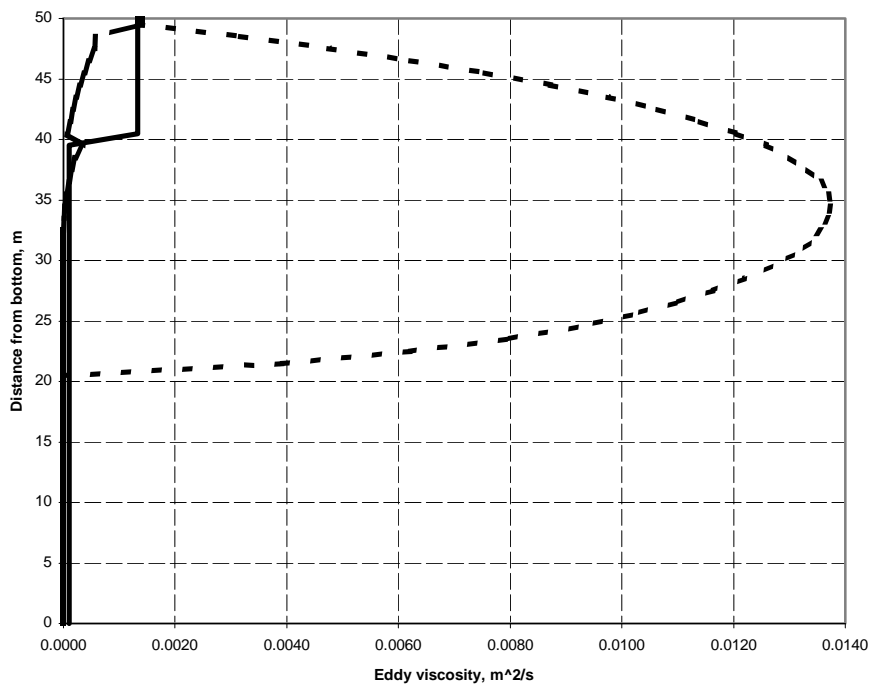


Fig.2. Variation of eddy viscosity with depth.

Differences in variation of eddy viscosity with depth shown in Figure 2 can explain why $\kappa\text{-}\epsilon$ model damps currents stronger in the upper 20-30 m layer. The eddy viscosity has a parabolic profile in the layer between water surface and 30 m with the maximum value of $0.01374 \text{ m}^2 \text{ s}^{-1}$ at a depth of 15 m and decreases to almost zero value below 30 m depth. This provides effective mixing and transfer of momentum in the upper active layer.

References

- Benqué J. -P., Haugel A. and Viollet P. -L. 1982. *Engineering applications of computational hydraulics*. Vol. II. Numerical models in environmental fluid mechanics. Pitman. 160 p.
- Imberger, J. and Patterson, J. C. 1981. A dynamic reservoir simulation model - DYRESM:5. In "Transport Models for Inland and Coastal Waters". H.B. Fischer (ed). Academic. Pp. 310-361.
- Kochergin V.P. and Timchenko I.E. 1987. *Monitoring of hydro-physical ocean fields*. Leningrad. Hydrometeoizdat. 280 p. [In Russian]
- Madsen O.S. 1977. A realistic model of the wind-induced Ekman boundary layer. *J. Phys. Oceanog.*, 7: 248-255.
- Svensson U. PROBE. 1998. Program for boundary layers in the environment. System description and manual. SMHI. Reports Oceanography N.24. 42 p.+ Appendices.

Differentiation of Suspended Bottom Deposits by Tidal Waves in Shallow Water

V. N. Zyryanov

Institute of Water Problems, Russian Academy of Sciences, Moscow, Russia;

E-mail: zyryanov@aqua.laser.ru

The problem of transport of suspended bottom deposits in a tidal flow in shallow water is an important component of the integrated problem associated with the dynamics of the coastal zone. The transport of a suspended admixture and associated lithodynamic processes occurring in shallow water are primarily defined by the joint action of tidal currents and wind waves. The transport of suspended matter by wind waves has been studied for a long time, whereas the problem of bottom transformation under the influence of tidal currents is at the initial stage of research. Interest in this problem has grown in relation to the problems of developing new gas deposits in the arctic seas.

The asymmetry of a tidal wave in shallow water is an important factor determining the process of suspended matter transport in the tidal flow when tidal flows are stronger but less prolonged than the ebb flows. An attempt is made in (Aubrey and Speer, 1983) to apply precisely this asymmetry to explain nonzero residual transport of suspended matter in the onshore direction.

Nevertheless, tidal asymmetry is not the only reason for residual transport. As was shown in (Postma, 1961), residual transport of suspended matter in the onshore direction is also induced by a symmetric tidal wave with a decreasing onshore direction.

At present, the two most extreme time scales, corresponding to quasi-stationary (riverine) flows and rapidly oscillating motions (wind waves), have been studied extensively while investigating the problem of suspended matter transport. Tidal flows fall in the middle of these time scales and are not related to either the first or the second type.

This work deals with the study of the peculiarities of suspended matter transport and evolution of a solitary sand macroform in the shallow zone of a tidal sea.

Residual tidal transport of water or, as it is sometimes called, residual tidal circulation (RTC) is a quasi-stationary component of the velocity of the currents in a tidal sea, which appears as a result of averaging the velocity over the period of the tidal wave. The residual tidal circulation has significantly smaller velocities as compared to the tidal current, but nevertheless, these residual currents together with the wind and gradient currents have precisely the main

influence on the formation of the temperature and salinity fields and on the distribution of admixtures in a tidal sea. This is one of the reasons why so much attention is being paid to the investigation of tidal residual currents.

It is especially important to know the properties of residual tidal currents in the coastal zones of tidal seas, where pollution and admixtures are mainly transported by the continental runoff.

Sea floor transformation by tidal waves was studied in a semi-infinite channel using theoretical and experimental methods within a gradient-viscous model of tidal flow in shallow water with a depth less than the thickness of the Stokes layer

$$h < h_{st} = \sqrt{AT} ,$$

where A is the vertical turbulence viscosity and T is the period of a tidal wave (Zyryanov and Reshetkov, 1999). The results of laboratory experiments confirm the formation of inverse dunes in the tidal flow.

A new hydrodynamic effect: formation of a residual alongshore current by tides in a shallow water, when the water depth h becomes less than the thickness of the Stokes layer was described in (Zyryanov and Reshetkov, 1999). It is also shown that a residual tidal transport (RTT) of water is formed to the right of the direction of the main tidal wave in the coastal region of the sea with supercritical depths $h < h_{st}$. Thus, the coast is on the left side of the residual current. The maximum velocities of the residual tidal transport are reached at the marine boundary of the zone of supercritical depths, and they can be as large as $1-2 \text{ cm}\cdot\text{s}^{-1}$. The results of a laboratory experiment confirming the theoretical results are presented.

Formulation of the problem

On the basis of experimental studies of the tidal currents in shallow water (Debol'skii et al., 1984) and other theoretical works (Zyryanov and Leibo, 1985; Zyryanov and Muzylev, 1988; Zyryanov, 1995), we found that the flow in long gravity waves is characterized by a gradient-viscous regime and the pressure gradient is balanced by the turbulent friction stress in the equation of momentum conservation under the condition that the depth is less than the thickness of the Stokes layer. The depth $h < h_{st}$ is called the supercritical depth (Zyryanov and Leibo, 1985). The sufficient condition for the existence of the gradient-viscous regime is the supercritical depth h and low Froude number

$$Fr = U^2 / gh \ll 1$$

(Zyryanov and Muzylev, 1988; Zyryanov, 1995). The value of the depth for a semidiurnal tidal wave is equal to 12-17 m if the value of the turbulent exchange coefficient characteristic of shallow-water tidal estuaries is $A \sim 102 \text{ cm}^2 \cdot \text{s}^{-1}$ (Debol'skii et al., 1984).

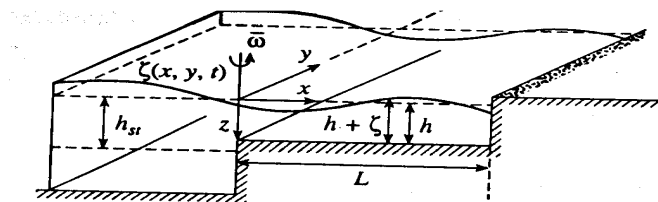


Fig.1. Scheme for the formulation of the problem.

We shall consider before the problem under the assumption of a semi-infinite coastal zone with a constant depth h , which is less than the critical depth for the given tidal wave with a period T (Fig. 1). The width of the zone is assumed to be much greater than its depth and much less than the external Rossby radius of deformation; thus, we can neglect the Coriolis acceleration in the first

order of the approximation. Let us choose the axes of the left-hand Cartesian coordinate system in the following way: X-axis in the direction of the propagation of the front of the tidal wave, Y-axis parallel to the front of the wave, and Z-axis directed vertically downwards (Fig. 1). The origin of the coordinate system is at the non-disturbed surface of the sea, at the marine edge of the shallow-water zone. We use the gradient-viscous approximation, then, taking into account the Coriolis force for the homogeneous fluid, we shall have the following system of dynamic equations:

$$\frac{\partial}{\partial z} \left[A(x, y, z, t) \frac{\partial U}{\partial z} \right] + fV = \frac{1}{\rho_0} \frac{\partial p}{\partial x} \quad (1)$$

$$\frac{\partial}{\partial z} \left[A(x, y, z, t) \frac{\partial V}{\partial z} \right] - fU = \frac{1}{\rho_0} \frac{\partial p}{\partial y} \quad (2)$$

$$g\rho_0 = \frac{\partial p}{\partial z}, \quad (3)$$

$$\frac{\partial U}{\partial x} + \frac{\partial V}{\partial y} + \frac{\partial W}{\partial z} = 0, \quad (4)$$

$$\frac{\partial S}{\partial t} + U \frac{\partial S}{\partial x} + V \frac{\partial S}{\partial y} + (W + \omega_0) \frac{\partial S}{\partial z} = k_x \frac{\partial^2 S}{\partial x^2} + k_y \frac{\partial^2 S}{\partial y^2} + k_z \frac{\partial^2 S}{\partial z^2} \quad (5)$$

where $A(x, y, z, t)$ is the kinematic coefficient of vertical turbulent exchange, which is assumed constant $A(x, y, z, t) = A = \text{const}$; U , V and W are the horizontal and vertical components of the velocity vector, respectively; f is the Coriolis parameter, ρ_0 is the fluid density; p is the pressure in the fluid; $S(x, y, z, t)$ is the concentration of suspension; ω_0 is the fall velocity of the particles in the suspension and bottom deposits; and k_x , k_y and k_z are horizontal and vertical coefficients of suspension diffusion, respectively, which are assumed to be constant.

Let us designate the elevation of the free surface as $\zeta(x, y, t)$ then, the total depth will be equal to

$$H(x, y, t) = h(x, y, t) + \zeta(x, y, t).$$

The boundary conditions are the following:

at the free surface of the fluid, $z = -\zeta(x, y, t)$

$$\text{a zero wind: } A \frac{\partial U}{\partial z} = A \frac{\partial V}{\partial z} = 0, \quad (6)$$

$$\text{the kinematic condition: } W \Big|_{z=-\zeta} = -\frac{\partial \zeta}{\partial t} + \left(U \frac{\partial \zeta}{\partial x} + V \frac{\partial \zeta}{\partial y} \right) \Big|_{z=-\zeta} \quad (7)$$

$$\text{zero suspension transport is } \left[k_z \frac{\partial S}{\partial z} - (W + \omega_0) S \right] \Big|_{z=-\zeta} = 0; \quad (8)$$

at the bottom $z = h(x, y, t)$:

$$\text{the nonslip condition for the fluid is } U \Big|_{z=h} = V \Big|_{z=h} = W \Big|_{z=h} = 0; \quad (9)$$

$$\text{the suspension transport from the bottom is } k_z \frac{\partial S}{\partial z} \Big|_{z=h} = \frac{f + |f|}{2}, \quad (10)$$

where

$$f = |\zeta_x| \frac{Rg(h + \zeta)}{U_e^2} - R$$

is the function of the source of solid admixture, ζ_x is the slope of the surface; R is an empirical coefficient ($R=0.0086 \text{ kg m}^{-2} \text{ s}^{-1}$); U_e is the critical value of the dynamic velocity; when

$$U_*^2 = |\zeta_x| g(h + \zeta) \geq U_e^2 ,$$

tidal currents erode the bottom, and when

$$U_*^2 = |\zeta_x| g(h + \zeta) < U_e^2$$

there is no erosion and suspension is not transport into water. Condition (10) describes this pulse regime (Zyryanov and Reshetkov, 1999).

A tidal harmonic wave with period equal to T propagating from the deep water region ($x < 0$) along the normal to the marine boundary of the shallow-water area would generate a level displacement at the boundary of the shallow water (see Fig. 1):

$$\zeta(0, y, t) = \zeta^0 \sin(\omega t), \quad \omega = 2\pi/T \quad (11)$$

The gradient-viscous regime of the dynamics of tidal waves in shallow water of supercritical depth is described by a parabolic equation for the level [10]:

$$\frac{\partial \zeta}{\partial t} = \frac{g}{3A} \nabla \cdot [(h + \zeta)^3 \nabla \zeta] + \frac{2gf}{15A^2} \nabla \times [(h + \zeta)^5 \nabla \zeta] , \quad (12)$$

where

$$\nabla = \left(\frac{\partial}{\partial x}, \frac{\partial}{\partial y} \right), \quad (\cdot), (\times)$$

are the scalar and vector products, respectively.

Solution of equation (12) with boundary condition (11) and the condition of wave attenuation at infinity for $x \rightarrow \infty$ in neglecting the Coriolis parameter in the first order approximation was obtained in (Zyryanov and Muzylev, 1988) using decomposition of the level into an asymptotic series with respect to a small parameter $\varepsilon = \zeta^0/h$:

$$\begin{aligned} \zeta = & -h\varepsilon e^{-kx} \sin(\omega t - kx) - \\ & -h\varepsilon^2 \left[\frac{3}{4}(1 - e^{-2kx}) + \frac{3}{2}e^{-2kx} \cos(2\omega t - 2kx) - \frac{3}{2}e^{-\sqrt{2}kx} \cos(2\omega t - \sqrt{2}kx) \right] + O(\varepsilon^2) \end{aligned} \quad (13)$$

where k is found from the dispersion relation

$$k = k_0 \left(1 - \frac{9}{8}\varepsilon^2 + \dots \right), \quad k_0 = \sqrt{\frac{3\omega A}{2gh^3}} \quad (14)$$

The stationary part of the solution of (13)

$$\frac{3}{4}h\varepsilon^2(1 - e^{-2kx})$$

describes nonlinear level pumping (Zyryanov and Leibo, 1985; Zyryanov and Muzylev, 1988; Zyryanov, 1995). One can easily see from (1), (2), and (3) that the velocity profile will be parabolic in neglecting the Coriolis parameter.

Equation (5) will have the form

$$\omega_0 \frac{\partial S}{\partial z} = k_z \frac{\partial^2 S}{\partial z^2} \quad (15)$$

The solution of the equation (15) with boundary conditions (8), (10) is given by the expression

$$S(x, z, t) = \frac{f + |f|}{2\omega_0} \exp\left[\frac{\omega_0}{k_z}(z - h)\right] \quad (16)$$

Variation of the transport of suspended admixture

$$q(t) = \int_0^{h+\zeta} U S dz ,$$

calculated using relations (13), (14), and (16) during a tidal cycle for point $x = 6$ km with the depth of the channel $h = 5$ m at the value of $\zeta_0 = 0.5$ m in (11), is shown in Fig. 2. The integral of this transport over the period

$$I = \int_0^T q(t) dt$$

is positive. This means that there is an onshore residual suspension transport at each point of the shallow zone. Its value decreases approximately exponentially with the distance from the sea boundary of zone (Fig. 3). From this follows an important conclusion: in the case of non-deficit erosion of the bottom, deposits of sediments would occur over the entire zone of eroding velocities. The closer the point to the sea boundary of a zone l , the more intensive is the process. With a decrease in depth, this process decreases due to reducing the depth and consequently the decrease in tidal velocities.

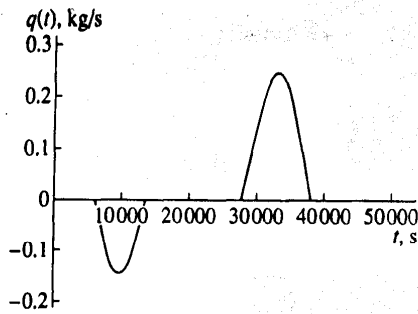


Fig. 2. Tidal evolution of the integral transport of suspension $q(t) = \int_0^{h+\zeta} US dz$ at the point $x = 6$ km of a semi-infinite channel when the values of the parameters are $\omega_0 = 1.5$ cm/s, $A = 0.01$ m²/s, $R = 0.0086$ kg m⁻² s⁻¹, $U_e = 0.041$ m/s, $\varepsilon = 0.1$, $h = 5$ m, and $\zeta = 0.5$ m.

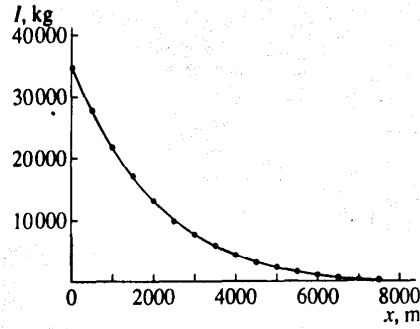


Fig. 3. Variation of residual integral transport of suspension $I = \int_0^T q(t) dt$ along the channel. The parameters are the same as in Fig. 2.

For each sediment fraction the critical distance from a sea boundary of a shallow zone exists farther with a tidal wave cannot transfer this fraction. In the first order approximation by ε it may be expressed by the inequality

$$x_i \leq -\frac{1}{k} \ln \left[\frac{(U_e^{(i)})^2}{\sqrt{2\zeta_0} k g h} \right]$$

It is apparent that the regime of bottom transformation described above is valid under the condition of equivalent erosion of the bottom at each point of the channel. This, however, is rarely encountered in practice. Finite (localized) forms of bottom sediments in the form of sand ridges located on a weakly eroded floor are usually observed in reality. Deficit zones would appear at the edges of these forms and the process of bottom transformation would be more complicated.

We emphasize that the existence of a nonzero average over the tidal period onshore transport of suspended particles in the tidal current is confirmed by the results of some field measurements.

Dynamics of finite bottom forms

The process of formation and transportation of localized bottom ridges under the influence of the tidal current was studied using the methods of numerical and laboratory modeling. The Cauchy problem for the equation of bottom deformation with account for relations (13) and (16) was solved in the first case. The initial form of the ridge was specified in the numerical experiment in the form of a part of a parabola with a height of 0.5 m and a length of $L = 10$ km, located on the non-eroded floor of the channel with a depth of $h = 5$ m. The results of numerical solution are

shown in Fig. 4, where one can see that the symmetric ridge was transformed into a dune under the influence of the tidal wave. Its left (sea side) slope becomes steeper, and the right slope becomes flatter. At the same time, the dune slowly moves in the onshore direction. The displacement of the left boundary of the ridge during a time of $t=7T$ was equal to 0.8 km, the displacement of the right boundary was equal 3.6 km.

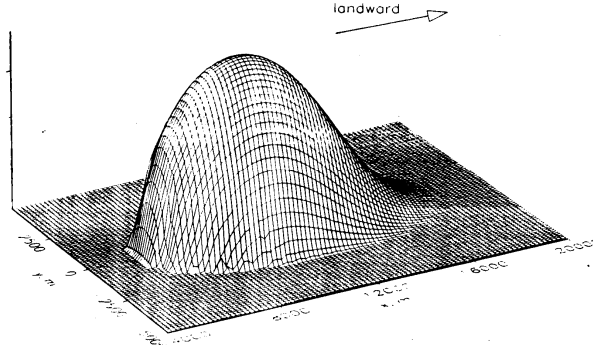


Fig. 4. The result of the numerical experiment. Formation of an inverse dune.

Residual water and suspended admixture transport

To find the solution when the width of supercritical depth is finite, we shall use the same approach as in (Postma, 1961) and seek the solution of equation (16) in the form of an asymptotic series with respect to $\varepsilon = \zeta^0/h$. Averaging equation (16) over the period of the tide and taking into account condition (15), we obtain

$$\frac{g}{3A} \left\langle (h + \zeta)^3 \frac{\partial \zeta}{\partial x} \right\rangle = 0, \quad (17)$$

where

$$\langle \phi \rangle = \frac{1}{T} \int_0^T \phi dt.$$

We can see that the expression (17) is the invariant, that is, the integral transport normal to the coast, averaged over the period, is equal to zero. Now, applying the averaging operation to the component of the integral transport along the coast S_y , we obtain the expression for the residual alongshore water transport:

$$\langle S_y \rangle = \frac{2gf}{15A^2} \left\langle (h + \zeta)^5 \frac{\partial \zeta}{\partial x} \right\rangle. \quad (18)$$

Finally, we shall obtain the expression for residual alongshore transport

$$\langle S_y \rangle = \frac{2gf h^6 \varepsilon^2}{15A^2 L} \frac{d}{dx} (\tilde{f} \tilde{f}^*), \quad (19)$$

where asterisk means complex conjugation and

$$\tilde{f} = \frac{\cosh[\tau(x-1)]}{\cosh(\tau)}, \quad \tau = (2\alpha)^{-1/2}(1+i), \quad \alpha = \frac{gh^3}{3AL^2\omega}, \quad (20)$$

i is the imaginary unit.

The distribution of the residual transport for several values of L including the infinite width of the shallow-water zone is shown in Fig. 5. One can see that when $L > 50$ km, we can practically use the approximation for the infinite width of the shallow-water zone. Residual alongshore water transport is formed in the zone of supercritical depths in the negative direction by Y . The latter means that, if we look in the direction of the residual current, the coast would always be on the left. This remarkable theoretical result was obtained for the first time for the case of the infinite

width of the shallow-water zone in paper (Zyryanov, 1995) and had experimental confirmation in paper (Zyryanov and Reshetkov, 1999).

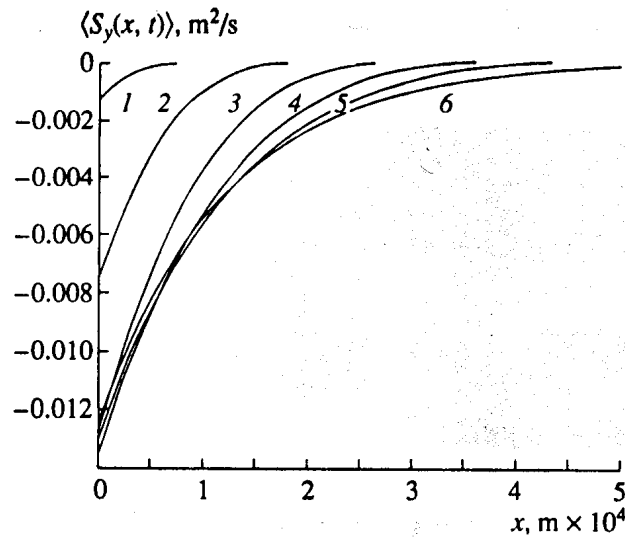


Fig.5. Graphs of the integral transport of the residual longshore water and suspended admixture transport for different values of the shallow-water zone with a width of L : (1) -10 km; (2) -20 km; (3) -30 km; (4) -40 km; (5) -50 km, and (6) - ∞ . The values of the parameters are: $h = 5$ m, $A = 0.01$ m²/s, $f = 1.32 \cdot 10^{-4}$, $\varepsilon = 0.1$

Discussion of the results

As was shown above, the average transport of suspended particles in the tidal flow in shallow water over the tidal period is nonzero and directed onshore. Its values decrease with the growth in the distance from the boundary of the shallow water area with the sea. It is interesting that, unlike the transport of suspended matter, the fluid transport average over the tidal period at any point of the channel is zero (Zyryanov and Muzylev, 1988). The latter means that there is a nonzero residual Stokes velocity in the tidal wave.

The results of numerical calculations showed that under the influence of a tidal wave a solitary sand macroform is transformed into an asymmetric dune. Its slope closest to the shore becomes flatter and the distant one (offshore) becomes steeper. The macroform moves in the onshore direction. Macroforms of the dune and antidune types are well known in river flows. The dune is oriented with its steep ("lee") slope in the direction of the suspended matter transport; the antidune, on the contrary, is oriented against the transport of sediments. Both macroforms move in the direction of their steep slope; that is, the dune moves in the direction of the sediment transport, and the antidune moves against the transport.

A new type of a macroform, an inverse dune was generated, which is an antidune by its form, because it is oriented with its steep slope against the residual transport of the suspended matter, and a dune by its motion. The results of the laboratory experiments confirmed the correctness of the theoretical results.

The transport of deposits is one of the least studied problems of the hydrodynamics of the shallow zone in tidal seas. It was shown in (Antsyferov and Arutyunyan, 1992) that to calculate the transport of deposits by tidal currents it is possible to use the methods for stationary flows averaging the displace period. The latter means that the displacement of the particles should occur along the line of the wave propagation. The result obtained in this work indicates that for finely dispersed suspension, which remains in the suspended condition during the entire tidal cycle, the residual displacement by tidal current would occur not along the line of the tidal wave propagation but over a normal to that direction.

So, differentiation of suspended bottom deposits by tidal waves in shallow water on fractions takes place not only along the direction of a tidal wave propagation but also in the angle 90° to the right from the direction of wave propagation.

In conclusion, we emphasize that the mechanism of residual transport formation described in the article is caused by viscous effects in the shallow-water zone of a tidal sea. When the depths are significantly greater than the thickness of the Stokes layer h_{St} viscous effects would not be significant, and the residual water transport would be generated mainly due to the nonlinear motion of the fluid and correspondingly due to the evolution of the potential vorticity (Garreau and Maze, 1992). It was, however, correctly noted in (Huthnance, 1993) that we have to account for viscosity even in the deep-water zones in order to avoid, for example, zero values of the residual Lagrangian water transport along closed geostrophic contours. As was shown in (Zyryanov, 1995), nonlinear terms of the equation of momentum conservation in the Stokes layer $h < h_{St}$ have an order of $(h/h_{St})^2$ as compared to viscous ones. From this it follows that in the region of supercritical depths $h < h_{St}$, the non-viscous mechanism would be weaker in the formation of the residual transport than the viscous one at least by a factor of $(h/h_{St})^2$.

The result obtained is also interesting because it points to the formation of the residual tidal circulation in bays and inlets in the band of supercritical depths, which goes around the basin of a bay in an anticyclonic way, whereas around the islands located in the zone it goes in a cyclonic way.

References

- Antsyferov, S.M. and Arutyunyan, G.E., 1992. Studies of Displacement of the Sediment Suspended by a Tidal Flow, *In* Proektirovanie, stroitel'svo i ekspluatatsiya morskikh portovykh sooruzhenii (Design, Construction, and Exploitation of Marine Port Arrangements), Moscow: Soyuzmorniiiproekt, 1992, pp. 12-26. [In Russian]
- Aubrey, D.G. and Speer, P.E., 1983. *Sediment Transport in a Tidal Inlet*. Woods Hole Oceanogr. Inst., *Tech. Rep.*, WHO 1-83-20.
- Debol'skii, V.K., Zyryanov, V.N., and Mordasov, M.A., 1984. On the Turbulent Exchange in a Tidal Mouth under the Presence of an Ice Cover, *In* Dinamika i termika rek i vodokhranilishch (Dynamics and Thermal Conditions of Rivers and Reservoirs), Moscow: Nauka, 1984, pp. 279-290. [In Russian]
- Garreau, P. and Maze, R., 1992. Tidal Rectification and Mass Transport over a Shelf Break. A Barotropic Frictionless Model, *J. Phys. Oceanogr.*, **22**: 719-731.
- Huthnance, J.M., 1993. Tidal Rectification and Mass-Transport over a Shelf Break: A Barotropic Frictionless Model. Comments, *J. Phys. Oceanogr.*, **23**: 1893.
- Muzylev, S.V., Lifshits, V.Kh., Petrov, M.P., and Titov, V.S., Variability of Hydrophysical Parameters in a Shallow-Water Estuary in Winter, *In* Gidrofizicheskie protsessy v rekakh i vodokhranilishchakh (Hydrophysical Processes in Rivers and Reservoirs), Moscow: Nauka, pp. 237-246. [In Russian]
- Postma, H., 1961. Transport and Accumulation of Suspended Matter in the Dutch Wadden Sea, *Neth. J. Sea Res.*, **1**: 148-190.
- Zyryanov, V.N. and Leibo, A.B., 1985. Evolution of a Tidal Wave in a River Mouth Covered with Ice, *In* Gidrofizicheskie protsessy v rekakh i vodokhranilishchakh (Hydrophysical Processes in Rivers and Reservoirs), Moscow: Nauka, pp. 246-257. [In Russian]
- Zyryanov, V.N. and Muzylev, S.V., 1988. Nonlinear Sea-Level Pumping by Tides in a Shallow Sea, *Dokl. Akad. Nauk SSSR*, **298**: 454-458. [In Russian]
- Zyryanov, V.N., 1995. *Topograficheskie vikhri v dinamike morskikh techenii* (Topographic Eddies in the Dynamics of Marine Currents), Moscow: Inst. Vodnykh Problem Ross. Akad. Nauk. [In Russian]
- Zyryanov, V.N. and Reshetkov, A.B., 1998. Sediment Transport and Sea Floor Transformation by Tidal Waves in Shallow Water. *Oceanology*, **38**: 679-686.
- Zyryanov, V.N. and Reshetkov, A.B., 1999. Residual Water Transport by Longshore Tidal Currents along the Coast in Shallow Water. *Oceanology*, **39**: 296-305.

Modelling circulation and temperature regime in great stratified lakes

L.A. Rukhovets, G.P. Astrakhantsev, V.N. Poloskov

Institute for Economics and Mathematics at St.Petersburg, Russ. Acad. Sci., Chaikovsky st. 1, 191187
St.Petersburg, Russia, E-mail: leor@emi.spb.su

Introduction

The main aim of modeling hydrodynamics of great stratified lakes (in our case Ladoga and Onega) is to provide information on abiotic processes, which define to a high extent functioning of the lake ecosystem, for the ecosystem model. In great stratified lakes, hydrophysical conditions have a high variability, especially during a vegetation period. For instance, the temperature in Lake Ladoga may vary in horizontal and vertical up to 15°C (Tikhomirov, 1982).

A characteristic property of ecosystem functioning for a great stratified lake is its long response to the change of loading. This time is comparable to that of water exchange. Thus, in order to forecast a response of the ecosystem to this change it is natural to use long-term average values of external forcing. Circulation that corresponds to such conditions can be considered as climatic. According to the classification done by Filatov (1983), a climatic circulation is a general lake circulation together with currents in the near-shore zone, i.e. processes, spatial scales of which are comparable to the size of a lake.

The models for numerical studies of Lake Ladoga hydrodynamics have been used for a long time. Detailed information on Lake Ladoga modelling is present in (Filatov, 1991). These investigations mostly used numerical diagnostic models.

In present paper, we evaluate the effect of quality of simulating lake hydrodynamics on adequacy of the simulated ecosystem functioning. All considerations are based on the Lake Ladoga observational data. The answer whether changes in lake hydrodynamics affect the lake ecosystem will be also given.

Numerical models of the lake's hydrothermodynamics

To reproduce the climatic circulation in Lake Ladoga, the authors have proposed two numerical models (Astrakhantsev et al., 1987, 1988). Both these models represent the approximation of the same mathematical model (Marchuk & Sarkisjan, Eds., 1980), which is based on common assumptions of Boussinesque, hydrostatics and incompressibility of fresh water, and uses linearized equations of motion and a non-linear equation of heat transfer. A full description of the model and validation of its application for simulating a climatic circulation is given in (Astrakhantsev et al., 1997, 1998).

Results of modeling the Lake Ladoga circulation

For the first time, a climatic circulation in Lake Ladoga was simulated in (Astrakhantsev et al., 1987, 1988). Qualitative and quantitative analysis of results has shown that a numerical model in general adequately simulates large-scale dynamics of the deep stratified reservoir. As a numerical grid used at that time was rather rough, containing only 300 grid points to describe the lake surface, it was not possible to describe many features of the thermal structure in Lake Ladoga with adequate accuracy. Notice that the temperature, along with nutrients, is one of the main parameters that control the development of primary production in the lake. Results (Astrakhantsev et al., 1988) show that the temperature distribution was reproduced rather roughly, especially concerning the development of such phenomena as thermal bar and thermocline. As a result, drawbacks in definition of the spatial distribution of nutrients led to the non-adequate description of phytoplankton production.

Having used a new numerical model with a higher order of approximation (Astrakhantsev et al., 1998; Rukhovets et al., 2000), authors reproduced a year-round climatic circulation of Lake Ladoga on the numerical grid with 4000 grid points describing the lake surface and with 20 layers in vertical. Results of simulations show that the development of the thermal structure during the open-water period, including main dates of the thermocline development, is in a good accordance with observational data (Tikhomirov, 1968; 1982). The development of the ice cover was also simulated, with dates of formation and melting quite close to long-term averages. Absence of the polynya (ice-hole) in the central part of Lake Ladoga (Filatov, 1991) can be considered as a drawback of the ice cover reproduction.

Due to results of simulations, variability of currents is high in the upper layer, especially during the period of stratification. Reproduced currents in the vicinity of frontal zones – thermal bar and thermocline – correspond to existing ideas. The model simulates all main features of large-scale dynamics. Vertical currents vary in the range $10^{-6} - 10^{-4} \text{ m}\cdot\text{s}^{-1}$ that corresponds to observational data (Filatov, 1983; 1991).

Thus, the model (Astrakhantsev et al., 1998; Rukhovets et al., 2000) allows reproducing the year-round circulation and thermal structure in Lake Ladoga with better results than those from the previous model (Astrakhantsev et al., 1987, 1988). Fig. 1 represents results of simulations from both models (a, b) and the distribution of the surface temperature based on averaged observational data from the last century (Naumenko et al., 2000), c. Notice that results of simulations differ from each other.

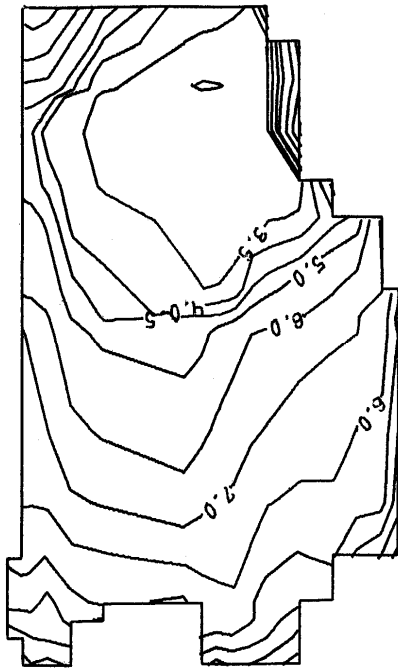
Effect of hydrodynamics on the ecosystem functioning

Turnover of nutrients is one of the main parameters of the ecosystem functioning. Comparison of modeled and observational nutrient distributions during the open-water period is a common test for model verification. Table 1 represents results of such test. Columns 1 and 2 contain modeled data received with use of the ecosystem model (Menshutkin et al., 1998), and column 3 presents averaged observational data (Petrova and Terzhevik, 1992; Rumyantsev and Drabkova, 2002). Results in column 1 are based on hydrodynamics from (Astrakhantsev et al., 1988), in column 2 on (Astrakhantsev et al., 1998; Rukhovets et al., 2000). Estimates of the total phosphorus concentration P_{total} are made for four regions presenting Lake Ladoga according to the depth distribution (Petrova & Terzhevik, 1992): region I is a coastal area where the depths are < 15 m; region II with depths from 15 m to 52 m; region III with the depths 52-89 m; region IV is the abyssal area of the lake where depths are > 89 m. As seen, modelled results based on the later model better correspond to observational data.

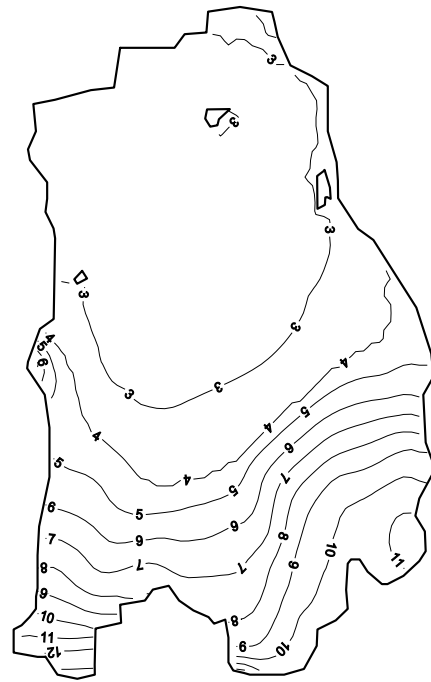
Table 1

Average concentrations of total phosphorus ($\mu\text{g}\cdot\text{l}^{-1}$) during the period of open water (observational data and computed results).

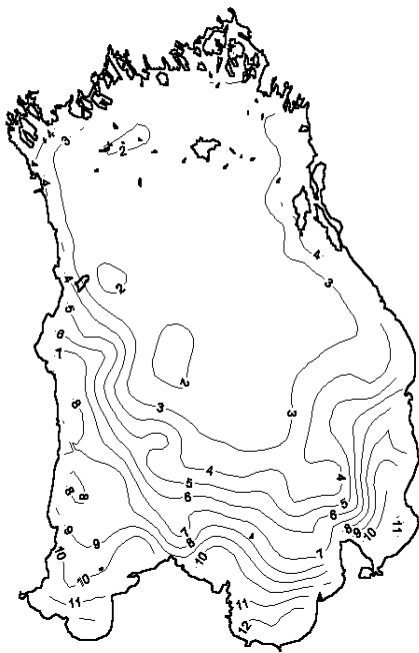
	1976-1980			1981-1983			1984-1986			1987-1989			1990-1995			1996-2000		
	1	2	3	1	2	3	1	2	3	1	2	3	1	2	3	1	2	3
I	29	31	46	32	33	37	29	29	32	30	30	31	-	29	31	-	20	26
II	28	27	27	29	28	27	28	26	24	28	26	23	-	25	20	-	18	20
III	27	25	26	29	27	22	28	25	21	27	25	20	-	24	18	-	18	18
IV	27	24	24	28	26	22	27	25	22	27	24	20	-	24	16	-	17	18
Whole lake	28	25	26	30	27	23	28	25	22	28	25	21	-	23	19	-	18	19



a)



b)



c)

Fig. 1. Surface temperature distribution in Lake Ladoga at the beginning of June: a) simulated with use of (Astrakhtsev et al., 1987, 1988); b) simulated with use of (Astrakhtsev et al., 1998; Rukhovets et al., 2000); c) averaged observational data (from Naumenko et al., 2000).

Improvement of hydrodynamic information increases reliability of modeling the phosphorus turnover, and this is a main conclusion from numerical experiments with different models of Lake Ladoga hydrodynamics. Despite the fact that a result is expected, it confirms that a simulation of the lake ecosystem development can be improved not making the ecosystem model more complicated.

In future, further numerical experiments with use of the model (Menshutkin et al., 1998) and aforementioned numerical grid are planned. They are essential in sight of increasing interest to the impact of global climate change on functioning of ecosystems of such great stratified lakes as Ladoga and Onega.

Acknowledgements

The study was performed within the framework of the project 03-05-65392 financed by the Russian Fund for Basic Research.

References

- Astrakhtantsev G.P., Egorova N.B. & Rukhovets L.A., 1987. Numerical modeling of the year-round circulation in deep lakes. *Dokl. Acad. Nauk SSSR*, 296: 1331-1334 [In Russian].
- Astrakhtantsev G.P., Egorova N.B. & Rukhovets L.A., 1988. Modelirovanie techenii i termicheskogo regima Ladojskogo ozera [Modelling currents and thermal structure in Lake Ladoga]. Leningrad, Institute of Limnology, preprint. 44 p. [In Russian].
- Astrakhtantsev G.P., Egorova N.B., Petrova N.A., Pisulin I.V., Raspletina G.F., Rukhovets L.A., 1997. Lake Ladoga ecosystem model *In Nevskaya guba – opit modelirovaniya*. Ed. by V.V. Menshutkin. St.-Petersburg, p. 44-125. [In Russian].
- Astrakhtantsev, G.P., Poloskov, V.N., Rukhovets, L.A., 1998. Numerical model of the Lake Ladoga: model of the climatic circulation and ecosystem model //Proceedings of workshop in Helsinki, May, № 5/1998, pp. 80-97.
- Astrakhtantsev G.P., Minina T.R., Petrova N.A., Poloskov V.N., Rukhovets L.A., 2003. Modelirovaniye zoobentosa i issledovanie ego roli v obmene fosforom na granitse voda-dno v Ladojskom ozere [Modelling zoobenthos and studying its role in phosphorus exchange through the interface water-sediment in Lake Ladoga]. *Vodnye resursy* [Water Resources], N 2. [In Russian].
- Filatov N.N. Dinamika ozer [Lake hydrodynamics]. Leningrad, Gidrometeoizdat, 1983. 165 pp. [In Russian].
- Filatov N.N., 1991. Gidrodinamika ozer [Hydrodynamics of lakes]. St. Petersburg. Nauka, 200 pp. [In Russian].
- Marchuk G.I., Sarkisyan A.S. (eds). 1980. Matematicheskiye modeli tsirkulyatsii v okeane [Mathematical models of ocean circulation]. Novosibirsk. 341 p. [In Russian].
- Menshutkin V.V., Astrakhtantsev G.P., Yegorova N.B., Rukhovets L.A., Simo T.L. & Petrova N.A., 1998. Mathematical modeling the evolution and current conditions of Ladoga Lake ecosystem. *Ecological Modelling*, 107: 1-24.
- Naumenko M, Guzivaty V., Karetnikov S. 1999. Spatial distribution of daily mean surface temperatures in Lake Ladoga from May to November. *In Peltonen A., Gronlund & Viljanen (eds). Proc. Third Int. Lake Ladoga Symp., University of Joensuu. Publ. of Karelian Institute. No. 129. 2000. p.442-447.*
- Petrova N.A. & Terzhevik A.Yu. (Eds.), 1992. *Ladozhskoe ozero – kriterii sostoyaniya ecosystemy*. [Lake Ladoga, ecosystem condition criteria.], St.Petersburg: Nauka, 328 p. [In Russian].
- Rumyantsev V.A., Drabkova V.G. (Eds.), 2002. *Ladozhskoe ozero – proshloe, nastoyashee, budushee* [Lake Ladoga: Past, Present and Future]. St.Petersburg, Publishing House Nauka, 327 p. [In Russian].
- Rukhovets L.A., Astrakhtantsev G.P., Menshutkin V.V., Minina T.R., Petrova N.A., Poloskov V.N. 2000. Ladozhskoye ozero – rezultaty i perspektivy [Lake Ladoga: Results and perspectives]. *In Ladozhskoye ozero*. Edited by N.N. Filatov. Petrozavodsk, pp. 405-425 [In Russian].
- Rukhovets L.A., Astrakhtantsev G.P., Menshutkin V.V., Minina T.R., Petrova N.A., Poloskov V.N., 2003: Development of Lake Ladoga Ecosystem Models: Modelling of the Phytoplankton Succession in the Eutrophication Process. I. Accepted in *Ecol. Modelling*.
- Tikhomirov A.I., 1968. Temperaturniy regime i zapasy tepla Ladozhskogo ozera [Thermal structure and heat content of Lake Ladoga]. *In Teplovoy regim Ladozhskogo ozera*, pp. 144-217 [In Russian].
- Tikhomirov A.I., 1982. *Termika krupnyh ozer* [Thermal structure of great lakes]. Leningrad, Publishing House Nauka, 232 p. [In Russian].

Comprehensive investigations of hydrophysical processes in tidal and non tidal estuaries of the Baltic and White Seas

N.Filatov¹, I. Neelov², D. Pozdnjakov² and A.Filatov³

¹ Northern Water Problems Institute, Russian Academy of Sciences, Petrozavodsk, Russia.

² Nansen International Environmental and Remote Sensing centre, St. Petersburg, Russia.

³ Center of Ecological Safety, Russian Academy of Sciences, S. Petersburg

Introduction

The White Sea and Gulf of Finland joint research projects are described herein in general lines with the major emphasis being placed on the pursued methodological approach, which was based on a concerted use of numerical hydrodynamic/ecological modeling means, remote sensing and special physical experiments conducted from research vessel. A comprehensive study of two different Estuaries in tidal White Sea and non tidal - Neva River of the Baltic Sea were carried out. It included our investigations of the indigenous physical processes aimed at estimating the mechanisms of water movements and water exchange in different cases and under conditions of climate changes. The main attention was paid to such features as circulation patterns, upwellings, frontal zones, marginal filters or barrier effects in the estuaries. On the basis of space imagies, the analysis of the data from SeaWifs and NOAA satellites and the results of sub-satellite observations was performed, with the result of revealing of the variability of water movement patterns in estuaries. (Johannessen et al, 2002).

The experimentally established tendencies in climate changes in the region were analyzed. Some numerical thermohydrodynamic and ecological models were developed. It was shown that the barrier effect plays a very significant role in the distribution of polluted water in estuaries (Lisitsin, 1999).

Model description

The model is intended to simulate the seasonal and interannual variability in hydrological and chemistry-biological characteristics of the White Sea and Gulf of Finland (Neelov, 1997). This version of the model consists of hydrodynamic and thermodynamic (ice module inclusive) units. The model is designed for eventual embedding a chemico-biological module and further investigation of the White Sea and Eastern Part Gulf of Finland ecosystems (Savchuk and Fulf, 1996). In what follows, the results of simulations of the White Sea and Gulf of Finland circulation patterns during the time period 1948- 2000 are presented. Mean monthly fields/spatial distributions of water temperature, salinity and marine water movements are given both taking into account and neglecting the tidal mechanisms. Established is that due to tidal effects there is a decrease of inflow of the Barents Sea waters to the White Sea.

The model is based on the equations of movements of a viscous and incompressible liquid in spherical co-ordinates in the approximations of Boussinesq and hydrostatics.

$$\frac{\partial u}{\partial t} = -\frac{g}{r \sin \theta} \frac{\partial \zeta}{\partial \lambda} - \frac{g}{\rho_0 r \sin \theta} \frac{\partial}{\partial \lambda} \int_{-z}^0 \rho dz + lv + \frac{\partial}{\partial z} k_m \frac{\partial u}{\partial z} + A \Delta u ;$$
$$(1) \frac{\partial v}{\partial t} = -\frac{g}{r} \frac{\partial \zeta}{\partial \theta} - \frac{g}{\rho_0 r} \frac{\partial}{\partial \theta} \int_{-z}^0 \rho dz - lu + \frac{\partial}{\partial z} k_m \frac{\partial v}{\partial z} + A \Delta v .$$

Equation of heat and salt transfer:

$$\frac{\partial(T,S)}{\partial t} + \frac{1}{r \sin \theta} \left[\frac{\partial u(T,S)}{\partial \lambda} + \frac{\partial v(T,S) \sin \theta}{\partial \theta} \right] + \frac{\partial w(T,S)}{\partial z} = \frac{\partial}{\partial z} k_{t,s} \frac{\partial(T,S)}{\partial z} + A_{(T,S)} \Delta(T,S) \quad (2)$$

Equation of continuity of hydrostatics and state is used in the UNESCO form. At the surface of the ocean, components of wind stress are considered.

For closing the equation system, a methodology analogous to (Neyelov and Oumnov, 1997) is used, i.e. a local equation of turbulent energy balance is expressed as:

$$\frac{\partial b}{\partial t} = k_m \left[\left(\frac{\partial u}{\partial z} \right)^2 + \left(\frac{\partial v}{\partial z} \right)^2 + \frac{g}{\rho_0} \alpha_\rho \frac{\partial \rho}{\partial z} \right] - \varepsilon + \frac{\partial}{\partial z} k_b \frac{\partial b}{\partial z}.$$

where b is a specific kinetic energy of turbulence.; α_b, α_ρ are parameters; ε dissipation of the turbulent energy as specified by the Kolmogorov- Obukhov hypothesis:

$$\varepsilon = c_\varepsilon b^2 / k_b; \quad k_b = 0.2L\sqrt{b}; \quad k_m = S_{mom}L\sqrt{b}; \quad k_{t,s} = S_{heat}L\sqrt{b}$$

where $c_\varepsilon = 0,09$, L = scale of turbulence determinable from the Montgomery generalized formula with due account of stratification:

$$L = L_0(1 - \alpha_R R_i);$$

$$\text{where } L_0 = \frac{\chi}{H} Z_H Z_\zeta Z_0;$$

Z_H = distance between the bottom and the point for which the calculation is performed ;

Z_ζ = distance between the water surface and the same point;

$$\alpha_R \sim 3; \quad Z_0 = 1 - \beta_1 H^{-2} Z_H Z_\zeta;$$

$0 \leq \beta_1 \leq 4$ = truncation parameter ;

$$R_i = - \frac{g}{\rho_0} \frac{\partial \rho}{\partial z} / \left[\left(\frac{\partial u}{\partial z} \right)^2 + \left(\frac{\partial v}{\partial z} \right)^2 \right]$$

R_i = Richardson number, Gh = functions of the Richardson number.

The model of ice cover evolution is based on the equations of ice movement using the viscous-plastic rheology. For calculating heat fluxes directed to the water/ice-air interface, the method suggested by Orlanski (1976) is used. The flux of solar shortwave radiation is calculated from the Zillman (1972) expression.

Taken from the NCEP/NCAR archive, the daily meteorological data for the time period 1948-2000 are used as the model forcing parameters. These data have a spatial resolution of 2° latitude by 2° longitude. The archive is formatted as an array of binary code-files of direct access, which assures a serious reduction of calculation time. These meteorological data are subjected to linear interpolation into the simulated domain.

To set up the boundary conditions, mean climatic values of river discharge and the Barents Sea boundary conditon characteristics were employed.

Estimated were the impact of climate change on to the watershed territory and the White Sea ecosystem .

Remote Sensing data

It is important to underscore that both water bodies, viz, Onega Bay of the White Sea and the easternmost Gulf of Finland are by all accounts marine eutrophic aquatic environments. Bathymetric features (relatively low depths), fairly high summer water temperatures, proximity to strand lands, and hence being subject to land and river runoffs discharging into the water bodies,

large amounts of waters rich in nutrients, suspended matter and soil humus, indicate that in the sense of hydrooptics these are Case II waters with all the ensuing consequences for passive optical remote sensing. This conclusion will further be substantiated by the results of shipborne/laboratory in situ measurements, the discussion of which follows this section.

It appears worthwhile to analyse the chl field retrieved with SeaDAS from the perspective of the nature of inaccuracies arising from the application of the standard OC4 retrieval algorithm. According to our analysis, it becomes clear that OC4 erroneously gives higher values of chl in the areas with enhanced concentrations of either sm or doc. Indeed, according to the water circulation patterns, the waters of rivers (e.g. Kem' and Onega) move anti-clockwise along the coastline of Onega Bay being rich in doc and sm respectively. It is exactly within coastline areas where OC4 erroneously gives particularly high concentrations of chl.

Comparing the chl and sm spatial distributions, it is interesting to point out that large areas of decreased concentrations of sm (i.e. transparent waters) coincide with enhanced concentration of chl. Contrarily, in the impounded (by a flooding-protection dike) region of the Neva River Bay and right beyond it, the areas of high concentrations of sm correspond to low contents of chl. These features comply well with the local bathymetry and hydrodynamic patterns discussed above. The same holds for the northern coastline of the Gulf. This is further substantiated by the causal analysis of doc spatial distribution over the easternmost part of the Gulf of Finland. The doc concentrations are most pronounced along the southern coastline of the water area under consideration. This is a result of topographic effects, water currents and physicochemical specific conditions: rather shallow, low-salinity areas subjected to strong currents, land-, river runoff and sewage effluents rich in humus/dissolved organics.

A distinguishing feature of the above SeaWiFS images taken over both Onega Bay in the White Sea and the Gulf of Finland is a strongly pronounced heterogeneity of the spatial distributions of all CPAs – a property inherent in the sophisticated nature of aquatic environments with non-Case I waters, and is a result of a simultaneous and conjoint influence of physicochemical impacts from the ambient land areas, bottom relief and the inherent water movement patterns. The principal problem of processing space images of the White Sea resides in their enhanced optical complexity: these waters contain in substantial amounts a number of colour producing agents. As a result, all of them contribute to the composite signal subject to processing and inferring the desired component. The algorithm suggested and applied to the interpretation of the space imagery taken over Onega Bay of White Sea proved to be successful, which is substantiated by both direct comparisons with synchronized in situ determinations and expert analyses of the field of water temperature, prevailing current patterns and water salinity spatial distribution.

Based on these comparisons between in situ measurements, SeaDAS and L-M retrieval data, it appears justifiable to assume that the L-M procedure assures an adequate restoration of the desired water quality parameters even in optically most complex waters (i.e. non-case I waters) in the White Sea. For the pelagic waters (which optically are generally less complex), the task of water quality retrieval is easier and, hence obviously credible when processed with the L-M code. Consequently, the spatial distributions of chl, sm and doc are believed to be the first trustworthy images of water quality parameter fields in the White Sea obtained from space.

Some results

The Gulf of Finland

The Gulf of Finland is an estuary-type body of water. The Gulf stretches further east to the Neva river estuary cutting far into the land. The narrowest (12-15 km) eastern part of the Gulf of Finland is called the Neva Bay. Due to the intensive transport of sedimentary material by the rivers Neva, Narva and some others the bottom in the Gulf's eastern part is formed by flat accumulative plains at a depth of 30-50 m. The Gulf of Finland total water surface area is 29 571 sq. km (about 7 % of the total Baltic Sea area). The water mass volume is 1103 km³ (about 5 % of

the total Sea volume). The length of the Gulf of Finland is 398 km, with mean depth 29 m and maximum depth 123 m. The total annual river runoff is 114 km³.

The thermohaline structure of the Gulf's water masses forms under a powerful desalinating effect due to river runoff with the general tendency of water salinity decline with increasing depth and approaching the eastern apex of the Gulf. Hence, the surface water salinity in the Gulf decreases to 2-3‰, and the permanent halocline layer typical of the Baltic Sea is present only in relatively deep, offshore areas.

Owing to the river runoff the spatial distribution of water salinity at the surface shows a general round-the-year tendency towards the salinity increase from 1-2 ‰ in the east to 6-6.5 ‰ in the west.

Tides in the Gulf of Finland are insignificant, and follow an irregular diurnal and semidiurnal pattern. The tide amplitude in the central part of the Gulf of Finland is 5-10 cm, growing to 10-20 cm at the apex of the Gulf.

The pattern of the water level oscillations induced by the binodal seiche in the Baltic Sea – Gulf of Finland system is somewhat different. The range of oscillations in the eastern Gulf of Finland is between 30-50 cm, being 40-60 cm in the south-western Baltic.

The regime of currents in the Gulf of Finland is a result of interactions between a variety of processes on various temporal and spatial scales. The most important processes are: wind drift, river runoff, storm surge swell, seiches, inertial currents. Thus, as regards the genesis, the types of currents in the Gulf of Finland are wind-driven, runoff-induced, gradient, density and compensating, which sum up into the general water circulation pattern.

The surface currents in the Gulf of Finland indicate the presence of a large number of eddies and flow meandering. The major factor controlling the spatial variability of the current velocities and directions in the Gulf of Finland is its morphometry. Water masses from the Baltic Sea penetrate the Gulf forming a current flowing from the east along the southern coast. The water masses transformed by the Gulf of Finland flow out along its northern coast. Fig. 1 illustrates a possible position of the frontal zone in the Gulf of Finland.

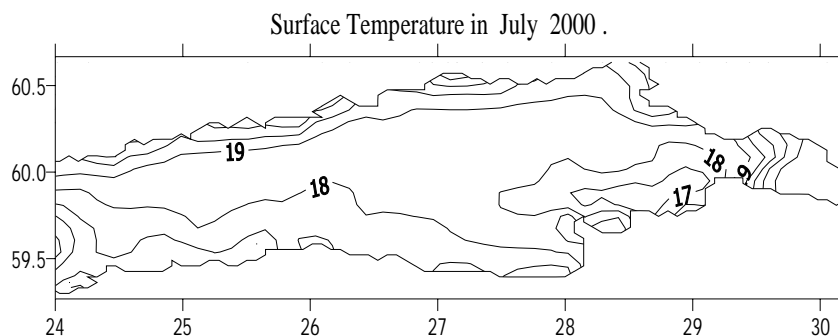


Fig. 1. Surface temperature distribution in the Gulf of Finland according to the numerical modeling

Results of numerical simulations (Fig. 1), the relevant remote sensing data and field experiments collectively demonstrate the presence of frontal zones – barrier effects which keep about 80 % of polluted waters in upper part of the estuary. The location of these frontal zones depends upon the specific nature of mixing fresh and marine offshore waters. The barrier effect is generally generated within isohalines of 3-4‰. The thermal front contours here are fussy. The barrier effect is mostly due to both the specificity of water movements within the estuary and the influence of storm-induced positive setups. Since water flow-driven fronts are dominant in this region, their identification from satellite data is possible through the retrieval of spatial distributions of concentrations of phytoplankton chlorophyll, suspended minerals, dissolved organics and SST.

The thus obtained data indicate that the role of flow waters coming from the eastern Gulf had been overestimated.

The White Sea

The White Sea is a shallow, tide-controlled sea characterised by significant water exchange processes. Bounded by 69°N and 63°N, and 32°E and 45°E, the White Sea region is located on the northern outskirts of the north-western region of Russia. The sea surface is about 90000 km², and it is 90800 km², including islands. The maximal depth is 350 m, the average depth is 67 m. The water body volume is 6000 km³. The White Sea is a typical shelf sea, which can be divided into three parts: northern, central and southern. There are several large bays in the sea. The bottom relief of the White Sea is irregular; the depths vary strongly throughout the sea. The water exchange between the White and Barents Seas considerably fluctuates due to the relief unevenness. It plays an important role in the formation of hydrophysical, hydrochemical and hydrobiological regimes of the sea. The Onega Bay is separated from the central part of the sea by the Solovecky Islands. This is the shallowest part with the depths between 5 and 25 m.

A typical feature of water temperature distributions in the sea is the existence of two kinds of vertical distribution of water masses. In the Funnel, Throat, Mezen and Onega Bays it is homogeneous, in the Dvinsky and Kandalacsha Bays as well in the Pool it is stratified. The Barents Sea current brings to the White Sea about 26 % of the total annual heat input. The salinity of offshore waters in the predominant part of the water area is about 24,7‰ despite of a significant desalination of sea waters induced by river runoff. Brackish waters remain only in the northern parts of the White Sea bays and mainly in the vicinity of the inflowing river banks. The role of river runoff is extremely important. The annual amount of river runoff reaches 4% of the White Sea water volume. It controls the water exchange rate between the White and Barents Seas and determines to a large extent the extant water circulation patterns. The total number of rivers is 5563 with the cumulative length of 26.7 thousand km. The total annual river runoff into the sea is 259 km³. The river runoff plays an important role in the development of the sea hydrophysical and chemical regimes. The White Sea currents result mostly from a joint effect of baroclinity, bottom relief (JEER), tides and winds. Hydrodynamic features of the sea are defined by a relatively small size of the sea and strong river runoff. The greatest speeds of currents (50-100 cm·s⁻¹) are found in the Mezen Bay, Throat and near the Solovecky islands. Water movements are relatively slow during winter when the sea is covered by ice. An important source of currents is tides. In the White Sea, predominant are quasi 12-h fluctuations.

Tides in the White Sea play a very significant role in the formation of the thermo-hydrodynamical regime in this sea. The tidal water level fluctuations are highest in the Mezen Bay. They equal 10 m here, 3.5 m in the Throat, 3 m in the Onega Bay, 2-2.5 m in the Kandalakshski Bay.

The developed 3-D thermohydrodynamic model of water circulation in the White Sea reproduces reasonably faithfully the seasonal and interannual variabilities in the hydrological characteristics as well as in ice cover. The White Sea tidal effects were equally simulated and assessed in terms of their significance. It is shown that taking into account the action of tidal wave M2 brings about a 20% decrease in water exchange rates with the Barents Sea. The results of hydrodynamic simulations are indicative that 1) the tidal effects are very essential in terms of the water surface and water movements pattern formations; the simulated velocities proved to be about 5-7 cm·s⁻¹; 2) a surficial runoff current originates in the Dvina River mouth and then moves on to the Winter coastline; 3) nearby the bottom, in the Throat there is a countercurrent into the White Sea, which brings the Barents Sea water. Another countercurrent is found to be located in the Dvina River Bay. Neglecting the tidal component leads to a nearly along-the coast direction of the current, which is particularly important when simulating the current patterns in the Gorlo area

of the White Sea. A quantitative assessment of tidal effects on the circulation patterns of the White Sea is essential in terms of discharge rates: the discharge rate of inflowing waters from the Barents Sea is by 2-3 Sverdrups less than it is en the tidal effect is neglected. It accounts for about 20%. Therefore, it can be believed well established that the tidal effect sensibly affects long-period processes in the White Sea through lowering the water exchange rates with the Barents Sea. The other spectacular effect produced by tidal effects is a formation of a stable zone of upwelling around the Solovetskie Islands. In August, the water salinity in surface waters is noticeably lower, especially so in near estuarine areas, which is naturally due to a seasonal increase in river discharge.

Dominating in the White Sea are tidal and water flow-driven fronts (Dolotov et al., 2002). This brings about a significant difference in the mechanisms of front formation in comparison with the Gulf of Finland. At the river-sea barrier the major portion of suspended matter settles down as the salinity reaches the level of 21‰. The vertical profile of the suspended matter lacks of well-formed maxima, which is due to a strong influence of water-inflow0driven mixing. Delimitation of frontal/barrier zones in the White Sea from satellite imagery is only possible when SeaWiFS and NOAA are concertedly employed. Unlikely the boundaries of salinity, the location of a thermal front can differ from the patterns of spatial distribution of phytoplankton chlorophyll, suspended minerals and dissolved organics. This is discussed in detail in our oral presentation..

Fig. 2 illustrates the results of simulations of thermohydrodynamics in the Onega Bay with due account and neglect of tides.

Thus the role of tides in both the formation of the thermohydrodynamic regime and determining the processes of exchange at the estuary/open sea is explicitly shown.

Based on the results of numerical simulations, shown are the possible variations in both the marine thermohydrodynamic regime and ecosystem under a climatic scenario previously assessed using the ECHAM-4 model. Fig. 4 indicates that a 2°C air temperature change will be followed by one per mille increase of water salinity. This in turn will entail some variations in the hydrological and chemico-biological characteristics.

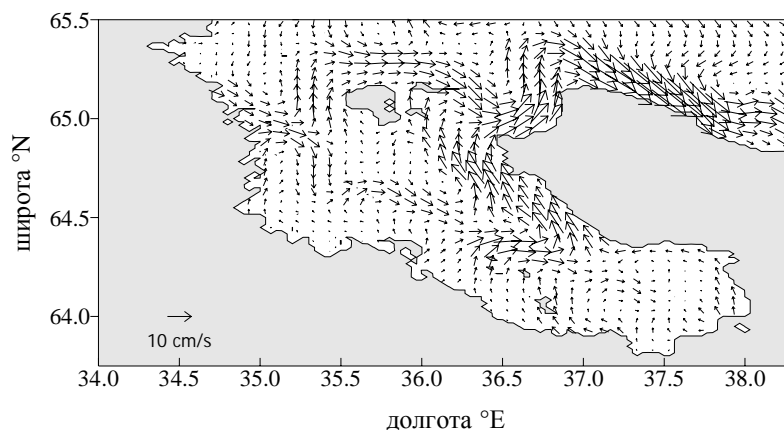


Fig. 2a . Simulated surface currents in the Onega Estuary of the White Sea when calculated without tides.

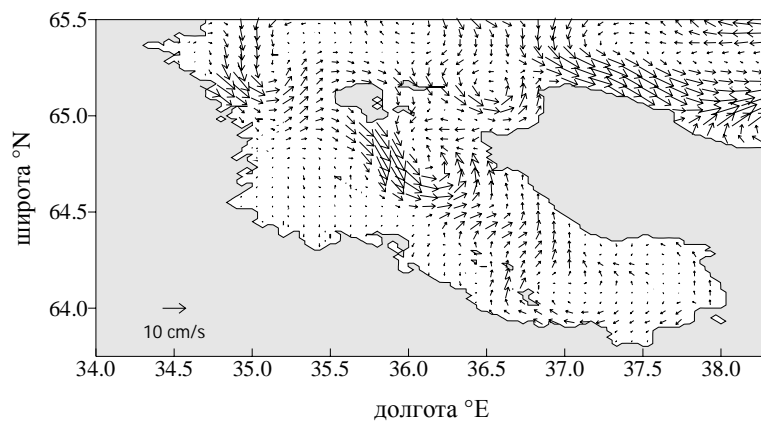


Fig. 2b. Simulated surface currents in the Onega Estuary of the White Sea when calculated with tides.

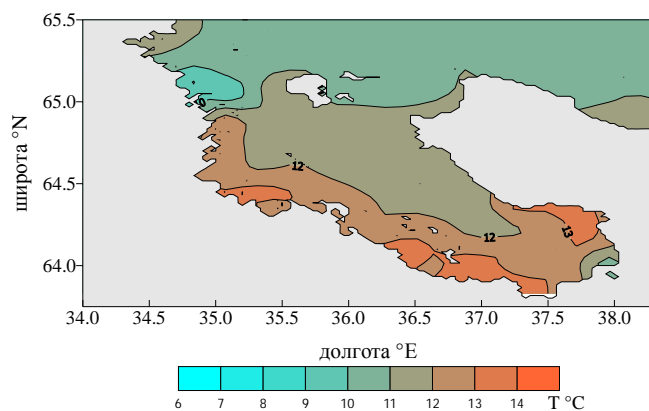


Fig. 3a. Simulated surface temperatures in the Onega Estuary of the White Sea when calculated without tides.

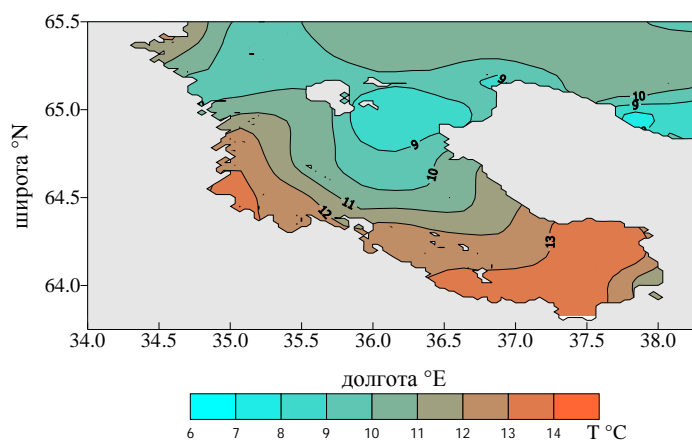


Fig. 3b. Simulated surface temperatures in the Onega Estuary of the White Sea when calculated without tides.

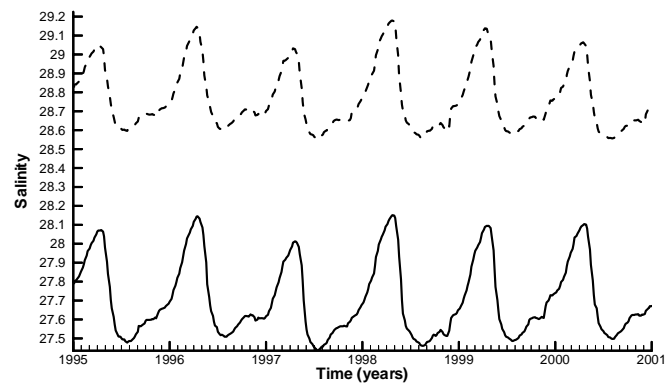


Fig. 4. The mean salinity in the White Sea . The solid curve is a control run, the dashed line corresponds to the explored climate scenarios (an increase of the mean temperature by 2°C and a decrease of river discharge by 20%).

Validation of the model calculations was also performed by comparing the simulated phytoplankton distributions with the chlorophyll special distributions as retrieved from SeaWiFS images taken over the White Sea during the vegetation seasons. The satellite data are explicitly confirmative in favour of adequacy of the simulated distributions.

Acknowledgements

This work was supported by the INKO-Copernicus project ICA2-CT-2000-10014 and INTAS project 99-674.

References

- Dolotov Yu.S., Filatov N.N., Nemova N.N. et al., 2002. The study of dynamics of the water, suspended matter, anthropogenic pollution, and the ecosystem living conditions in the estuaries (by the example of the Karelian Coast of the White Sea). *Oceanology*. **42**. Supp. 1. S135-S147.
- Lisitzin A.P., 1999. The continental-ocean boundary as a marginal filter in the World Ocean. *In* Biogeochemical Cycling and Sediment Ecology. J.S. Gray, W. Ambrose Jr., Szaniawska (eds.). Dordrecht: Kluwer Academic Publishers. 1999. P. 69-109.
- Neyelov, I.A., Oumnov A.A., 1997. A model of the Neva River Bay ecological system. *In*: The Neva River Bay: experience in modeling (Ed. V.V. Menshoutkin). St.Petersburg. pp. 183-218.
- Galperin, B., Kantha, L.H., Hassd, S., Rosati, A., 1988, A quasi-equilibrium turbulent energy model for geophysical flows. *J. Atmos. Sci.*, **45**: 55-62.
- Hibler III, W.D., 1979. A dynamic thermodynamic sea ice model. *J. Phys. Oceanogr.* **9**: 815-846.
- Johannessen O.M., Liaskovski A., Pozdnyakov D., Filatov N., Pettersson L., Bobylev L., 2003. SeaWiFS detects spatial features of the White Sea water quality parameters. *Remote Sensing of Environment* (in press).
- Orlanski, I., 1976. A simple boundary condition flows for unbounded hyperbolic. *J. Comput. Phys.* **21**: 251-269.
- Palma, E.D., Matano, R.P., 2000. On the implementation of open boundary conditions for a general circulation model: The three-dimensional case. *J. Geophys. Res.* **105**: 8605-8627.
- Savchuk, O., Wulf, F., 1996, Biogeochemical Transformations of Nitrogen and Phosphorus in the Marine Environment. *In*: Coupling Hydrodynamic and Biogeochemical Processes in Models for the Baltic Proper. System Ecology Contributions No.2 Stockholm University. 79 p.
- Zilliman, J.W., 1972. *A study of some aspects of the radiation and heat budgets of the southern hemisphere oceans*. Meteorol. Study. Rep. 26, Bur. of Meteorol., Dep. of the Inter., Canberra, A.C.T. 562 p.